THE CERN LARGE HADRON COLLIDER: ACCELERATOR AND EXPERIMENTS

LHC Machine

Lyndon Evans[1] **and Philip Bryant (editors)**[2]

European Organization for Nuclear Research
CERN CH-1211, Genève 23, Switzerland
E-mail: *lyn.evans@cern.ch*

ABSTRACT: The Large Hadron Collider (LHC) at CERN near Geneva is the world's newest and most powerful tool for Particle Physics research. It is designed to collide proton beams with a centre-of-mass energy of 14 TeV and an unprecedented luminosity of 10^{34} cm^{-2}s^{-1}. It can also collide heavy (Pb) ions with an energy of 2.8 TeV per nucleon and a peak luminosity of 10^{27} cm^{-2}s^{-1}. In this paper, the machine design is described.

KEYWORDS: Acceleration cavities and magnets superconducting; Beam-line instrumentation; Hardware and accelerator control systems; Instrumentation for particle accelerators and storage rings — high energy.

---

[1]Corresponding author.

[2]This report is an abridged version of the LHC Design Report (CERN-2004-003).

Contents

Chapter 1

Introduction

The Large Hadron Collider (LHC) is a two-ring-superconducting-hadron accelerator and collider installed in the existing 26.7 km tunnel that was constructed between 1984 and 1989 for the CERN LEP machine. The LEP tunnel has eight straight sections and eight arcs and lies between 45 m and 170 m below the surface on a plane inclined at 1.4% sloping towards the *Léman* lake. Approximately 90% of its length is in molasse rock, which has excellent characteristics for this application, and 10% is in limestone under the Jura mountain. There are two transfer tunnels, each approximately 2.5 km in length, linking the LHC to the CERN accelerator complex that acts as injector. Full use has been made of the existing civil engineering structures, but modifications and additions were also needed. Broadly speaking, the underground and surface structures at Points 1 and 5 for ATLAS and CMS, respectively, are new, while those for ALICE and LHCb, at Points 2 and 8, respectively, were originally built for LEP.

The approval of the LHC project was given by the CERN Council in December 1994. At that time, the plan was to build a machine in two stages starting with a centre-of-mass energy of 10 TeV, to be upgraded later to 14 TeV. However, during 19956, intense negotiations secured substantial contributions to the project from non-member states, and in December 1996 the CERN Council approved construction of the 14 TeV machine in a single stage. The non-member state agreements ranged from financial donations, through inkind contributions entirely funded by the contributor, to in-kind-contributions that were jointly funded by CERN and the contributor. Confidence for this move was based on the experience gained in earlier years from the international collaborations that often formed around physics experiments. Overall, non-member state involvement has proven to be highly successful.

The decision to build LHC at CERN was strongly influenced by the cost saving to be made by re-using the LEP tunnel and its injection chain. The original LEP machine was only made possible by something that was once referred to by N. Cabbibo, INFN, Italy, as the exo-geographic transition. Although at its founding, CERN was endowed with a generous site in the Swiss countryside, with an adjacent site for expansion into the even emptier French countryside, the need for space outstripped that available when the super-proton synchrotron, or SPS, was proposed. In this instance, the problem was solved by extensive land purchases, but the next machine, LEP, with its 27 km ring, made this solution impractical. In France, the ownership of land includes the underground volume extending to the centre of the earth, but, in the public interest, the Government can

buy the rights to the underground part for a purely nominal fee. In Switzerland, a real estate owner only owns the land down to a "reasonable" depth. Accordingly, the host states re-acted quickly and gave CERN the right to bore tunnels under the two countries, effectively opening a quasiinfinite site that only needed a few "islands" of land ownership for shafts. In 1989, CERN started LEP, the world's highest energy electron-positron collider. In 2000, LEP was closed to liberate the tunnel for the LHC.

The LHC design depends on some basic principles linked with the latest technology. Being a particle-particle collider, there are two rings with counter-rotating beams, unlike particle-antiparticle colliders that can have both beams sharing the same phase space in a single ring. The tunnel geometry was originally designed for the electron-positron machine LEP, and there were eight crossing points flanked by long straight sections for RF cavities that compensated the high synchrotron radiation losses. A proton machine such as LHC does not have the same synchrotron radiation problem and would, ideally, have longer arcs and shorter straight sections for the same circumference, but accepting the tunnel "as built" was the cost-effective solution. However, it was decided to equip only four of the possible eight interaction regions and to suppress beam crossings in the other four to prevent unnecessary disruption of the beams. Of the four chosen interaction points, two were equipped with new underground caverns.

The tunnel in the arcs has a finished internal diameter of 3.7 m, which makes it extremely difficult to install two completely separate proton rings. This hard limit on space led to the adoption of the twin-bore magnet design that was proposed by John Blewett at the Brookhaven laboratory in 1971. At that time, it was known as the "two-in-one" super-conducting magnet design [1] and was put forward as a cost saving measure [2, 3], but in the case of the LHC the overriding reason for adopting this solution is the lack of space in the tunnel. The disadvantage of the twin bore design is that the rings are magnetically coupled, which adversely affects flexibility. This is why the Superconducting Super Collider (SSC) was designed with separate rings [4].

In the second half of the twentieth century, it became clear that higher energies could only be reached through better technologies, principally through superconductivity. The first use of superconducting magnets in an operational collider was in the ISR, but always at 4 K to 4.5 K [5]. However, research was moving towards operation at 2 K and lower, to take advantage of the increased temperature margins and the enhanced heat transfer at the solid-liquid interface and in the bulk liquid [6]. The French Tokamak Tore II Supra demonstrated this new technology [7, 8], which was then proposed for the LHC [9] and brought from the preliminary study to the final concept design and validation in six years [10].

The different systems in the LHC will be reviewed in more details in the following chapters. The principal references used for the technical design are the early design studies [11, 12] and the LHC Design Report [13], which is in three volumes.

Chapter 2

Main machine layout and performance

2.1 Performance goals

The aim of the LHC is to reveal the physics beyond the Standard Model with centre of mass collision energies of up to 14 TeV. The number of events per second generated in the LHC collisions is given by:

$$N_{\text{event}} = L\sigma_{\text{event}} \tag{2.1}$$

where σ_{event} is the cross section for the event under study and L the machine luminosity. The machine luminosity depends only on the beam parameters and can be written for a Gaussian beam distribution as:

$$L = \frac{N_b^2 n_b f_{\text{rev}} \gamma_r}{4\pi \varepsilon_n \beta*} F \tag{2.2}$$

where N_b is the number of particles per bunch, n_b the number of bunches per beam, f_{rev} the revolution frequency, γ_r the relativistic gamma factor, ε_n the normalized transverse beam emittance, $\beta*$ the beta function at the collision point, and F the geometric luminosity reduction factor due to the crossing angle at the interaction point (IP):

$$F = \left(1 + \left(\frac{\theta_c \sigma_z}{2\sigma*}\right)^2\right)^{-1/2} \tag{2.3}$$

θ_c is the full crossing angle at the IP, σ_z the RMS bunch length, and $\sigma*$ the transverse RMS beam size at the IP. The above expression assumes round beams, with $\sigma_z \ll \beta$, and with equal beam parameters for both beams. The exploration of rare events in the LHC collisions therefore requires both high beam energies and high beam intensities.

The LHC has two high luminosity experiments, ATLAS [14] and CMS [15], both aiming at a peak luminosity of $L = 10^{34} \text{cm}^2 \text{s}^1$ for proton operation. There are also two low luminosity experiments: LHCB [16] for B-physics, aiming at a peak luminosity of $L = 10^{32} \text{cm}^2 \text{s}^1$, and TOTEM [17] for the detection of protons from elastic scattering at small angles, aiming at a peak luminosity of $L = 2 \times 10^{29} \text{cm}^2 \text{s}^1$ with 156 bunches. In addition to the proton beams, the LHC will also be operated with ion beams. The LHC has one dedicated ion experiment, ALICE [18], aiming at a peak luminosity of $L = 10^{27} \text{cm}^2 \text{s}^1$ for nominal lead-lead ion operation.

The high beam intensity required for a luminosity of $L = 10^{34}$cm^{2}s^1 excludes the use of anti-proton beams, and hence excludes the particle-anti-particle collider configuration of a common vacuum and magnet system for both circulating beams, as used for example in the Tevatron. To collide two counter-rotating proton beams requires opposite magnetic dipole fields in both rings. The LHC is therefore designed as a proton-proton collider with separate magnet fields and vacuum chambers in the main arcs and with common sections only at the insertion regions where the experimental detectors are located. The two beams share an approximately 130 m long common beam pipe along the IRs. The exact length is 126 m in IR2 and IR8, which feature superconducting separation dipole magnets next to the triplet assemblies, and 140 m in IR1 and IR5, which feature normal conducting magnets and therefore longer separation dipole magnets next to the triplet assemblies. Together with the large number of bunches (2'808 for each proton beam), and a nominal bunch spacing of 25 ns, the long common beam pipe implies 34 parasitic collision points at each experimental insertion region. For four experimental IRs, this implies a total of 136 unwanted collision points. Dedicated crossing angle orbit bumps separate the two LHC beams left and right from the IP in order to avoid collisions at these parasitic collision points.

There is not enough room for two separate rings of magnets in the LEP/LHC tunnel and, for this reason, the LHC uses twin bore magnets that consist of two sets of coils and beam channels within the same mechanical structure and cryostat. The peak beam energy depends on the integrated dipole field around the storage ring, which implies a peak dipole field of 8.33 T for the 7 TeV in the LHC machine and the use of superconducting magnet technology.

2.2 Performance limitations

2.2.1 Beam-beam limit

The maximum particle density per bunch is limited by the nonlinear beam-beam interaction that each particle experiences when the bunches of both beams collide with each other. The beam-beam interaction is measured by the linear tune shift given by:

$$\xi = \frac{N_b \, r_p}{4\pi\varepsilon_n} \tag{2.4}$$

in which r_p is the classical proton radius $r_p = e^2/(4\pi\varepsilon_0 m_p c^2)$. Experience with existing hadron colliders indicates that the total linear tune shift summed over all IPs should not exceed 0.015. With three proton experiments requiring head-on collisions, this implies that the linear beam-beam tune shift for each IP should satisfy $\xi < 0.005$.

2.2.2 Mechanical aperture

The geometrical aperture of the LHC arcs is given by the beam screen dimensions. The beam screen has a height of approximately 2 × 17.3 mm and a total width of 2 × 22 mm. Setting the minimum aperture of 10 σ in terms of the RMS beam size, and allowing for tolerances for the linear machine imperfections and the magnet alignment and geometry, implies a peak nominal beam size of 1.2 mm. The minimum mechanical aperture of 10 σgs prescribed by the LHC beam cleaning system. When combined with a peak β-function of 180 m in the LHC arcs, this implies a maximum

acceptable transverse beam emittance of $\varepsilon_n = 3.75$ μm. The limit on the linear beam-beam tune shift and the mechanical aperture of the LHC therefore limit the maximum bunch intensity to $N_b = 1.15 \times 10^{11}$.

Furthermore, the mechanical aperture of the triplet magnets limits the minimum attainable β^* value at the IPs and the maximum attainable crossing angle orbit bump in the experimental interaction regions. Both these parameters limit the peak luminosity in the LHC machine.

2.2.3 Maximum dipole field and magnet quench limits

The maximum beam energy that can be reached in the LHC is limited by the peak dipole field in the storage ring. The nominal field is 8.33 T, corresponding to an energy of 7 TeV. However, the actual field attainable in the storage ring depends on the heat load and temperature margins inside the cryo-magnets and therefore on the beam losses during operation. A high dipole field therefore requires efficient operation with minimum beam losses.

2.2.4 Energy stored in the circulating beams and in the magnetic fields

A total beam current of 0.584 A corresponds to a stored energy of approximately 362 MJ. In addition to the energy stored in the circulating beams, the LHC magnet system has a stored electro-magnetic energy of approximately 600 MJ, yielding a total stored energy of more than 1 GJ. This stored energy must be absorbed safely at the end of each run or in the case of a malfunction or an emergency. The beam dumping system and the magnet system therefore provide additional limits for the maximum attainable beam energies and intensities.

2.2.5 Heat load

Although synchrotron radiation in hadron storage rings is small compared to that generated in electron rings, it can still impose practical limits on the maximum attainable beam intensities, if the radiation has to be absorbed by the cryogenic system. In addition to the synchrotron-radiation heat load, the LHC cryogenic system must absorb the heat deposition from luminosity-induced losses, impedance-induced losses (resistive wall effect) and electron-cloud bombardment.

2.2.6 Field quality and dynamic aperture

Field quality errors compromise the particle stability in the storage ring, and hence loss-free operation requires a high field quality. A characterizing feature of superconducting magnets is the decay of persistent currents and their 'snap back' at the beginning of the ramp. Achieving small beam losses therefore requires a tight control of the magnetic field errors during magnet production and during machine operation. Assuming fixed limits for the beam losses (set by the quench levels of the superconducting magnets), the accuracy of the field quality correction during operation and its limitation on machine performance can be estimated.

2.2.7 Collective beam instabilities

The interaction of the charged particles in each beam with each other via electromagnetic fields and the conducting boundaries of the vacuum system can result in collective beam instabilities. Generally speaking, the collective effects are a function of the vacuum system geometry and its surface properties. They are usually proportional to the beam currents and can therefore limit the maximum attainable beam intensities.

2.2.8 Luminosity lifetime

The luminosity in the LHC is not constant over a physics run, but decays due to the degradation of intensities and emittances of the circulating beams. The main cause of the luminosity decay during nominal LHC operation is the beam loss from collisions. The initial decay time of the bunch intensity, due to this effect, is:

$$\tau_{\text{nuclear}} = \frac{N_{\text{tot},0}}{L\sigma_{\text{tot}}k} \tag{2.5}$$

where $N_{\text{tot},0}$ is the initial beam intensity, L the initial luminosity, σ_{tot} the total cross section ($\sigma_{\text{tot}} = 10^{25}$ cm^{-2} at 14TeV) and k the number of IPs. Assuming an initial peak luminosity of $L = 10^{34}$ cm^{-2}s^{-1} and two high luminosity experiments, the above expression yields an initial decay time of $\tau = 44.85$ h. Equation 2.5 results in the following decay of the beam intensity and luminosity as functions of time:

$$N_{\text{tot}}(t) = \frac{N_{\text{tot},0}}{1 + t/\tau_{\text{nuclear}}} \tag{2.6}$$

$$L(t) = \frac{L_0}{(1 + t/\tau_{\text{nuclear}})^2}. \tag{2.7}$$

The time required to reach $1/e$ of the initial luminosity is given by:

$$t_{1/e} = (\sqrt{e} - 1)\tau, \tag{2.8}$$

yielding a luminosity decay time of $\tau_{\text{nuclear},1/e} = 29$ h.

Other contributions to beam losses come from Toucheck scattering and from particle losses due to a slow emittance blow-up. Emittance blow-up can be caused by the scattering of particles on residual gas, the nonlinear force of the beam-beam interaction, RF noise, and IBS scattering effects.

The synchrotron radiation damping in the LHC decreases the bunch dimensions at top energy and can partially compensate the beam size blow-up due to the above effects. Following the arguments set out in the Pink Book (1991 Design Study) [19], it is assumed that the radiation damping process just cancels the beam blow up due to the beam-beam interactions and RF noise. Approximating further the decay by an exponential process, the net luminosity lifetime can be estimated as:

$$\frac{1}{\tau_L} = \frac{1}{\tau_{\text{IBS}}} + \frac{1}{\tau_{\text{rest gas}}} + \frac{1}{\tau_{\text{nuclear},1/e}} \tag{2.9}$$

Assuming an IBS time constant of 80 hour and a rest gas time constant of 100 hour with the above nuclear decay time gives a net estimate of the luminosity lifetime of,

$$\tau_L = 14.9 \, h. \tag{2.10}$$

2.2.9 Average turnaround time

Filling the LHC requires 12 cycles of the SPS synchrotron, and each SPS fill requires 3 to 4 cycles of the PS synchrotron. The SPS and PS cycling time are 21.6 s and 3.6 s, respectively, yielding a total LHC filling time of approximately 4 minutes per beam. Assuming that each LHC aperture requires an additional 4 SPS cycles for the injection set up (3 pilot bunches and one nominal intensity), and that the LHC operators require at least two minutes to evaluate the measurements of each pilot bunch shot and to readjust the machine settings, the total (minimum) LHC injection time becomes 16 minutes. The minimum time required for ramping the beam energy in the LHC from 450 GeV to 7 TeV is approximately 20 minutes. After a beam abort at top energy, it takes also approximately 20 minutes to ramp the magnets down to 450 GeV. Assuming a programmed check of all main systems of say 10 minutes, the total turnaround time for the LHC is of the order of 70 minutes, which should be considered as a theoretical minimum.

After 10 years of HERA machine operation, on average, only every third proton injection leads to a successful proton fill at top energy. The average time between the end of a luminosity run and a new beam at top energy in HERA is approximately 6 hours, compared to a theoretical minimum turnaround time of approximately 1 hour, i.e., 6 times longer. Thus for a minimum turnaround time for the LHC of 1.15 hours, the practical experience at HERA implies that the average turnaround time will be 7 hours.

2.2.10 Integrated luminosity
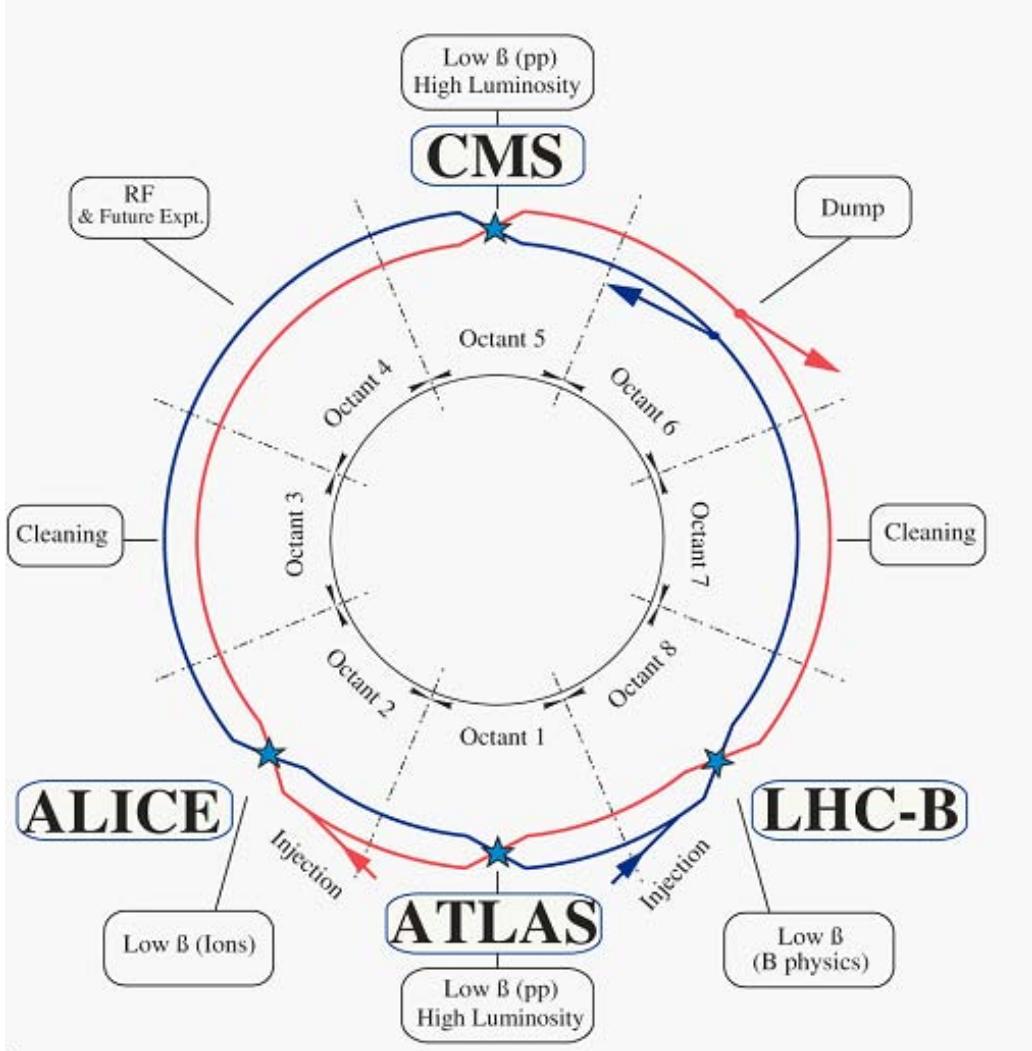
Integrating the luminosity over one run yields,

$$L_{\text{int}} = L_0 \tau_L \left[1 - e^{-T_{\text{run}}/\tau_L} \right] \tag{2.11}$$

where T_{run} is the total length of the luminosity run. The overall collider efficiency depends on the ratio of the length of the run to the average turnaround time. Assuming the machine can be operated for 200 days per year and assuming the luminosity lifetime of 15 hours obtained earlier, the optimum run time is 12 hours or 5.5 hours, for the average turnaround times of 7 hours and 1.15 hours, respectively. This leads to a maximum total integrated luminosity per year of $80\,\text{fb}^{-1}$ to $120\,\text{fb}^{-1}$, depending on the average turnaround time of the machine.

2.3 Lattice layout
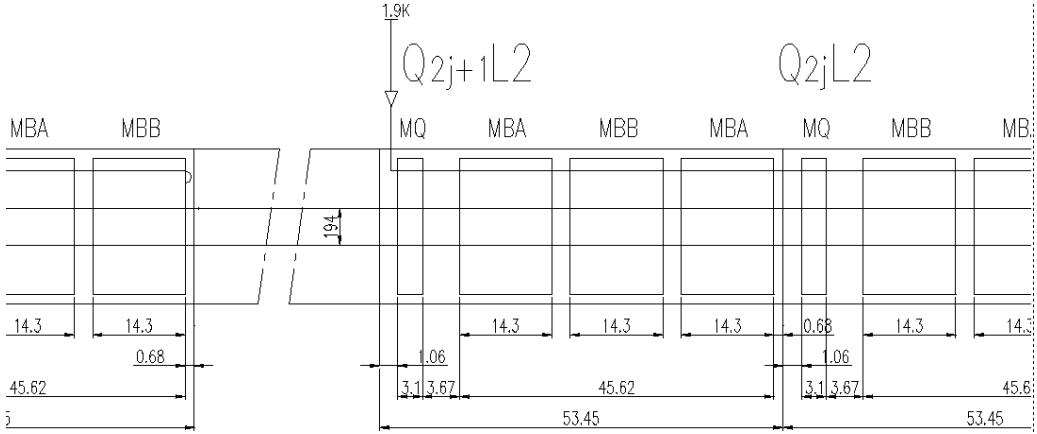
The basic layout of the LHC follows the LEP tunnel geometry: see figure 2.1. The LHC has eight arcs and eight straight sections. Each straight section is approximately 528 m long and can serve as an experimental or utility insertion. The two high luminosity experimental insertions are located at diametrically opposite straight sections: the ATLAS experiment is located at Point 1 and the CMS experiment at Point 5. Two more experimental insertions are located at Point 2 and Point 8, which also include the injection systems for Beam 1 and Beam 2, respectively. The injection kick occurs in the vertical plane with the two beams arriving at the LHC from below the LHC reference plane. The beams cross from one magnet bore to the other at four locations. The remaining four straight sections do not have beam crossings. Insertions at Points 3 and 7 each contain two collimation

Figure 2.1: Schematic layout of the LHC (Beam 1- clockwise, Beam 2 — anticlockwise).

systems. The insertion at Point 4 contains two RF systems: one independent system for each LHC beam. The straight section at Point 6 contains the beam dump insertion, where the two beams are vertically extracted from the machine using a combination of horizontally deflecting fast-pulsed ('kicker') magnets and vertically-deflecting double steel septum magnets. Each beam features an independent abort system. The LHC lattice has evolved over several versions. A summary of the different LHC lattice versions up to version 6.4 is given in ref. [20].

The arcs of LHC lattice version 6.4 are made of 23 regular arc cells. The arc cells are 106.9 m long and are made out of two 53.45 m long half cells, each of which contains one 5.355 m long cold mass (6.63 m long cryostat), a short straight section (SSS) assembly, and three 14.3 m long dipole magnets. The LHC arc cell has been optimized for a maximum integrated dipole field along the arc with a minimum number of magnet interconnections and with the smallest possible beam envelopes. Figure 2.2 shows a schematic layout of one LHC half-cell.
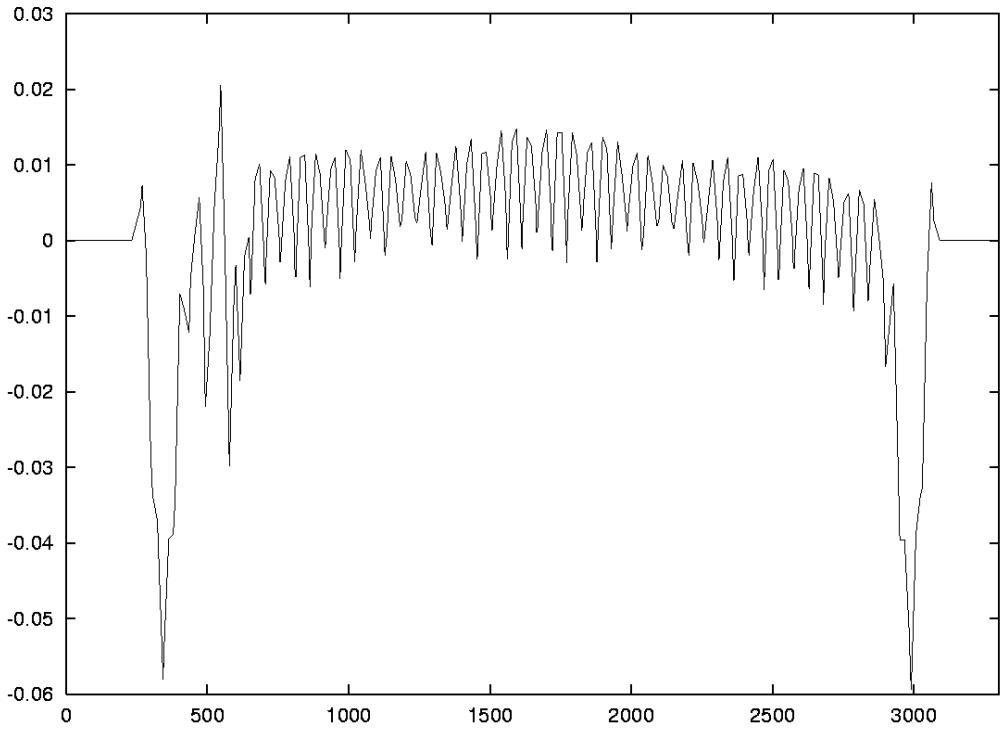
Figure 2.2: Schematic layout of an LHC half cell (distances in m).

The two apertures of Ring 1 and Ring 2 are separated by 194 mm. The two coils in the dipole magnets are powered in series, and all dipole magnets of one arc form one electrical circuit. The quadrupoles of each arc form two electrical circuits: all focusing quadrupoles in Beam 1 and Beam 2 are powered in series, and all defocusing quadrupoles in Beam 1 and Beam 2 are powered in series. The optics of Beam 1 and Beam 2 in the arc cells is therefore strictly coupled via the powering of the main magnetic elements.

A dispersion suppressor is located at the transition between an LHC arc and a straight section, yielding a total of 16 dispersion suppressor sections. The aim of the dispersion suppressors is threefold:

- Adapt the LHC reference orbit to the geometry of the LEP tunnel.

- Cancel the horizontal dispersion arising in the arc and generated by the separation / recombination dipole magnets and the crossing angle bumps.

- Facilitate matching the insertion optics to the periodic optics of the arc.

A generic design of a dispersion suppressor uses standard arc cells with missing dipole magnets. The LEP dispersion suppressor, which defined the geometry of the tunnel, was made of 3.5 cells with a 90° phase advance. With the 2.5 times longer LHC dipole and quadrupole magnets, only two LHC cells can fit in the same distance. This layout can still accurately follow the LEP tunnel geometry, but the shortened dispersion suppressor cannot fully cancel the horizontal dispersion if the dispersion suppressor cells are powered in series with the arc cells. Full cancellation of the horizontal dispersion requires individual powering of the dispersion suppressor quadrupoles. To this end, the dispersion suppressor cells are equipped with special, medium current, quadrupoles except at IR3 and IR7, which do not have enough space to house the large 6000 A power supplies required for the individual powering of the dispersion suppressor quadrupoles. Instead, the quadrupoles in these regions are powered in series with the arc quadrupoles, and each dispersion suppressor quadrupole is equipped with a trim quadrupole that requires a smaller 500 A power supply. This solution solves the space problem, but limits the flexibility in those insertions.

Figure 2.3: Horizontal deviation between the LHC and LEP geometries (in metres).

The straight sections in the tunnel are approximately 528 m long. A quadrupole spacing equivalent to the spacing in the arc cells allows approximately ten insertion region quadrupole magnets. The exact number and arrangement of these insertion quadrupoles depends on the requirements specific to each insertion. Assuming a midpoint symmetry for the insertion optics, this provides 5 independent parameters for matching 6 optical constraints (β_x, β_y, α_x, α_y, μ_x and μ_y) at the transition points to the dispersion suppressors, assuming that the dispersion functions can be matched via the dispersion suppressor. In order to provide the missing flexibility for matching, the dispersion suppressors are used as optical buffers between the arc and the insertion. In fact, the dispersion suppressors have to be extended into the neighbouring arcs using the arc trim quadrupole of the first arc cell to add four more free parameters for the final matching. The drawback of this scheme is that it does not provide a strictly separate functionality between the dispersion suppressor and the insertion region.

The LHC arcs are mainly positioned radially to the exterior of the theoretical position of the LEP machine by up to 4 cm, with the maximum excursions occurring near the arc transition to the dispersion suppressor. However, to keep total LHC circumference equal to the LEP circumference, the positive offset of the LHC machine in the arcs is compensated by a larger excursion in the opposite direction inside the dispersion suppressors. See figure 2.3. The LHC is divided into 8 independent sectors (the arcs between two consecutive straight sections).

2.4 Corrector circuits

The corrector magnets located in the arcs of the LHC can be split into two distinct categories:

- The lattice corrector magnets placed on both sides of the main quadrupoles in the SSS cryostats.

- The spool-piece correctors which are thin nonlinear windings attached directly to the extremities of the main dipoles.

In contrast to the main dipole circuits and the two main quadrupole families, the arc corrector magnets can be adjusted independently for the two beams. The different types and main functionalities of the lattice corrector magnets are summarized below.

2.4.1 Arc orbit corrector magnets MCB

Horizontal and vertical orbit corrector magnets, MCBH and MCBV, are installed at each focusing (QF) and defocusing (QD) quadrupole respectively, making a total of 23 or 24 orbit correctors per ring, per arc and per transverse plane, depending on the polarity of the quadrupole at mid-arc. They are designed to achieve a maximum kick of 80.8 μrad at 7 TeV for a nominal current of 55 A.

2.4.2 Chromaticity or lattice sextupoles, MS

Chromaticity sextupoles, MS, are installed at each focusing and defocusing quadrupole of the lattice. The chromaticity sextupoles are split into four families in each sector of each ring. Two families, SF and SD, are installed at QF and QD, respectively. These are further divided into two interleaved sub-families '1' and '2'. Only two SF and SD families are needed to correct the natural chromaticity of each ring. This includes the contributions from the arc and/or the contribution from the low-β insertions in collision. The present scheme can also correct the second order chromaticity and minimize the off-momentum beating induced by the inner triplet magnets in collision mode.

2.4.3 Lattice skew sextupoles, MSS

In each ring and each sector of the machine, four focusing sextupoles (2 SF1s and 2 SF2s situated mid arc) are rotated by 90° and are powered in series to generate a skew sextupole field for compensation of the chromatic coupling induced by the a_3 component of the main dipoles. This scheme guarantees extremely good compensation of the second order chromaticity induced by chromatic coupling, with a minimum impact on the third-order skew resonances and on the off-momentum β-beating.

2.4.4 Tune-shift or tuning quadrupoles, MQT

Two families of 8 tuning quadrupoles per ring and per sector, QTF and QTD, equip the short straight sections from Q14 to Q21 (left and right). Since the main quadrupole circuits are powered in series in Ring 1 and Ring 2, the phase advance per arc cell cannot be changed independently for

the two beams. Therefore, independent tune adjustments for each beam can only be done by re-tuning the phase advances of the LHC insertions (essentially IR4) or by using the MQT corrector magnets. In principle, the latter are strong enough to achieve tune shifts of slightly more than one unit at 7 TeV. However, due to the large β-beating and dispersion mismatch induced, they will be limited to much smaller tune shifts in nominal operation, of the order of $\Delta Q \sim \pm 0.1$.

2.4.5 Arc skew quadrupole corrector magnets, MQS

In both rings, each sector of the machine is equipped with two pairs of skew quadrupole magnets MQS at Q23 and Q27 (left and right) which are just MQT type magnets rotated by $45°$. The two pairs are either powered in series, in Sectors 1-2, 3-4, 5-6, 7-8 for Ring 1 and in Sectors 2-3, 4-5, 6-7, 8-1 for Ring 2, or split into two independent families in the other sectors. This layout allows compensation of the coupling coefficient due to the systematic $a2$ errors of the main dipoles for each sector, but implies that only four corrector circuits are available for correction of the random coupling errors. The betatron phase advances between the MQSs of the same family are such that the coupling compensation can be made without generating too large a vertical dispersion.

2.4.6 Landau damping or lattice octupoles, MO
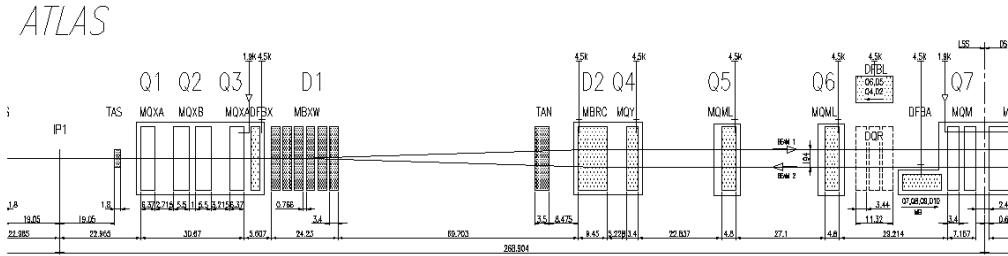
Each short straight section not equipped with MQT or MQS type magnets contains a lattice octupole MO, making a total of 168 MO type magnets per ring, for the Landau damping of coherent oscillations caused by collective effects. These magnets will be powered in four families per sector, subdividing them into focusing and defocusing magnets, OF and OD, for Ring 1 and Ring 2.

2.4.7 Spool-piece corrector magnets

In addition to the lattice corrector magnets, each bore of the main dipoles will carry a small sextupole corrector magnet (MCS) at one end (Type B magnet), and every other dipole will be equipped with an octupole-decapole spool-piece (MCDO) at the opposite end (Type A magnet). The MCS magnets will be connected in series to form two families per sector, one for each ring. The same will apply for the octupole and decapole corrector magnets. The MCS spool-pieces are designed to compensate the b_3 field integral of the main dipoles in each sector of the machine, in order to correct its impact on the linear chromaticity up to top energy. On the other hand, the MCDO spool-piece corrector magnets mainly preserve the dynamic aperture of the LHC at injection.

2.5 High luminosity insertions (IR1 and IR5)

Interaction regions 1 and 5 house the high luminosity experiments of the LHC and are identical in terms of hardware and optics, except that the crossing-angle is in the vertical plane in Point 1 and in the horizontal plane in Point 5. The small β-function values at the IPs are generated between quadrupole triplets that leave ± 23 m free space about the IP. In this region, the two rings share the same vacuum chamber, the same low-beta triplet magnets, and the D1 separation dipole magnets. The remaining matching section (MS) and the dispersion suppressor (DS) consist of twin-bore

Figure 2.4: Schematic layout of the right side of IR1 (distances in m).
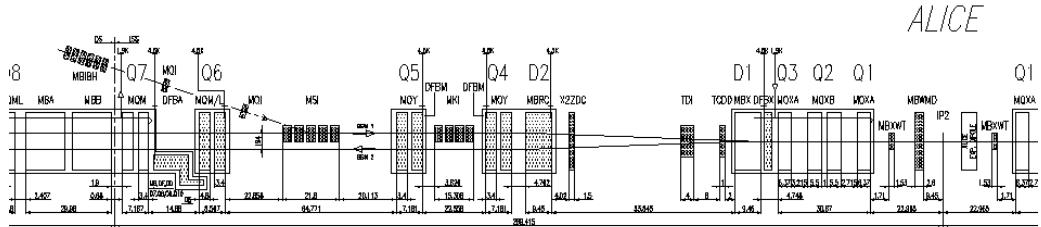
magnets with separate beam pipes for each ring. From the IP up to the DS insertion the layout comprises:

- A 31 m long superconducting low-β griplet assembly, operated at a temperature of 1.9 K and providing a nominal gradient of 205 T/m.

- A pair of separation / recombination dipoles separated by approximately 88 m.

- The D1 dipole located next to the triplet magnets, which has a single bore and consists of six 3.4 m long conventional warm magnet modules yielding a nominal field of 1.38 T.

- The following D2 dipole, which is a 9.45 m long, twin bore, superconducting dipole magnet, operating at a cryogenic temperature of 4.5 K with a nominal field of 3.8 T. The bore separation in the D2 magnet is 188 mm and is thus slightly smaller than the arc bore separation.

- Four matching quadrupole magnets. The first quadrupole following the separation dipole magnets, Q4, is a wide-aperture magnet operating at a cryogenic temperature of 4.5 K and yielding a nominal gradient of 160 T/m. The remaining three quadrupole magnets are normal-aperture quadrupole magnets, operating at a cryogenic temperature of 1.9 K with a nominal gradient of 200 T/m.
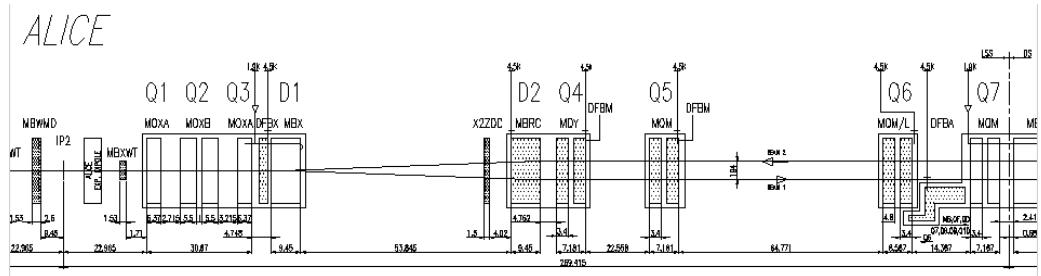
Figure 2.4 shows the schematic layout of IR1 on the right hand side. The triplet assembly features two different quadrupole designs: the outer two quadrupole magnets, made by KEK, require a peak current of 6450 A to reach the nominal gradient of 205 T/m, whereas the inner quadrupole block, consist of two quadrupole magnets made by FNAL, requires a peak current of 10630 A. The triplet quadrupoles are powered by two nested power converters: one 8 kA power converter powering all triplet quadrupole magnets in series and one 6 kA power converter supplying additional current only to the central two FNAL magnets. The Q1 quadrupole next to the IP features an additional 600 A trim power converter. Two absorbers protect the cold magnets from particles leaving the IP. The TAS absorber protects the triplet quadrupole magnets, and the TAN absorber, located in front of the D2 dipole magnet, protects the machine elements from neutral particles.

2.6 Medium luminosity insertion in IR2

The straight section of IR2 (see figures 2.5 and 2.6) houses the injection elements for Ring-1, as well as the ion beam experiment ALICE. During injection, the optics must obey the special con-

Figure 2.5: Schematic layout of the matching section on the left side of IR2 (distances in m).
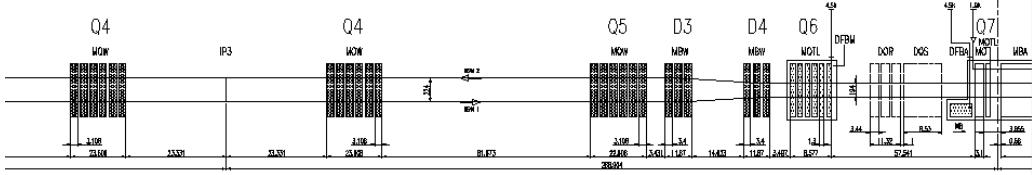
Figure 2.6: Schematic layout of the matching section on the right side of IR2 (distances in m).

straints imposed by the beam injection for Ring-1, and the geometrical acceptance in the interaction region must be large enough to accommodate both beams in the common part of the ring, with a beam separation of at least 10σ.
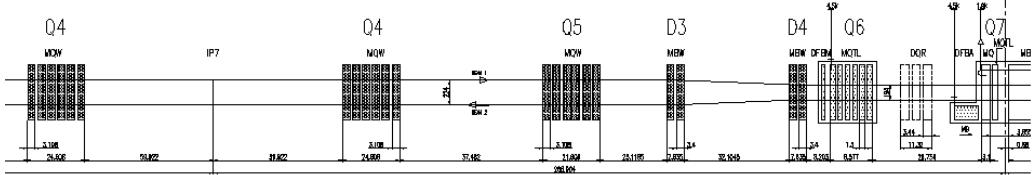
The triplet quadrupoles are powered in series and are followed by the separation / recombination dipoles D1 and D2, which guide the beams from the interaction region into two separated vacuum chambers. The quadrupoles Q4, Q5, Q6, Q7, Q8, Q9 and Q10 are individually powered magnets. The aperture of Q4 is increased to provide sufficient space for the crossing-angle orbit separation. The aperture of Q5 left of the IP is increased to provide sufficient aperture for the injected beam. The injection septum MSI is located between Q6 and Q5 on the left-side and kicks the injected beam in the horizontal plane towards the closed orbit of the circulating beam (positive deflection angle). The injection kicker MKI is located between Q5 and Q4 on the left-hand side of the IP and kicks the injected beam in the vertical plane towards the closed orbit of the circulating beam (negative deflection angle). In order to protect the cold elements in case of an injection failure, a large absorber (TDI) is placed 15 m upstream from the D1 separation / recombination dipole on the left side of the IP. The TDI absorber is complemented by an additional shielding element 3 m upstream of the D1 magnet and two additional collimators installed next to the Q6 quadrupole magnet. In order to obtain an optimum protection level in case of injection errors, the vertical phase advance between MKI and TDI must be 90°, and the vertical phase advance between the TDI and the two auxiliary collimators must be an integer multiple of 180°. The matching section extends from Q4 to Q7, and the DS extends from Q8 to Q11. In addition to the DS, the first two trim quadrupoles of the first arc cell (QT12 and QT13) are also used for matching.

MOMENTUM CLEANING INSERTION

Figure 2.7: Schematic layout of the matching section on the right side of IR3 (distances in m).

BETATRON CLEANING INSERTION
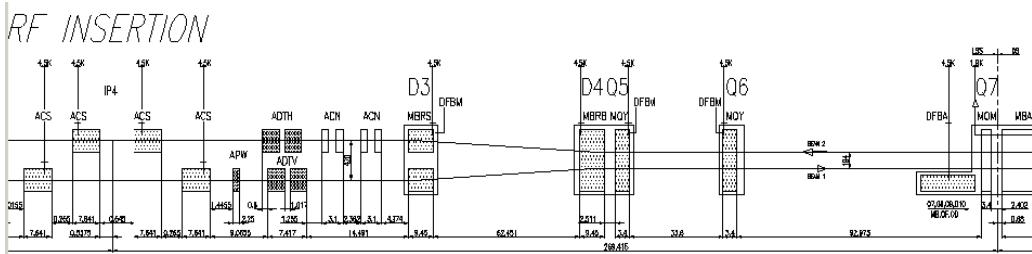
Figure 2.8: Schematic layout of the matching section on the right side of IR7 (distances in m).

2.7 Beam cleaning insertions in IR3 and IR7

The IR3 insertion houses the momentum cleaning systems of both beams, while IR7 houses the betatron cleaning systems of both beams. Particles with a large momentum offset are scattered by the primary collimator in IR3, and particles with a large betatron amplitudes are scattered by the primary collimator in IR7. In both cases, the scattered particles are absorbed by secondary collimators. Figures 2.7 and 2.8 show the right hand sides of IRs 3 and 7, respectively.

In IR7, the layout of the LSS between Q7L and Q7R is mirror symmetric with respect to the IP. This allows a symmetrical installation for the collimators of the two beams and minimizes the space conflicts in the insertion. Starting from Q7 left, the quadrupole Q6 (made of 6 super-conducting MQTL modules) is followed by a dog-leg structure made of two sets of MBW warm single bore wide aperture dipole magnets (2 warm modules each). The dogleg dipole magnets are labelled D3 and D4 in the LHC sequence, with D3 being the dipole closer to the IP. The Primary Collimators are located between the D4 and D3 magnets, allowing neutral particles produced in the jaws to point out of the beam line, and most charged particles to be swept away. The inter-beam distance between the dogleg assemblies left and right from the IP is 224 mm, i.e., 30 mm larger than in the arc. This increased beam separation allows a substantially higher gradient in the Q4 and Q5 quadrupoles, which are made out of 6 warm MQW modules. The space between Q5 left and right from the IP is used to house the secondary collimators at appropriate phase advances with respect to the primary collimators.

In IR3, the most difficult constraint was to generate a large dispersion function in the straight section. Since the layout of the DS cannot be changed in IR3, this constraint means that the natural dispersion suppression generated in the DS is over-compensated. To fix this, Q6 and Q5 were moved towards each other by a substantial amount, thus shrinking the space granted to the dog-leg structure D4-D3. It was therefore necessary to add a third MBW element to D3 and D4 in IR3. Apart from this, IR3 and IR7 are identical.

Figure 2.9: Schematic layout of the matching section on the right side of IR4 (distances in m).

2.8   RF insertion in IR4

IR4 (see figure 2.9) houses the RF and feed-back systems, as well as some of the LHC beam instrumentation. The RF equipment is installed in the old ALEPH (LEP) cavern, which provides a large space for the power supplies and klystrons. Because both RF systems are installed in this cavern, large drift spaces are necessary between the quadrupoles. This makes the insertion look similar to IR6. Furthermore, the two independent RF systems for Beam 1 and Beam 2 require a larger than nominal beam separation. The increased beam separation is provided by two pairs of dipole magnets. These dogleg dipole magnets are labelled D3 and D4 in the LHC sequence, with D3 being the dipole magnets closer to the IP. The inter-beam distance between the dogleg magnets is 420 mm, i.e., 226 mm larger than in the arcs. In contrast to IR3 and IR7, the dogleg magnets in IR4 are superconducting.

2.9   Beam abort insertion in IR6
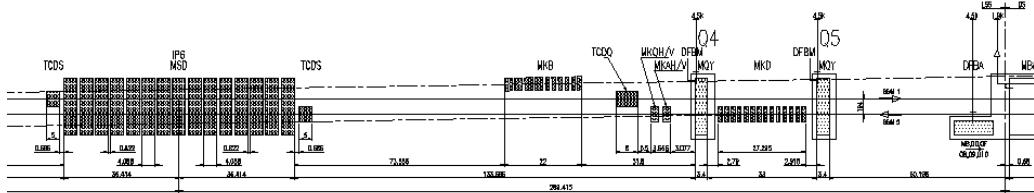
IR6 (see figure 2.10) houses the beam abort systems for Beam 1 and Beam 2. Beam abort from the LHC is done by kicking the circulating beam horizontally into an iron septum magnet, which deflects the beam in the vertical direction away from the machine components to absorbers in a separate tunnel. Each ring has its own system, and both are installed in IR6. In order to minimize the length of the kicker and of the septum, large drift spaces are provided. Matching the β-functions between the ends of the left and right DS requires only four independently-powered quadrupoles. In each of the dispersion suppressors, up to six quadrupoles can be used for matching. The total of sixteen quadrupoles is more than sufficient to match the β-functions and the dispersion, and to adjust the phases. There are, however, other constraints to be taken into account concerning apertures inside the insertion.

Special detection devices protect the extraction septum and the LHC machine against losses during the abort process. The TCDS absorber is located in front of the extraction septum and the TCDQ in front of the Q4 quadrupole magnet downstream of the septum magnet.

2.10   Medium luminosity insertion in IR8

IR8 houses the LHCb experiment and the injection elements for Beam 2 (see figures 2.11 and 2.12). The small β-function values at the IP are generated with the help of a triplet quadrupole assembly

BEAM DUMP INSERTION
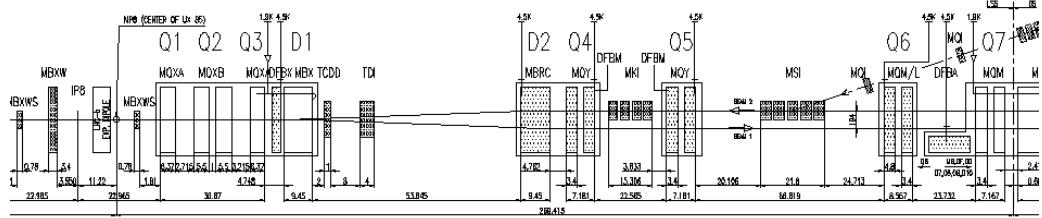
Figure 2.10: Schematic layout of the matching section on the right side of IR6 (distances in m).
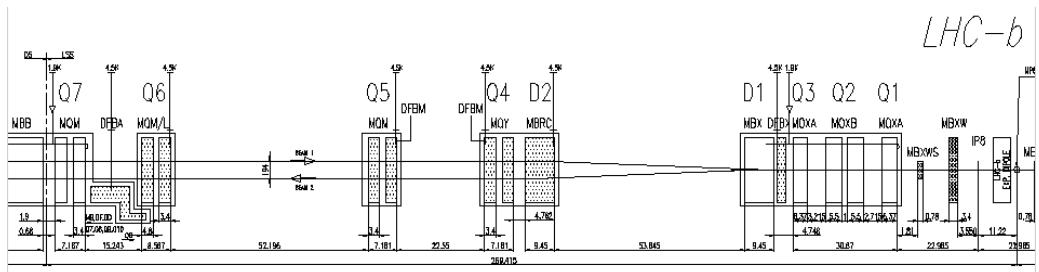
that leaves ±23 m of free space around the IP. In this region, the two rings share the same vacuum chamber, the same low-beta triplet magnets, and the D1 separation dipole magnet. The remaining matching section (MS) and the DS consist of twin-bore magnets with separate beam pipes for each ring. From the IP up to the DS insertion the layout comprises:

- Three warm dipole magnets to compensate the deflection generated by the LHCb spectrometer magnet.

- A 31 m long superconducting low-β triplet assembly operated at 1.9 K and providing a nominal gradient of 205 T/m.

- A pair of separation / recombination dipole magnets separated by approximately 54 m. The D1 dipole located next to the triplet magnets is a 9.45 m long single-bore superconducting magnet. The following D2 dipole is a 9.45 m long double bore superconducting dipole magnet. Both magnets are operated at 4.5 K. The bore separation in the D2 magnet is 188 mm and is thus slightly smaller than the arc bore separation.

- Four matching quadrupole magnets. The first quadrupole following the separation dipole magnets, Q4, is a wide aperture magnet operating at 4.5 K and yielding a nominal gradient of 160 T/m. The remaining three matching section quadrupole magnets are normal aperture quadrupole magnets operating at 1.9 K with a nominal gradient of 200 T/m.

- The injection elements for Beam 2 on the right hand side of IP8. The 21.8 m long injection septum consists of 5 modules and is located between the Q6 and Q5 quadrupole magnets on the right-hand side of the IP. The 15 m long injection kicker consists of 4 modules and is located between the Q5 and Q4 quadrupole magnets on the right-hand side of the IP. In order to protect the cold elements in case of injection failure, a large absorber (TDI) is placed 15 m in front of the D1 separation / recombination dipole magnet, right from the interaction point. The TDI is complemented by an additional shielding element (TCDD) between the TDI and D1 magnet (placed 3 m in front of D1) and by two additional collimators, placed at the transition of the matching section, left from the interaction point, to the next DS section.

In order to provide sufficient space for the spectrometer magnet of the LHCb experiment, the beam collision point is shifted by 15 half RF wavelengths (3.5 times the nominal bunch spacing ≈ 11.25 m) towards IP7. This shift of the collision point has to be compensated before the beam returns to the dispersion suppressor sections and requires a non-symmetric magnet layout in the matching section.

Figure 2.11: Schematic layout of the matching section on the right side of IR8 (distances in m).


Figure 2.12: Schematic layout of the matching section on the left side of IR8 (distances in m).

Chapter 3

Magnets
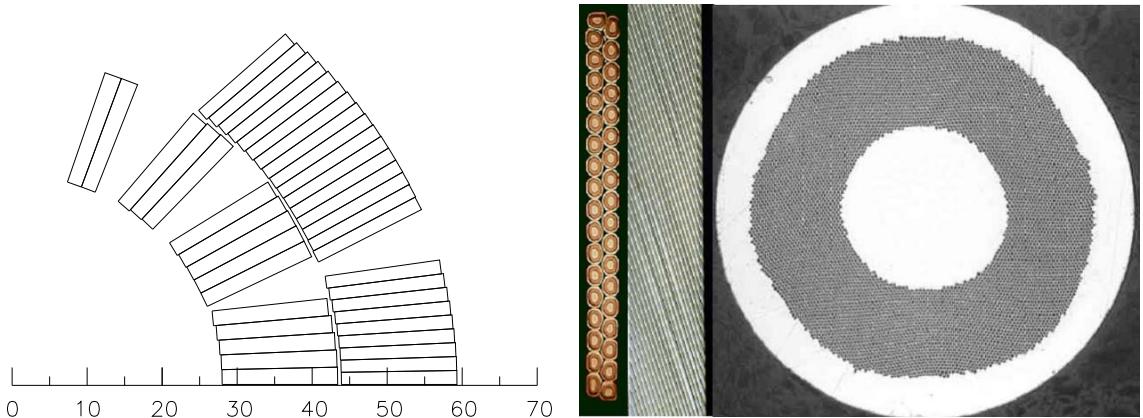
3.1 Overview

The Large Hadron Collider relies on superconducting magnets that are at the edge of present technology. Other large superconducting accelerators (Tevatron-FNAL, HERA-DESY and RHIC-BNL) all use classical NbTi superconductors, cooled by supercritical helium at temperatures slightly above 4.2 K, with fields below or around 5 T. The LHC magnet system, while still making use of the well-proven technology based on NbTi Rutherford cables, cools the magnets to a temperature below 2 K, using superfluid helium, and operates at fields above 8 T. One detrimental effect of reducing the temperature by more than a factor of two is the reduction of the heat capacity of the cable by almost an order of magnitude. As a result, for a given temperature margin (difference between the critical temperature of the superconductor and the operating temperature), the energy deposition that can trigger a quench is substantially reduced. This means that the temperature margin must be significantly larger than that used in previous projects and that a tighter control of movements and heat dissipation inside cables is needed. Since the electromagnetic forces increase with the square of the field, the structures retaining the conductor motion must be mechanically much stronger than in earlier designs.

In addition, space limitations in the tunnel and the need to keep costs down have led to the adoption of the "two-in-one" or "twin-bore" design for almost all of the LHC superconducting magnets. The two-in-one design accommodates the windings for the two beam channels in a common cold mass and cryostat, with magnetic flux circulating in the opposite sense through the two channels. This makes the magnet structure complicated, especially for the dipoles, for which the separation of the two beam channels is small enough that they are coupled both magnetically and mechanically.

3.2 Superconducting cable

The transverse cross-section of the coils in the LHC 56 mm aperture dipole magnet (figure 3.1) shows two layers of different cables distributed in six blocks. The cable used in the inner layer has 28 strands, each having a diameter of 1.065 mm, while the cable in the outer layer is formed

Figure 3.1: Conductor distribution in the dipole coil cross-section (*X*-axis in mm on left). Picture of cables and strand on right.

from 36 strands, each of 0.825 mm diameter. The main parameters of the two cables are given in table 3.1.

The filament size chosen (7 μm for the strand of the inner layer cable and 6 μm for the strand of the outer layer cable) allows the fabrication of superconducting wires by a single stacking process. The filament size for each type of strand is optimised in order to reduce the effects of the persistent currents on the sextupole field component at injection. The residual errors are corrected by small sextupole and decapole magnets located at the end of each dipole.

Table 3.2 shows the peak field (B_p) for the two layers of cable, the field margin and the temperature margin when the magnet operates at 8.33 T. The field margin is defined as the ratio of the operating field to the expected quenching field at the short-sample limit (B_{ss}). The reference temperature of the bath is 1.9 K (helium between coil inner radius and cold bore). Also shown are the current density in the copper at B_0 = 8.33 T, and, in the case of a quench, the expected hot-spot temperature in the outer layer and maximum quench voltage, calculated in the adiabatic approximation.

During ramping and discharge of the current in the dipole magnet, the main losses and field errors are generated by inter-strand coupling currents and by persistent currents inside the filaments. The power losses due to inter-strand coupling currents depend strongly on the coating of the strands and the compression of the coils at low temperature. They are proportional to $(dB/dt)^2$ and inversely proportional to the inter-strand contact resistance R_c. Losses for a twin-aperture dipole have been estimated at 180 mW/m for a charging time of 1200 s, corresponding to an energy of 220 J/m transmitted to the helium bath and to specific power dissipation in the cables of 0.077 mW/cm^3.
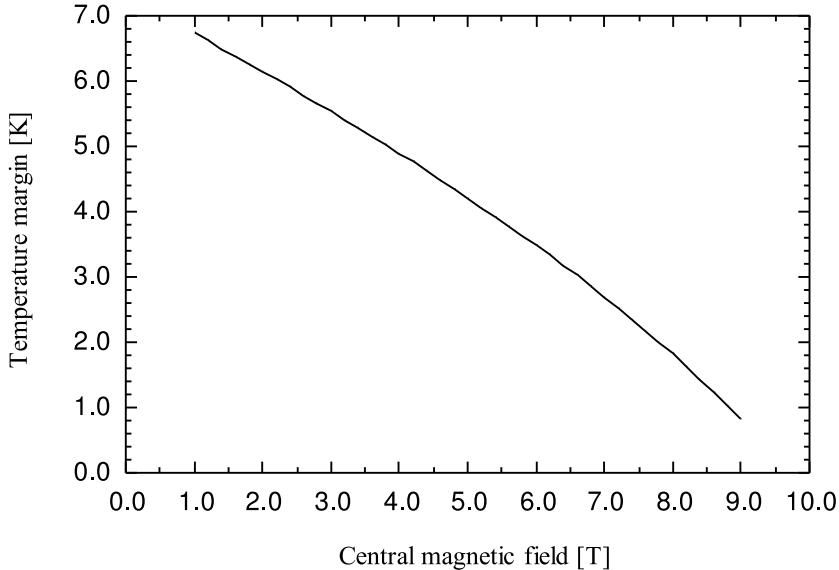
In the case of a discharge of the machine, the upper limit of the time constant is given by the characteristics of the diode heat sink of the quench protection system and the quench propagation to other magnets via bus-bars. In the 10 m long magnets tested, a linear discharge from 8.33 T with dB/dt of 0.12 T/s did not initiate a quench. An exponential discharge with a time constant of 100 s leads to a load of 500 J/m. These values are mainly due to hysteresis losses and are calculated with an inter-strand contact resistance of 10 $\mu\Omega$, the lowest expected.

Table 3.1: Strand and cable characteristics of main dipoles (MB) and main quadrupoles (MQ).

	Inner Layer MB	Outer Layer MB Both layers MQ
Strand		
Coating type	Sn5wt%Ag	Sn5wt%Ag
Diameter after coating [mm]	1.065 ± 0.0025	0.825 ± 0.0025
Copper to superconductor ratio	1.65 ± 0.05	1.95 ± 0.05
Filament diameter [μm]	7	6
Number of filaments	$\sim$ 8'900	$\sim$ 6'500
RRR	$\geq$ 150	$\geq$ 150
Twist pitch after cabling [mm]	18 ± 1.5	15 ± 1.5
Critical current [A] 10 T, 1.9 K	$\geq$ 515	
9 T, 1.9 K		$\geq$ 380
ΔM AT 0.5 T AND 1.9 K [MT]	$\leq$ 30	$\leq$ 23
Cable		
Number of strands	28	36
Cable dimension (at room temperature)		
Mid-thickness at 50 MPa [mm]	1.900 ± 0.006	1.480 ± 0.006
Thin edge [mm]	1.736	1.362
Thick edge [mm]	2.064	1.598
Width [mm]	$15.10^{-0.02}_{+0}$	$15.10^{-0.02}_{+0}$
Keystone angle [degree]	1.25 ± 0.05	0.90 ± 0.05
Transposition pitch [mm]	115 ± 5	100 ± 5
Aspect ratio	7.95	10.20
MIITS [300 K] [MA^2 s]	45 [8T]	30 [6T]
Critical current I$_c$ [A] 10 T, 1.9 K	> 13750	
9 T, 1.9 K		> 12960
dI$_c$/dB [A/T]	> 4800	> 3650
Inter-strand cross contact resistance [$\mu\Omega$]	$\geq$ 15	$\geq$ 40
RRR	$\geq$ 70	$\geq$ 70
No cold welds and no cross-overs of strands allowed		

Table 3.2: Expected quench performance and temperature margin ($B_0 = 8.33$ T, $I_0 = 11'800$ A, $T_{\text{bath}} = 1.9$ K).

| Layer	B_p [T]	B_margin [%]	ΔT[K] margin	J_cu[A/mm^2]	T_max quench [K]	V_max [V]
Inner layer	8.57	85.7	1.51	760		
Outer Layer	7.46	85.8	1.57	928	375	500
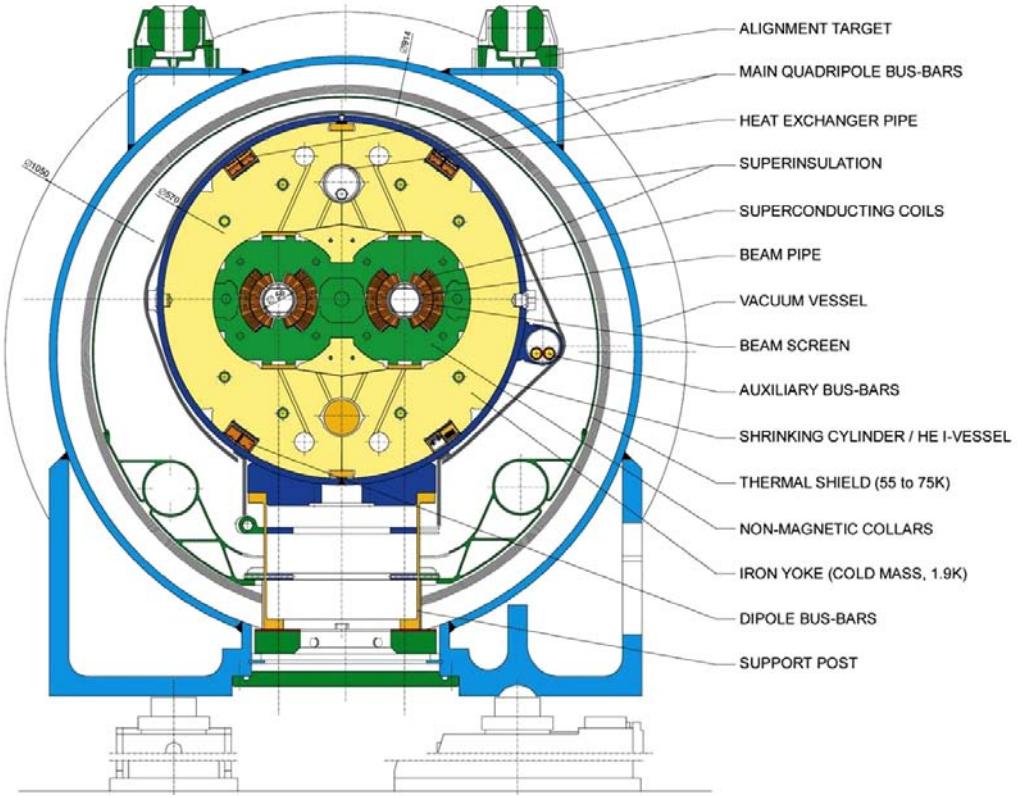
Figure 3.2: Variation of the temperature margin of the inner layer for T_{bath} = 1.9 K.

A superconductor stays in the superconducting state when the temperature, the magnetic field, and the current density are below their critical values. The temperature margin shown in table 3.2 corresponds to the difference between the bath temperature and the critical temperature at the design field and current. The temperature margin as a function of the operating field for the inner layers, and for a bath temperature of 1.9 K, is shown in figure 3.2.

3.3   Main dipole cold mass

The LHC ring accommodates 1'232 main dipoles: 1'104 in the arc and 128 in the DS regions. They all have the same basic design. The geometric and interconnection characteristics have been targeted to be suitable for the DS region, which is more demanding than the arc. The cryodipoles are a critical part of the machine, both from the machine performance point of view and in terms of cost. Figure 3.3 shows the cross section of the cryodipole. The three European companies that have been collaborating with CERN throughout the prototype phase manufactured the series cryodipole cold masses. To reduce costs, co-ordinate orders, and obtain the highest possible degree of uniformity, CERN supplies most of the critical components and some of the main tooling. Thus CERN becomes, all at the same time: the magnet designer, the supplier of superconducting cables and most components, and the client. The dipole manufacturers are responsible for good quality construction that is free from faults. In order to help the cold mass manufacturers during the start-up phase, there have been two contracts with each manufacturer: first a pre-series contract (for the first 30 cold masses), then a series contract (for the remaining 386 cold masses). The components supplied by CERN for the two types of contract are shown in table 3.3.

Tests on the first 15 m-long prototype of the second generation showed that transport of the fully assembled cryodipole is critical. For this reason, the cold masses are put in their cryostats at CERN. Apart from the obvious cryogenics and vacuum considerations, the cryostating is also

Figure 3.3: Cross-section of cryodipole (lengths in mm).

an important operation for the geometry and the alignment of the magnet, which is critical for the performance of the magnets in view of the large beam energy and small bore of the beam pipe. The core of the cryodipole is the "dipole cold mass", which contains all the components cooled by superfluid helium. Referring to figure 3.3, the dipole cold mass is the part inside the shrinking cylinder/He II vessel. The dipole cold mass provides two apertures for the cold bore tubes (i.e. the tubes where the proton beams will circulate) and is operated at 1.9 K in superfluid helium. It has an overall length of about 16.5 m (ancillaries included), a diameter of 570 mm (at room temperature), and a mass of about 27.5 t. The cold mass is curved in the horizontal plane with an apical angle of 5.1 mrad, corresponding to a radius of curvature of about 2'812 m at 293 K, so as to closely match the trajectory of the particles. The main parameters of the dipole magnets are given in table 3.4.

The successful operation of LHC requires that the main dipole magnets have practically identical characteristics. The relative variations of the integrated field and the field shape imperfections must not exceed $\sim 10^{-4}$, and their reproducibility must be better than 10^{-4} after magnet testing and during magnet operation. The reproducibility of the integrated field strength requires close control of coil diameter and length, of the stacking factor of the laminated magnetic yokes, and possibly fine-tuning of the length ratio between the magnetic and non-magnetic parts of the yoke. The structural stability of the cold mass assembly is achieved by using very rigid collars, and by opposing the electromagnetic forces acting at the interfaces between the collared coils and the magnetic yoke with the forces set up by the shrinking cylinder. A pre-stress between coils and retaining structure

Table 3.3: CERN supplied components for the dipole cold masses.

Component	"Pre-Series" Contract	"Series" Contract
Superconducting cables (for inner & outer layers)	x	x
Polyimide tapes for cable and Cu wedges, insulation (two types)	x	x
Copper wedges (4 types)	x	x
Head spacers sets (for inner & outer layers)	x	
Inter-layer spacers	x	
Layer-jump boxes	x	
Layer-jump filling pieces	x	
Cable stabilisers (3 types)	x	
Quench heaters	x	
Polyimide (in rolls) for the coils' ground insulation	x	x
Collars (6 types)	x	x
Cold Bore tubes (insulated)	x	x
Low-carbon steel half-yoke & insert laminations	x	x
Non-magnetic steel half-yoke & insert laminations	x	x
Busbars subassemblies (ready to be mounted)	x	x
Shrinking half-cylinders	x	x
Spool piece correction magnets (sextupole and decapole/octupole)	x	x
End covers	x	x
Helium heat exchanger tube	x	x
Interconnection bellows	x	x
Instrumentation (including the wires) for the Cold Mass	x	x
Auxiliary busbar pipe	x	x
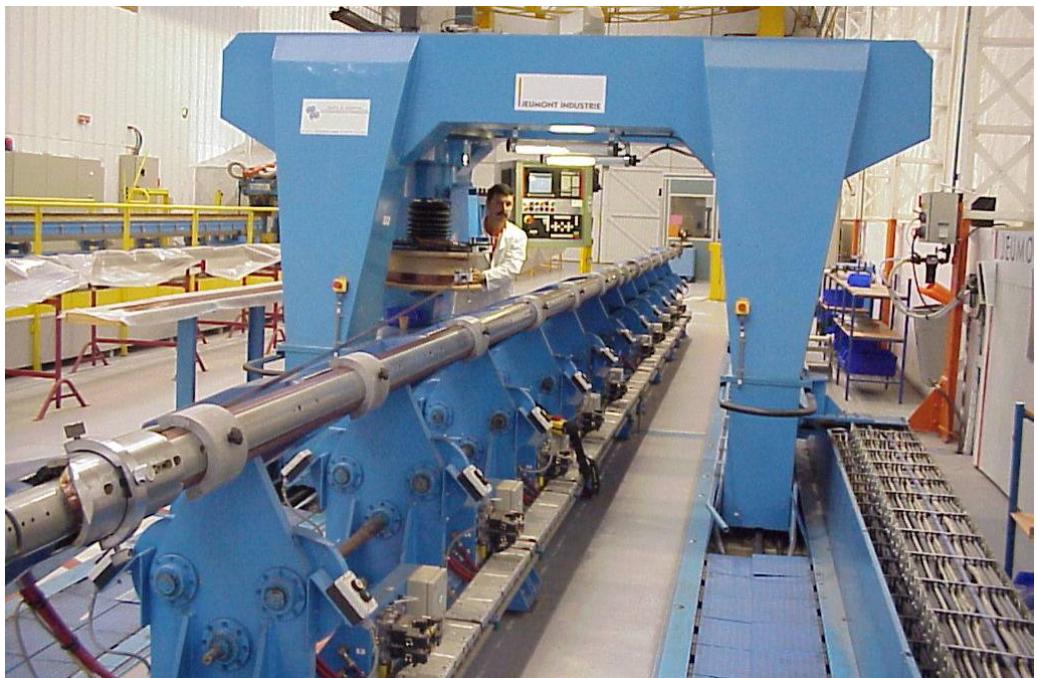
(collars, iron lamination and shrinking cylinder) is also built-in. Because of the larger thermal contraction coefficient of the shrinking cylinder and austenitic steel collars with respect to the yoke steel, the force distribution inside the cold mass changes during cool down from room temperature to 1.9 K. The sensitivity of the force distribution in the cold mass structure to the tolerances on all the major components and parameters (collars, laminations, inserts, coil pre-stress, and shrinking cylinder circumferential stress) has been checked by finite element analysis computations applying statistical methods. Some 3000 geometries were computed under high-field conditions; in all cases, strictly positive contact forces were found at the interfaces between yoke halves and between the yoke and collared coils.

The coils were manufactured in a clean area with adequate air circulation, air filtration, and an airlock access. Coil winding is done with a "winding machine": see figure 3.4. During winding, the conductors and spacers are maintained in place by tools designed for this purpose. In particular, the conductor must always be clamped in place in the straight parts before winding the coil ends. Special tooling for forming and pressing the conductors at the ends is also used. After winding, the coil is prepared for the curing phase while still lying on the mandrels. This operation takes place in a dedicated curing press. This press is equipped with moulds whose inner diameter is the outer
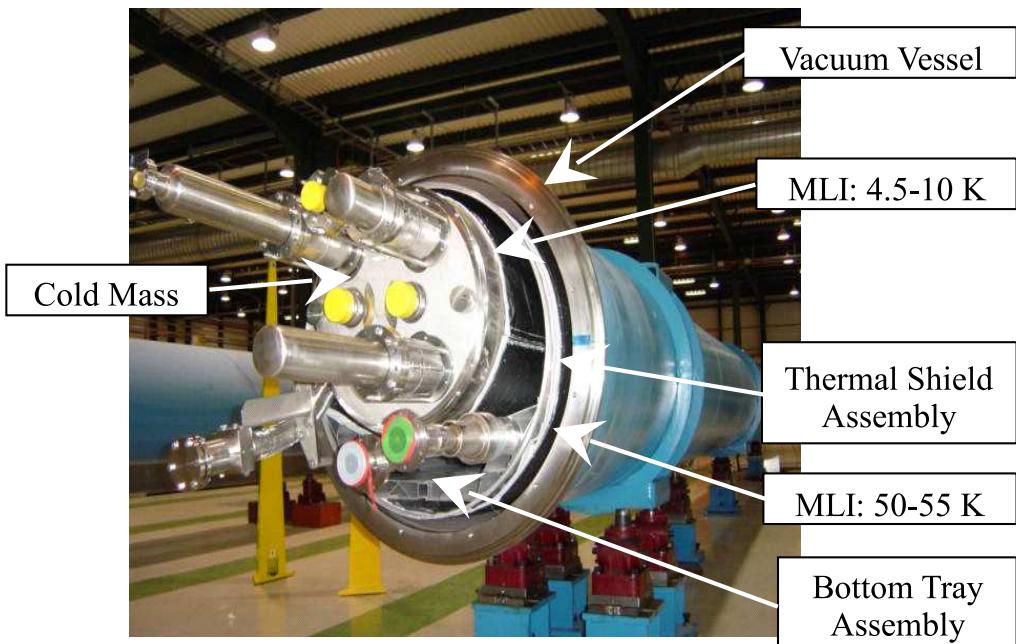
Table 3.4: Main parameters of the dipole cold mass.

	Value	Unit
Injection field (0.45 TeV beam energy)	0.54	T
Current at injection field	763	A
Nominal field (7 TeV beam energy)	8.33	T
Current at nominal field	11850	A
Inductance at nominal field	98.7	mH
Stored energy (both apertures) at nominal field	6.93	MJ
Ultimate field	9.00	T
Current at ultimate field	12840	A
Stored energy (both apertures) at ultimate field	8.11	MJ
Maximum quench limit of the cold mass (from short samples)	9.7	T
Operating temperature	1.9	K
Magnetic length at 1.9 K and at nominal field	14312	mm
Distance between aperture axes at 1.9 K	194.00	mm
Cold mass sagitta at 293 K	9.14	mm
Bending radius at 1.9 K	2803.98	m
Inner coil diameter at 293 K	56.00	mm
Number of conductor blocks / pole	6	
Number of turns / pole, inner layer	15	
Number of turns / pole, outer layer	25	
Electromagnetic forces / coil quadrant at nominal field		
Horizontal force component (inner and outer layer)	1.8	MN/m
Vertical force component (inner and outer layer)	0.81	MN/m
Electromagnetic forces / coil quadrant at ultimate field		
Horizontal force component (inner and outer layer)	2.1	MN/m
Vertical force component (inner and outer layer)	0.94	MN/m
Axial electromagnetic force at each ends at nominal field	0.40	MN
Coil aperture at 293 K	56.00	mm
Cold tube inner diameter at 293 K	50.00	mm
Cold tube outer diameter at 293 K	53.00	mm
Cold mass length at 293 K (active part)	15.18	m
Cold mass diameter at 293 K	570.0	mm
Cold mass overall length with ancillaries	16.5	m
Total mass	~ 27.5	t

diameter of either the inner or the outer layer. In addition, the moulds are equipped with heating systems that allow the coils to be cured at 190±3°C under a maximum pressure of 80-90 MPa.

**Figure 3.4**: A winding machine for the superconducting coils.

Figure 3.5: LHC dipole cryomagnet assembly.
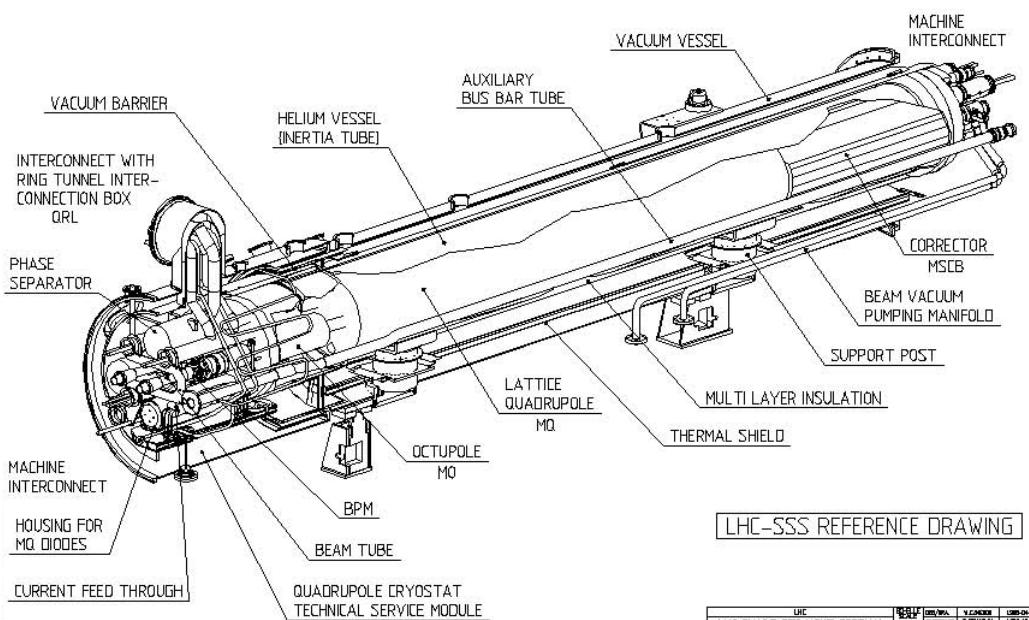
3.4 Dipole cryostat

The vacuum vessel consists of a long cylindrical standard tube with an outer diameter of 914 mm (36 inches) and a wall thickness 12 mm. It is made from alloyed low-carbon steel. The vessel has stainless steel end flanges for vacuumtight connection via elastomer seals to adjacent units. Three support regions feature circumferential reinforcement rings. Upper reinforcing angles support alignment fixtures. An ISO-standard flanged port is located azimuthally on the wall of the vessel at one end. In normal operation, the vessel will be under vacuum. In case of a cryogenic leak, the pressure can rise to 0.14 MPa absolute, and a sudden local cooling of the vessel wall to about 230 K may occur. The steel selected for the vacuum vessel wall is tested to demonstrate adequate energy absorption during a standard Charpy test at -50°C. A front view of the cryodipole is shown in figure 3.5.
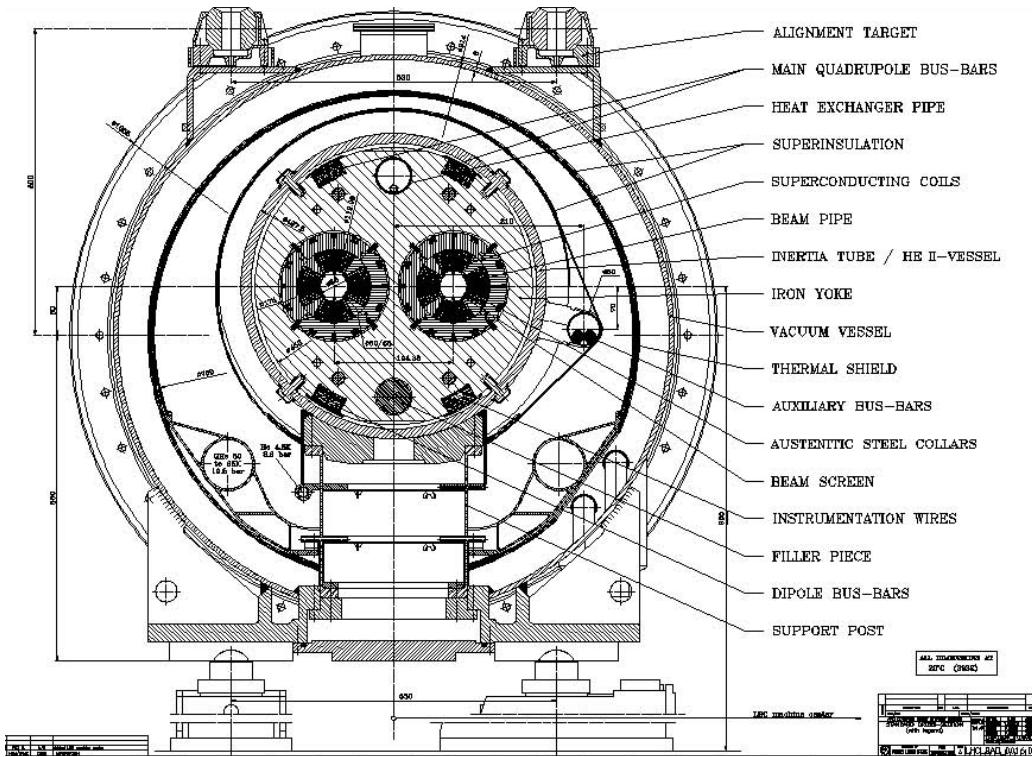
3.5 Short straight sections of the arcs

Figure 3.6 shows a perspective view while figure 3.7 illustrates the cross-section of an SSS. The cold masses of the arc SSSs contain the main quadrupole magnets, MQ, and various corrector magnets. On the upstream end, these can be either octupoles, MO, tuning quadrupoles, MQT, or skew quadrupole correctors, MQS. On the downstream end the combined sextupole-dipole correctors, MSCB are installed. These magnets are mounted inside a so-called inertia tube which is closed by end covers. This structure provides the helium vessel for these magnets and at the same time the mechanical stiffness of the assembly. The upstream flat end cover also supports the beam position monitors and the container for the quench protection diode stack of the main quadrupoles. The downstream, dished end cover has the connection tubes mounted with bellows for the interconnections to the adjacent dipole cold mass. Running through the SSSs are the two beam tubes, the heat exchanger tube, and the main dipole and quadrupole bus-bars as well as the spool bus-bars which interconnect the correctors of the dipole cold masses. The powering of the corrector magnets inside the short straight section cold masses is made via bus-bars placed in a tube located outside the cold mass, called line N. The cold masses are mounted into their cryostats to which the technical service modules, called QQS, are attached on the upstream end. These modules house the interconnections to the adjacent upstream dipole, the outlets of the wires for the instrumentation, and local corrector powering. In every second unit, the interconnection to the separate cryogenic feed line (QRL) and the phase separators are present. One out of four straight sections is equipped with a vacuum barrier for sectorising the cryostat vacuum. At the same positions, there are connection tubes and pressure plugs inside the upstream bus-bars to separate the local helium circuits of the machine.

Because of the lower electromagnetic forces, the two apertures do not need to be combined, but are assembled in separate annular collaring systems. This is in contrast to the case of the main dipoles. Computations, since confirmed by measurements, have shown that the magnetic coupling between the two apertures is negligible. This remains true even when the two apertures are excited with very different currents. Table 3.5 shows the design parameters of the main quadrupoles.

Figure 3.6: Short straight section with jumper.

Figure 3.7: Cross-section of SSS at quadrupole cold mass inside cryostat.

Table 3.5: Parameter list for main quadrupole magnets at 7.0 TeV.

Integrated Gradient	690	T
Nominal Temperature	1.9	K
Nominal Gradient	223	T/m
Peak Field in Conductor	6.85	T
Temperature Margin	2.19	K
Working Point on Load Line	80.3	%
Nominal Current	11870	A
Magnetic Length	3.10	m
Beam Separation distance (cold)	194.0	mm
Inner Coil Aperture Diameter (warm)	56.0	mm
Outer Coils Diameter	118.44	mm
Outer Yoke diameter	452	mm
Collar Material	Austenitic Steel	
Yoke Material	Low Carbon Steel	
Yoke Length including End Plates	3250	mm
Cold Mass Length Between End Covers	5345	mm
Total Mass Including Correctors	6500	kg
Number of turns per Coil (pole)	24	
Number of turns per coil inner layer (2 blocks)	2+8	
Number of turns per coil outer layer (2 blocks)	7+7	
Cable length per coil (pole)	160	m
Cable length per two-in-one quadrupole	1280	m
Bare Cable	Same as dipole outer layer	
Insulation Thickness 1st layer	50	μm
2nd layer	37.5	μm
3rd layer (adhesive)	50+5	μm
Self-inductance, one aperture	5.6	mH
Stored energy, one aperture	395	KJ
Electromagnetic forces: Resultant in x-dir	537	KN
Resultant in y-dir	-732	KN

3.6 Orbit and multipole correctors in the arcs

About 3'800 single aperture and 1'000 twin aperture corrector magnets will be used in the LHC. The 194 mm beam separation gives sufficient lateral space to build all correctors as single bore modules, with a nominal working point between 40 – 60% along the load line. Twin aperture units

Table 3.6: Overview of corrector magnet types and location.

Name	Description	Location
MCS	Sextupole multipole corrector	Main MBA & MBB dipoles
MCDO	Nested Decapole-Octupole multipole corrector	Main MBA dipoles
MSCB	Sextupole-Dipole Corrector (lattice chromaticity & orbit). Exists in 4 variants with all combinations of normal & skew fields.	Main quadrupoles (SSS), dispersion suppressors
MQT, MQS	Tuning and Skew Quadrupoles	Main quadrupoles (SSS)
MO	Octupole Lattice Corrector (Landau damping)	Main quadrupoles (SSS)
MCBC, MCBY	Dipole correctors (orbit)	Insertion region and dispersion suppressors
MQTL	Long Trim Quadrupole	Insertion region and dispersion suppressors
MCBX MCBXA = MCBX+MCSTX	Inner Triplet nested Horizontal & Vertical Dipole Orbit corrector. MCBX with a nested 6-pole, 12-pole corrector insert.	Inner Triplets
MQSX	Skew quadrupole	Inner Triplets
MCSOX	Nested skew sextupole, octupole, skew octupole corrector package	Inner Triplets

are assembled by keying corresponding modules into laminated support structures. The assembly by keying ensures mechanical precision and allows flexibility during mounting, since the same type of module is used for a normal or skew magnet. To optimise the cost of the corrector magnets, common design and fabrication principles are applied. A summary of the corrector magnet types is given in table 3.6.

3.7   Insertion magnets

The insertion magnets are superconducting or normal conducting and are used in the eight insertion regions of the LHC. Four of these insertions are dedicated to experiments, while the others are used for major collider systems (one for the RF, two for beam cleaning, and one for beam dumping). The various functions of the insertions are fulfilled by a variety of magnets, most based on the technology of NbTi superconductors cooled by superfluid helium at 1.9 K. A number of stand-alone magnets in the matching sections and beam separation sections are cooled to 4.5 K, while in the radiation areas, specialised normal conducting magnets are installed. The different magnet types will be described in the following sections, organized according to the machine sectors to which they belong. The type and distribution of magnets amongst the eight insertions are summarized in table 3.7.

Table 3.7: Types and number of magnets used in the LHC insertion regions.

Magnet type	IR1 ATLAS	IR2 ALICE	IR3 Cleaning	IR4 RF	IR5 CMS	IR6 Dump	IR7 Cleaning	IR8 LHCb
Main dipoles and quadrupoles (DS)								
MB	16	16	16	16	16	16	16	16
MQ	2	2	10	2	2	2	10	2
Superconducting insertion quadrupoles and correctors (DS and MS)								
MQMC	2	2	-	2	2	2	-	2
MQM	6	10	-	4	6	2	-	10
MQML	8	6	-	4	8	4	-	6
MQY	2	6	-	4	2	4	-	6
MQTL	2	2	24	2	2	2	24	2
MSCB	2	2	2	2	2	2	2	2
MCBC	12	13	10	8	12	6	10	13
MCBY	6	9		4	6	4		9
Normal conducting quadrupoles (Cleaning insertions)								
MQWA/B(Q4,Q5)	-	-	24	-	-	-	24	-
Superconducting separation dipoles								
MBX (D1)	-	2	-	-	-	-	-	2
MBRC (D2)	2	2	-	-	2	-	-	2
MBRS (D3)	-	-	-	4	-	-	-	-
MBRB (D4)	-	-	-	4	-	-	-	-
Normal conducting separation and correction dipoles								
MBXW (D1)	12	-	-	-	12	-	-	-
MBW (D3)/(D4)	-	-	12	-	-	-	8	-
MCBWH/V	-	-	8	-	-	-	8	-
Inner triplets and associated correctors								
MQXA (Q1, Q3)	4	4	-	-	4	-	-	4
MQXB (Q2)	4	4	-	-	4	-	-	4
MCBX	6	6	-	-	6	-	-	6
MQSX	2	2	-	-	2	-	-	2
Multipole packages	2	2	-	-	2	-	-	2
Normal conducting compensator dipoles in ALICE and LHCb experiments								
MBWMD	-	1	-	-	-	-	-	-
MBXWT	-	2	-	-	-	-	-	-
MBXWH	-	-	-	-	-	-	-	1
MBXWS	-	-	-	-	-	-	-	2

3.8 Dispersion suppressors

The main dipoles in the dispersion suppressors have the same characteristics and the same cryostats as the arc, with a minor difference in the cryogenic circuits in some of the cryodipoles. These

Table 3.8: Main parameters of the dispersion suppressor quadrupole cold masses.

Cold mass position	Magnets	Operating temperature (K)	Length (mm)	Mass (kg)	No. units
Q11	MQ+MQTL+MSCB	1.9	6620	7416	16
Q10, Q8 (other than IR3/7)	MQML+MCBC	1.9	6620	7416	24
Q10, Q8 (IR3/7)	MQ+MQTL+MCBC	1.9	6620	7416	8
Q9 (other than IR3/7)	MQMC+MQM+MCBC	1.9	8020	9310	12
Q9 (IR3/7)	MQ+2 MQTL+MCBC	1.9	8020	9310	4

dipoles are installed two per half-cell. The half-cell from Q10 to Q11 is longer than the others, and the extra length is bridged by a connection cryostat, which is adjacent to quadrupole Q11 in all IRs. The connection cryostats ensure the continuity of the beam pipes, the cryogenic fluids, and the electrical bus-bars.
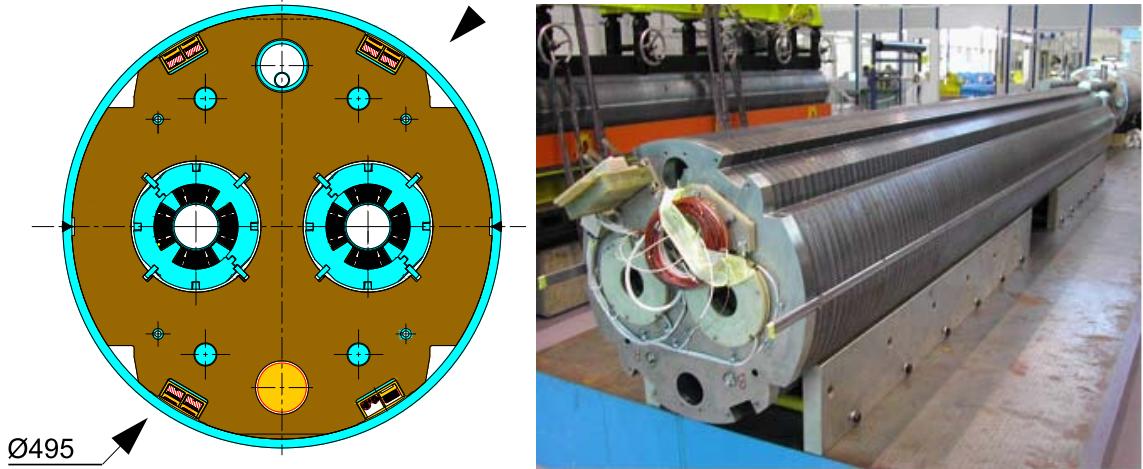
The superconducting quadrupoles in the dispersion suppressors are based on the MQ and MQM-type magnets (next section). The main parameters of the dispersion suppressor quadrupole cold masses are given in table 3.8. Their cryostats closely follow the design of the SSS cryostat, where the standard section of the vacuum vessel is modified in accordance with the length of the cold mas.

3.9 Matching section quadrupoles

The tuning of the LHC insertions is provided by the individually powered quadrupoles in the matching and dispersion suppressor sections. The matching sections consist of stand-alone quadrupoles arranged in four half cells, but the number and parameters of the magnets are specific for each insertion. Apart from the cleaning insertions, where specialized normal conducting quadrupoles are used in the high-radiation areas, all matching quadrupoles are superconducting magnets. Most of them are cooled to 4.5 K, except the Q7 quadrupoles, which are the first magnets in the continuous arc cryostat and are cooled to 1.9 K.

CERN has developed two superconducting quadrupoles for the matching sections: the MQM quadrupole, featuring a 56 mm aperture coil, which is also used in the dispersion suppressors, and the MQY quadrupole, with an enlarged, 70 mm coil aperture. Both quadrupoles use narrow cables, so that the nominal current is less than 6 kA, substantially simplifying the warm and cold powering circuits. Each aperture is powered separately, but a common return is used, so that a three-wire bus-bar system is sufficient for full control of the apertures.

The MQM quadrupole, figure 3.8, consists of two identical, independently powered apertures, which are assembled together in a two-in-one yoke structure. Three versions of the MQM quadrupole are required for the LHC, with magnetic lengths of 2.4 m, 3.4 m and 4.8 m. The main parameters of the quadrupole are listed in table 3.9. In total, 84 MQM magnets are required for the LHC dispersion suppressors and matching sections.
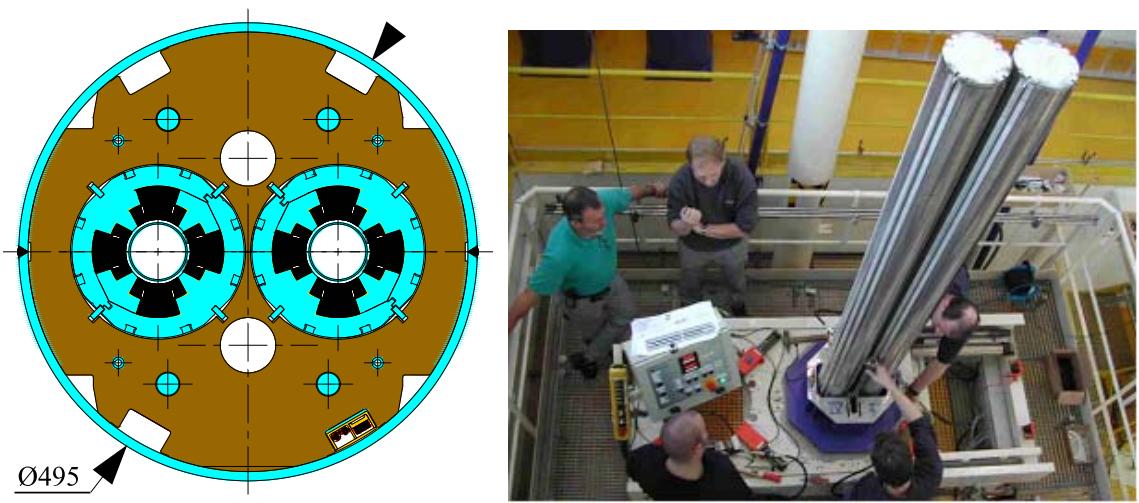
Figure 3.8: Cross-section of MQM quadrupole (left) and a 5 m long MQM magnet on the test stand (right) (dimensions in mm).

Table 3.9: Main parameters of the MQM-type quadrupoles.

Coil inner diameter	56 mm
Magnetic length	2.4/3.4/4.8 m
Operating temperature	1.9/4.5 K
Nominal gradient	200/160 T/m
Nominal current	5390/4310 A
Cold bore diameter OD/ID	53/50 mm
Peak field in coil	6.3 T
Quench field	7.8 T
Stored energy per aperture	64.3 kJ/m
Inductance per aperture	4.44 mH
Quench protection	Quench heaters, two independent circuits
Cable width	8.8 mm
Mid-thickness	0.84 mm
Keystone angle	0.91 deg.
No of strands	36
Strand diameter	0.475 mm
Cu/SC Ratio	1.75
Filament diameter	6 μm
j_c, (4.2 K and 5 T)	2800 A/mm^2
Mass (2.4/3.4/4.8 m)	3100/4300/6000 kg
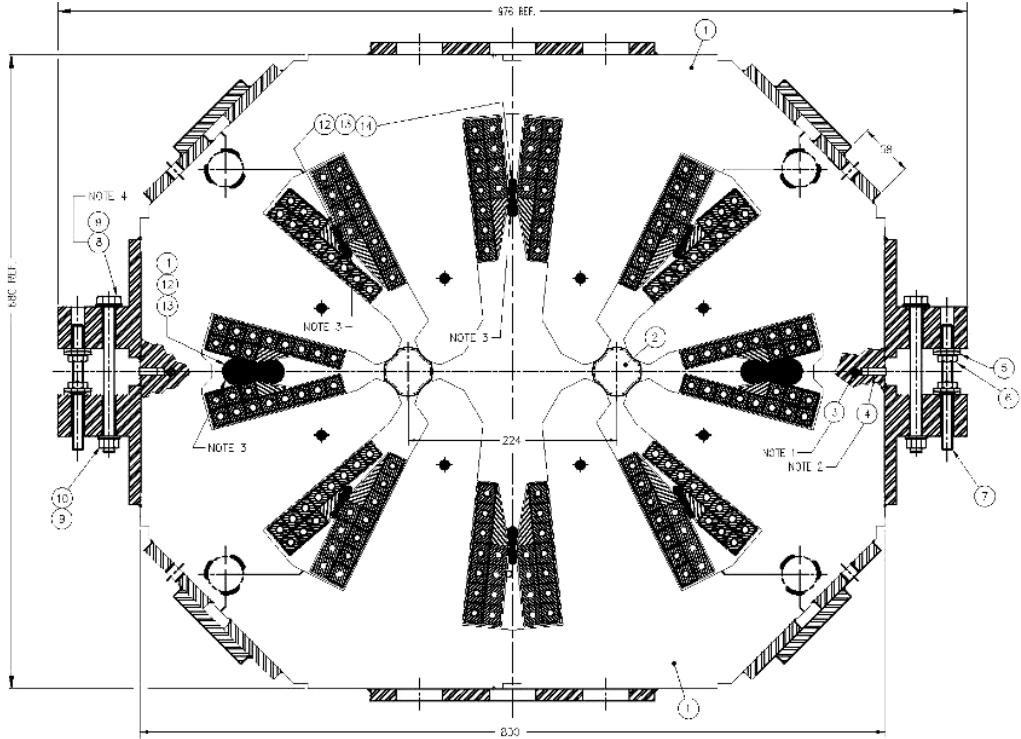
The MQY wide-aperture quadrupole, figure 3.9, consists of two individually powered apertures assembled in a common yoke structure. The coil aperture of the magnet is 70 mm and its magnetic length 3.4 m. The main parameters of the quadrupole are given in table 3.10. In total, 24 MQY magnets are required for the LHC matching sections.

Figure 3.9: Cross-section of MQY quadrupole (left) and assembly of the magnet (right) (dimensions in mm).

Table 3.10: Main parameters of the MQY matching quadrupole.

Coil inner diameter	70 mm
Magnetic length	3.4 m
Operating temperature	4.5 K
Nominal gradient	160 T/m
Nominal current	3610 A
Cold bore diameter OD/ID	66.5/62.9 mm
Peak field in coil	6.1 T
Quench field	7.5 T
Stored energy	479 kJ
Inductance	73.8 mH
Quench protection	Quench heaters,
	two independent circuits
Cable width, cable 1/2	8.3/8.3 mm
Mid-thickness, cable 1/2	1.285/0.845 mm
Keystone angle, cable 1/2	2.16/1.05 deg.
No of strands, cable 1/2	22/34
Strand diameter, cable $1/2$	0.735/0.475 mm
Cu/SC Ratio, cable 1/2	1.25/1.75
Filament diameter, cable 1/2	6/6 μm
j_c, cable 1/2, (4.2 K and 5 T)	2670/2800 A/mm^2
Mass	4400 kg

**Figure 3.10**: Cross-section of the MQW twin aperture normal conducting matching quadrupole (dimensions in mm).

In the cleaning insertions IR3 and IR7, each of the matching quadrupoles Q4 and Q5 consists of a group of six normal conducting MQW magnets. This choice is dictated by the high radiation levels due to scattered particles from the collimation system, and therefore the use of superconducting magnets is not possible. The cross-section of the quadrupole is shown in figure 3.10. It features two apertures in a common yoke (2-in-1), which is atypical for normal conducting quadrupole magnets, but is needed because of transverse space constraints in the tunnel. The two apertures may be powered in series in a standard focusing/defocusing configuration (MQWA), or alternatively in a focusing/focusing configuration (MQWB) in order to correct asymmetries of the magnet. In a functional group of six magnets, five are configured as MQWA, corrected by one configured as MQWB. As in most normal conducting magnets, the field quality is iron-dominated and therefore defined by the shape of the magnetic poles. In order to achieve the necessary field quality, the separation between poles is adjusted and verified to within a tenth of a millimetre by tightening rods along the length of the magnet. The total number of quadrupole magnets in each of the two insertions is 24. Altogether 52 magnets of this type, including 4 spares, have been built by Canadian industry in collaboration with TRIUMF and CERN. The design parameters are given in table 3.11.

3.10 Matching section separation dipoles

The separation dipoles are used in several insertions to change the beam separation from the nominal 194 mm in the LHC arcs. In the experimental insertions, a pair of D1-D2 dipoles brings the two beams onto a collision orbit at the IP and then separates the beams again beyond the IP. To reduce

Table 3.11: Main parameters of the MQW normal conducting quadrupole magnet.

Magnet type	MQWA	MQWB
Magnetic length	3.1 m	
Beam separation	224 mm	
Aperture diameter	46 mm	
Operating temperature	$< 65°$ C	
Nominal gradient	35 T/m	30 T/m
Nominal current	710 A	600 A
Inductance	28 mH	
Resistance	37 mΩ	
Conductor X-section	20.5 x 18.0 mm^2 inner poles	
	17.0 x 17.0 mm^2 outer poles	
Cooling hole diameter	7 mm inner poles,	
	8 mm outer poles	
Number of turns per magnet	8 x 11	
Minimum water flow	28 l/min	
Dissipated power at I$_{nom}$	19 kW	14 kW
Mass	11700 kg	

the long-range beam-beam effects, the first separation dipole D1 is placed immediately upstream of the low-β triplet. In the high-luminosity insertions, high radiation levels are expected, and more robust normal conducting magnets, MBXW, are used. In the ALICE and LHCb insertions, D1 is a stronger superconducting magnet, MBX, allowing more space for the injection systems. In all cases, the D2 separation dipole, MBRC, is a twin-aperture superconducting magnet. In the cleaning insertions, the pair of D3-D4 dipoles separates the beams to 224 mm to accommodate the collimation system, while in the RF insertion the beam separation is 420 mm, so that individual RF cavities can be installed for each beam. The radiation levels in the cleaning insertions require the use of normal conducting dipoles, MBW (both for D3 and D4), while superconducting dipoles, MBRB (D4) and MBRS (D3), are used in the RF insertion.

The MBX (D1), MBRB/C (D4/D2) and MBRS (D3) dipoles are designed and built by BNL (USA) on the basis of the RHIC lattice dipole [21]. The MBX magnets are designed with one RHIC-style cold mass in a RHIC-style cryostat, and the MBRS magnets are designed with two such cold masses side-by-side in a common cryostat. The cold masses are built straight, without the 47 mm sagitta of the RHIC magnets. The MBRB and MBRC magnets are built with coils that are pre-stressed with stainless steel collars. These collared coils are assembled into yokes with common outside dimensions but with two aperture spacing, depending on the type. The main parameters of the magnets are given in table 3.12.
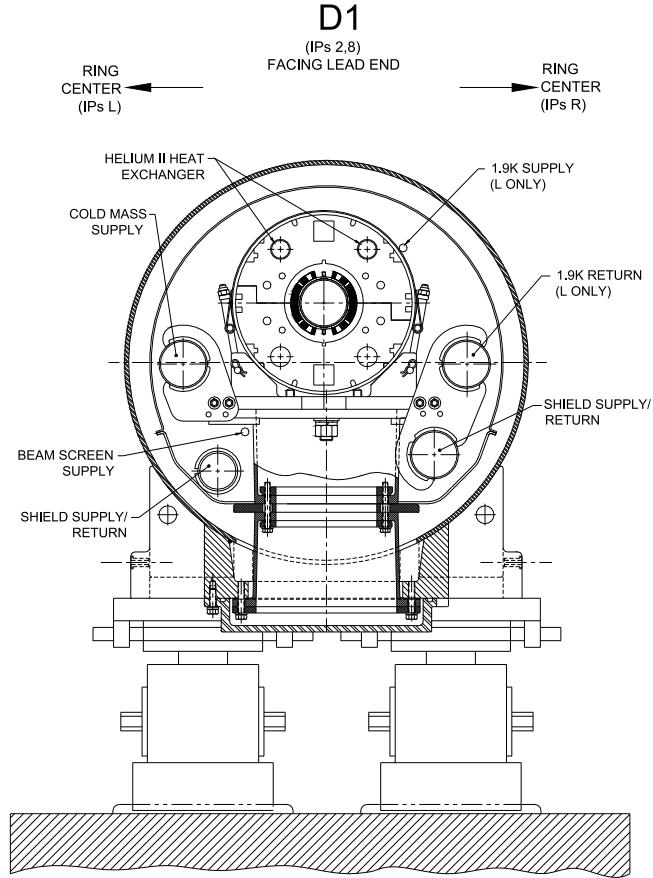
The MBX dipole cross-section is shown in figure 3.11. Many of its design features are identical to the RHIC main dipoles. However, the magnet is equipped with two heat exchangers, allowing it to be cooled to 1.9 K, and it has a larger cold bore (OD 78 mm) than the RHIC dipole. Another feature is the use of quench heaters as active protection elements. These modifications require additional cryogenic and electrical instrumentation compared to the original RHIC design.

Table 3.12: Main parameters of the MBX, MBRB/C and MBRS superconducting separation dipoles.

Coil inner diameter	80 mm
Magnetic length	9.45 m
Nominal field	3.8 T
Operating temperature	1.9 K (MBX)
	4.5 K (MBRB/C, MBRS)
Nominal current	5750 A (MBX, MBRS)
	6050 A (MBRB/C)
Aperture separation	188 mm (MBRC)
	194 mm (MBRB)
	414 mm (MBRS)
Cold bore diameter OD/ID	78/74 mm (MBX)
	73/69 mm (MBRB/C, MBRS)
Peak field in coil	4.2 T
Quench field	4.8 T
Stored energy per aperture	470 kJ
Inductance per aperture	25.8 mH
Quench protection	Quench heaters,
	two independent circuits per aperture
Cable width	9.73 mm
Mid-thickness	1.166 mm
Keystone angle	1.2 deg.
No of strands	30
Strand diameter	0.648 mm
Cu/SC Ratio	1.8
Filament diameter	6 μm
j_c	2500 A/mm^2 (4.2 K and 5 T)
Mass	4500 kg (MBX)
	13500 kg (MBRS)
	24500 kg (MBRB/C)

The MBRB magnet is a two-in-one magnet with parallel fields in the two apertures. The MBRC is similar in design (its cross-section is shown in figure 3.12) and differs only by the nominal aperture spacing (188 mm). In addition, to allow installation of the beam screens, the cold bore in MBRB is slightly off-centred from the IP side. The cross-talk between parallel fields in the two apertures is reduced by additional iron around the median plane, resulting in an oval shape of the cold mass. Its outer dimensions are identical in the vertical plane to the LHC main dipole, so that standard LHC support posts and other cryostat elements can be used in a 9.8 m long vacuum tank.
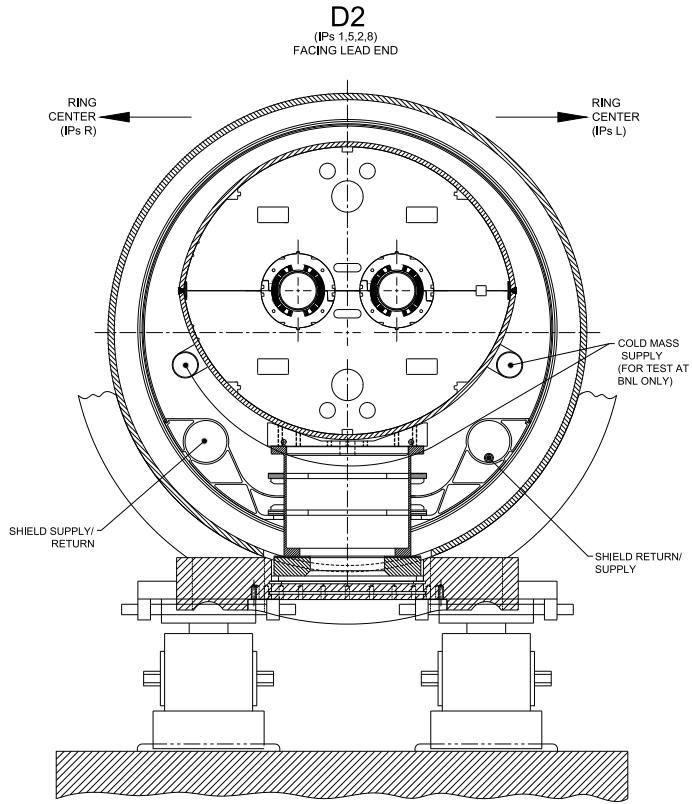
The MBRS separation dipole consists of two MBX-like cold masses assembled in a 9.6 m long cryostat, as shown in figure 3.13. The cold masses are aligned to a separation of 414 mm
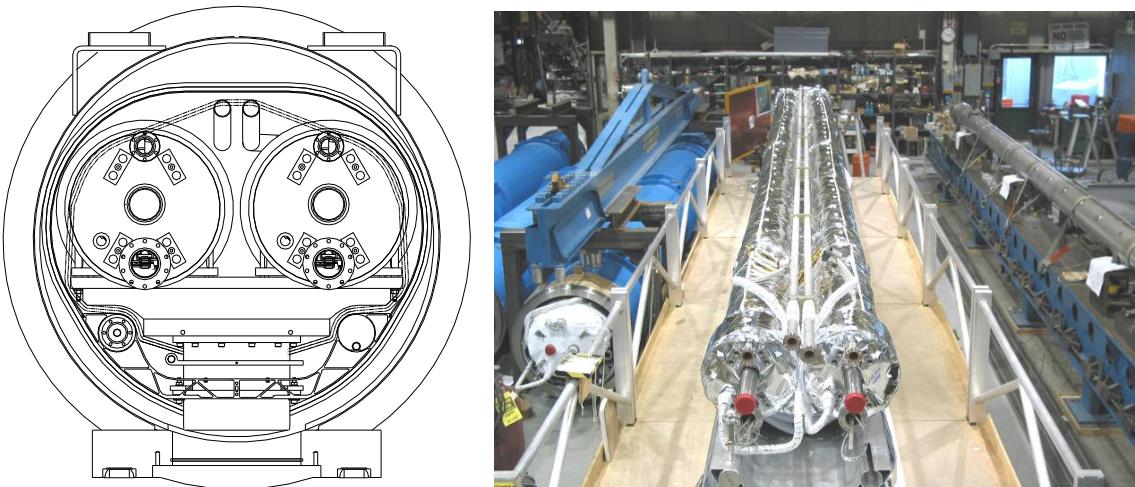
Figure 3.11: Cross-section of the MBX (D1) cryodipole, of same design as the RHIC main dipole.

using three transverse beams, connected to the upper plates of standard LHC dipole posts. Other cryostat elements are identical to MBRB. The magnet interfaces on the non-IP side with the QQS service module, which provides the connection to the cryogenics and powering services. On the IP side, provisions are made for interconnecting MBRS with the MSRU undulator [22] designed to produce synchrotron radiation for transversal beam profile measurement.

The MBW and MBXW normal conducting dipoles are designed and built by BINP, Novosibirsk, Russia, employing a well-established technology of epoxy-impregnated coils in a laminated window-frame steel yoke: see figures 3.14 and 3.15. The two coils of both types of magnet consist of three pancakes that are wound from a hollow rectangular copper conductor. The conductor is insulated with glass-fibre tape and impregnated with epoxy resin. The yoke is laminated from insulated magnetic steel sheets of 1.5 mm thickness to reduce eddy currents that are generated during ramping. The laminations are held together by welded plates. The shape of the end-plates and shims is adjusted to compensate the magnetic end effects. The coils are fixed in the yoke by stainless steel clamps at the end of the magnet and further supported by separation blocks in the mid-plane. The magnets are manufactured as two half-cores that are clamped together with studs and nuts along the side cover plates. The main parameters of the magnets are given in table 3.13.

Figure 3.12: Cross section of the MBRC (D2) cryodipole at a support post location.

Figure 3.13: Cross-section of the MBRS dipole (left) and assembly of the MBRS cold masses at BNL (right).

The field quality of normal conducting magnets is defined by the shape of the steel poles. In order to guarantee good field quality, the punching of the laminations is controlled to within 0.05 mm in the vicinity of the apertures. The lamination stacks and the clamping of the two half-magnets

Table 3.13: Main parameters of the MBW and MBXW separation dipoles.

| Magnet type	MBW	MBXW
Magnetic length	3.4 m	
Beam separation	194–224 mm	0–27 mm
Gap height	52 mm	63 mm
Coil Protection temperature	$< 65°$ C	
Nominal field	1.42 T	1.28 T
Nominal current	720 A	690 A
Inductance	180mH	145 mH
Resistance	55 mΩ	60 mΩ
Conductor X-section	18 x 15 mm^2	
Cooling hole diameter	8 mm	
Number of turns per magnet	2 x 42	2 x 48
Minimum water flow	19 l/min	
Dissipated power at I$_{nom}$	29kW	29 kW
Mass	18000 kg	11500 kg
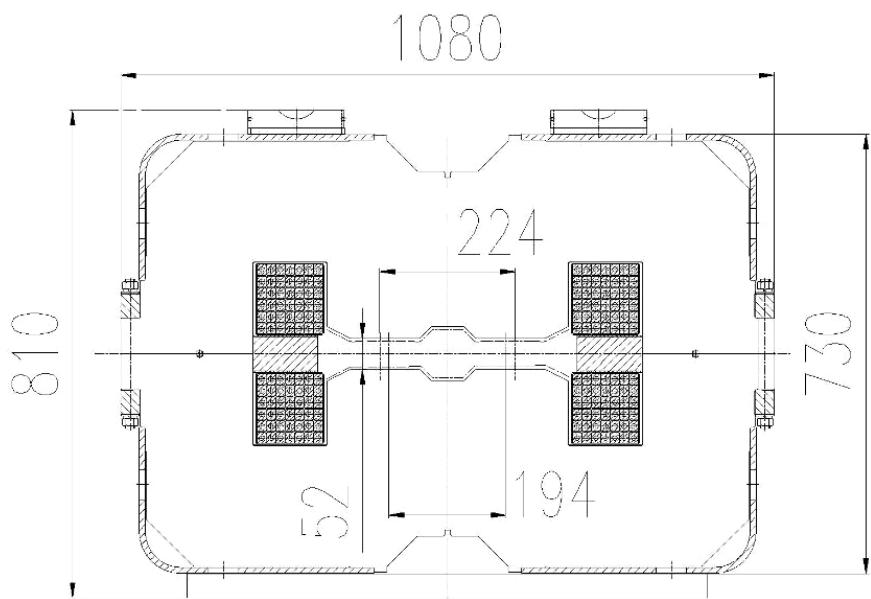
are also controlled to within a tenth of a millimetre. Access to the laminations on the top and the sides of the magnet allows the verification of the magnet assembly after production. Specifications require a sag of less than 0.5 mm and a twist of less than 1 mrad. All these parameters are checked to assure quality during production and to guarantee the required field quality.

The MBW magnet, shown in figure 3.14, features a pole shape with varying gap height and two positions for the beam pipes (194 mm to 224 mm), while employing a standard H-type dipole construction. The two coils consist of three pancakes with 14 windings. The overall number of MBW magnets produced by BINP is 24, including 4 spares.
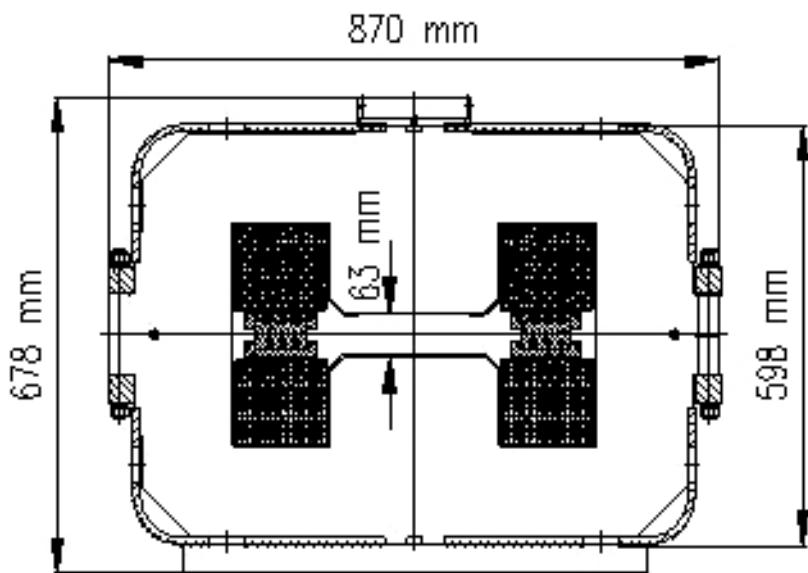
The cross-section of the MBXW, shown in figure 3.15, features a coil with three pancakes with 16 turns each, wound using the same copper conductor as for the MBW. Since both beams run through a single pipe, the pole region is 120 mm wide with a gap height of 63 mm. Small shims, placed along the sides of the pole, are part of the punched laminations and homogenize the field in the aperture. The total number of MBXW magnets built by BINP is 29, including 4 spares.

3.11 Low-beta triplets

The low-β triplet, figure 3.16, is composed of four single-aperture quadrupoles with a coil aperture of 70 mm. These magnets are cooled with superfluid helium at 1.9 K using an external heat exchanger system capable of extracting up to 10 W/m of power deposited in the coils by the secondary particles emanating from the proton collisions. Two types of quadrupoles are used in the triplet: 6.6 m long MQXA magnets designed and developed by KEK, Japan, and 5.7 m long MQXB magnets designed and built by FNAL, USA. The magnets are powered in series with 7 kA, with an additional inner loop of 5 kA for the MQXB magnets. Together with the orbit correctors MCBX, skew quadrupoles MQSX, and multipole spool pieces supplied by CERN, the low-β quadrupoles
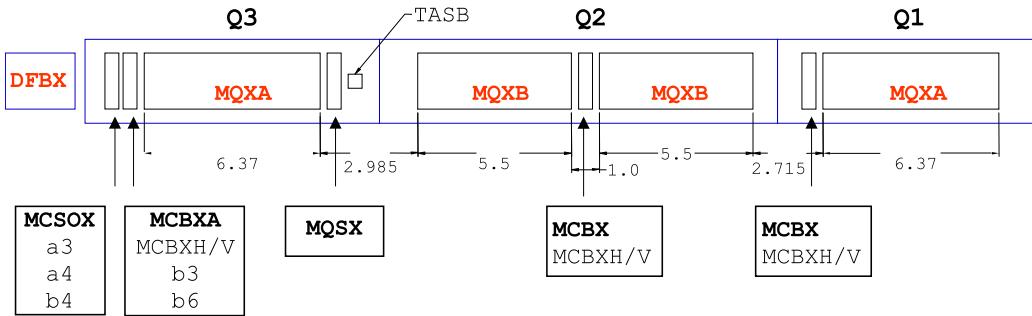
Figure 3.14: Cross-section of the normal conducting separation dipole MBW (dimensions in mm).
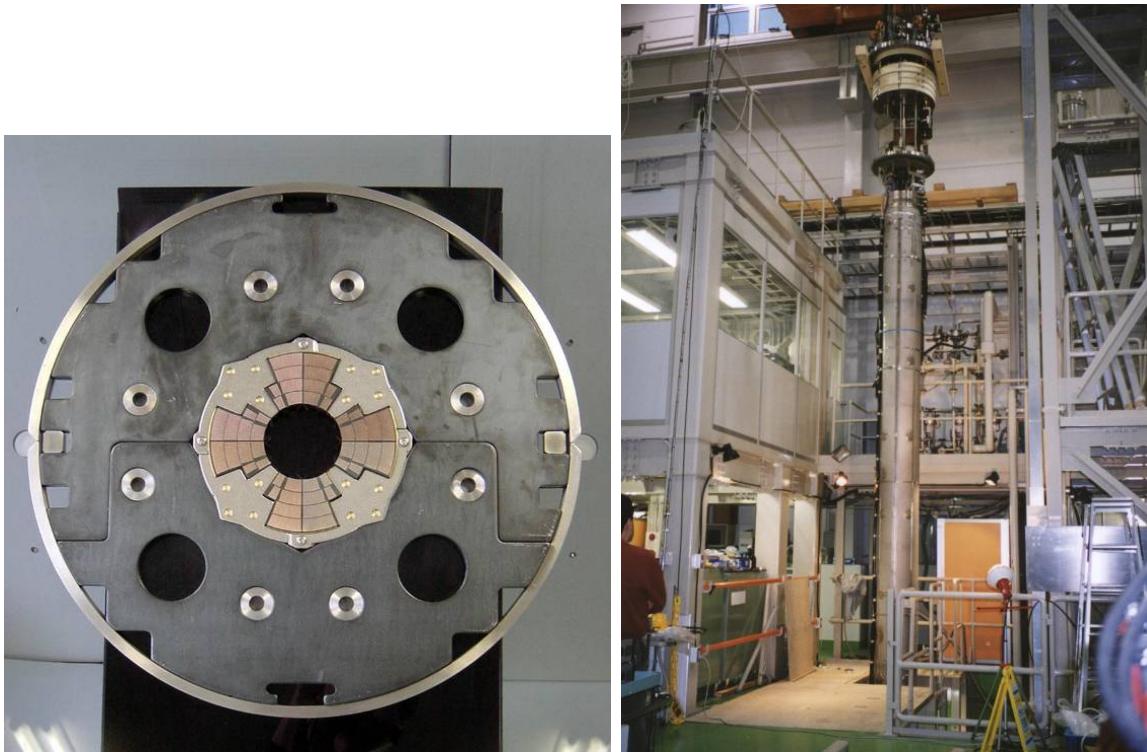

Figure 3.15: Cross-section of the normal conducting separator dipole magnet MBXW.

are completed in their cold masses and cryostated by FNAL. The cryogenic feed-boxes (DFBX), providing a link to the cryogenic distribution line and power converters, are designed and built by LBNL, USA.

Figure 3.16: Schematic layout of the low-β triplet (distances in m).
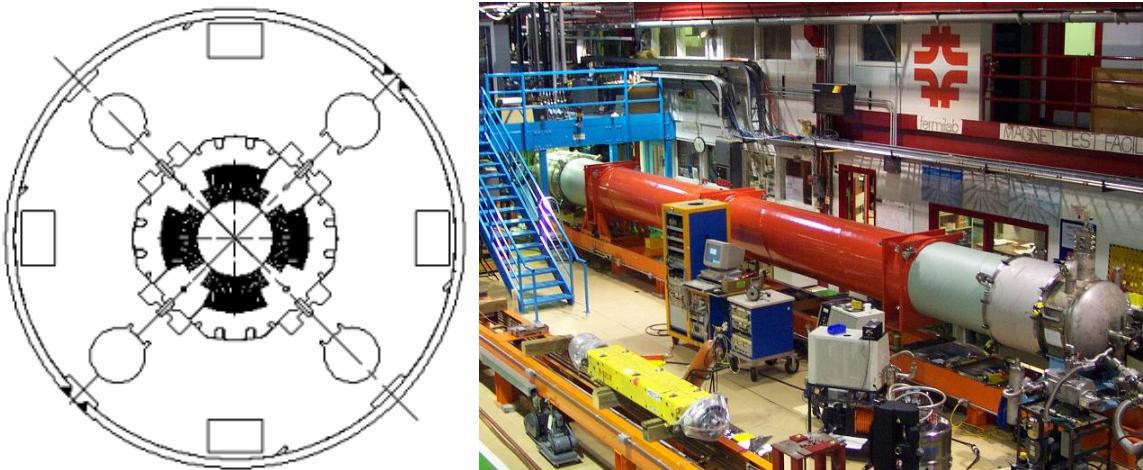
Figure 3.17: Cross-section of the MQXA low-β quadrupole (left) and MQXA quadrupole ready for tests in the vertical cryostat at KEK (right).

Alongside the LHC main dipoles, the high-gradient, wide-aperture low-β quadrupoles are the most demanding magnets in the collider. They must operate reliably at 215 T/m, sustain extremely high heat loads in the coils and high radiation dose during their lifetime, and have a very good field quality within the 63 mm aperture of the cold bore.

The design of the MQXA quadrupole is based on a four-layer coil using 11 mm wide Rutherford-type graded NbTi cables. The coils are wound and cured in two double layers and are assembled using 10 mm wide spacer-type collars (see figure 3.17). The pre-stress in the coils and their rigidity is provided by the yoke structure, which consists of horizontally split laminations keyed at the mid-plane. The main parameters of the magnet are given in table 3.14.

Table 3.14: Main parameters of the MQXA low-β quadrupole.

Coil inner diameter	70 mm
Magnetic length	6.37 m
Operating temperature	1.9 K
Nominal gradient	215 T/m
Nominal current	7149 A
Cold bore diameter OD/ID	66.5/62.9 mm
Peak field in coil	8.6 T
Quench field	10.7 T
Stored energy	2300 kJ
Inductance	90.1 mH
Quench protection	Quench heaters,
	two independent circuits
Cable width, cable 1/2	11/11 mm
Mid-thickness, cable 1/2	1.487/1.340 mm
Keystone angle, cable 1/2	2.309/1.319 deg.
No of strands, cable 1/2	27/30
Strand diameter, cable 1/2	0.815/0.735 mm
Cu/SC Ratio, cable 1/2	1.2/1.9
Filament diameter, cable 1/2	10/10 μm
j_c, cable1/2, (4.2 K and 6 T)	2200/2160 A/mm^2
Mass	9600 kg

Figure 3.18: Cross-section of the MQXB low-β quadrupole (left) and Q2 quadrupole on test in FNAL (right).

The MQXB design features a two-layer coil, with each layer individually wound using a 15.4 mm wide Rutherford-type NbTi cable (see figure 3.18). The coils are assembled using free-standing collars, which provide the pre-stress and counteract the magnetic forces. The collared

Table 3.15: Main parameters of the MQXB low-β quadrupole.

Coil inner diameter	70 mm
Magnetic length	5.5 m
Operating temperature	1.9 K
Nominal gradient	215 T/m
Nominal current	11950 A
Cold bore diameter OD/ID	66.5/62.9 mm
Peak field in coil	7.7 T
Quench field	9.2 T
Stored energy	1360 kJ
Inductance	19.1 mH
Quench protection	Quench heaters, two independent circuits
Cable width, cable 1/2	15.4/15.4 mm
Mid-thickness, cable 1/2	1.456/1.146 mm
Keystone angle, cable 1/2	1.079/0.707 deg.
No of strands, cable 1/2	37/46
Strand diameter, cable 1/2	0.808/0.650 mm
Cu/SC Ratio, cable 1/2	1.3/1.8
Filament diameter, cable 1/2	6/6 μm
j_c, cable 1/2 (4.2 K and 5 T)	2750/2750 A/mm2
Mass	5700 kg

assembly is aligned in the yoke structure with precision keys, and the magnet is enclosed in a stainless steel helium vessel consisting of half-shells welded at the pole plane. The design parameters of the magnet are given in table 3.15.
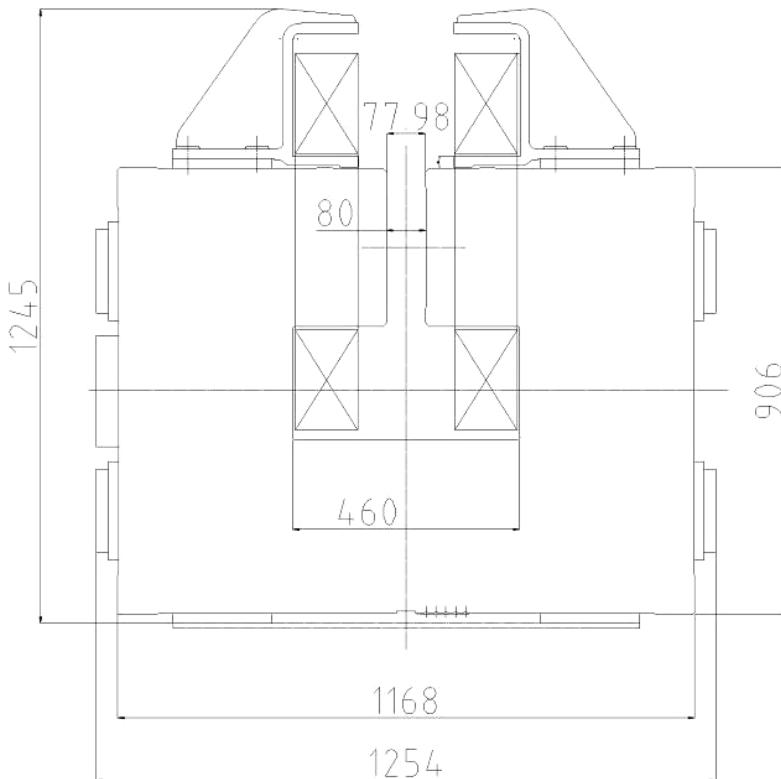
There are also a number of superconducting and normal conducting corrector magnets in the insertions.

3.12 Compensator dipoles in ALICE and LHCb experiments

The effect of the spectrometer dipoles in the ALICE (IR2) and LHCb (IR8) experiments on the beam is compensated in both cases with three dipoles, one placed symmetrically with respect to the IP and two weaker dipoles placed next to the inner triplets. The dipole field of the ALICE spectrometer, which produces a vertical kick on the beam, is compensated with a MBWMD and two MBXWT magnets. The MBWMD is a magnet from the SPS complex, originally built for the ISR beam lines (type HB2, turned vertical). Its main parameters are shown in table 3.16, and its cross section is shown in figure 3.19. The LHCb dipole, which produces a horizontal kick on the beam, is compensated by an MBXWH magnet and two MBXWS magnets. The MBXWH is in fact an MBXW separation dipole, discussed above, and the MBXWT and MBXWS magnets are short versions of the MBXW dipole. The parameters of these magnets are given in table 3.16. All MBXW type magnets are designed and built by BINP, Russia.

Table 3.16: Main parameters of the compensator dipoles for ALICE and LHCb (the magnets in the first three columns have the same cross-section as MBXW).

| Magnet type	MBXWH	MBXWT	MBXWS	MBWMD
Magnetic length	3.4 m	1.5 m	0.8 m	2.6 m
Gap height		63 mm		80 mm
Coil protection temperature		$< 65°$ C		$< 65°$ C
Nominal field	1.24 T	1.20 T	1.33 T	1.32 T
Current at nominal field	670 A	630 A	780 A	475 A
Inductance	145 mH	70 mH	35 mH	639 mH
Resistance	60 mΩ	40 mΩ	20 mΩ	172 mΩ
Conductor X-section		18 x 15 mm^2		16.3 x 10.8 mm^2
Cooling hole diameter		8 mm		6.6 mm
Number of turns per magnet		2 x 48		2 x 102
Minimum water flow	19 l/min	5 l/min	7 l/min	20 l/min
Dissipated power at I$_{nom}$	27 kW	16 kW	12 kW	39 kW
Mass	11500 kg	5800 kg	3700 kg	20500 kg

Figure 3.19: Cross-section of the normal conducting compensation dipole MBWMD for ALICE (dimensions in mm).

Chapter 4

The RF systems and beam feedback

4.1 Introduction

The injected beam will be captured, accelerated and stored using a 400 MHz superconducting cavity system, and the longitudinal injection errors will be damped using the same system. This choice defines the maximum allowable machine impedance, in particular for higher order modes in cavities [23]. Transverse injection errors will be damped by a separate system of electrostatic deflectors that will also ensure subsequent transverse stability against the resistive wall instability [24]. A new capture system at 200 MHz to reduce injection loss and ease operation has been proposed and designed. It will be installed at a later stage, if the injected emittance increases when intensities much higher than nominal are reached. All RF and beam feedback systems are concentrated at Point 4 and extend from the UX45 cavern area into the tunnel on either side. The klystron power plant and racks of equipment for the different systems are in both the UX45 and US45 sides of the cavern. Point 4 is already equipped with klystron power converters to be reused from LEP.

The beam and machine parameters that are directly relevant to the design of the RF and Beam Feedback systems are given in table 4.1. At nominal intensity in the SPS, an emittance of 0.6 eVs has now been achieved, giving a bunch length at 450 GeV of 1.6 ns. The phase variation along the batch due to beam loading is within 125 ps. This emittance is lower than originally assumed, and as a result, an RF system in the LHC of 400.8 MHz can be used to capture the beam with minimal losses, accelerate, and finally store it at top energy. Higher frequencies, while better for producing the short bunches required in store, cannot accommodate the injected bunch length.

There will be some emittance increase at injection, but this will be within the capabilities of the RF system for acceleration and, in particular, will be below the final emittance needed in storage. This final emittance is defined by intra-beam scattering lifetime in the presence of damping due to synchrotron radiation, RF lifetime and instability threshold considerations. Controlled emittance increase will be provided during acceleration by excitation with band-limited noise, the emittance increasing with the square root of the energy to optimise both narrow and broadband instability thresholds [23].

The final emittance at 7 TeV (2.5 eVs) and a maximum bunch length given by luminosity considerations in the experiments, leads to a required maximum voltage of 16 MV / beam. Transient beam-loading, coming from the high RF beam current ($\sim$ 1 A) combined with the long beam

Table 4.1: The Main Beam and RF Parameters.

	Unit	Injection 450 GeV	Collision 7 TeV
Bunch area (2σ)*	eVs	1.0	2.5
Bunch length (4σ)*	ns	1.71	1.06
Energy spread (2σ)*	10^{-3}	0.88	0.22
Intensity per bunch	10^{11} p	1.15	1.15
Number of bunches		2808	2808
Normalized rms transverse emittance V/H	μm	3.75	3.75
Intensity per beam	A	0.582	0.582
Synchrotron radiation loss/turn	keV	-	7
Longitudinal damping time	h	-	13
Intrabeam scattering growth time - H	h	38	80
- L	h	30	61
Frequency	MHz	400.789	400.790
Harmonic number		35640	35640
RF voltage/beam	MV	8	16
Energy gain/turn (20 min. ramp)	keV	485	
RF power supplied during acceleration/ beam	kW	~ 275	
Synchrotron frequency	Hz	63.7	23.0
Bucket area	eVs	1.43	7.91
RF (400 MHz) component of beam current	A	0.87	1.05

* The bunch parameters at 450 GeV are an upper limit for the situation after filamentation, $\sim$100 ms after each batch injection. The bunch parameters at injection are described in the text.
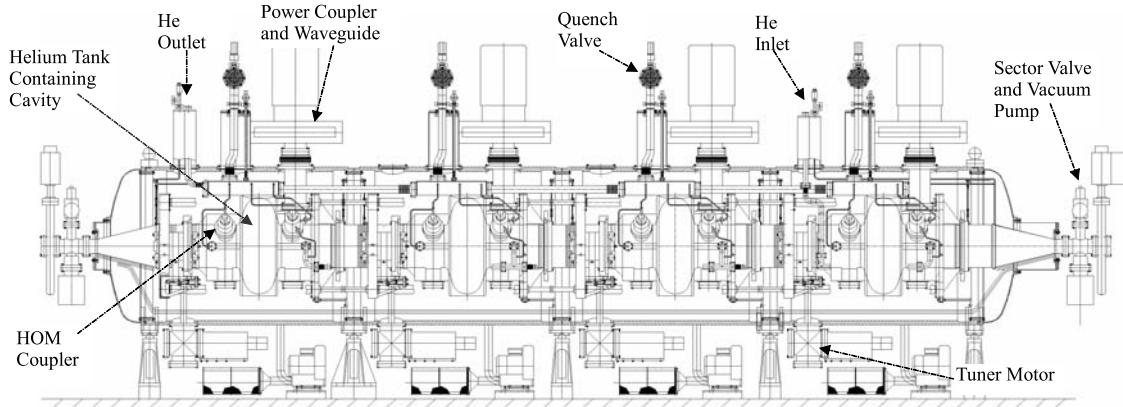
gap ($\sim 3\,\mu$s) due to the abort gap dominates the design of the LHC RF system and leads to the choice of SC cavities with a wide beam aperture (30 cm). With high RF voltage per cavity and the low R/Q due to the wide aperture, the stored energy in the cavity is high, and the cavity field phase swing due to reactive beam loading in the beam gap is minimized. Furthermore, the required voltage is achieved with fewer cavities than with a copper system and, again due to the wide beam aperture, the R/Q of the Higher Order Modes(HOM) in the cavity are lower. With strong HOM damping in the cavity, the total machine impedance can be kept low.

During acceleration the real power supplied to the beams is relatively small (275 kW/beam), but the installed power required to control these beams is much larger. The challenge in the design of the RF system is to minimize the beam handling power in order to arrive at acceptable levels for the power couplers. If separate cavities can be used for each beam, the RF beam current, and hence transient beam-loading in the cavities, is halved, and the coupler power requirement at injection is also reduced to more realistic levels. An added advantage is the possibility of independent control of the beams. However, the standard distance between beams in the machine, 194 mm, is insufficient. Consequently, the beam separation is increased in the RF region to 420 mm by means of special superconducting dipoles. With the increased separation and also by staggering the cavities longitudinally, the "second" beam can pass outside the cavity. It must still, however, pass through the cryostat.

4.2 Main 400 MHz RF Accelerating System (ACS)

The two independent RF systems must each provide at least 16 MV in coast, while at injection about 8 MV is needed. The frequency of 400 MHz is close to that of LEP, 352 MHz, allowing the same proven technology of niobium sputtered cavities to be applied. All reactive beam power has to be carried by the RF couplers. The present design, using single cell cavities each with 2 MV accelerating voltage, corresponding to a conservative field strength of 5.5 MV/m, minimizes the power carried by the RF window. Even so, the peak power requirements for the coupler are significantly higher than previously achieved on superconducting cavities. A large tuning range is required to compensate the average reactive beam component. Each RF system has eight cavities, with $R/Q = 45\ \Omega$ and of length $\lambda/2$ grouped by four with a spacing of 3 $\lambda/2$ in one common cryostat [25]. Each cavity is driven by an individual RF system with klystron, circulator and load. Complex feedback loops around each cavity, described below, allow precise control of the field in each cavity, important for the unforgiving high-intensity LHC proton beam. The use of one klystron per cavity also avoids problems such as coupling between cavities and ponderomotive oscillations that plagued the LEP-RF system when one klystron supplied eight cavities. Energy and phase errors at injection require strong coupling between cavity and klystron (low external Q, Q_{ext}) but the higher field in coast demands a high Q_{ext} to limit the power needed. The power coupling must therefore vary during the ramp. The variable coupler has a range of $Q_{ex} = 10{,}000$ to $Q_{ext} = 200{,}000$. To control the transient beam-loading, the installed power is 300 kW — the average RF power being much lower. Simulations [26] have shown that under some conditions the power to be handled can be even higher for a fraction of a μs; hence the RF drive has to be limited to avoid klystron saturation. Simulations also show that short reflected power spikes, much larger than the installed RF power, are possible, the energy being taken from the beam or the cavity stored energy. Therefore, the peak power capabilities of circulator and loads have to be increased correspondingly. Due to the staging of the 200 MHz capture system the 400 MHz RF system has to provide all injection damping. Simulations have verified that this is possible but the system's power-handling capabilities are stretched to the limits. All HOMs have to be damped as strongly as possible, partly for machine impedance reasons but also to avoid extracting excessive RF power from the beam through the coupler. To couple to the different polarities of the multi-pole modes, two wide-band HOM couplers are used placed at 120° around the circumference. The wideband couplers have a notch filter at 400 MHz which causes reduced coupling to these modes. Two dipole modes at $\sim$500 MHz (TE$_{111}$) and $\sim$534 MHz (TM$_{110}$) respectively are particularly dangerous since they do not propagate in the tubes of the inter-cavity beam tubes with 700 MHz cut-off frequency. A second set of narrow band couplers is therefore needed for these two modes, resulting in a total of four HOM couplers for each cavity.

The use of niobium sputtering on copper for construction of the cavities has the important advantage over solid niobium that susceptibility to quenching is very much reduced. Local heat generated by small surface defects or impurities is quickly conducted away by the copper. During the low-power tests, the 21 cavities produced, all reached an accelerating field of twice nominal without quenching. The niobium sputtered cavities are insensitive to the Earth's magnetic field and special magnetic shielding, as needed for solid niobium cavities, is not required. Four cavities, each equipped with their helium tank, tuner, HOM couplers and power coupler, are grouped together in

Figure 4.1: Four-cavity cryomodule.

a single cryomodule, see figures 4.1 and 4.2. The conception of the cryomodule is itself modular; all cavities are identical and can be installed in any position. If a problem arises with a cavity it can "easily" be replaced. The cavity is tuned by elastic deformation, by pulling on a harness using stainless-steel cables that are wound around a shaft. A stepping motor, fixed to the outside of the cryostat, drives the shaft. The motor therefore works in normal ambient conditions and can be easily accessed for maintenance or repair.

Each cryomodule has a single inlet for liquid helium and a single outlet for the helium evaporated by static and dynamic losses. The level is regulated by the input valve using feedback from superconducting wire level gauges in the cryomodule. The static losses are 150 W per module. At nominal field the RF losses are 100 W and at twice the nominal field 800 W per module, making the total losses 250 W and 950 W, respectively. For operation at nominal field the pressure inside the helium tank has to be carefully controlled to avoid frequency variations of the cavity, the sensitivity being an appreciable 150 Hz/mbar. The maximum excursion around the nominal value of 1350 mbar has been fixed to ±15 mbar. The operation of the cavities will be critical from the point of view of safety: They have been designed to withstand a maximum pressure of 2 bar and will be connected to the QRL line D in which pressure can rise to up to 20 bar if magnets quench. A pressure switch will therefore close the output valve if the pressure is above 1500 mbar.

The 400 MHz superconducting RF cavities have three different and independent types of vacuum systems: for the cavity, the secondary beam and the cryostat. The cavities are pumped at room temperature by two 60 l/s ion pumps mounted at each end of the RF modules. At 4.5 K, an additional huge pumping speed of more than 300,000 l/s, for hydrogen, comes from the cryogenic pumping of the cavity walls. The background pressure, without RF, will be very low and not measurable using the Penning gauges ($<10^{-12}$ mbar). Pressure signals provided for RF control are a hardware interlock from the ion pumps to cut the high voltage and readout from the Penning gauges, one per coupler, to limit the RF power, for example during conditioning. Signals for vacuum control come from both Pirani and Penning gauges mounted on the pumping ports. The cavity vacuum can be isolated by two all-metal valves at the ends of each module, to maintain vacuum during transport and installation. Due to the size of the cryostat, the second beam has to pass in its own vacuum tube through the cryostat insulation vacuum. The chambers are made of

Figure 4.2: Four-cavity module during assembly.

stainless steel tube (ID 67 mm, 1.5 mm thick), coated by electro-deposition with a copper film 1 mm thick to give low impedance, and then coated with NEG to reduce the pressure and avoid electron cloud effects. The insulation vacuum is less demanding in terms of pressure, the modules being pumped to 10^{-3} mbar before being cooled down. When cold, the insulation vacuum also benefits from the cryogenic pumping of the cold surfaces and the operating pressure will decrease to 10^{-7} mbar. Turbo molecular pumps are used and pressures are measured using Penning and Pirani gauges.

A maximum of 4800 kW of RF power will be generated by sixteen 300 kW 400 MHz klystrons. Each klystron will feed, via a Y-junction circulator and a WR2300 (half height) waveguide line, a single-cell SC cavity. The average waveguide length will be about 22 m. The klystrons, the circulators and loads, the HV interface bunkers and the control racks will be located on the ground floor of the UX45 cavern, approximately 6 m below the level of the beam lines. The klystrons have been developed by a European company, according to CERN specifications. The main operating parameters at the rated output power are shown in table 4.2. Most auxiliary equipment for the klystrons has been recuperated from the LEP RF system, modified where necessary. This includes the power supplies for the focusing coils, the power supplies for the klystron vacuum pumps, the 200 W solid-state RF driver amplifiers and the arc detectors.

Each klystron will be protected against reflections by a three-port junction circulator. To ensure stable klystron operation a temperature control system will automatically adjust the circulator's magnetic field to compensate for the ferrite temperature variations, keeping optimum input matching and isolation at all forward power levels. For better performance and to reduce size, 330 kW ferrite loaded waveguide absorbers will be used as the port 3 terminations, instead of water-loads. Other advantages of these ferrite loads are higher bandwidth and low variation in reflected phase with absorbed power.
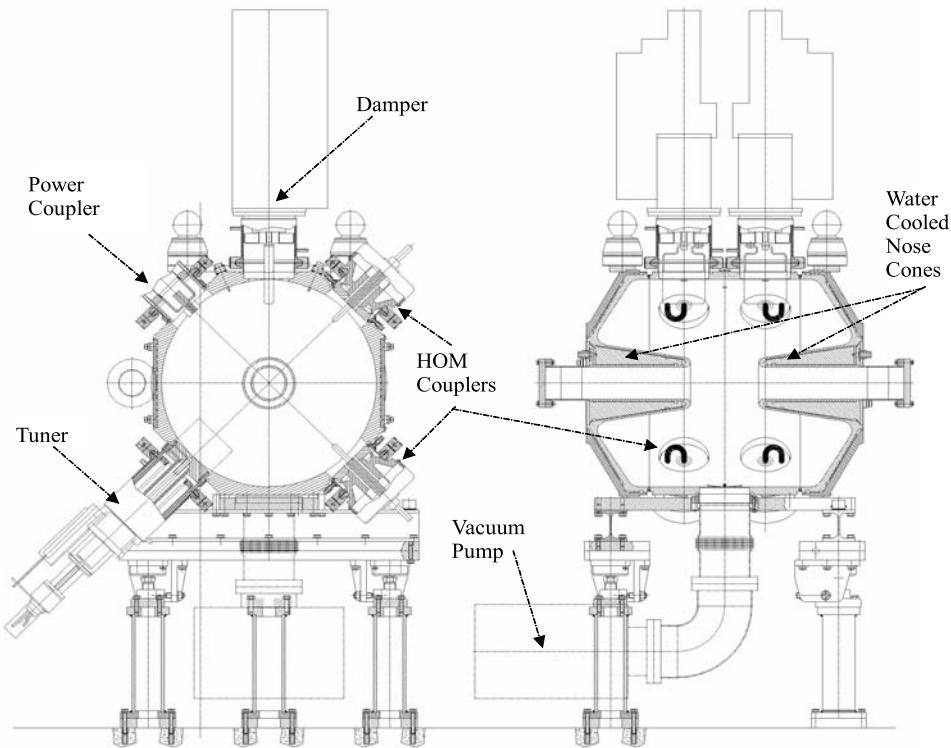
Table 4.2: Characteristics of the RF power equipment.

Klystron:	
Output power	300 kW
Operating frequency f_0	400.8 MHz
DC to RF conversion efficiency	$\geq 62\%$
Operating voltage	≤ 54 kV
Maximum beam current	9 A
Gain	≥ 37 dB
Group Delay at $f_0 \pm 1$MHz and 1 dB below rated output power	≤ 120 ns
1 dB bandwidth	$\geq \pm 1$ MHz
Circulator:	
Operating frequency f_0	400.8 MHz
Type	3-port junction circulator
Ports	WR2300 half-height waveguide
Maximum CW forward power	300 kW
Maximum CW reflected power	330 kW, at any phase
Insertion loss at rated forward power	$\leq$ -0.1 dB
Isolation:	
a) within frequency range $f_o \pm 0.25$ MHz	$\leq$ -28 dB
b) within frequency range $f_o \pm 12$ MHz	$\leq$ -20 dB
Group delay at $f_o \pm 0.25$ MHz	≤ 30 ns

4.3 Staged 200 MHz Capture System (ACN)

If the injected bunch emittance from the SPS approaches 1 eVs, the resulting bunch length given by the maximum available voltage in the SPS, combined with the phase and energy errors expected, leads to unacceptable losses from the 400 MHz buckets in the LHC. Various schemes to cope with this have been studied: more voltage in the SPS, or a higher harmonic RF system in the SPS etc. but the solution retained is a separate 200 MHz capture system in the LHC. Studies and simulations [26] have shown that by installing 3 MV/beam, capture losses can be significantly reduced. Again transient beam-loading is the major issue and determines the installed power of 300 kW per cavity. A full RF system using four standing-wave cavities has been designed, space has been reserved at Point 4, basic civil engineering work has been undertaken and a complete power chain for one cavity will be tested, but due to the significant improvements in the longitudinal emittance of the beam from the SPS the 200 MHz system will not be installed in the machine for initial commissioning.

The 200 MHz standing-wave cavity design is based on the SPS SWC cavities, see figure 4.3. The nominal frequency is 200.210 MHz. The main constraints on the design were the reduced diameter imposed by the 420 mm separation between the two beams and the necessity of keeping essential monopole HOM frequencies away from multiples of the 40 MHz bunch frequency. These

Figure 4.3: ACN 200 MHz cavity mounted on its support.

constraints result in slightly higher shunt impedance and lower quality factor. With $R/Q = 192\ \Omega$ and $Q_0 = 30'000$ the power dissipated at a nominal field of 0.75 MV is 69 kW. Particular attention was therefore paid to the design of the cooling channels to evacuate this large amount of power. Components such as the four HOM couplers, the tuner (200 kHz range) and the two fundamental mode dampers will be recuperated from the SPS SWC cavities and refurbished. A new power coupler, based on the new SPS TWC one, will be used.

4.4 Transverse damping and feedback system (ADT)

The LHC transverse feedback system (ADT) combines three principal functions: it damps transverse injection errors, prevents transverse coupled bunch instabilities (dipole modes) and can excite transverse oscillations for beam measurements [27]. There are four independent systems, one per plane and per ring. Each system comprises two modules, each consisting of two kicker units. Each kicker unit has one power amplifier with two tetrodes installed directly under the kicker vacuum tank. The horizontal kickers and power amplifiers for ring 1 are installed left of the IP4 and the vertical kickers and power amplifiers for ring 1 are to the right. The installation for ring 2 is asymmetric with respect to ring 1. Kickers and power amplifiers of ring 2 are interleaved with those of ring 1. This arrangement optimizes the beta functions to maximize kick strength. Space has been left for a future upgrade of one extra module per ring and plane to boost the total system capability by 50%. The systems work in base band, from below 3 kHz up to > 20 MHz.

4.5 Low-level RF

The low-level RF system comprises four sub-systems, the Cavity Controller, the Beam Control, RF Synchronization and the Longitudinal Damper. It also uses the longitudinal pickups (APW). The system described below is for the 400 MHz RF system. The requirements for the low level of the 200 MHz system are similar in many respects and the design will closely follow this system. There is one cavity controller for each individual cavity. It has two main functions; to provide adequate control of the phase and amplitude of the voltage in the cavity and to keep the power demanded at acceptable levels. To achieve this it comprises a number of separate loops, see figure 4.4. The Klystron Polar Loop keeps the gain and phase constant from the RF modulator input to the cavity main coupler input. It compensates the large change in phase shift when the klystron beam voltage is changed ($\sim$30°/kV), the smaller phase shift variation with circulator temperature and the gain and phase modulation caused by power supply ripples (50 Hz, 600 Hz), on the power supply ($\sim$ 35° RF peak to peak measured on the second klystron). The loop bandwidth is approximately 1 kHz. The RF Feedback Loop reduces the effects of the cavity impedance by compensating variations in the beam-induced voltage. The loop delay is $\sim$ 650 ns. A 20 dB impedance reduction (open loop gain of 10) is specified at the exact RF frequency, reducing to zero at 1 MHz. The 1-Turn Feed-forward loop provides an extra 10-15 dB reduction of the beam loading at the RF frequency. In addition, a 1-Turn Feedback provides 20 dB gain on the revolution frequency sidebands to control transient effects. It reduces the impedance in a band extending to $\sim$1 MHz on each side of the RF frequency. The Tuner Loop maintains a given phase between incident power and cavity field. It has to be controlled in such a way that power transients due to the passage of batches and gaps are minimised (half-detuning). The Set Point defines the desired voltage in the cavity. It should ideally be constant. However, some bunch-to-bunch variation is allowed as a compromise between an ideal voltage and the ability of the klystron to deliver transient power spikes. In addition to this function, the Set Point module also injects the drive from the Longitudinal Damper.

All signals used in the loops are logged in two different memories, one for observation and one for post-mortem. For slow signals 6 s of data are kept with one sample/100 μs, whereas fast signals are logged at a rate of 40 MHz to observe the effects on each bunch, the last ten turns ($\sim$1 ms) being stored. In addition a base band network analyzer is included: an arbitrary function can be injected into the loops and the corresponding outputs at various points enable the transfer function to be obtained, as is done in PEPII [27]).
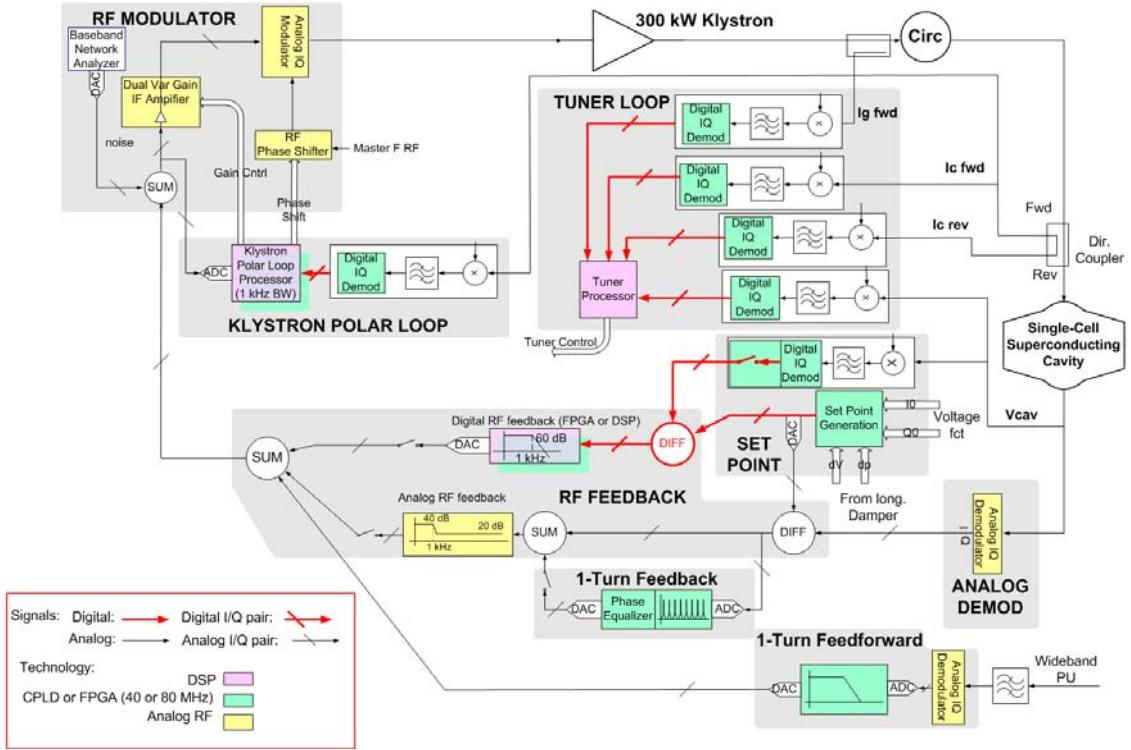
Figure 4.4: The cavity controller (one per cavity).

Chapter 5

Vacuum system

5.1 Overview

The LHC has three vacuum systems: the insulation vacuum for cryomagnets, the insulation vacuum for helium distribution (QRL), and the beam vacuum. The insulation vacua before cool-down do not have to be better than 10^{-1} mbar, but at cryogenic temperatures, in the absence of any significant leak, the pressure will stabilise around 10^{-6} mbar. The requirements for the beam vacuum are much more stringent, driven by the required beam lifetime and background at the experiments. Rather than quoting equivalent pressures at room temperature, the requirements at cryogenic temperature are expressed as gas densities normalised to hydrogen, taking into account the ionisation cross sections for each gas species. Equivalent hydrogen gas densities should remain below 10^{15} H$_2$ m^{-3} to ensure the required 100 hours beam lifetime. In the interaction regions around the experiments, the densities will be below 10^{13} H$_2$ m^{-3} to minimise the background to the experiments. In the room temperature parts of the beam vacuum system, the pressure should be in the range 10^{-10} to10^{-11} mbar.

All three vacuum systems are subdivided into manageable sectors by vacuum barriers for the insulation vacuum and sector valves for the beam vacuum. Sector lengths are 428 m in the QRL and 214 m for the magnet insulation vacuum. The beam vacuum is divided into sectors of various lengths, in most cases the distance between two stand-alone cryomagnets. However, there are no sector valves in the cold arc, leading to a length for this single sector of approximately 2'900 m.

A number of dynamic phenomena have to be taken into account for the design of the beam vacuum system. Synchrotron radiation will hit the vacuum chambers, in particular in the arcs; and electron clouds (multipacting) could affect almost the entire ring. Extra care has to be taken during the design and installation to minimise these effects, but conditioning with beam will be required to reach nominal performance.

5.2 Beam vacuum requirements

The design of the beam vacuum system takes into account the requirements of 1.9 K operation and the need to shield the cryogenic system from heat sources, as well as the more usual constraints

Table 5.1: The nuclear scattering cross sections at 7 TeV for different gases and the corresponding densities and equivalent pressures for a 100 h lifetime.

GAS	Nuclear scattering cross section(cm^2)	Gas density (m^{-3}) for a 100 hour lifetime	Pressure (Pa) at 5 K, for a 100 hour lifetime
H_2	$9.5 \ 10^{-26}$	$9.8 \ 10^{14}$	$6.7 \ 10^{-8}$
He	$1.26 \ 10^{-25}$	$7.4 \ 10^{14}$	$5.1 \ 10^{-8}$
CH_4	$5.66 \ 10^{-25}$	$1.6 \ 10^{14}$	$1.1 \ 10^{-8}$
H_2O	$5.65 \ 10^{-25}$	$1.6 \ 10^{14}$	$1.1 \ 10^{-8}$
CO	$8.54 \ 10^{-25}$	$1.1 \ 10^{14}$	$7.5 \ 10^{-9}$
CO_2	$1.32 \ 10^{-24}$	$7 \ 10^{13}$	$4.9 \ 10^{-9}$

set by vacuum chamber impedances. Four main heat sources have been identified and quantified at nominal intensity and energy:
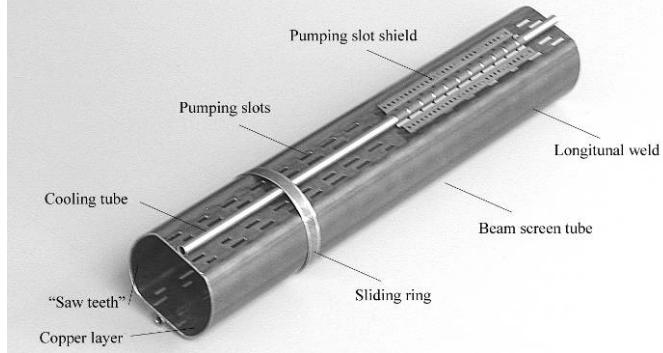
- Synchrotron light radiated by the circulating proton beams (0.2 W m^{-1} per beam, with a critical energy of about 44 eV);

- Energy loss by nuclear scattering (30 mW m^{-1} per beam);

- Image currents (0.2 W m^{-1} per beam);

- Energy dissipated during the development of electrons clouds, which will form when the surfaces seen by the beams have a secondary electron yield which is too high.

Intercepting these heat sources at a temperature above 1.9 K has necessitated the introduction of a beam screen. The more classical constraints on the vacuum system design are set by the stability of the beams, which sets the acceptable longitudinal and transverse impedance [29, 30], and by the background conditions in the interaction regions.

The vacuum lifetime is dominated by the nuclear scattering of protons on the residual gas. The cross sections for such an interaction at 7 TeV vary with the gas species [31, 32] and are given in table 5.1, together with the gas density and pressure (at 5 K) compatible with the requested 100 hour lifetime. This number ensures that the contribution of beam-gas collisions to the decay of the beam intensity is small as compared to other loss mechanisms; it also reduces the energy lost by scattered protons in the cryomagnets to below the nominal value of 30 mW m^{-1} per beam.

5.3 Beam vacuum in the arcs and dispersion suppressors

The two beams are confined in independent vacuum chambers from one end of the continuous cryostat to the other, extending from Q7 in one octant to Q7 in the next octant. Cold bores with an inner diameter of 50 mm, part of the cryomagnets, are connected together by so-called cold-interconnects which compensate length variations and alignment errors. A beam position monitor, with an actively-cooled body, is mounted on each beam in each SSS (i.e. at each quadrupole). An actively-cooled beam screen is inserted into the cold bore of all magnets, connection cryostats and shuffling modules containing the current leads.

Figure 5.1: Conceptual design of the LHC beam screen.
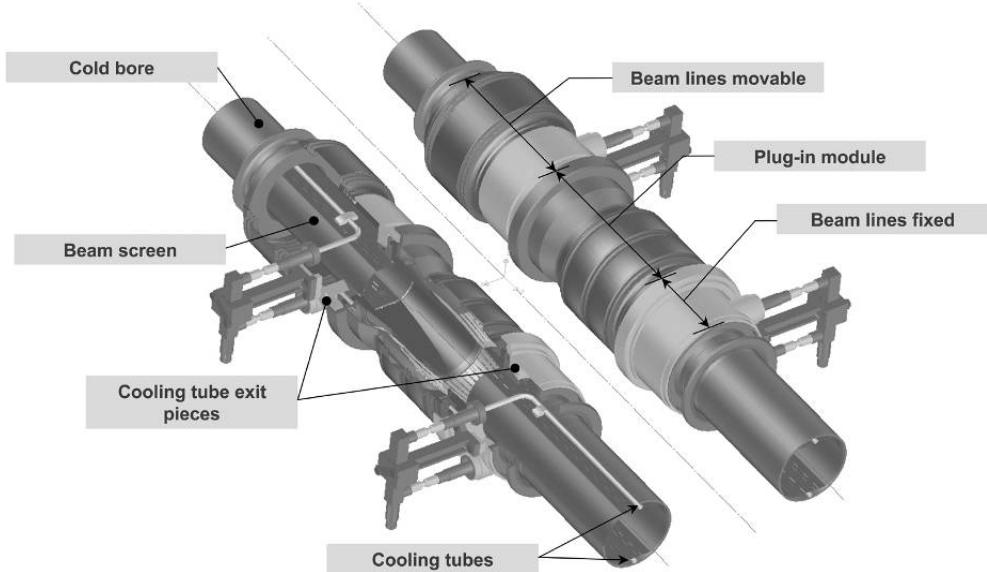
5.3.1 Beam screen (figure 5.1)

A racetrack shape has been chosen for the beam screen, which optimises the available aperture while leaving space for the cooling tubes. The nominal horizontal and vertical apertures are 44.04 mm and 34.28 mm, respectively. Slots, covering a total of 4% of the surface area, are perforated in the flat parts of the beam screen to allow condensing of the gas on surfaces protected from the direct impact of energetic particles (ions, electrons and photons). The pattern of the slots has been chosen to minimise longitudinal and transverse impedance and the size chosen to keep the RF losses through the holes below 1 mW m^{-1}. A thin copper layer (75 μm) on the inner surface of the beam screen provides a low resistance path for the image current of the beam. A saw-tooth pattern on the inner surface in the plane of bending helps the absorption of synchrotron radiation.
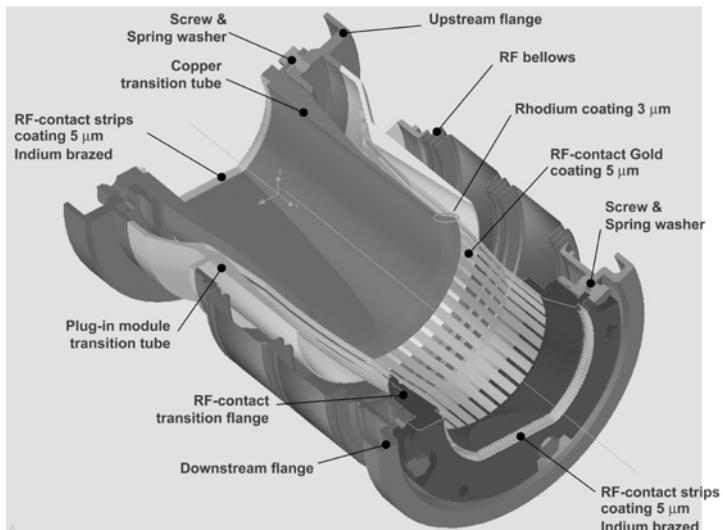
The beam screen is cooled by two stainless steel tubes with an inner diameter of 3.7 mm and a wall thickness of 0.53 mm, allowing for the extraction of up to 1.13 W/m in nominal cryogenic conditions. The helium temperature is regulated to 20 K at the output of the cooling circuit at every half-cell, resulting in a temperature of the cooling tubes between 5 K and 20 K for nominal cryogenic conditions. The cooling tubes are laser welded onto the beam screen tube and fitted at each end with adaptor pieces which allow their routing out of the cold bore without any fully penetrating weld between the helium circuit and the beam vacuum. Sliding rings with a bronze layer towards the cold bore are welded onto the beam screen every 750 mm to ease the insertion of the screen into the cold bore tube, to improve the centering and to provide good thermal insulation. Finally, since the electron clouds can deposit significant power into the cold bore through the pumping slots, the latter are shielded with copper beryllium shields clipped onto the cooling tubes. The net pumping speed for hydrogen is reduced by a factor of two, which remains acceptable.

5.3.2 Cold interconnects (figures 5.2 and 5.3)

Beam vacuum interconnects ensure the continuity of the vacuum envelope and of the helium flow, as well as a smooth geometrical transition between beam screens along the 1'642 twin aperture superconducting cryomagnets installed in the continuous cryostat. The physical beam envelope must have a low electrical resistance for image currents and minimise coupled bunch instabilities [29]. It must also have a low inductance for the longitudinal single-bunch instability. The maximum DC
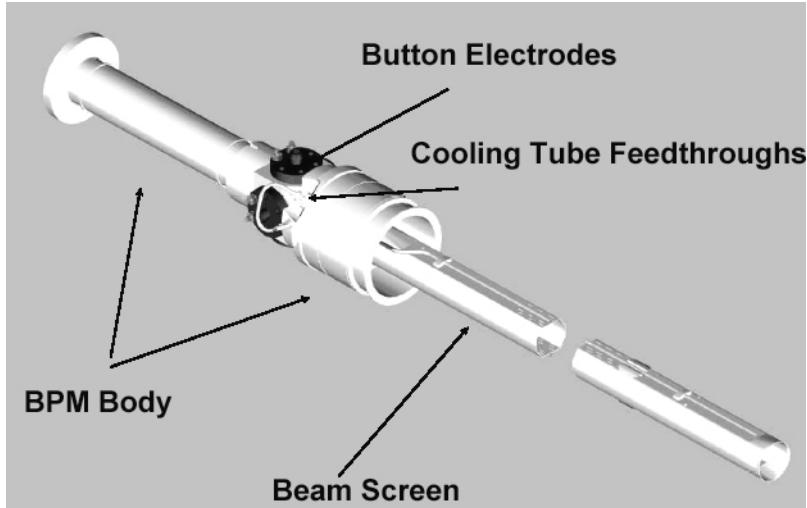
Figure 5.2: Layout and components of the interconnects for the LHC arc beam vacuum.

Figure 5.3: Details of the interconnect "plug-in module".

resistance allowed at room temperature for a complete interconnect is 0.1 mΩ. In order to meet these requirements, a complex interconnect module integrates a shielded bellows to allow thermal expansion, as well as for compensation of mechanical and alignment tolerances between two adjacent beam screens. The shielding of the bellows is achieved by means of a set of sliding contact fingers made out of gold-plated copper-beryllium, which slide on a rhodium-coated copper tube.

Figure 5.4: Principal layout of an arc beam position monitor.

5.3.3 Beam position monitor bodies and supports (figure 5.4)
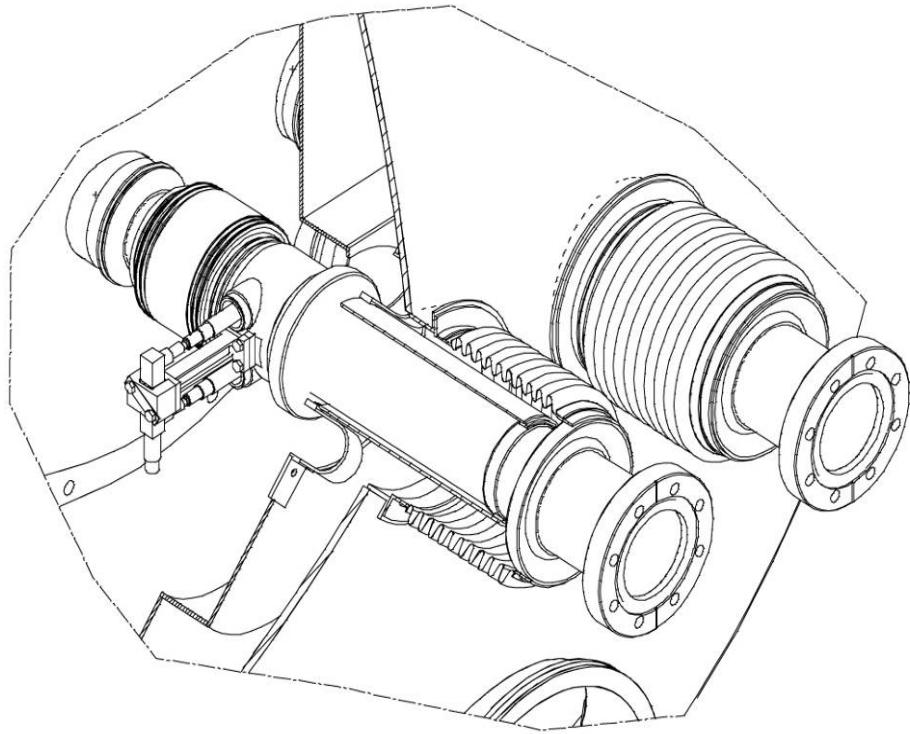
A beam position monitor (BPM) equipped with four button electrodes is installed on each beam in every short straight section in the continuous cryostat of the arc. In a few places, a strip-line monitor replaces the button type. The body holding the electrode, and the connecting "drift length" to the cold bore, form an integral part of the beam vacuum chamber, by extending the cold bores of the quadrupole magnets. The BPM body is actively cooled in series with the beam screen. A thin copper layer (100 μm) is electrodeposited on both the BPM body and the support to ensure low DC resistance and uniform cooling over the drift length.

5.4 Beam vacuum in the insertions

Room temperature chambers alternate with stand-alone cryostats in the IRs. The room temperature part includes beam instrumentation, accelerating cavities, experiments, collimation equipment, and the injection and ejection kickers and septa, as well as some of the dipole and quadrupole magnets where superconducting elements are not used. In these regions, the vacuum systems for the two beams sometimes merge, notably in the four experimental insertions, but also in some special equipment like the injection kickers and some beam stoppers.

5.4.1 Beam screen

The beam screen is only required in the cold bores of the stand-alone cryostats. It is derived from the arc type, but uses a smaller (0.6 mm) steel thickness and comes in various sizes, to match different cold bore diameters. The orientation of the beam screen in the cold bore is adapted to the aperture requirements, which means that the flat part with the cooling tubes can be either vertical or horizontal. The saw-tooth structure has been abandoned for these beam screens, since synchrotron radiation hitting the screen in these regions is at least ten times less intense than in the arc, and because fitting the saw teeth at the appropriate location of the beam screen would be too expensive.

Figure 5.5: Details of a cold-to-warm transition.

5.4.2 Cold interconnections and Cold-Warm Transitions

The required interconnections between multiple magnets in a single stand-alone cryostat (e.g. the inner triplet) are based on the design of the arc type. In some cases, however, they not only have to compensate for thermal expansion and minor alignment errors, but also for beam separation and cold bore diameter transitions in the adjacent beam pipes. Other complications come from the beam screens that are rotated by 90° in some locations as compared to the arc, and the occasional need to integrate pumping ports into interconnects, leading to non-standard solutions. The combined interface variations result in 24 different interconnect assemblies to be used in the 278 cold beam vacuum interconnects of the DS sections and LSSs.

A cold-to-warm transition (CWT) has to be installed for the beam vacuum tubes at the end of every cryostat (figure 5.5) as an interface between the cryogen-cooled beam pipes and the room temperature beam pipes. Each circulating beam will pass 108 CWTs per turn (superconducting cavities excluded). In total there will be 200 individual CWTs, taking into account that most elements have two apertures. The CWT compensates for the longitudinal and transverse thermal displacements of the cold bores and beam screens with respect to the insulation vacuum end cover. It also allows the differential thermal displacements between the beam screen and the cold bore. The design of the CWT is a compromise between beam impedance and thermal impedance requirements. The heat load to be intercepted by the thermal anchor at 100 K is less than 6 W per CWT, while the static heat load to the 20 K level must remain below 2.5 W per CWT (1.3 W by thermal radiation and 1.2 W by thermal conduction).

5.4.3 Room temperature beam vacuum in the field free regions

The baseline for the room temperature beam vacuum system is to use 7 m long OFS copper chambers, with an inner diameter of 80 mm and fitted with standard DN100 Conflat^{TM} flanges. The thickness of the copper is 2 mm, and the chambers are coated with TiZrV non evaporable getter (NEG) [33]. After activation at low temperature (200°C), the getter provides distributed pumping and low outgassing to maintain a low residual gas pressure, as well as a low secondary electron emission yield to avoid electron multipacting. The chambers are connected by means of shielded bellows modules, some of them including pumping and diagnostic ports.

5.4.4 Beam vacuum in room temperature magnets

A number of room-temperature magnets, most of them located in the cleaning insertions around Points 3 and 7, will be equipped with extruded OFS copper chambers, with either elliptic or circular cross-sections, and fitted with standard DN100 Conflat^{TM} flanges. The thickness of the copper is 2 mm, and the chambers are NEG coated. The MBXW (also referred to as D1) chambers are an exception, in so far as they have a wall thickness of 3 mm and are fitted with DN150 flanges.
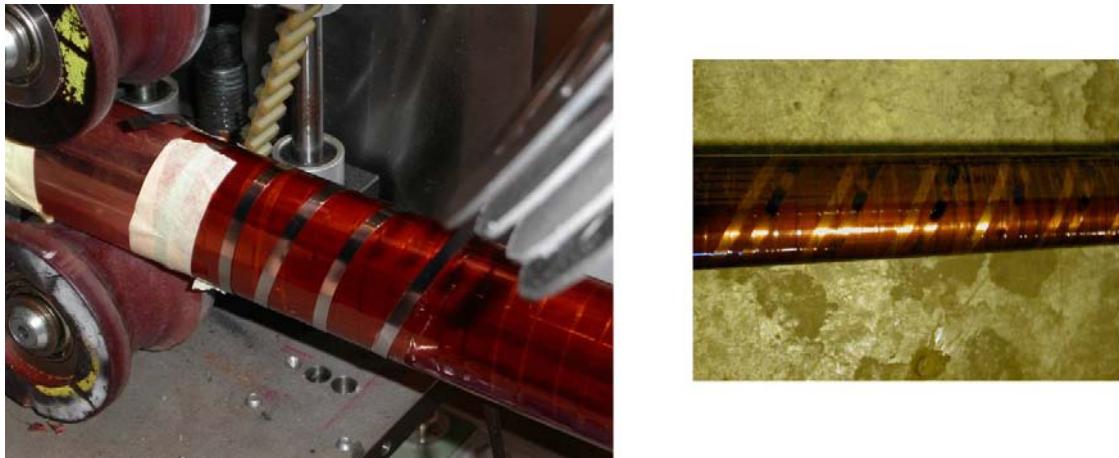
5.4.5 Bake-out and NEG activation

The required pressures in the insertion regions, and the need to activate the NEG coating, call for a bakeout system able to heat every component to 250°C (300°C for uncoated chambers). The baseline is to have mobile heating and regulation equipment. However, in the many highly radioactive areas around the ring, permanently installed heating equipment may become mandatory to reduce the radiation dose to personnel during maintenance activities.
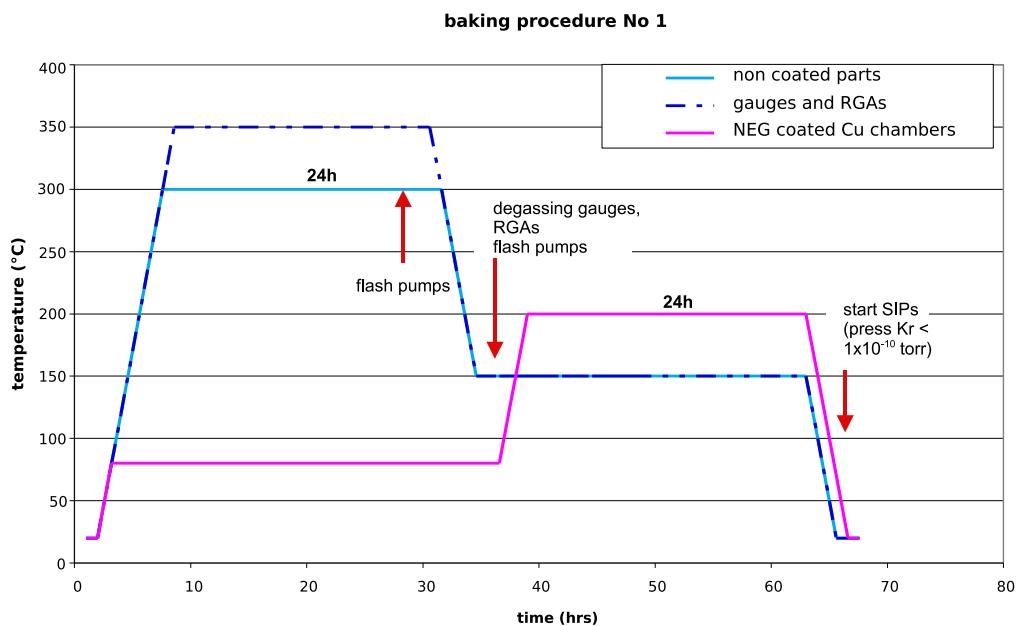
For the standard chambers, classical methods, like heating tapes and insulation shells are likely to be the cheapest for permanently installed equipment, heating jackets can be used for removable heating equipment. Although more expensive than tapes, jackets are much more robust when it comes to mounting and demounting them. They also need significantly less manpower.

For the chambers in room temperature magnets, an original concept of a wound sandwich made out of stainless steel as heating elements and polyimide foils as insulation material has been developed and validated, see figure 5.6. This technique allows the space required for heating and insulation to be reduced to typically 0.3 mm. Aluminising the top layer of the polyimide further reduces the radiated power. A considerable cost reduction can be obtained compared to using coaxial heaters.

The proposed bakeout sequence is optimised to take into account the NEG activation. In the first part of the bakeout cycle, all non-coated elements will be heated to 300°C (gauges and gas analysers to 350°C) for 24 hours, while the coated parts are left at 80°C to prevent absorption of water without an early activation of the NEG. The temperature of the non-coated parts is then reduced to 150°C and 24 hours of NEG activation at 200°C can start. The whole process (figure 5.7) takes about 65 hours.

Figure 5.6: Wrapping of the stainless steel strips as bakeout heaters and a close up view of a finished chamber before the addition of the aluminised layer.
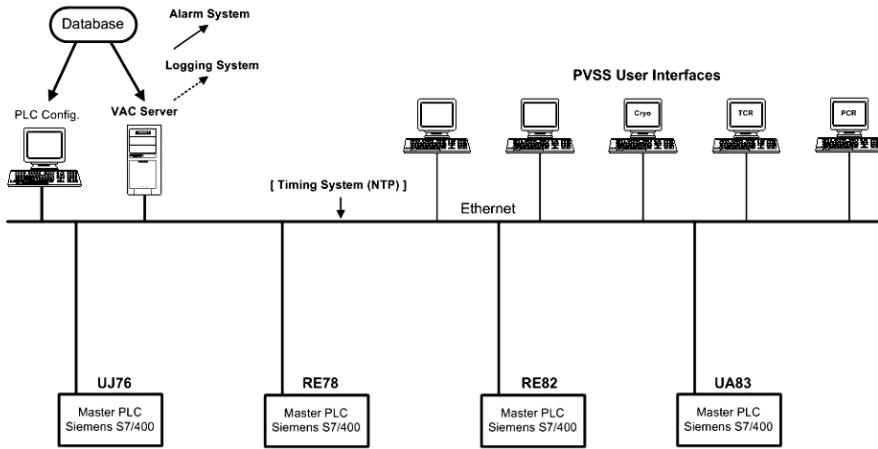
Figure 5.7: Proposed bakeout cycle with NEG activation.

5.5 Insulation vacuum

The insulation vacuum includes the magnet cryostats and the QRL, see table 5.2. Vacuum barriers at the jumper connections maintain separation of the two systems, however, longitudinal vacuum barriers can be by-passed. The configuration of the insulation vacuum barriers and cryogenic circuits permit warming of individual machine cells. The insulation vacuum is characterised by the large volumes that need to be pumped and the large amount of multilayer reflective insulation (MLI), which introduces a high gas load. This requires high-capacity mobile pumping groups ($64 \text{ m}^3 \text{ h}^{-1}$) and an appropriate strategy for leak detection to provide an acceptable pump-down time.

Table 5.2: Main characteristics of the insulation vacuum sectors.

	Cryomagnet	QRL
Volume (m^3)	80	85
Length (m)	214	428
MLI (m^2/m)	200	140
Sectors per arc	14	7

Figure 5.8: Architecture of the higher level of the vacuum control system, example for Sector 7-8.

5.6 Vacuum controls

The controls for the three vacuum systems are based on an industrial solution using PLCs and a central SCADA supervision system connected via Ethernet to the master PLCs (see figure 5.8).

A Profibus^{TM} link is used to connect slave PLCs and mobile equipment to the master PLCs. The slave PLCs control off-the-shelf or CERN developed hardware control crates, which are hard-wired to pumps, gauges and valves in the tunnel. In order to minimise the cabling costs, signal and control wires are grouped into large multicore cables and locally dispatched to the equipment via junction boxes. Most of the control equipment is located in radiation free areas, such as the alcoves. However, the gauges in the arcs are supplied by local equipment situated in areas where the expected annual dose remains below 10 Gy per year.

Extensive tests have been performed in the North Area of the SPS on the radiation resistance of commercially available vacuum control equipment. Based on these tests and on the requirement to minimise the cables, the power supplies for the cold cathode gauges can be bought from industry, while those for the Pirani gauges have been developed in-house. The turbo-molecular pumps needed for the insulation vacuum can also be supplied by industry.

One specific requirement of the vacuum control system is the requirement to dynamically reconfigure the layout. This is a consequence of using mobile pumping and diagnostic equipment. It must be possible to detect equipment when it is connected or disconnected from the Profibus^{TM} link, without having to manually update a database. A prototype link with mobile equipment has been successfully tested in the laboratory. The general architecture and the SCADA program have been operational in the SPS since 2002, thus validating the concept.

Chapter 6

Powering and protection

6.1 Overview

A very large number of superconducting and normal conducting magnets will be installed in the LHC, and most magnets of a given type in the same sector will be powered in series families. In total, the LHC will have 1'612 different electrical circuits for superconducting and normal conducting magnets. To limit the stored magnetic energy and the voltages that will be experienced during energy extraction (a quench), magnet families do not extend over more than one sector. In most cases, however, the stored energy is still sufficient to damage superconducting magnets, and hence a sophisticated protection system is essential.
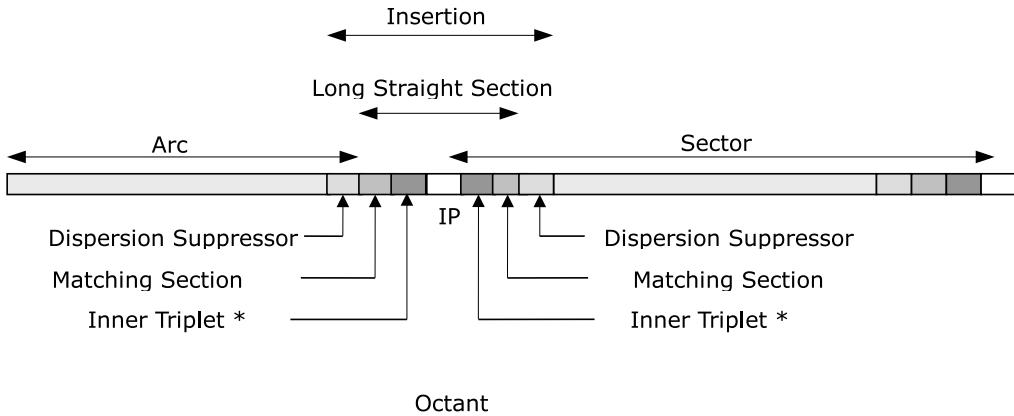
6.2 Powering circuits

The LHC magnets are powered in eight independent and symmetric sectors (see figure 6.1). Within these sectors, more than 40 different cryostats house the superconducting magnets, while the normal conducting magnets are located in the LSSs close to the IPs (except for IP 4, where there are no normal conducting magnets). The higher radiation levels in the cleaning insertions (IR3 and IR7) and around experiments with high luminosity (IP2 and IP8) prevent the use of superconducting magnets. Here normal conducting magnets are employed. Eight long arc cryostats span the major part of the circumference and contain the main bending and focusing magnets. Smaller cryostats located around the interaction points house magnets that are specifically required for each insertion.

The total of 1'612 electrical circuits is composed of 131 types, connecting main bending magnets, magnets for beam focusing, dipole field correctors, or higher order correctors. Some types appear in each of the eight sectors (e.g. the main dipole circuit), while others are only present in dedicated insertions (as, for example, a warm compensator for the ALICE experiment). The detailed description of this complex electrical system is available in the LHC Reference Database [34], which also contains the connection information for all 1'612 electrical circuits.

The eight sectors have been subdivided into 28 powering sub-sectors of four different types, as shown in figure 6.2.

- 8 Arc Powering Sub-sectors, containing all powering equipment related to magnets in the arc cryostats.

Figure 6.1: Sectors and octants in the LHC.
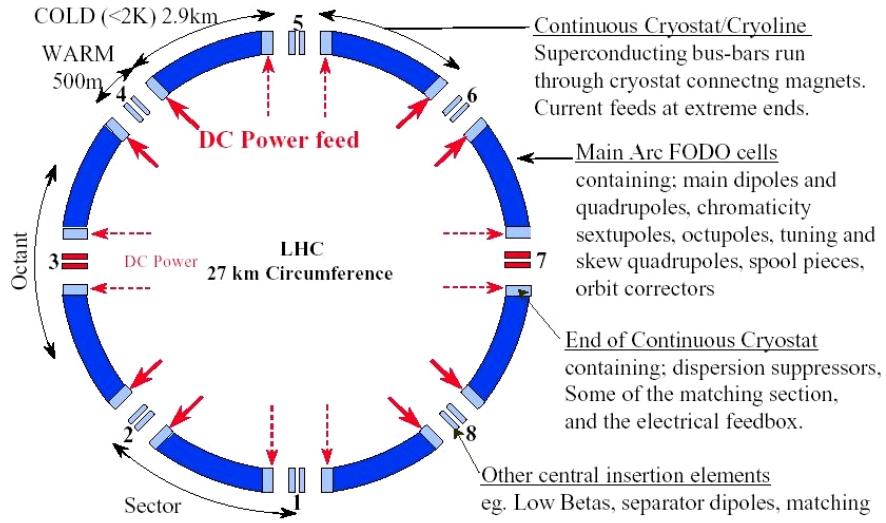
- 8 Powering Sub-sectors for powering of the inner triplet cryostats, housing the magnets for Q1 to Q3 for the insertions with physics experiments and additionally D1 in the insertions 2 and 8.

- 12 Powering Sub-sectors to power magnets in smaller cryostats in the matching sections, containing individually powered quadrupoles and separation and combination dipoles.

- 7 Powering Sub-sectors for powering of normal conducting magnets left and right of an IP.

Every electrical circuit and the associated electrical components in the LHC tunnel is allocated to a Powering Sub-sector. As such, the powering in each of the powering sub-sectors is independent of the powering of the other sub-sectors.
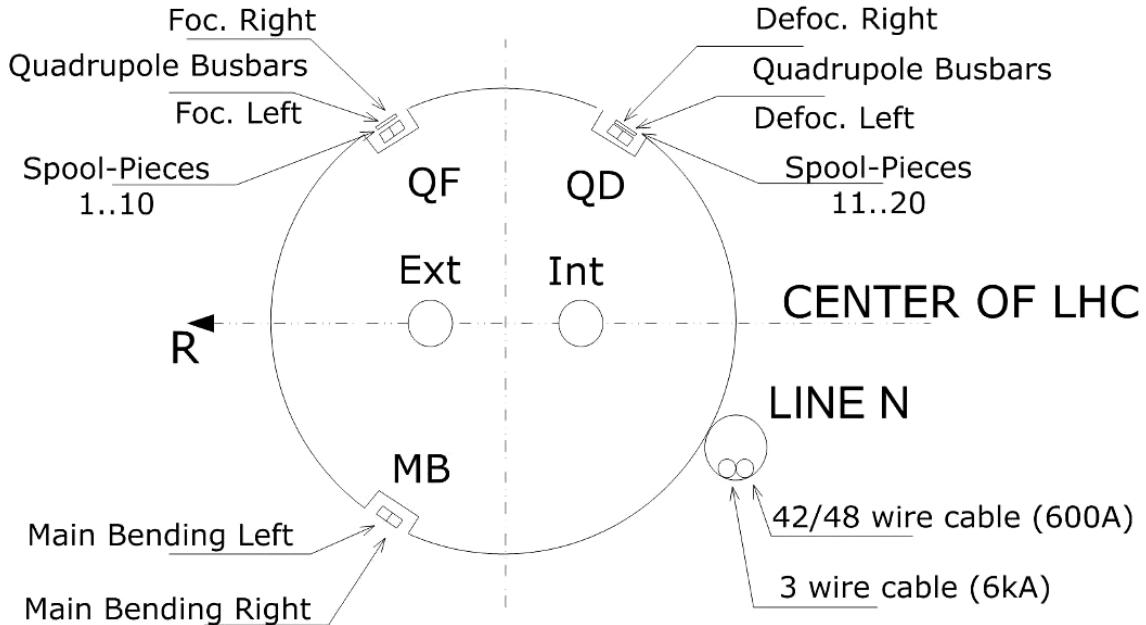
Each of the eight symmetrical LHC sectors will contain one electrical circuit (called RB), connecting all main bending magnets in series. The main quadrupoles are powered in each sector in two electrical circuits (RQF and RQD) dedicated to focusing and defocusing the two beams. The power converters for these three main circuits in each of the eight sectors are located in an underground area (UA) close to the even insertion regions. The currents enter the cryostat through a nearby DFBA feedbox. The stored energy in these circuits amounts to 1.22 GJ for the main dipole[1] and 20 MJ for each of the main quadrupole circuits. For the main dipole circuit an energy extraction system (consisting of a high current switch in parallel with the extraction resistor) is placed on either side of the arc cryostat, while only one system for either of the quadrupole circuits is sufficient. Figure 6.2 illustrates the powering layout for the eight long arc cryostats.

A number of higher-order correctors are installed in every dipole assembly in the long arc cryostat to compensate the field errors of the main dipoles. Two different types of dipole assemblies are installed alternately in the LHC arcs. In addition to the main dipole coil on each of the two beam pipes the MBA type provides a combined decapole-octupole-corrector (MCDO) at the connection side of the cryo-assembly and a sextupole corrector (MCS) at the far end of the cryo-assembly.

---

[1]At ultimate energy and using the measured value for the inductance (100 mH).

Figure 6.2: Powering of the eight arc cryostats.

Figure 6.3: Cross-section of LHC arc cryo-assembly with bus-bars.

The MBB type only contains a sextupole corrector at the far end beside the main dipole coil. All correctors of a given family are connected in series for each of the two beams. The circuit families RCS, RCO and RCD (Sextupole, Octupole and Decapole) are connected throughout the cryostat via twenty so-called spool-piece bus-bars, (grouped in bundles of five bus-bars), located on top of the two main quadrupole bus-bars (see figure 6.3).
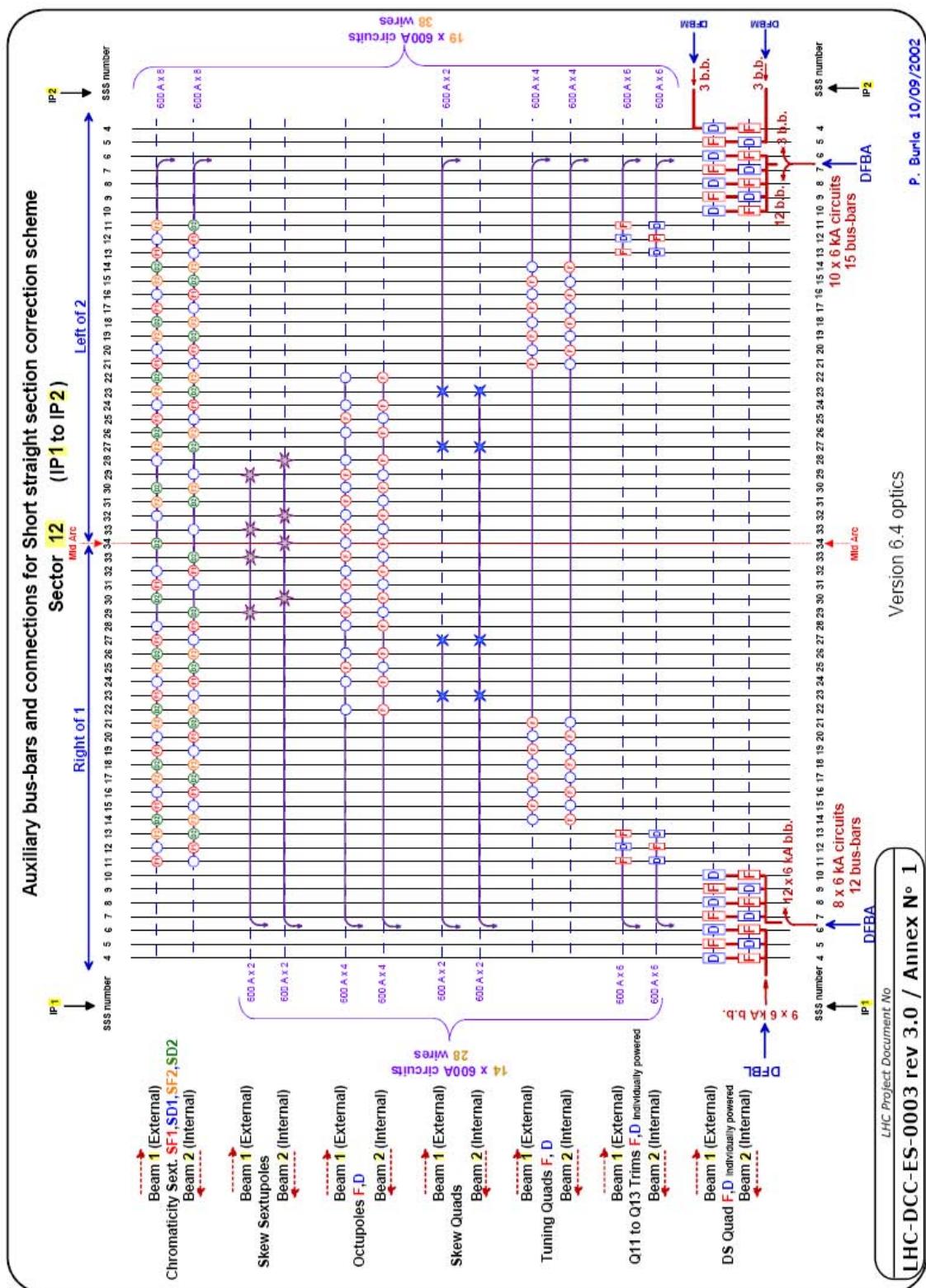
The SSSs in the LHC arcs contain two independent main quadrupole magnet coils, two higher-order corrector magnets at the upstream connection side, and two orbit corrector dipoles

Table 6.1: Correctors in the arc SSS.

Circuit Function	Families	Magnet Type	Circuit Type
Tuning Quadrupoles	2 families/arc	MQT	RQTF, RQTD
Skew Quadrupoles	In even sectors, Beam 1 & in odd sectors Beam 2: 2 families/arc	MQS	RQS
	In odd sectors, Beam 1 & in even sectors Beam 2: 1 family/arc	MQS	RQS
Chromaticity Sextupoles	4 families/arc	MS	RSF1, RSF2, RSD1, RSD2
Skew Sextupoles	1 family/arc	MSS	RSS
Octupoles	2 families/arc	MO	ROF, ROD

as well as two sextupoles at the downstream side. The orbit corrector magnets are powered with currents of up to 60 A (120 A for SSSs in the DS sections) and are connected to the power converter via current feedthroughs, mounted on a flange on the SSS service module. The correctors on the so-called "connection end" of the SSS are routed throughout the arc cryostat via a special cable, consisting of 42 (sometimes exceptionally 48) superconducting wire cables. This cable does not run through the magnets but through a special pipe (line N), which is attached to the outside of the cold masses. This special cable is connectable only in the upstream interconnection plane of each SSS in the arc (see figure 6.4). To limit the number of wires and hence the size of this cable, each wire will be used in two different electrical circuits, as shown in figure 6.4. An overview of the corrector family types in the arc SSS can be found in table 6.1.

There are also circuits (for mainly individually powered magnets) for the DS and MS regions, the normal conducting magnets in the cleaning insertions, the separation regions, experimental insertion regions including the low-beta inner triplets, and the RF insertion.

Figure 6.4: Example of the correction circuit layout (sector 12).

Figure 6.5: 13 kA CERN prototype HTS current lead.

6.3 Powering equipment

6.3.1 Current leads

For the 1'612 electrical circuits in the LHC, a total of 3'286 current leads are needed to connect the superconducting wires or cables to the power supply cables, which are at ambient temperature. The design of these leads aims at high reliability and low heat load. A total of 1'070 leads, operating between 600 A and 13 kA, incorporate a section with high-temperature superconducting (HTS) material (see figure 6.5). The higher investment costs are amply compensated by the low heat load. All other leads use copper as conductor. To feed the electrical circuits of the inner triplet magnets with up to 600 A, 112 gas cooled leads are used. The remaining 2'104 leads feed the 60 A or 120 A electrical circuits of the orbit corrector dipoles, the sextupoles of the inner triplets, and the octupole and dodecapole correctors.

6.3.2 Electrical feedboxes

The HTS current leads described above are mounted in cryogenic electrical distribution feedboxes (DFB). The limited space in the LHC tunnel requires the use of two different strategies. If the space is sufficient, the current is transferred to the arc magnets or to standalone magnets through locally installed DFBs. When the integration of a DFB close to the superconducting magnets is not possible, the magnets are powered through superconducting links (DSL) that connect the DFBs and the superconducting magnets at distances between 70 m and 500 m. There are four different types of DFBs listed in table 6.2.

Table 6.2: List of DFB and their current leads.

DFB type	Number	Type of leads (nb/DFB)
DFBA	16	13kA (2-6), 6kA (0-15), 600A (0-52), 120A(0-8)
DFBM	23	6kA (0-5), 600A(0-4), 120A(0-12)
DFBL	5	6kA (0-5), 600A(0-44), 120A(0-12)
DFBX	8	7.5kA (4-6), 600A (10), 120A (14)
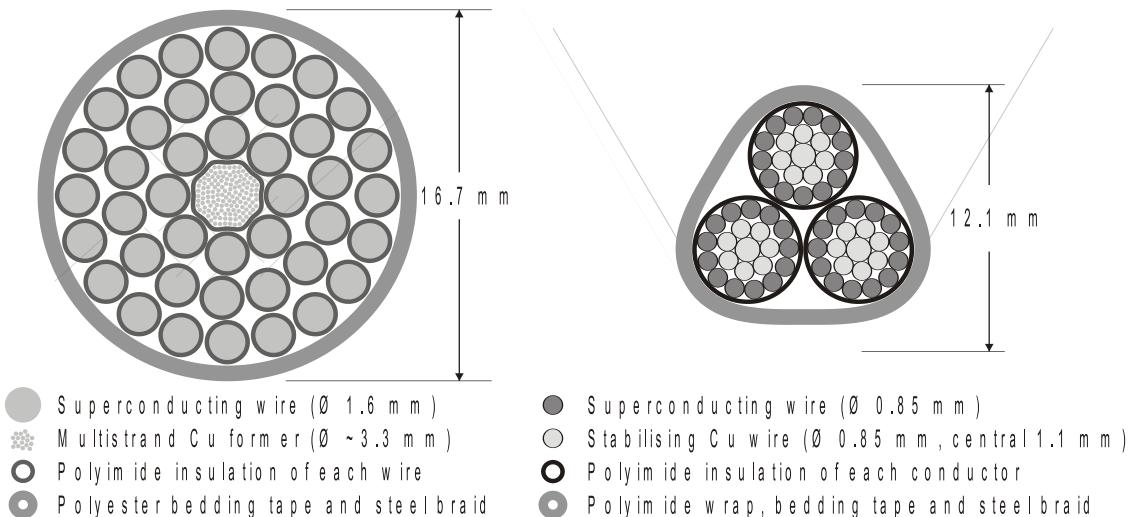
Table 6.3: DSL summary.

Name	Description
DSLA	Type-1: connects the DFBLA current feedbox located in alcove RR13 to the three magnet cryostats of Q6, Q5, and Q4D2 in the LHC main tunnel.
DSLB	Type-1: connects the DFBLB current feedbox located in alcove RR17 to the three magnet cryostats of Q6, Q5, and Q4D2 in the LHC main tunnel.
DSLC	Type-2: connects the DFBLC current feedbox located in the UJ33 alcove to the DFBAF current feedbox located in the LHC main tunnel. The routing is from the UJ33 alcove through the UP33 tunnel (about 46 m long) and then through a part of the LHC main tunnel (about 462 m long).
DSLD	Type-1: connects the DFBLD current feedbox located in alcove RR53 to the three magnet cryostats of Q6, Q5, and Q4D2 in the LHC main tunnel.
DSLE	Type-1: connects the DFBLE current feedbox located in alcove RR57 to the three magnet cryostats of Q6, Q5, and Q4D2 in the LHC main tunnel.

The DFBXs electrical distribution feedboxes provided under the USA-CERN collaboration, feed the inner triplets at Interaction Points 1, 2, 5 and 8.

6.3.3 Superconducting links

Whenever it is impossible to mount a DFB close to the magnets, the electrical current is transferred from the DFBs to the LHC magnets through superconducting links (DSL). The links carry currents in the range of 120 A to 6 kA. The nominal operating temperature ranges from 4.5 K to 6 K for the part which houses the superconducting cable and is about 70 K for the heat shielding. Five DSLs of two types will be needed in LSS 1, 3, and 5. Table 6.3 summarises the DSL with some technical details. The four type-1 DSLs are of similar design, differing only in the precise mechanical layout of their routing in the LHC tunnel. Their length is about 70 m, with two intermediate branches of about 3 m. They are located at LSS 1 and 5 on either side of the interaction points and connect a link current feedbox (DFBL) to the Q6, Q5 and Q4D2 magnet cryostats. The type-2 DSL serves as a superconducting power transmission line between two current feedboxes. It is exceptionally long, about 500 m, without any intermediate branches. It is located in Point 3 and connects the DFBLC in UJ33 to the arc current feedbox (DFBAF) on the right side of IP3. In addition to the power transmission function, it provides the cryogenics for DFBLC.

Figure 6.6: Cross sections of the 42 × 600 A cable (left) and the 3 × 6 kA cable (right).

6.3.4 Bus-bar systems

To connect the individual magnets within a family, superconducting bus-bars are used: see figure 6.3. Like the magnets, these busbars may also quench, and hence a protection is needed. There are four distinct classes of bus-bars. The high current connections are highly stabilized and quite rigid. The 600 A connections to the corrector magnets in the SSS are made using a 42 or 48 wire cable running outside the main cryostat in the Line N. The same pipe is also used to hold a cable of 6 kA conductors feeding the individually powered magnets in the continuous cryostat in the matching section and dispersion suppressor: see figure 6.6. Finally, the current for the spool pieces runs through straight wires mechanically attached to the quadrupole bus-bars.

6.3.5 Normal conducting cables

Normal conducting cables are also widely used. The heat losses of all the normal conducting magnets have a major impact on the installed cooling power in the tunnel and underground areas of the LHC. Cables and tubes carrying very high currents for the LHC main circuits and several other connections are therefore water cooled to decrease heat losses into the air.

6.4 Protection equipment

In most circuits, the stored magnetic energy is sufficient to destroy magnets and bus-bars. Protection of the equipment relies on the fast detection of resistive voltages, on a bypass of the current around the quenching parts, and on fast and reliable extraction of as much energy as possible. The large inductive voltages caused by current changes and the electrical noise in an accelerator environment, along with the high level of ionizing radiation, present the basic difficulties for detection. The energy bypass for the main LHC magnets is achieved using cold diodes in parallel with the magnet coils. At low temperatures, the turn-on voltage is normally high enough to prevent a bypass

leakage current. However, if the voltage across the diode reaches a few volts, the diode is turned on and heats up. At elevated temperatures, the turn-on voltage rapidly reaches the usual room temperature value of 0.7 V. Here the main difficulty is to avoid a partial overheating of the diode, which would result in an unequal current distribution over the junction area of the diode (current crowding). This, in turn, results in thermal run-away and a fusion of the pn junction. It is necessary to discharge the stored magnetic energy as quickly as possible, mainly to protect the diodes. All parts of the quench protection system are required to be safe and reliable. Moreover, in view of the large number of items, there is a potential problem with false triggers.

The quench detection systems for the main dipoles are based on a floating bridge detector, which continuously compares the voltages of the two apertures. The two magnet apertures of equal inductance and two balancing resistors form the bridge. These resistors also protect against over-currents through the instrumentation wires. The quadrupole magnets have the same kind of detector, comparing the voltage drops across two different poles, because the two apertures are powered separately. In the case of a quench, the floating bridge will become unbalanced, and the detector will activate directly the associated quench heater power supplies. These devices are located in racks under the main dipoles inside the LHC tunnel. In addition, these racks house the quench heater power supplies.

Each of the of HTS current leads is protected by a detector that compares the expected voltages with measured values across the resistive, as well the superconducting part, of the lead. The superconducting bus-bars of the corrector and insertion region magnets are included in the protection of the attached magnets, but the main 13kA bus-bars are a special case and have their own dedicated quench detector. No dedicated quench protection equipment is foreseen for circuits containing superconducting magnets powered with currents lower than 600A. In these cases, the power converter directly protects the magnet by detecting the over-voltage in the circuit caused by a quench.

6.4.1 Quench heater power supplies
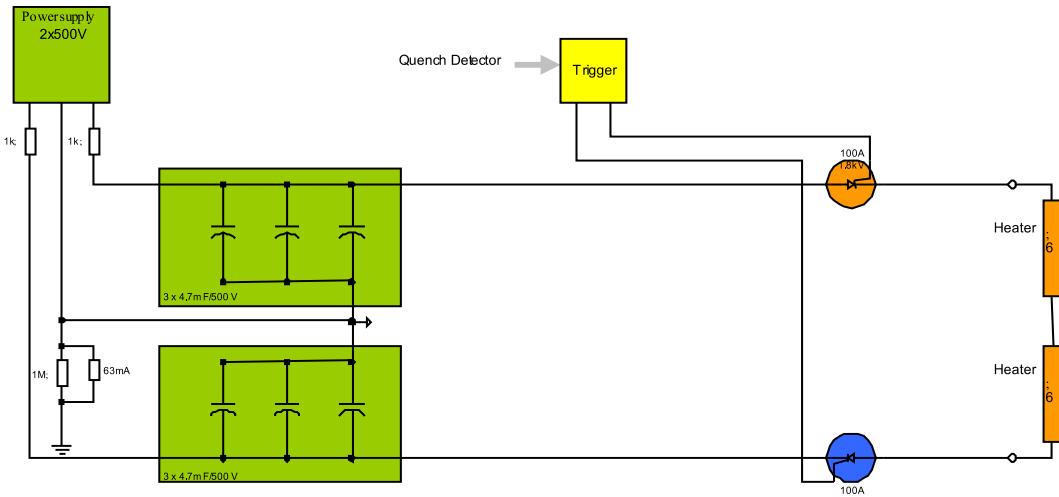
The quench heater power supplies (figure 6.7) store enough electrical energy to artificially quench a magnet. The quench heater strips, mounted on the coils of many LHC superconducting magnets, are heated up and spread the quench rapidly. This, in turn, decreases the energy density, and hence the maximum temperature in the quenching coils. Basically a triggered thyristor discharges an aluminium electrolytic capacitor bank, which is normally kept charged. The thyristor has ratings of 1.8 kV and 100 A, while the capacitor bank is formed by 2×3 capacitors of 4.7 mF / 500 V rating. These components have been extensively tested with respect to reliability, useful lifetime and radiation tolerance up to 200 Gy. The useful lifetime of the power supply under radiation is mainly limited by the two thyristors used for the discharge of the capacitor bank. Table 6.4 lists the quantities of electronics needed.

6.4.2 Energy extraction systems

The quench heaters spread the energy released in a quench over a larger volume, thereby reducing the maximum temperature. This is often sufficient to protect a single magnet. However, the energy stored in the other magnets, which are connected in series, might be too large to be absorbed. In

Table 6.4: Quench Protection Electronics, Summary.

Device	Qty.
Quench heater power supply	6076
Local quench detector (for MB and MQ magnets)	2016
Protection system for 600A corrector circuits	418
Protection system for insertion region magnets	172
Protection system for inner triplets	8
Protection system for 13kA superconducting busbars	80 slave + 8 master
Protection system for superconducting current leads	1198
Acquisition and monitoring controllers	2070

Figure 6.7: Quench heater power supply functional diagram.

this case, as much current as possible has to be routed around the quenching magnet by using a diode, but such a diode may not be able to absorb the total energy of the circuit. Also, energy absorbed by the diode has to be removed at cryogenic temperatures, which is more expensive and time consuming than at room temperature. On top of that, dumping the energy in the diodes takes a very long time. Therefore all major energy dumping systems have an external switch, bypassed by a dump resistor [35].

The energy extraction impacts on other systems in the power circuit. Voltage waves are created by the opening of the switches that sweep through the magnet chains. The amplitudes of the waves would exceed the ramping voltage without individual damping. For the MB strings, 100 Ω resistors connected across the dipole terminals serve this purpose. The effect on the precision of the current due to the leakage during current changes is negligible.

6.4.3 13 kA circuits

The maximum rate of current change must be limited to prevent eddy-current-induced quenches (quench-back), while ramping down the current in the main dipoles. The limit has been estimated

to be above 125 A/s for the LHC dipole circuits. Assuming an exponential current decay down from 13 kA, this corresponds to a time constant of 104 s. The inductance of all dipoles[2] in a sector is about 15.1 H. Hence the maximum voltage over a sector would be about 1900 V. With two, identical, series-inserted sub-systems, one with the circuit earthing at its mid-point (through 1 Ω), the maximum voltage to ground is limited to about ±475 V. The system requires the presence of bypass thyristors across the converter terminals to ensure circuit continuity after switch-off of the power source.

The basic criteria for the choice of extraction switches for the various circuits are reliability, lifetime, voltage drop (losses), and radiation hardness (for the units in the tunnel). A CERN/Russia collaboration resulted in a breaker with the following features:

- Two independent release systems: one completely passive, based on under-voltage release, the other active, based on a discharge pulse trigger.

- Magnetic displacement of the arc into the arc-chute, driven by the main current itself, providing fast and reproducible arc extinction, even at low currents.

- No mechanical catch and latch, the 'on' state being maintained entirely by the excitation of the holding coil.

- Arc-free separation of the main contacts, i.e., opening prior to separation of easily replaceable arc contacts.

- High overload and high current breaking capability combined with low 'on'-state losses.

Each extraction facility is composed of eight breakers, in four parallel branches, with two series-connected units each, to recover some of the redundancy lost by the parallel connection. All four branches must be closed in order to generate the 'power permit' for the circuit. A minimum of three branches is required for safe operation of the breakers; consequently, one branch may open accidentally during operation without forcing a beam abort. In case of accidental opening of a second branch, a 'power abort' is generated, opening all the switches for extraction in the circuit and dumping the beam.

In spite of the large energy difference, the dipole and quadrupole extraction resistors have many common design features. The basic principles for both types are:

- The absorber material has a low inductance and a low temperature coefficient.

- The operating temperature stays below 350°C at the end of the energy deposit.

- The equipment must always be available for extraction during powering of the magnet chain. It cannot rely on any external infrastructure, such as mains power or cooling water, for accepting the energy deposit.

- The resistor body is cooled by forced air, and the air is cooled by water. The units contain an air-to-water heat exchanger and a water reservoir, with sufficient capacity to ensure worst-case no-boiling conditions.

---

[2]Using the measured value of 100 mH per dipole.

- The cooling period is below two hours. Re-powering of the magnet chain is possible only after cooling of the resistor body.

- The material for the dipole resistors is radiation tolerant.

With an energy deposit of (ultimately) 625 MJ, a single 75 mΩ dipole unit would be 11 m long and have a mass of 8 t. For reasons of handling and space, an alternative solution, with three individual, parallel-connected sub-units of 225 mΩ and 220 MJ has been adopted. The resistor body consists of 84 series-connected stainless steel plates. Particular attention was paid to the need for free expansion-contraction, and for a uniform cooling across the resistor body, to avoid buckling, twisting and other deformation during the fast energy deposit and the slow cooling. The 6.6 mΩ (and 7.7 mΩ), 22 – 24 MJ quadrupole extraction resistor is small enough to be housed in a rack-sized cubicle.

6.4.4   600 A extraction equipment

The MCS, MCD, MO, MQS, MQT, MQTL and MS corrector circuit families are equipped with extraction systems for stored energy ranging from 2 kJ to 108 kJ. In this case, the extraction equipment consists of two series-connected, high-speed electro-mechanical, 3-phase AC breakers, with common and simultaneous operation of the three poles. In addition, the breakers are fitted with special DC arc-chutes. The total opening time is 17 ms (pulsed release) and 25 ms (zero-voltage release). For the corrector magnets and their bus bars the extraction time is a critical parameter, because of the limited amount of stabilising copper in the superconductors. Capacitive snubbers (typically 320 μF, bi-polar) are used for arc suppression, reducing the contact erosion, the total opening time (by 20%), and the acoustic noise (by 15-20 dB). The extraction resistors, 0.7 Ω or 0.2 Ω, are made from a low temperature coefficient material, such as Fe-Cr-Al.

6.4.5   Cold diodes

The main magnets are bypassed, as in HERA and RHIC, by diodes operating at cryogenic temperatures. During normal standby operation, the diodes have a low temperature turn-on voltage of a few volts, sufficiently high for the anticipated ramping rates. Once a quench has created sufficient resistance in a magnet and the corresponding voltage exceeds the diode turn-on voltage, the diodes start to conduct. They warm up and the 'knee-voltage' drops to lower values. It is important to achieve a 'knee-voltage' and resistance during the bypass operation which is as low as possible. The lower the effective resistance, the more current will be transferred out of the coil.

All dipoles or quadrupoles of a sector may be quenched during a discharge due to a malfunction. The non-uniform quench behaviour will cause the last quenching magnet and its diode to see a reverse voltage of 2'100 V (140 V for quadrupoles). Since there is no diode with such a blocking voltage, the diode will be destroyed. However, it will still protect the magnet. Clearly, the maximum reverse voltage is an important design parameter, along with the resistance to radiation. A special diffused diode was developed with a cold turn-on voltage of about 6 V, which falls to 0.96 V at room temperature (I = 15 kA). The cold reverse voltage is typically around 250 V.

Corrector magnets are protected by parallel resistors. The bypass currents during current changes are negligibly small.

6.4.6 Controllers

Acquisition and monitoring controllers enable the supervision of all electronic devices belonging to the quench protection system and transfer the data via a fieldbus link to the higher-level LHC control systems. These controllers exist in three different variants, differing only in the number of analogue and digital I/O channels. The hardware is based on a micro-converter of the ADuC831 type, which incorporates a 12 Bit 8 channel ADC with an 8'052 compatible microcontroller core, and an ASIC of the VY27257 type, implementing the WorldFip fieldbus protocol. All controllers are equipped with 62 kByte Flash EEPROM memory and 32 kByte static RAM. All controller boards have been successfully tested with respect to the radiation tolerance levels required in the LHC tunnel of 200 Gy.

6.4.7 Supervision of the Quench Protection System (QPS)

The QPS supervision software layer links the gateways (DQGTW) to the LHC general purpose software modules (LHC Alarms, LHC Logging, LHC Post Mortem, Machine Protection System, etc.). Some key features are listed below:

- The access to the data is based on views.

- It will be possible to access the QPS Supervision from an office with W2000/WXP computers, from the control room, and from the tunnel area.

- The interface to the hardware controllers is done by command/result data.

- This supervision handles the test mode, where all the QPS hardware can be checked with respect to their proper function.

- The QPS Supervision will always be available. Possible upgrades will be planned for shutdown periods.

- The QPS Supervision will be built in stages. The QPS architecture will support this.

6.5 Operational aspects and reliability

6.5.1 Electrical quality assurance

An electrical quality assurance plan is defined for the LHC machine environment in order to ensure the safe and correct functioning of all superconducting electrical circuits during its commissioning and operation. The plan has been worked out in close collaboration with all parties concerned with the installation and commissioning (i.e., the hardware commissioning working group). The steps in the electrical quality assurance plan for the machine assembly, commissioning, operation, and shutdown phases are as follows:

- Continuity, polarity, and electrical integrity verification during machine assembly until the closure of the helium enclosure of each sub-sector.

- Electrical measurements at ambient temperatures of reference parameters for each individual electrical circuit part of a sub-sector. These measurements are performed from the corresponding DFB.

- On-line monitoring during the cool-down of the integrity of electrical insulation of circuits and instrumentation for magnet protection.

- Electrical measurements of reference parameters at cold conditions before the powering of each individual electrical circuit of a sub-sector.

- Diagnostic measurements and verifications during sub-sector commissioning and machine operation.

- Yearly verification during shutdown periods of cold electrical components, such as the by-pass diodes.

- Verification of electrical circuit segments after in-situ repairs as well as after an exchange of electrical components.

6.5.2 Quench detectors

In order to increase the availability of each of the detection systems, it is foreseen to use the coherence of the two independent channels continuously, thereby reducing the probability for false quenches. A simulated quench signal can be sent from the control room. If one or more channels fail the test of the coherency it will generate a warning. Since this test implies the discharge of the quench heater power supplies, it can only be performed when the magnets are cold and not powered. When Quench Tests are performed monthly and repairs are carried out before re-powering the circuits (see below), the probability of missing a quench during 20 years of operation is below 1% [36].

The expected number of false quenches is around 10 per year. Since the powering of the detectors is not redundant, it is not possible to improve its reliability via checks. However, the number of false quenches will drop to less than 1 per year, if two supplies are connected in parallel. Due to the large investment required to double all the power supplies, it has been decided to install one power supply per local quench detector and provide the necessary space and cabling to install a redundant unit if operation experience shows it to be necessary.

Table 6.5 summarises the results for all the LHC quench detectors if monthly checks are carried out (see below). The expected probability of not missing any quench along the machine over 20 years is well above 95%.

6.5.3 Quench Heater Power Supplies (DQHDS)

Each of the 6'076 quench heater power supplies contains two banks of three capacitors each, connected in parallel. These are discharged in the quench heaters by triggering two thyristors in series with the strips. Four power supplies are installed per dipole. At least two have to be properly discharged to ensure the integrity of the coil. The quench heaters in the 13 kA and 6 kA quadrupoles are fed by two power supplies (except in the case of the MQY magnets, where four power supplies

Table 6.5: The probability to miss one quench in 20 years (RMQ) and the expected number of false quenches with a 95% confidence level for the different detector families.

Detector		Units	RMQ	False Quenches
DQQDL	Local	2016	0.991	197-238
DQQDI,T	Insertion and Inner Triplets	316	0.991	89-145
DQQDG	Correctors	351	0.997	120-187
DQQDC	Current Leads	1198	0.974	132-165

are required), and at least one of them (two for the MQY) has to be correctly fired to protect the magnet. The reliability analysis of the quench heater power supplies shows that quench tests on a regular time scale improve the reliability of the system. Monthly tests (and repairs) boost the reliability to react properly to all quenches during 20 years to 99.7% (99.9% for the quadrupoles). Incidentally, a high rate of quenches would have a benign effect on the reliability for this highly redundant system.

6.5.4 Energy extraction

As described earlier, the energy extraction systems are based on electro-mechanical breakers with high redundancy, using series and parallel connected current paths. During a machine run, one branch may open by accident without compromising operation. In the case that more than one branch is opened, all the other breakers of the facility will be forced to open. In the case of the main dipoles, the system at the other end of the arc is also opened. In the unlikely, but most dangerous, event that one branch of a system remains closed after an opening command, several cold diodes in the main magnets or resistors in the corrector magnets could be damaged, because the stored energy will not be dumped correctly. In this case, several pre-selected magnets will be fired. This will, unfortunately, lead to a huge load on the cryogenic system. The probability of one such failure in 20 years is about 0.03% in case of the 13 kA energy extraction systems, assuming a realistic failure rate of the breakers of 0.0001. This requires monthly checks and the use of the post-mortem information of all energy extractions which occur. Four power aborts due to quenches in the main magnets per operational week have been assumed. For the 600 A circuits, the space conditions allow the use of a third switch, which decreases the failure rate. In this case, the result is a failure probability of less than 1%.

In summary, only regular maintenance can keep the QPS alert, not to miss a quench, and also not to have a false trigger. Failing to provide regular maintenance means failure in operation of the accelerator. Some checks can be done while running, others require normal operation to be stopped. Finally a check will be done automatically, for example due to "normal" quenches. Table 6.6 summarises the required maintenance policy.

With all maintenance properly done and assuming the parameters mentioned above, an overall main failure probability over 20 years of 0.914 is to be expected.

Clearly, the maintenance will take time. The exact time will depend on the number and distribution of quenches happening during operation, which do not need to be tested any more. The strategy for the quench tests will then fully exploit the cryogenic capacity and the voltage

Table 6.6: Maintenance policy.

		Check	Inspection	Repair	Affected
Quench Detectors	DQQDL	Quench Test	Monthly	Monthly	All
		Post Mortem	After Quench	Before Power Permit	Quenched Magnet
		Coherency Test	On-line	Monthly	All
		Power Permit	On-line	Before Power Permit	Sub-sector
	Other	Quench Test	Monthly	Monthly	All
		Post Mortem	After Quench	Before Power Permit	Circuit
		Powering Test	On-line	Monthly	All
		Power Permit	On-line	Before Power Permit	Sub-sector
Heaters		Discharge Test	Monthly	Monthly	All
		Post Mortem	Quench	Before Power Permit	Quenched Magnet
Extraction	13kA	Open Check	Monthly	Monthly	All
		Post Mortem	Quench	Before Power Permit	Sub-sector
		False Opening	On-line	Monthly	All
		Power Permit	On-line	Before Power Permit	Sub-sector
	600A	Open Check	Monthly	Monthly	All
		Post Mortem	Quench	Before Power Permit	Sub-sector

rating of the various circuits in order to gain time. After a careful analysis of the data, repair or replacement of parts may be needed. Hence, to keep the systems working several days per month of intensive tests and repairs need to be anticipated. It should be noted that access to the sectors under test will normally not be possible.

Chapter 7

Cryogenic system

7.1   Overview

The LHC is unique among superconducting synchrotrons, because its operating temperature is below 2 K to maximise the field strength of the superconducting magnets with NbTi windings. The basic design as well as the main technical choices for the LHC cryogenic system have been described in Part III section 2 of the "White Book" [11] and in Part III section 2 of the "Yellow Book" [12].

The superconducting magnet windings in the arcs, the dispersion suppressors, and the inner triplets will be immersed in a pressurised bath of superfluid helium at about 0.13 MPa (1.3 bar) and a maximum temperature of 1.9 K [37]. This allows a sufficient temperature margin for heat transfer across the electrical insulation. As the specific heat of the superconducting alloy and its copper matrix fall rapidly with decreasing temperature, the full benefit in terms of stability margin of operation at 1.9 K (instead of at the conventional 4.5 K) may only be gained by making effective use of the transport properties of superfluid helium, for which the temperature of 1.9 K also corresponds to a maximum in the effective thermal conductivity. The low bulk viscosity enables the coolant to permeate the heart of the magnet windings. The large specific heat (typically 10^5 times that of the conductor per unit mass, 2×10^3 times per unit volume), combined with the enormous heat conductivity at moderate flux (3'000 times that of cryogenic-grade OFHC copper, peaking at 1.9 K) can have a powerful stabilising action on thermal disturbances. To achieve this, the electrical insulation of the conductor must preserve sufficient porosity and provide a thermal percolation path, while still fulfilling its demanding dielectric and mechanical duties. This cooling requirement applies during both ramping and stored-beam operation. In the case of fast current discharge, the temperature excursion may be larger but must still remain below the helium II/helium I phase transition (lambda line). In the long straight sections, with the exception of the inner triplets and the superconducting dipoles D1, the field strength and heat extraction requirements are such that operation at 1.9 K is not necessary. The superconducting windings of these magnets will be immersed in a bath of saturated helium at 4.5 K.

The cryogenic system must be able to cope with the load variations and a large dynamic range induced by the operation of the accelerator as well as being able to cool-down and fill the huge cold mass of the LHC, 37×10^6 kg, within a maximum delay of 15 days while avoiding

thermal differences in the cryo-magnet structure higher than 75 K. The cryogenic system must be also able to cope with resistive transitions of the superconducting magnets, which will occasionally occur in the machine, while minimising loss of cryogen and system perturbations. It must handle the resulting heat release and its consequences, which include fast pressure rises and flow surges. The system must limit the propagation to neighbouring magnets and recover in a time that does not seriously detract from the operational availability of the LHC. A resistive transition extending over one lattice cell should not result in a down time of more than a few hours. It must also be possible to rapidly warm up and cool down limited lengths of the lattice for magnet exchange and repair. Finally, it must be able to handle, without impairing the safety of personnel or equipment, the largest credible incident of the resistive transition of a full sector. The system is designed with some redundancy in its subsystems.
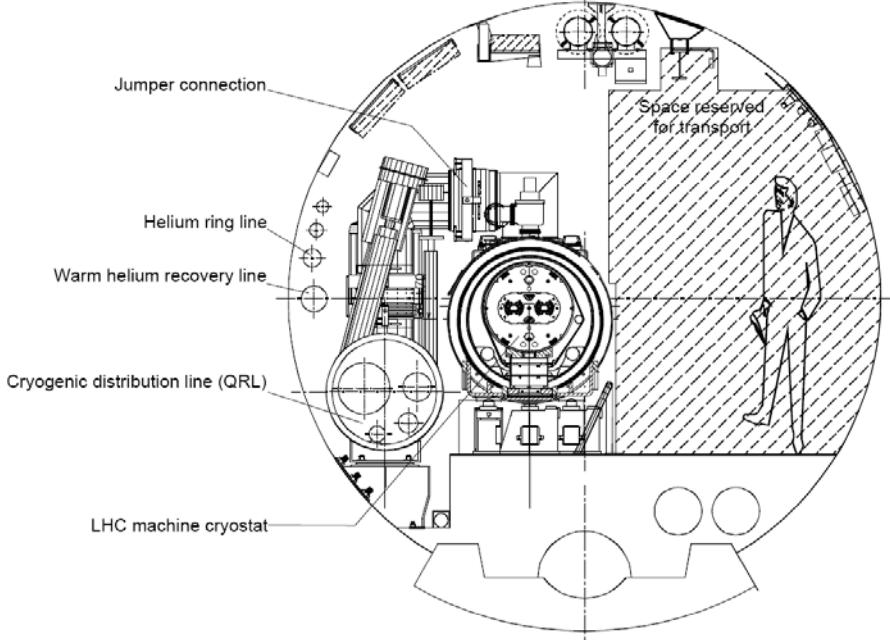
7.2 General architecture

The main constraints on the cryogenic system result from the need to install the system in the existing LEP tunnel and to re-use LEP facilities, including four refrigerators. The limited number of access points to the underground area is reflected in the architecture of the system. The cooling power required at each temperature level will be produced by eight refrigeration plants and distributed to the adjacent sectors over distances up to 3.3 km. To simplify the magnet string design, the cryogenic headers distributing the cooling power along a machine sector, as well as all remaining active cryogenic components in the tunnel, are contained in a compound cryogenic distribution line (QRL). The QRL runs alongside the cryo-magnet strings in the tunnel and feeds each 106.9 m-long lattice cell in parallel via a jumper connection (figure 7.1).
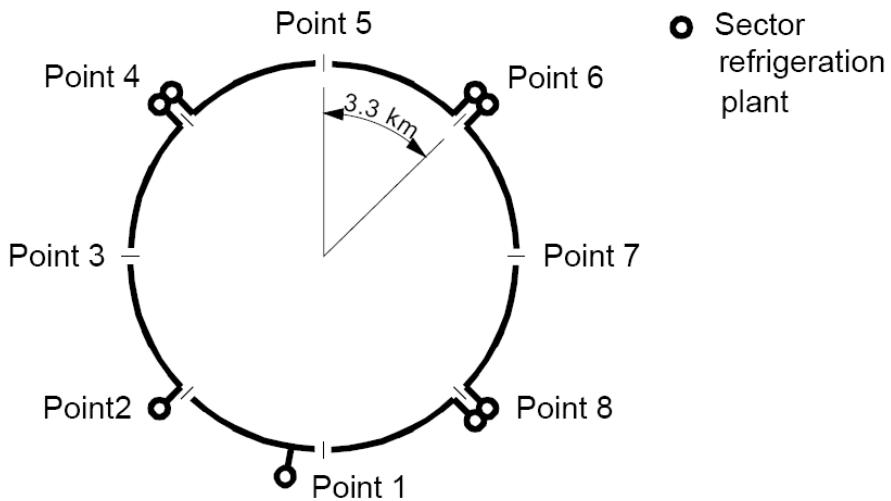
The LHC tunnel is inclined at 1.41% with respect to the horizontal, thus giving height differences of up to 120 m across the tunnel diameter. This slope generates hydrostatic heads in the cryogenic headers and could generate flow instabilities in two-phase, liquid-vapour, flow. To avoid these instabilities, all fluids should be transported over large distances in a mono-phase state, i.e., in the super-heated-vapour or supercritical region of the phase diagram. Local two-phase circulation of saturated liquid can be tolerated over limited lengths, in a controlled direction of circulation. Equipment is installed as much as possible above ground to avoid the need for further excavation, but certain components have to be installed underground near the cryostats. For reasons of safety, the use of nitrogen in the tunnel is forbidden, and the discharge of helium is restricted to small quantities only.

Figure 7.2 shows the general layout of the cryogenic system with five "cryogenic islands" at access Points 1.8, 2, 4, 6 and 8, where all refrigeration equipment and ancillary equipment is concentrated. Equipment at ground level includes electrical substations, warm compressors, cryogen storage (helium and liquid nitrogen), cooling towers, and cold boxes. Underground equipment includes lower cold boxes, 1.8 K refrigeration unit boxes, interconnecting lines, and interconnection boxes. Each cryogenic island houses one or two refrigeration plants that feed one or two adjacent tunnel sectors, requiring distribution and recovery of the cooling fluids over distances of 3.3 km underground.

Figure 7.3 shows the general architecture of the system. A refrigeration plant comprises one 4.5 K refrigerator and one 1.8 K refrigeration unit. The 4.5 K refrigerator is either one of the
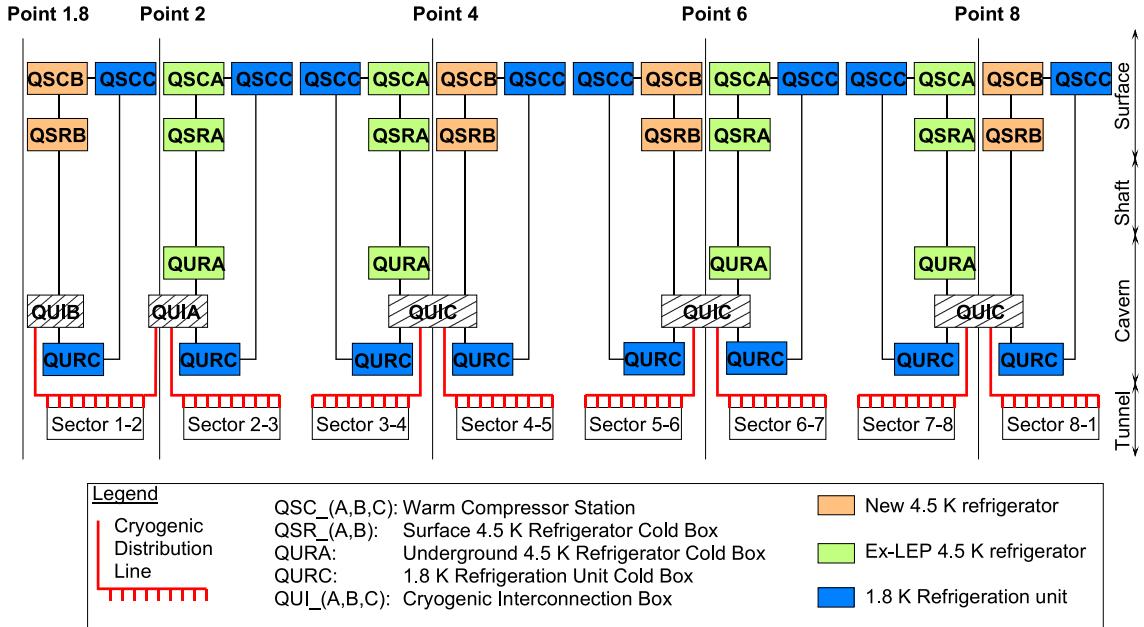
Figure 7.1: Transverse cross-section of the LHC tunnel.

Figure 7.2: General layout of the cryogenic system.

four split-cold-box refrigerators recovered from LEP, or one of the four new integrated-cold-box refrigerators. At each cryogenic island, an interconnection box couples the refrigeration chains and the cryogenic distribution lines. Due to lack of space for two refrigeration plants at Point 2 and the need at Point 1.8 for a large refrigeration capacity for cryo-magnet testing, the 4-point symmetry was broken, and two refrigeration plants at Points 4, 6 and 8, but only one plant at Points 1.8 and 2, were installed. The drawback of this architecture affects Sector 2-3, which has only limited redundancy.
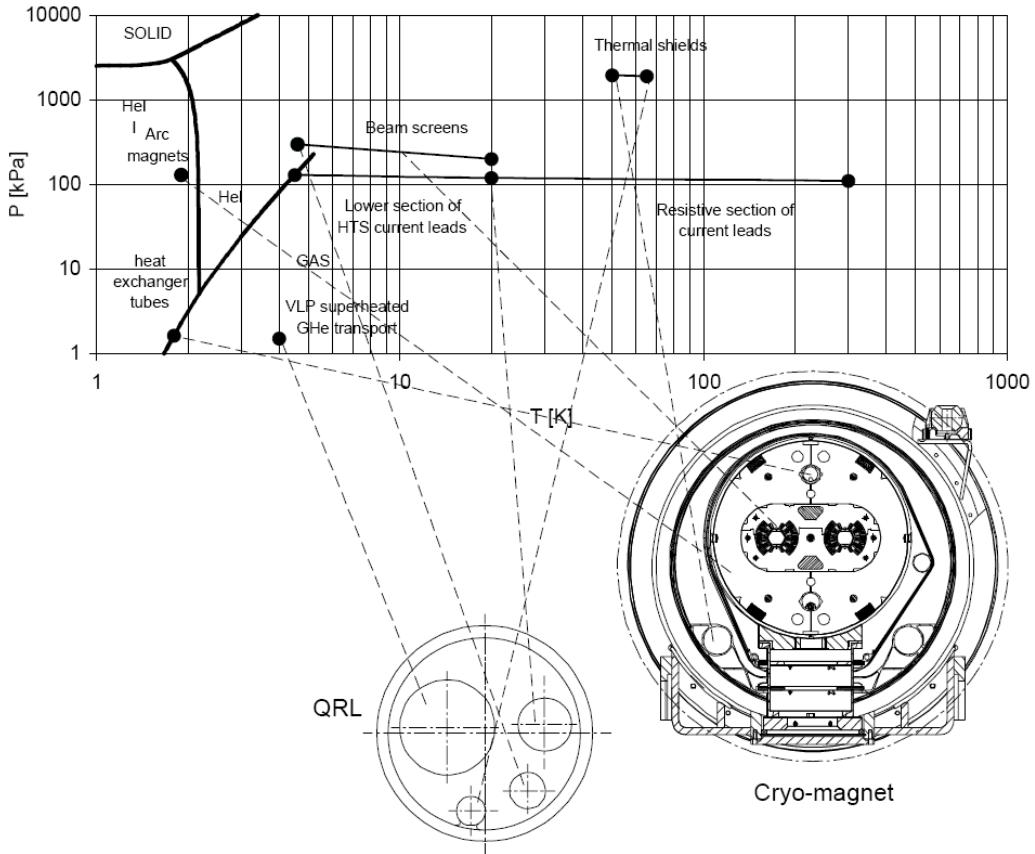
Figure 7.3: General architecture of the cryogenic system.

7.3 Temperature levels

In view of the high thermodynamic cost of refrigeration at 1.8 K, the thermal design of the LHC cryogenic components aims at intercepting the main heat influx at higher temperatures; hence the multiple-staged temperature levels in the system. The temperature levels are:

- 50 K to 75 K for the thermal shield protecting the cold masses,

- 4.6 K to 20 K for lower temperature interception and for cooling the beam screens that protect the magnet bores from beam-induced loads.

- 1.9 K quasi-isothermal superfluid helium for cooling the magnet cold masses,

- 4 K at very low pressure for transporting the superheated helium flow coming from the distributed 1.8 K heat exchanger tubes across the sector length to the 1.8 K refrigeration units,

- 4.5 K normal saturated helium for cooling some insertion region magnets, RF cavities, and the lower sections of the HTS current leads,

- 20 K to 300 K cooling for the resistive upper sections of the HTS current leads [38].

To provide these temperature levels, use is made of helium in several thermodynamic states: figure 7.4. The cryostats and cryogenic distribution line (QRL) combine several techniques for limiting heat influx, such as low-conduction support posts, insulation vacuum, multi-layer reflective insulation wrapping, and low-impedance thermal contacts, all of which have been successfully applied on an industrial scale.
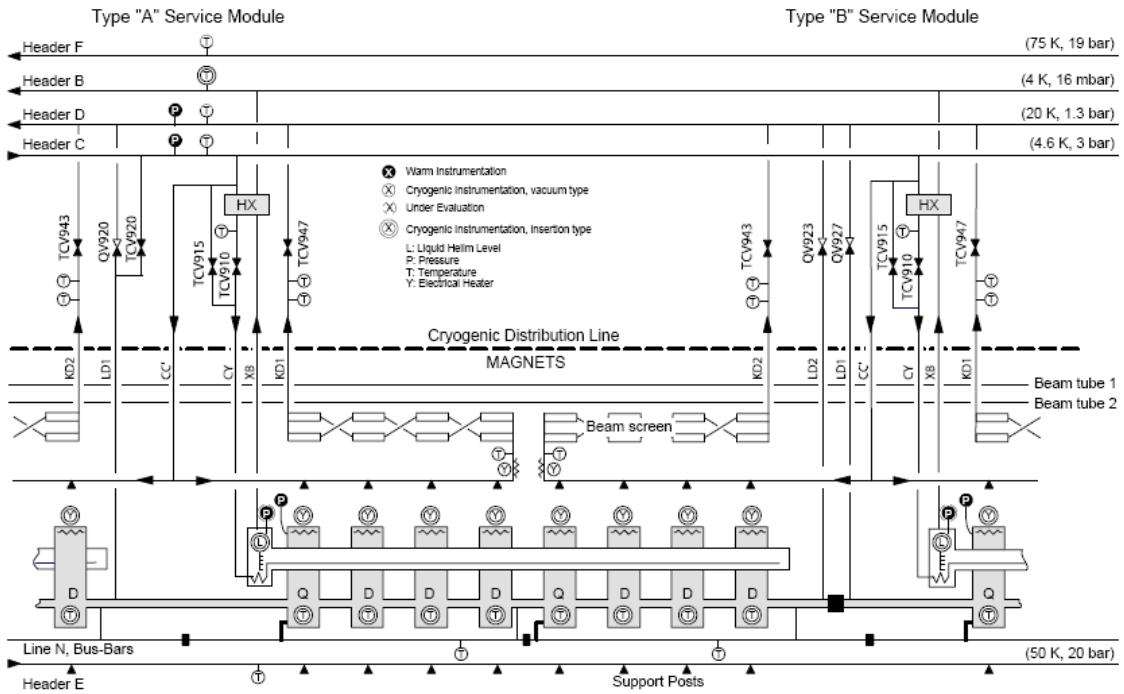
Figure 7.4: Thermodynamic states of helium in the LHC cryogenic system.

7.4 Cooling scheme

7.4.1 Arc and dispersion suppressor cooling loops

The cooling flow scheme for the arcs and DS regions is shown in figure 7.5. The first level of thermal shielding and heat interception in the magnet cryostats and the QRL is provided by forced circulation of gaseous helium under pressure at a temperature between 50 K and 75 K, through headers E and F respectively. The cryo-magnets operate in a static bath of pressurised helium II, cooled by heat exchange with flowing saturated helium II. Low-pressure vapour resulting from the vaporisation of the saturated helium II is returned to the refrigerator by header B. Supercritical helium is distributed by header C and is used to a) fill the cryo-magnet baths, b) to produce — after subcooling and Joule-Thomson expansion — the saturated helium II flowing in the full cell length heat exchanger tube and c) feed line C' that cools the cold heat intercepts in the support posts at about 5 K, in series with the beam screens that operate between about 5 K and 20 K. The resulting gaseous helium is returned to the refrigerator by header D.
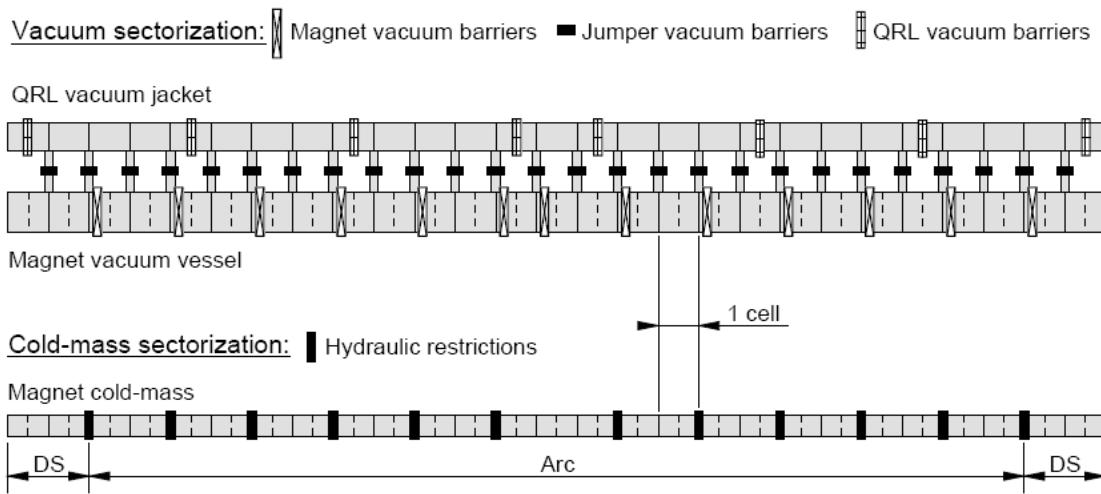
The performance of such a scheme depends critically on the thermo-hydraulic behaviour of the two-phase helium II flowing in quasi-horizontal tubes. This has been modelled at CERN and CEA Grenoble and demonstrated that over a large range of vapour quality, most of the tube cross-section is occupied by the vapour flow, which then controls the overall pressure drop. For

Figure 7.5: Thermodynamic cryogenic flow scheme and instrumentation of an LHC lattice cell.

vapour velocities of up to a few m s^{-1}, the drag between the two phases remains small, so that the liquid flows separately from the vapour, almost as if in a single phase open channel. Under these conditions, the heat transfer is mainly controlled by the wetted area inside the tube, which can be adequately predicted by simple models. Other important factors controlling the heat transfer across the tube wall are the conductivity of the tube and the Kapitza thermal resistance at the solid-liquid interfaces. By using a 53.4 mm inner diameter tube of OFHC copper with a wall thickness of 2.3 mm, the total transverse impedance when fully wetted can be kept down to about 0.3 mK m^2 W^{-1}, and the practical heat transfer capability of the partially wetted bayonet heat exchanger is thus typically a few mK m W^{-1}. The final validation of this cooling scheme was performed on a full scale magnet string equivalent to one LHC cell.

Within a sector, the tunnel slope results in elevation differences up to 50 m, equivalent to a hydrostatic head of up to 70 kPa (700 mbar). To avoid the negative effects of this hydrostatic head, the cold masses within a sector have been sub-sectorised by adding hydraulic restrictions every two or three cells (figure 7.6). These restrictions also limit the propagation of resistive transitions caused by warm helium flowing from magnet to magnet. The cryogenic vacuum is also sub-sectorised in order to limit the extent of a degraded vacuum zone caused by a possible helium leak from the internal circuit. On the cryo-magnet side, the vacuum barriers are in the SSS cryostats every two cells, and, in the QRL, vacuum barriers are placed every four cells. The jumper connection between the QRL and the magnet cryostats always contains a vacuum barrier. The two sub-sectorisation schemes also make it possible to warm-up and re-cool-down a limited length of the machine (up to 600 m) for minor interventions. The removal of magnets, however, requires the complete sector to be warmed up.

Figure 7.6: Cold-mass and cryogenic vacuum sub-sectorisation.

7.4.2 Matching section cooling loops
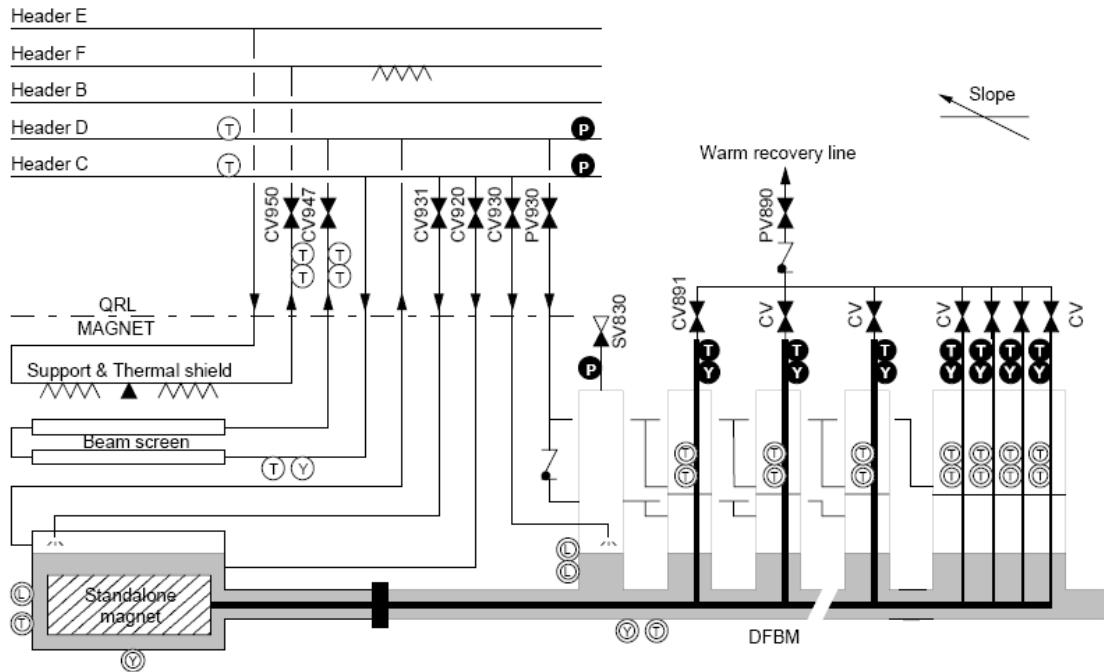
The special magnets in the matching sections that do not require 1.9 K operate in baths of saturated helium I at 4.5 K. These magnets are generally a single quadrupole or dipole with correctors (standalone), or a single quadrupole and dipole in series with correctors (semi-standalone). Figure 7.7 shows the basic cooling scheme. There is an actively cooled heat intercept at about 70 K. The cold mass is filled and the liquid level actively maintained by helium supplied from QRL header C. The vapour outlet is into the QRL header D, whose pressure of about 0.13 MPa (1.3 bar) directly determines the corresponding magnet's saturated liquid bath temperature at about 4.5 K. The stand-alone and semi-stand-alone magnets receive their powering through a dedicated interface, which in the majority of cases connects to a local DFB or to a superconducting link.

7.4.3 Inner triplet cooling loops
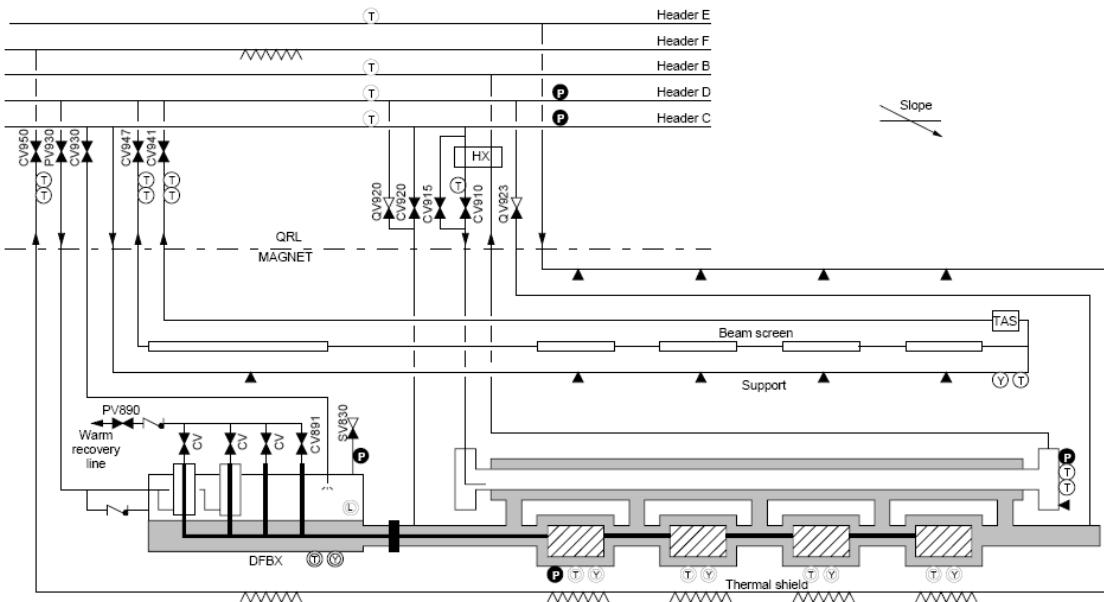
The inner triplet quadrupoles in the IRs are subject to heating due to secondary beam particles of up to 10 W m^{-1} in the high luminosity insertions of Points 1 and 5, and up to 2 W m^{-1} in the low-luminosity insertions in Points 2 and 8. Although this represents a much higher heat load than in the arcs, the quadrupoles can be cooled by a scheme similar to that in the standard arcs. A large-diameter, corrugated, copper heat exchanger tube inside a stainless steel tube is placed outside and parallel to the cold mass in the cryostat. Figure 7.8 shows the cryogenic flow scheme and instrumentation for a high luminosity insertion inner triplet.

7.5 Cryogenic distribution

The central nodes of the cryogenic distribution system are situated in the underground caverns. These are the cryogenic interconnection boxes (QUI) which provide the connection between the different cryogenic sub-systems at each of the five feed-points: surface 4.5 K cold boxes, underground 4.5 K lower cold boxes, 1.8 K refrigeration unit boxes, and the QRL. The upper cold boxes

Figure 7.7: Cryogenic flow scheme and instrumentation of a 4.5 K standalone magnet.

Figure 7.8: Cryogenic flow scheme and instrumentation of an inner triplet cell.

of the new 4.5 K refrigerators are linked to the interconnection boxes via four vertical helium transfer lines that pass down the main LHC shafts. The QUIs are located between 80 m and 145 m below ground, depending on the access point. The lower cold boxes of the refrigerators recovered from LEP and those of the 1.8 K refrigeration units are connected to the interconnection boxes

Table 7.1: Installed refrigeration capacity in the LHC sectors.

Temperature level	High-load sector	Low-load sector
50-75 K [W]	33'000	31'000
4.6-20 K [W]	7'700	7'600
4.5 K [W]	300	150
1.9 K LHe [W]	2'400	2'100
4 K VLP [W]	430	380
20-280 K [g s^{-1}]	41	27

via 12 underground helium transfer lines. Finally, the QRL feeds helium at different temperatures and pressures to the cooling loops and other devices for each of the eight sectors, starting from the QUIs and running along the tunnel.

7.6 Refrigeration plants

The refrigeration capacity of the sectors listed in table 7.1 corresponds to ultimate operation, without contingency, assuming the heat load levels calculated in 1997. Since ordering the refrigerators, the electron cloud predictions have increased the heat loads. Consequently, the installed capacity can no longer cope with the estimated ultimate demand, but it still fulfills the nominal demand of about 5.3 kW per sector.

7.6.1 4.5 k refrigerators
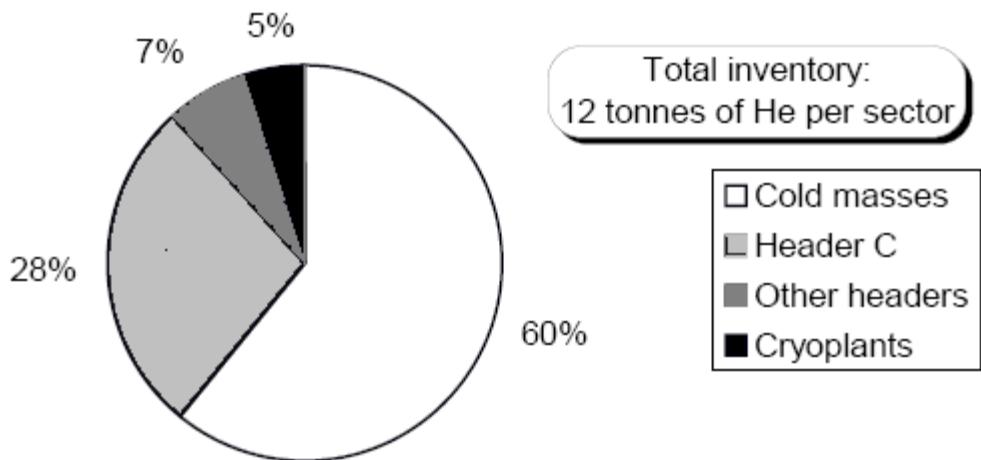
The refrigeration of the LHC sectors requires mixed-duty operation of the cryogenic helium refrigerators, in order to fulfil a variety of isothermal and non-isothermal cooling duties. This amounts to a total equivalent entropic capacity of 144 kW at 4.5 K, thus making the LHC the world's most powerful helium refrigeration system. In accordance with the policy for re-using as much as possible of the LEP equipment, CERN equipped the new "high-load" areas with four new refrigerators and upgraded four existing LEP refrigerators for the "low-load" areas.

7.6.2 1.8 k refrigerators

The efficient production of 1.8 K refrigeration in the multi-kW range can only be achieved through combined cycles making use of sub-atmospheric cryogenic compressors and heat exchangers. Considerable R&D was performed by CERN in liaison with CEA and industry before eight 1.8 K refrigeration units were procured industrially. The 1.8 K units are interconnected with the 4.5 K units.

7.7 Cryogen storage and management

Helium is mainly contained in the magnet cold masses, which require a minimum filling ratio of 15 l m^{-1} of superfluid helium for enthalpy buffering, and in the header C of the QRL. Figure 7.9 shows the helium inventory per sector. The total inventory is 96×10^3 kg. Initially, on-site helium

Figure 7.9: Helium inventory per sector.

storage was provided for half of this inventory, but in a second phase more storage is being added. CERN is also offering the possibility that gas-distribution companies can re-sell part of the helium inventory on the market during shutdowns, if the whole machine is warmed up and the on-site storage is insufficient.

CERN also needs liquid nitrogen for cool down operations and for the regeneration of purifiers. Liquid nitrogen is not used in the tunnel for safety reasons. For a normal cool down of a sector, the 600 kW pre-cooler will use a maximum of 1'260 ton of liquid nitrogen.

Chapter 8
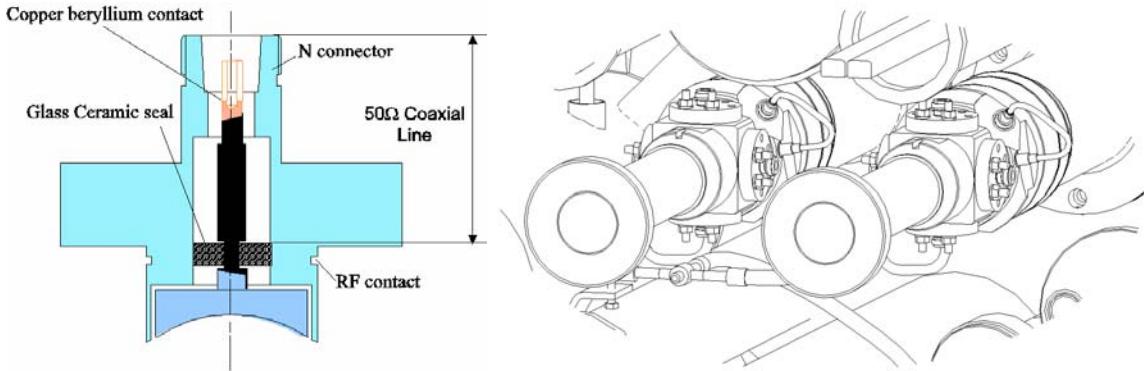
Beam instrumentation

8.1   Beam position measurement

A complete list of the beam position monitors associated with orbit and trajectory measurements is given in table 8.1. There are three types of monitor: 24 mm button electrode monitors, 34 mm button electrode monitors, and 120 mm stripline monitors. These are assembled in 13 different types of housing, depending on the vacuum chamber dimension and the interface with neighbouring equipment. The orbit and trajectory measurement system has been developed to fulfill the functional specifications described in [39]. The system consists of 516 monitors per ring, all measuring in both the horizontal and vertical planes. The acquisition electronics is capable of 40 MHz bunch-by-bunch measurements and will provide closed orbit feedback at 1 Hz.

Table 8.1: List of beam position monitor types in LHC.

Type	Electrode Type	Name	Number
Standard Arc	24 mm Button	BPM	720
Dispersion suppressor & Q7	24 mm Button	BPM	140
Standard BPM for vertical beam screen	24 mm Button	BPMR	36
Enlarged Aperture BPM for horizontal beam screen	34 mm Button	BPMYA	24
Enlarged Aperture BPM for vertical beam screen	34 mm Button	BPMYB	12
Warm LHC BPM for MQWA	34 mm Button	BPMW	36
Enlarged Warm LHC BPM for ADTV/H	34 mm Button	BPMWA	8
Enlarged Warm LHC BPM for D2	34 mm Button	BPMWB	16
Combined Button & Shorted Stripline BPMs	24 mm Button + 150 mm Stripline	BPMC	16
Cryogenic Directional Stripline Coupler for Q2	120 mm Stripline	BPMS	8
Warm Directional Stripline Coupler for Q1	120 mm Stripline	BPMSW	8
Warm Directional Stripline Coupler for D1	120 mm Stripline	BPMSX	4
Warm Directional Stripline Coupler for DFBX	120 mm Stripline	BPMSY	4
	TOTAL		1032
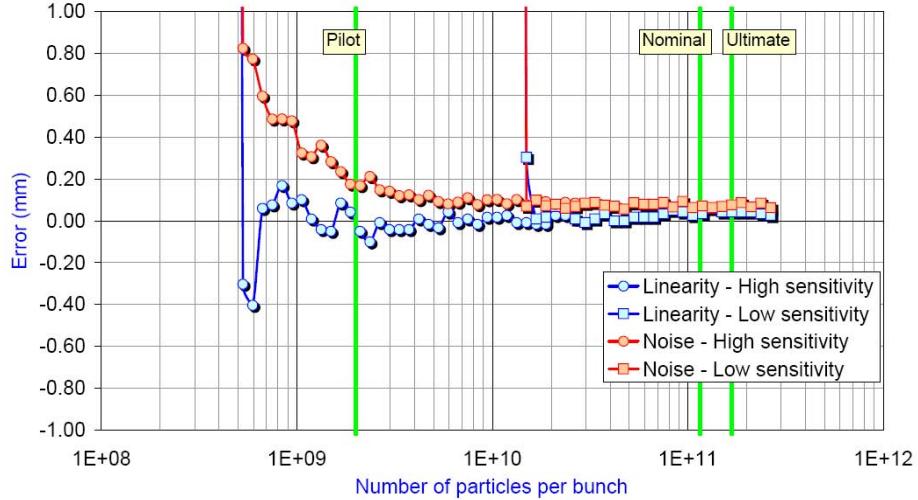
Figure 8.1: (a) 24 mm button electrode, (b) Mounted BPM bodies.

The majority of the LHC beam position monitors (860 of the 1'032) are of the arc type (see figure 8.1) consisting of four 24 mm diameter button electrode feedthroughs mounted orthogonally in a 48 mm inner diameter beam pipe. The electrodes are curved to follow the beam pipe aperture and are retracted by 0.5 mm, to protect the buttons from direct synchrotron radiation from the main bending magnets. Each electrode has a capacitance of 7.6 ±0.6 pF, and is connected to a 50 Ω coaxial, glass-ceramic, UHV feedthrough.

The inner triplet BPMs in all interaction regions are equipped with 120 mm, 50 Ω directional stripline couplers (BPMS×), capable of distinguishing between counter rotating beams in the same beam pipe. The location of these BPMs (in-front of Q1, in the Q2 cryostat and after Q3) was chosen to be as far as possible from parasitic crossings to optimise the directivity. The 120 mm stripline length was chosen to give a signal similar to the button electrode, so allowing the use of the same acquisition electronics as for the arcs. All cold directional couplers use an Ultem® dielectric for use in a cryogenic environment, while the warm couplers use a Macor® dielectric to allow bake-out to over 200°C.

The cleaning insertions in Points 3 and 7 are equipped with warm 34 mm diameter button electrode BPMs (BPMW) fitted either side of the MQWA magnets. The electrodes are an enlarged version of the arc BPM button. The same button electrodes are also used for the cold BPMs in the matching sections either side of the four interaction regions as well as for the warm BPMs located near the D2 magnets and either side of the transverse damper (ADTV/H). The BPMC, installed in Point 4, are combined monitors consisting of one BPM using standard 24 mm button electrodes for use by the orbit system, and one BPM using 150 mm shorted stripline electrodes for use in the transverse damper system.

The LHC orbit and trajectory acquisition system is based on a Wide Band Time Normaliser (WBTN) [40] capable of processing the analogue signals from the pick-up at 40 MHz. The resulting signal is transmitted via a fibre-optic link, treated, digitised using a 10-bit ADC and processed by a VME64x Digital Acquisition Board (DAB) developed by TRIUMF, Canada. The performance of the WBTN electronics with intensity is shown in figure 8.2. The system is expected to function with between 2×10^9 and 2×10^{11} charges per bunch. A summary of the expected performance of the complete acquisition system for standard arc BPMs is presented in table 8.2.

Figure 8.2: Performance of the LHC WBTN system as a function of intensity.

Table 8.2: Expected performance of the LHC BPM system for standard arc BPMs.

Range of Operation (±6mm)	Pilot Bunch (5x10⁹)		Nominal Bunch (1.1x10¹¹)		Ultimate Bunch (1.7x10¹¹)	
	Single	Average over 224 turns	Single	Average over 224 turns	Single	Average over 224 turns
Resolution (μm rms)	130	9	50	5	50	5
Non-Linearity (±μm)	100					
Scale Error (±%)	1					
Calibrator Offset (±μm)	50					
Intensity Offset (±μm)	25					
BPM & Gauge Mechanical Offset (±μm)	125					
Survey Measurement Precision (μm rms)	50					
Electrical Axis Offset (±μm)	113					
Uncertainty of MA wrt GA (μm rms)	150					
Geometric Non-Linearity (±μm)	100					
Total Offset (±μm)	363					
Relative Accuracy [offset ignored] (±μm)	302	155	183	154	183	154
Global Accuracy (±μm)	472	394	406	393	406	393

8.2 Beam current transformers

Beam current transformers of two different kinds will provide intensity measurements for the beams circulating in the LHC rings, as well as for the transfer lines from the SPS to LHC, and from LHC to the dumps. The transformers will all be installed in sections where the vacuum chamber is at room temperature and where the beams are separated.

The fast beam current transformers (FBCTs) will be capable of integrating the charge of each LHC bunch. This provides good accuracy for both bunch to bunch measurements and average measurements, intended mainly for low intensity beams, for which the DCCT accuracy will be limited. For redundancy, two transformers, with totally separated acquisition chains, will be placed in each ring. These will be located in Point 4. Each beam dump line will also be equipped with two redundant FBCTs, using the same acquisition electronics, for monitoring the ejected beam. In order to get good performance, there will be a DC restoration with a successive integrator and S/H circuitry used in the ring. The result of integration is digitized and stored in memory. Beam synchronous timing with 40 MHz frequency is used to trigger the system. The measurement precision

for the pilot beam of 5×10^9 protons in a single bunch is expected to be around 5% (worst-case 10%), and for the nominal beam, below 1%. The transformer cores will use low droop, radiation hard material, with a specified droop below $2\%/\mu$s, and with the sensitivity approx. 1.25 V/A. Once injection is completed, the transformers will be used to measure the circulating bunches, by averaging the acquired bunch intensities over 20 ms, yielding to approximate precision of 1% for pilot beams.

The DC current transformers (DCCT) are based on the principle of magnetic amplifiers and will measure the mean intensity or current of the circulating beam and they can be used to measure the beam lifetime. Because of their operational importance, two of the devices will be installed in each ring. Currently a resolution of 2 μA can be reached but a 1 μA is targeted corresponding to 5×10^8 circulating particles. The temperature dependence of the output current is $\sim$5 μA per degree which makes either temperature stabilisation or frequent re-adjustment of the offset a necessity. With an intensity of 4.8×10^{14} protons and a lifetime of 25 h driven by proton-proton collisions the decay rate is 5×10^9 protons/s. With a measurement time of 10 s this decay should be seen with 1% precision. A resolution of 1 μA is, however, insufficient for measurement of the pilot beam which can only be achieved with the fast transformers. The front-end electronics generating the DC transformer feedback current should be placed as close as possible to the sensor in the ring. However, the radiation induced by the beam and by the RF cavities during their conditioning will be an issue. If the finest resolution is required for measuring the beam over the whole dynamic range, then an ADC of at least 20 bits, located in the front-end electronics is required. The data will be transmitted to the front end computer (DSC) installed in a surface building.

8.3   Beam loss system

The loss of a very small fraction of the circulating beam may induce a quench of the superconducting magnets or even physical damage to machine components. The detection of the lost beam protons allows protection of the equipment against quenches and damage by generating a beam dump trigger when the losses exceed thresholds. In addition to the quench prevention and damage protection, the loss detection allows the observation of local aperture restrictions, orbit distortion, beam oscillations and particle diffusion.

The loss measurement is based on the detection of secondary shower particles using ionisation chambers located outside of the magnet cryostats. The secondary particle energy flux is linear with the initiating protons parameters. To observe a representative fraction of the secondary particle flux detectors are placed at likely loss locations. The calibration of the damage and quench level thresholds with respect to the measured secondary particle energy deposition is simulation based.

The criteria used to define the dynamic range are given by the calculated damage and quench levels and the expected usage. The observation time range is defined by the fastest possible use of a beam dump trigger signal by the beam dump itself and the response time of the helium temperature measurement system. Different families of BLM monitors are defined to ease the monitor design (see table 8.3) [41].

Table 8.3: Functional families of BLM.

Type	Area of use	Dangerous consequences in the case of failures	Time resolution
BLMC	Collimation sections	yes	1 turn
BLMS	Critical aperture limits or critical positions	yes	1 turn
BLMA	All along the rings	no	2.5 msec
BLMB	Primary collimators	no	1 turn bunch-by-bunch

8.4 Transverse profile measurement

User requirements led to the definition of four functional modes to be mapped on the different types of hardware monitors:

- A single-pass monitor of high sensitivity (pilot beam) with a modest demand on accuracy and few restrictions on the beam blow-up due to the traversal.

- A "few-pass monitor" (typically 20 turns) dedicated for the intermediate to nominal intensity range of the injected beam for calibration or matching studies. The blow-up per turn should be small as compared to the effect to be measured.

- A circulating beam monitor, working over the whole intensity range. No blow-up is expected from such a monitor.

- A circulating beam tail monitor optimised to scan low beam densities. In this mode, one may not be able to measure the core of the beam. The measurement should not disturb the tail density significantly.

The monitor types include wire scanners, residual gas ionisation monitors and synchrotron light monitors using light from D2-type superconducting dipoles. Synchrotron light monitors are also under development for using light from superconducting undulators in each ring. Point 4 is the default location for all instrumentation.

8.5 Longitudinal profile measurement

This measurement is a dual application of the Transverse Profile Monitor light source [42] with the aim of using synchrotron light to measure bunch profiles with a dynamic range of 10^5, enabling measurements and monitoring of bunch lengths, tails, un-bunched beam, ghost bunches and the abort kicker rise time gap. A part of the synchrotron light generated by the superconducting dipoles and undulator magnets of the Transverse Profile Monitor is collected by a separate fixed mirror offset behind the transverse optics. It is estimated that 2×10^6 photons will be collected per passage

of each 1.1×10^{11} proton bunch. This intensity remains reasonably constant from injection energy up to 7 TeV. However, the spectral distribution changes with beam energy. At injection energy the undulator produces a distribution peaked around 950 nm but at higher energies the spectral profile extends from 200 nm to 2'000 nm, although only a part of this range can be used by the instrument. The photon flux reliably mimics the beam in both time and intensity. Two detection methods are under study at Lawrence Berkeley Laboratory.

An alternative system is to use an array of fast Single Photon Detectors (SPD) and time-of-flight recorders, continuously detecting the photon flux with the data being accumulated into registers.

8.6   Luminosity monitors

The nominal LHC luminosity for ATLAS (Point 1) and CMS (Point 5) is 10^{34} cm^{-2}s^{-1}, for beams of 2'808 bunches of 1.1×10^{11} protons each. The other two interaction regions will have lower nominal luminosities of the order of 10^{32} cm^{-2}s^{-1} for LHCb (Point 8) and 10^{30} cm^{-2}s^{-1} for ALICE (Point 2). With different filling patterns and optics, the global luminosity range is from 10^{26} to 10^{34} cm^{-2}s^{-1} and for the ion runs between 10^{24} cm^{-2}s^{-1} and 10^{27} cm^{-2}s^{-1}.

The proton beams are bunched with a bunch-to-bunch distance of 25 ns (or a multiple of 25 ns). This corresponds to a maximum bunch crossing frequency of 40 MHz. Under nominal conditions the beams do not collide head on, but with a small angle of the order of 150-200 μrad to avoid unwanted collisions near the interaction point. The plane containing the two beams (collision plane) can be rotated and be different in the four interaction regions.

The aim of the machine luminosity monitors [43] is to measure the interaction rates for the setup, the optimisation and the equalisation of the beams at the interaction regions. The monitors must be simple, fast and robust and preferably be of one design for all four interaction points. The requirements on accuracy go from around 10% for the beam finding mode to 0.25% for the collision feedback. Measurement times also vary from minutes in beam finding mode (very low luminosity) to one second at nominal luminosity. The monitors should also allow the measurement of the crossing angle with an accuracy better than 10 μrad in the range 0-200 μrad.

In order to detect and correct eventual bunch-by-bunch effects, a bunch-by-bunch luminosity measurement is also required. The detectors, readout and acquisition systems must therefore be capable of operating with a useful bandwidth of 40 MHz.

The machine luminosity monitors are flux monitors installed in the TAN absorbers 141 m away on both sides of the high luminosity IR1 and IR5 and at equivalent positions in IR2 and IR8. They measure the flux of the showers generated by the neutral particles created in the collisions (neutrons and photons). Neutral particles are chosen in order to suppress the background related to beam losses. The radiation dose to the detectors is very large, 170 MGy/yr, and poses a constraint on the choice of the technology. The detectors have a rectangular surface $\sim$10 cm $\times$ 10 cm. and each detector consists of four rectangular fast, pressurised, gas ionisation chambers, assembled in a 2×2 array, which is placed behind $\sim$30 cm of copper at the shower maximum inside the TAN. An alternative technology that is still under investigation consists of the use of polycrystalline CdTe discs in a 2×5 array.

8.7 Tune, chromaticity, and betatron coupling

Reliable measurement of betatron tune, and the related quantities tune-spread, chromaticity and betatron coupling, will be essential for all phases of LHC running from commissioning through to ultimate performance luminosity runs. For injection and ramping, the fractional part of the betatron tune must be controlled to ±0.003, while in collision the required tolerance shrinks to ±0.001. With the exception of Schottky scans and the "AC-dipole" excitation outside the tune peak, all tune measurement techniques involve some disturbance to the beam. The resulting emittance increase, while acceptable for some modes of running, has to be strongly limited for full intensity physics runs. Different tune measurement systems are therefore envisaged.

8.7.1 General tune measurement system

Use of standard excitation sources (single kick, chirp, slow swept frequency, and noise). It should operate with all filling patterns and bunch intensities and be commissioned early after the LHC start-up. Even with oscillation amplitudes down to 50 μm, a certain amount of emittance increase will result, limiting the frequency at which measurements can be made. It will therefore probably be unsuitable for generating measurements for an online tune feedback system.

8.7.2 AC dipole

This emittance-conserving beam excitation was studied at BNL for adiabatic resonance crossing with polarised hadron beams and it was realised that the same principle could be used to diagnose the linear and non-linear transverse beam dynamics. The principle is to excite the beam coherently at a frequency close to, but outside its eigenfrequencies, by an oscillating dipole field. Hence the name AC dipole is given to the exciter. In the simplified model of a linear oscillator, the beam is expected to oscillate at the exciter frequency with a phase shift of $\pi/2$. The energy of the coherent oscillation does not couple with the incoherent oscillations of the individual beam particles. There is therefore no change of beam emittance. The forced beam oscillation amplitude is inversely proportional to the difference of the betatron tune and the exciter frequency, which is the major parameter in the design of the AC-dipole strength. Ideally, one would like to create large oscillation amplitudes, which requires the excitation frequency to approach the betatron tune, but a certain difference has to be maintained to preserve the emittance.

8.7.3 High sensitivity tune measurement system

The beam is excited by applying a signal of low amplitude and high frequency to a stripline kicker. This frequency is close to half the bunch spacing frequency (40 MHz for the nominal 25 ns bunch spacing). The equivalent oscillation amplitude should be a few micrometers or less for a β-function of about 200 m. A notch filter in the transverse feedback loop suppresses the loop gain at this frequency, where instabilities are not expected to be a problem. If the excitation frequency divided by the revolution frequency corresponds to an integer plus the fractional part of the tune, then coherent betatron oscillations of each bunch build up turn by turn (resonant excitation). A batch

structure with a bunch every 25 ns "carries" the excitation frequency as sidebands of the bunch spacing harmonics. A beam position pick-up is tuned to resonate at one of these frequencies.

8.7.4 Chromaticity measurement

The chromaticity is measured by varying the mean radial position (or energy) of the beam by changing the RF frequency and measuring the tune.

At injection the linear chromaticity must be controlled to better than $\Delta Q' = \pm 1$ unit. This relaxes to ± 3 units in collision. During the "snap-back" phase of the magnet cycle at the beginning of the ramp, the b_3 multipole in the main dipoles can generate a chromaticity change of up to 2.7 units per second. Feed-forward, on-line reference magnet measurements and modelling will be used to control "snap-back".

8.7.5 Betatron coupling measurement

The working point of the LHC will be close to the diagonal and coupling compensation may be needed before making tune and chromaticity measurements. Two classical methods can be used to measure betatron coupling. The first method is the "closest tune approach" method and the second is the "kick" method.

8.8 Long-range beam-beam compensation

Due to the small bunch spacing, the LHC beams experience 15 'near-misses' on each side of every collision point. In IP1 and IP5, the beam separation is 9.5σ on average. In the other two collision points, the normalised separation is larger and their contribution to the long-range beam-beam effect can be neglected. The non-linear part of the long-range interactions is the dominant mechanism for single particle instability [44], even though the tune spread is small enough. A very fast diffusion in amplitude is observed for beam amplitudes of 6 to 8σ. The topology of the long-range interactions in LHC makes it possible to devise a simple but accurate weak-strong model where the weak beam, assumed round, is perturbed by currents flowing in wires on either side of the crossing points (strong beam). This model leads naturally to a compensation system [45] made of genuine wires, excited by a constant current for the average compensation of the bunches, or by a pulsed current in an option where the bunches would be individually corrected. It is planned to place these wires along the beam at positions where the beams are already in separate channels. They should be placed between the two channels for a horizontal crossing, and above or below for a vertical crossing. The beam-wire distance should be equal to the beam separation at the long-range interaction points (9.5σ). Studies of robustness show that they can be further retracted to 12σ, i.e., well in the shadow of the collimators. The wire excitation is 83 A m on each side of every crossing point. The β-function is not relevant (provided it is the same in both planes). The phase advance between perturbation and correction must be as small as possible, to correct all linear and non-linear terms. The strong focusing of the LHC low-β sections allows suitable positions to be found at 112 m from the crossing points, and space has been reserved.

Chapter 9

Control system

9.1 Introduction

The LHC control system will be an extension of the infrastructure already in use today for the LHC Injector Chain and the Technical Services. Nevertheless, the LHC will present unique challenges for the control system. The hardware is of unprecedented complexity and requires a precise and unambiguous description. Failures could lead to long cryogenic recovery times and long magnetic conditioning cycles. Operational efficiency will depend on both the technical services and the accelerator hardware control systems. The high stored energies and beam powers will require rigorous operational procedures, sophisticated diagnostics and real-time automation. The challenging design parameters and the large dynamic effects will only be mastered by a flexible control strategy, adapted to changing circumstances as the knowledge of the LHC improves.

9.2 Architecture

The LHC control system architecture is largely based on standard components employed worldwide for the control of accelerators and used during recent years for the CERN injectors (PS, SPS) and the LEP machine. However, there are two major changes in the LHC era:

- The consistent use of object-oriented technologies and design principles for the control of beam-related systems and,

- The wide use of industrial controls solutions for the supervision of complete subsystems of the LHC.

9.2.1 Overall architecture

As shown in figure 9.1, the LHC control system has three hierarchical layers of equipment communicating through the CERN Technical Network, a flat Gigabit Ethernet network using the TCP-IP protocol (section 9.2.2). Starting from the bottom of figure 9.1:

- *At the equipment level*, the various actuators, sensors and measurement devices are interfaced to the control system through three different types of front-end computers:
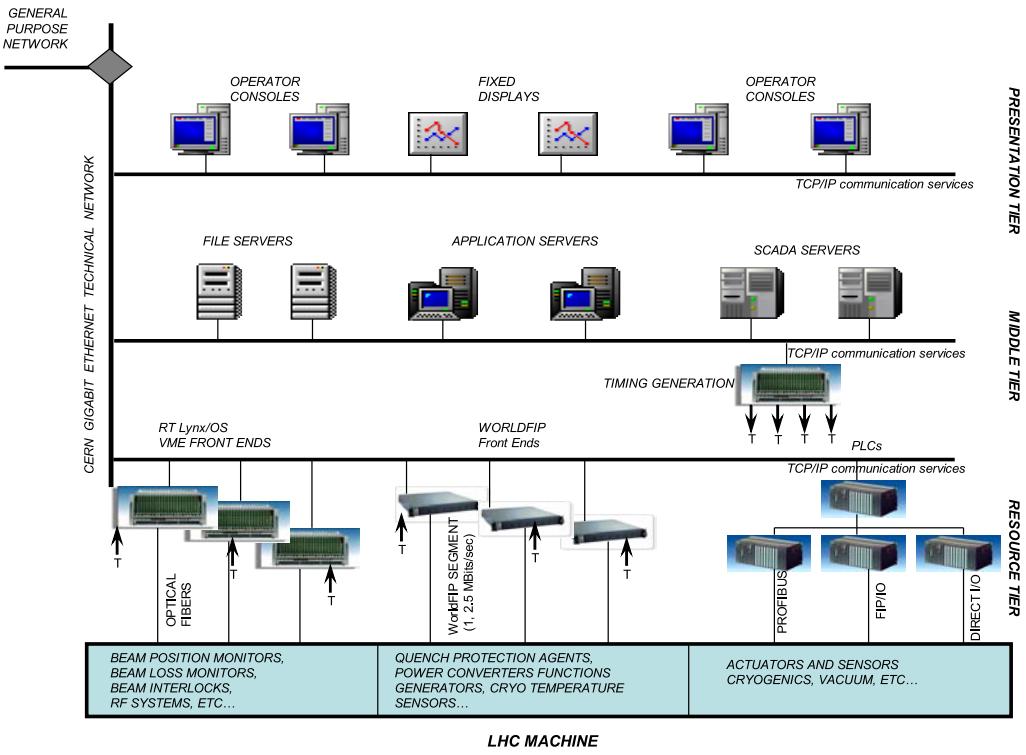
Figure 9.1: Control system architecture.

- **–** VME computers dealing with high performance acquisitions and real-time processing; these employ a large variety of I/O modules. Typically, the LHC beam instrumentation and the LHC beam interlock systems use VME front-ends.

- **–** PC based gateways interfacing systems where a large quantity of identical equipment is controlled through fieldbuses, such as the LHC power converters and the LHC Quench Protection System.

- **–** Programmable Logic Controllers (PLCs) driving various sorts of industrial actuators and sensors for systems such as the LHC Cryogenics systems or the LHC vacuum system.

- • *At the heart of the control system*, powerful UNIX servers host the operational files and run the LHC applications:

  - **–** Application servers hosting the software required to operate the LHC beams and running the Supervisory Control and Data Acquisition (SCADA) systems.

  - **–** Data servers containing the LHC layout and the controls configuration, as well as all the machine settings needed to operate the machine or to diagnose machine behaviour.

  - **–** Central timing, which provides the cycling information for the whole complex of machines involved in the production of the LHC beam, and the timestamp reference.

Processes running in these servers will communicate with the equipment access machines using various mechanisms and protocols such as the Common Object Request Broker Architecture (CORBA) and TCP-Modbus.

- **At the control room level**, consoles running the Graphical User Interfaces (GUI) will allow machine operators to control and optimise the LHC beams and to supervise the state of key industrial systems. Dedicated fixed displays will also provide real-time summaries of key machine parameters.

9.2.2 Network
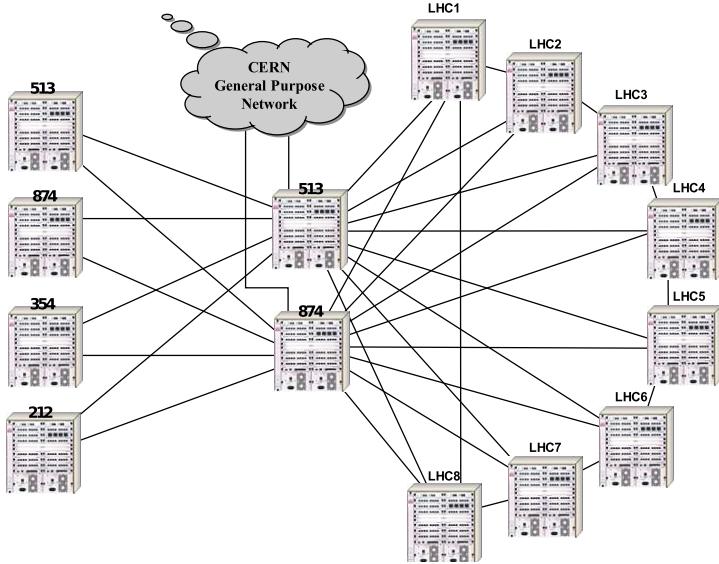
The control system for LHC relies on the CERN Technical Network. This network uses IP addresses of the form *172.18.xxx.xxx*. The address prefix prevents any direct communication between the technical network and the Internet. The infrastructure is interconnected with the General Purpose Network so that communications from within the Organization are still possible; however, the technical network can be completely isolated if required.

The technical network is a highly sub-netted, routed network that implements a high performance redundant backbone, reduces parasitic traffic, and keeps the overall structure maintainable. As shown in figure 9.2, the basic distribution is based on a redundant Gigabit Ethernet backbone using fibre optical distribution. The core consists of two redundant backbone routers located in the CERN computer centre and in the Prévessin control room, where most of the fibres terminate. These two central routers are interconnected in a redundant way to a series of regional routers located in the following buildings:

- The computer centre (building 513) for central services like Oracle databases and main file servers.

- The Meyrin control room (building 354) for the control of accelerators located on Meyrin site.

- The technical control room (building 212) for the supervision of the 2 CERN sites.

- The Prévessin control room (building 874) for the SPS control and other technical services located on the Prévessin site.

- Each LHC pit (SR building) for the LHC machine and technical services control.

In each technical building there are one or more "star points" configured to respect the maximum cable length of 100 m for 100-BaseT connections between the end-node and a high performance Fast-Ethernet switch. This switch usually has a 100 Mbps uplink to the closest regional router that may be upgraded to Gigabit if needed. Close to regional routers, 1 Gbit/s Ethernet may easily be made available if needed.

Active equipment in the network architecture is installed with a double power supply connected to two independent power sources (normal and secured), in order to ensure proper connectivity even in case of a power-cut on either 220 V distribution.

Figure 9.2: The CERN Technical network.

Because the technical network can be completely isolated from the external world, independent dedicated redundant name and time servers have been implemented. These servers are installed at different locations and connected to different regional routers to ensure full redundancy of the system. It must be noted that because the technical network infrastructure is interconnected with the general purpose network, security break-ins can be attempted on the devices connected to this infrastructure. End nodes security survey and updates must be made regularly.

9.3   Equipment access

9.3.1   The VME and PC Front End Computers

Most of the non-industrial accelerator hardware in the PS, SPS, and LHC sites is already connected to the control system via VME or PC based Front End Computers (FEC). These systems run a real-time operating system called LynxOS from LynuxWorks [46], or Red Hat Linux [47]. There will be several hundred FECs distributed in the surface buildings of the LHC and in some cases in the underground areas. Wherever possible, they will be diskless to increase reliability and will boot over the network.

A set of commercial or CERN-made hardware interface boards is being standardised for the LHC, together with the necessary device drivers (e.g. timing generators, timing receivers, beam interlock controllers, digital acquisition boards, WFIP cards, digitisers, etc.). The type of hardware (VME or PC), as well as the Operating System (Linux or LynxOS), will be selected according to the performance needed and the availability of the specific drivers.

These FECs will execute the equipment access software which is part of the *resource tier* (figure 9.1). This software accesses data from the hardware interface boards and provides it, either via subscription or command/response, to any software agent in the control system.

A dedicated FEC software framework (section 9.7.1) has been developed in order to simplify and standardise the software running in the FECs.

9.3.2 The PLCs

PLCs are increasingly used for controlling industrial equipment for LHC. This type of controller can be chosen when the process is not synchronised to accelerator timing and when the sampling period required is not smaller than 100 msec. PLCs offer ease of programming process logic via standard high-level languages (IEC-61131-3), cost efficiency, high reliability and adaptation to industrial environment. They are used in typical industrial controls fields such as electricity, water, gas, cooling, ventilation, but also in accelerator-specific fields of machine cryogenics, interlocks, vacuum, radio-frequency and beam extraction. PLCs are generally part of a complete subsystem including supervision (section 9.7.6). In a few cases, they are accessed through VME FECs. As with any other FEC in the Controls Infrastructure, PLCs benefit from generic facilities such as remote reset, monitoring and optional clock synchronisation.

9.3.3 The supported fieldbuses

The two fieldbuses used in the LHC accelerator, namely WorldFIP and Profibus, are among the three fieldbuses recommended at CERN. They are both supported by an internal CERN service. These fieldbuses typically allow longer distance and more robust protocols than Ethernet. In addition, they are the only means of connecting equipment located in the LHC tunnel or other radioactive areas.

9.3.4 The WorldFIP fieldbus

Table 9.1 summaries the LHC WorldFIP installation needs. WorldFIP is selected when the following features are required:

- Determinism (up to 10 μs); is required for:

  - The real-time control and synchronisation of LHC equipment.
  - High precision time distribution.
  - The management of periodic data.

- Robustness in severe environments and in particular:

  - Its resistance to electromagnetic noise (level 3).
  - Its good resistance to high radiation levels (based on robust semiconductors and a magnetic coupling ensuring galvanic isolation).

- Data Rates:

  - WorldFIP will be used to control largely distributed LHC systems at high data rates (1 MBits/s and 2.5 MBits/s).
  - High load factor possible (70 to 80% of the network bandwidth).

Table 9.1: WorldFIP Needs for the LHC machine.

LHC System	Required Time precision (ms)	Cable length (km)	Data rates
Magnet Protection	1	61	1 MBit/s
Power Converters	0.01	45	2.5 MBit/s
Beam Instrumentation	500	50	31.25 KBit/s
Radio Frequency	1	5	1 MBit/s
Cryogenics	500	90	1 MBit/s
Survey	1000	44	31.25 KBit/s

9.3.5 The Profibus fieldbus

Profibus has been selected for several applications in the LHC, such as fast kicker magnets, cooling and ventilation, vacuum, cryogenics, magnet and power interlock controllers. The main reasons to select Profibus for these applications are:

- The robustness of the protocol and simplicity of configuration.

- The large variety of remote I/O systems available with Profibus.

- The ease of integration with Siemens PLCs.

- The availability of radiation-tolerant remote I/O on Profibus.

- Its capacity to be used as an instrumentation bus (Profibus-PA) with a wide range of instrumentation products offering Profibus as standard means of connection.

9.4 Servers and operator consoles

The upper layers of the LHC control system (figure 9.1) will be deployed on operation consoles and fixed displays, files and applications servers to meet the requirements of the LHC applications software. The servers will be used to run the LHC middle-tier software, to host operational programs and data files, and also to offer specific services (web services for operation, fixed displays, SCADA servers, Database servers, etc.). The servers will run the Linux operating system. Emphasis will be put on the hardware reliability and availability issues by selecting multi-CPU architectures with redundant and hot swappable power supplies, discs and fans. Mirroring and RAID techniques will be used to ensure data integrity and error recovery.

9.5 Machine timing and UTC

9.5.1 Central beam and cycle management

The LHC beam production involves a long chain of injectors which need to be tightly synchronised. Moreover, the different types of beam to be produced for LHC are only a subset of the beams that the injectors have to produce for the rest of the experimental programme. All these beams are

produced in sequences of typically a few tens of seconds. The composition of these sequences changes many times a day, and the transition between different sequences has to be seamless. To manage the settings of the machines and to synchronise precisely the beam transfer from one injector to the other up to the LHC, a Central Beam and Cycle Manager (CBCM) is required. The CBCM will:

- Deliver General Machine Timing (GMT).

- Provide Beam Synchronous Timings (BST).

- Elaborate the "telegrams" specific to each machine and broadcast over the GMT networks.

A "telegram" describes the type of beam that has to be produced and provides detailed information for sequencing real-time tasks running in the FECs and for setting up equipment.

The CBCM drives seven separate GMT networks dedicated to the different CERN accelerators, including the LHC, and four BST networks, of which three are for the LHC and one for the SPS. To achieve extreme reliability, a CBCM runs in parallel on two different machines, with a selector module capable of seamlessly switching between them.

9.5.2 Timing generation, transmission and reception

Several hardware timing modules are required either to produce reference clocks and timing events, or to extract the timing pulses or the interrupts needed to drive the equipment from the distributed timing data. The following is a list of these modules.

- The CTSYNC module provides the "master" clocks from a 10 MHz oscillator which has a stability which is better than 10^{-10}.

- The CTGU module encodes events to be transmitted over the GMT network: the millisecond events, machine timing events, telegrams, and the Universal Coordinated Time (UTC) events.

- The CTGB is the driver module for the BST network; it uses the TTC technology [48]. The CTGB will also send the 1 pulse per second (1PPS) UTC time and some telegram events over these networks, hence its inclusion in the CBCM.

- The CTRP is a GMT multi-channel reception module. It comes in three formats: PMC, PCI, and VME and can generate timing pulses with very low jitter. The CTRP recognises the various types of timing events: UTC time, the telegrams, the millisecond and other machine events and can use them to trigger pre-programmed actions.

9.5.3 UTC for LHC time stamping

A key requirement for the LHC control system is the need for a timing reference to timestamp the accelerator data. UTC has been adopted as the standard of date and time for all CERN accelerators [49, 50]. UTC is the basis for the worldwide system of civil time. The motivation behind this decision was to eliminate the problems associated with the changes between the winter and summer standards, particularly for the change in October (CET changes from UTC+2H to UTC+1H) when the time is repeated for one hour.

Table 9.2: Required LHC time stamping accuracy.

System	Timestamp Accuracy
Beam Dump	
Beam Instrumentation	
Radio Frequency	< 0.05 ms
Injection (Kickers…)	
General Machine Timing	
Machine Interlocks	
Quench Protection	1 ms or better
Power Converter	
Feedbacks (orbit, tune …)	
Cryogenics	1 – 10 ms
Vacuum	
All other systems	

9.5.4 UTC generation, transmission and reception

The source of date and time for all CERN accelerators will be a Global Positioning System (GPS) time receiver connected to the CTGU. The GPS provides UTC referenced date and time plus a very accurate 1 PPS tick, which is used by the CTGUs to synchronise the UTC time.

At initialisation the CTGUs receive the date and time information from the GPS receiver then run independently, using the clock delivered by the CTSYNCH until a manual resynchronisation is carried out. CTGUs provide the time every second in UNIX standard format. UNIX time can then easily be converted by software into year, month, day, hour, minute and second.
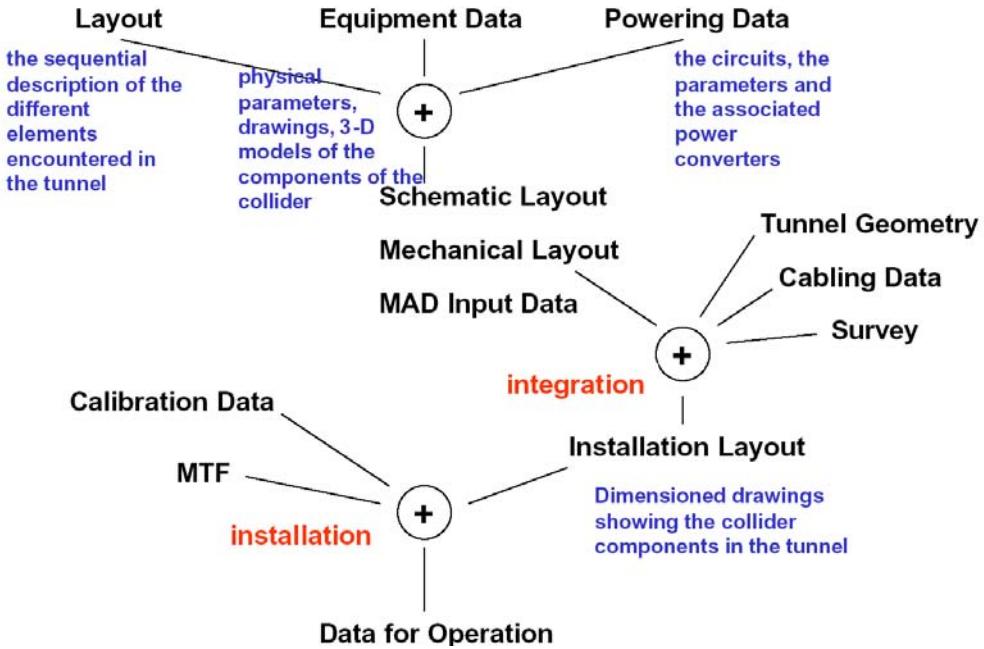
UTC time can be provided by the CTRP modules to timestamp the data to be logged with a 25 ns resolution. Using an optional CERN-developed chip the resolution can be brought down to 1 ns. The required time-stamping granularity for the different LHC systems [51] is shown in table 9.2. The 1 ns performance is required principally in the injector chain.

9.5.5 NTP time protocol

PLCs will use the Network Time Protocol (NTP) [52] to synchronise the time (section 9.2.2). NTP provides accuracies typically within a few milliseconds on LANs and up to a few tens of milliseconds on WANs. This accuracy is sufficient to properly tag most of the PLC data. Some PLCs that require higher precision for time-stamping their data will use the high precision 1 PPS tick from the CTRP; in this case, NTP will be used only to relate this tick to UTC time.

9.6 Data management

The LHC Machine will be of unparalleled complexity in terms of number of components and in the manipulation of operational parameters. A large number of signals will be made available to the control room, including over 100'000 from the cryogenics, machine protection, and beam

Figure 9.3: LHC Reference Database.

monitoring systems. Over 1'600 electrical circuits will power a wide variety of magnet systems. The quantity of data to be recorded for diagnostics after a "beam abort" has been estimated as a few gigabytes; during Hardware Commissioning, it is anticipated that 1 terabyte of information will be accumulated. Operation of the machine will rely on stringent control of the hardware settings. A complete beam operational history will be created in order to build a long term understanding of the accelerator performance. Such a variety and volume of data cannot be exploited without data management tools. Building on the experience of LEP construction and operation [53], Oracle has been selected as the strategic choice for data management at the LHC.

9.6.1 Offline and online data repositories

As shown in figure 9.3, the LHC Reference Database is being populated during the machine construction in order to manage the information essential for integration studies, installation, and hardware commissioning. This offline Database will be one of the sources of data that is required to configure the online LHC control room application software, providing essential information such as the layout, accelerator optics, and calibration information. The electrical circuit data, described in the next section, are an example of the use of the database both during construction and operation.

While the Reference Database will be an offline source of information during machine operation, several online databases — alarm archives, periodic data logging, Post Mortem event archive, and accelerators settings management — will be required to capture the operational history. These are described in the later sections of this chapter.

9.6.2 Electrical circuits

The powering layout of the LHC is extremely complex, comprising 1'232 main dipole magnets, about 450 quadrupole magnets, and several thousand corrector magnets, powered in 1'612 electrical circuits. The currents feeding the magnets range from 60 A (for small correctors) to 12 kA for main dipole and quadrupole magnets, while the energy stored in the superconducting magnets is about 10 GJ. About 80'000 high current connections have to be made and tested in the tunnel during the installation and commissioning phases.

To ensure the correct connection of the superconducting bus bars around the 27 km long machine, a detailed description of the electrical circuits and their elements has been added to the layout description of the machine in the LHC Reference Database [54]. This description has been linked to the existing data describing the physical and magnetic layouts. Changes of this powering information are very rare, and updates have to be performed only if there are major changes in the physical or powering layout of the machine. Information about the powering will be provided to users to:

- Perform the interconnections between cryo-assemblies in the long arc cryostats.

- Configure the powering interlock PLCs.

- Create MAD input files to calculate the beam optics.

- Display detailed circuit and equipment information via the web and the LHC equipment catalogue.

- Configure hardware state and beam parameter control room application software.

Integrity will be ensured by using the same information to generate the machine optics, make the circuit connections during assembly, configure the behaviour of the interlock system, and operate hardware and beams.

9.6.3 Control system configuration

The control system is composed of a large number of application programs, a middleware layer, VME- and PC-based FECs with control software, industrial PLCs, fieldbuses, and hardware interface modules. These components have shared characteristics, associated with their type or class, and specific addresses and parameters associated with their instances. All these data will be stored and described in an Oracle relational database, the *Controls Configuration Database*. This centrally managed configuration information allows the use of generic software on all levels. A layer of Java and C++ interfaces will enable all control room software to be data-driven, by fetching at runtime the layout, interconnection, access methods, and parameters of remotely controlled LHC equipment. All FECs can be automatically configured and bootstrapped with files generated from the database. Thanks to a generic design, the database also holds the controls configuration of the injection accelerator chain of the PS and SPS complexes. This common source of data will make it possible to have uniform controls data management throughout the accelerator chain, as well as effective sharing of tools and methods that use this data [56]. On top of the Configuration Database,

a Web browser service will allow exploration of all the information about the underlying controls hardware and software.

9.7 Communication and software frameworks

9.7.1 FEC software framework
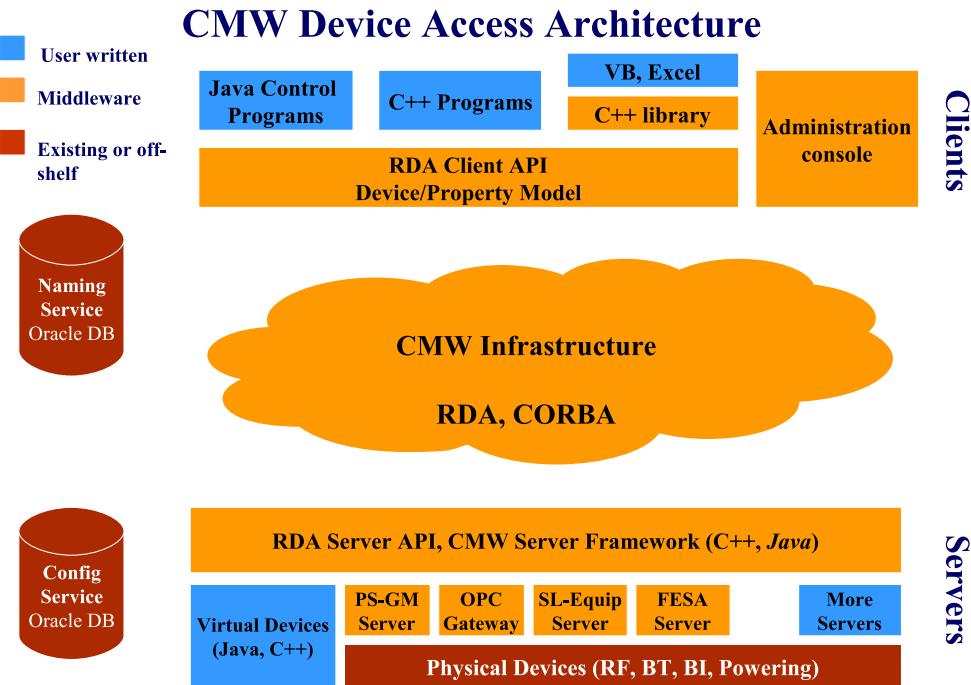
The software running in the LHC FECs will be developed using a specific framework, known as FESA. This framework is a complete environment for the equipment specialists to design, develop, test, and deploy real-time control software for the FECs. This framework is also the new standard for the LHC injector chain. The recurrent components of the equipment control software have been formalised into a generic model. It defines the structure of the real-time part of the software, which handles hardware and interrupts, together with the structure of the server task that handles external requests. In order to enhance the productivity and the maintainability of the code, a clear separation between the generic and the equipment specific parts is enforced, and automatic code generation is extensively used. As a result, the ratio between the generic/generated code and the developer-specific code is usually around 10 to 1. An object-oriented design and a C++ implementation have been used for supporting this approach.

For building the control software, the programmer is provided with a set of configuration tools for the creation and evolution of any FESA component. These tools are directly linked to the control system configuration DB (section 9.6.3). They are used for the definition of internal data structures, syntax of external commands, and binding between hardware events or external requests and treatment code. External requests are handled by dedicated server tasks that fully implement the device access model of the Controls Middleware, which is described in the next section. Compound data types are supported for data coherency and for performance purposes.

System-level services are provided for the operation of the FECs: handling of errors from the equipment software, monitoring of processes, etc. These dedicated services preserve the real-time behaviour of the FECs, and they support remote control for adjusting parameters, such as the trace level of a task, or for executing corrective action like restarting a process. The developers and the users (equipment-specialists, operators, and maintenance team) are also provided with a set of interactive tools, test programs and Java libraries which allow immediate testing of all the functionality of the software during its development and operation. These facilities are all generated in an automatic manner, without any specific code being required. The FESA framework is built for LynxOS and Linux platforms. The software tools are written in Java and are thus platform independent. No commercial software requiring a run-time license has been used.

9.7.2 Controls Middleware

The Controls Middleware (CMW) is the ensemble of protocols, Application Programming Interfaces (API), and software frameworks, which allow seamless communication between the software entities of the control system. Two conceptual models are supported: the device access model and the messaging model. The device access model is mainly used in the communication between the

CMW Device Access Architecture

Figure 9.4: The Device Access Model.

resource and middle tiers, while the messaging model is mainly used within the business tier, or between the business tier and applications running in the presentation tier.

9.7.3 Device access model

Figure 9.4 depicts the full architecture of the CMW device access model. The typical use of this communication model is between Java applications running in the middle tier and CMW equipment servers running in FECs. These processes communicate together through the Remote Device Access (RDA) API, which is available for both Java and C++ languages.

Within the device access model, all accelerator equipment can be accessed as "devices". A device is a named entity within the control system, which normally corresponds to a physical device (e.g., beam position monitor, power converter) or to a virtual controls entity (e.g., transfer line). Conceptually, each device has a number of properties that characterise its state. By getting the value of a property, the state of the device can be read. Accordingly, a device can be controlled by setting one of its properties with the required value. 'Get' and 'Set' operations can be either synchronous or asynchronous. In addition to the Get and Set operations on device properties, it is possible to monitor changes to the property via listeners (callbacks). It is often necessary to specify under which conditions the operation has to take place, for instance, to which cycle of the machine the operation applies. These conditions are commonly referred to as context or filter. A list of properties, together with their type description and the semantic of the assessors, is referred to as a contract. Contracts typically serve a specific purpose, such as measurements or settings of a device.

9.7.4 Messaging model

Complementary to the device access model, the messaging model allows any software process to send and receive asynchronous messages in a loosely coupled way. Various application programs for accelerator controls naturally exchange data via asynchronous messages: timing and logging events, notifications, and alarms are typical examples of data which is asynchronously generated from a various set of producers, and which is potentially of interest for multiple consumers. The LHC control system software relies on the Java Message Service (JMS) as the messaging solution for Java-based controls application. The JMS specification adds a standard and vendor-independent API that enables the development of portable, message-based applications in the Java programming language. Moreover, JMS is a strategic technology for the Java 2 Platform Enterprise Edition (J2EE). The LHC Alarm Service is a typical example of a messaging system relying on the publish-and-subscribe paradigm: it subscribes to alarm notifications published by several processes and, after processing, redistributes the result to dedicated consoles and any other controls software component that subscribed to the appropriate alarm content hierarchy.

9.7.5 The J2EE framework for machine control

Applications controlling the LHC beams must handle a great variety of tasks, such as visualisation of data, and significant computation, together with database and equipment access. These applications rely on several services such as security, transactions (to make sure that complex operations are performed automically), and remote access or resource management. The requirements dictate a move towards a modular and distributed architecture. Such an architecture offers a clear separation between the GUI (the user interface), the control (the core business of the application), the model (the abstract model of the accelerator control), and the devices (the physics equipment) that are controlled.

For LHC, a 3-tier architecture is being implemented, in which the middle-tier is responsible for providing all services and for coordinating the client applications running on the operator consoles. In this architecture, shown in figure 9.4, applications are running both in the operational consoles of the presentation tier and in dedicated servers of the middle-tier. The consoles are responsible for the GUI applications and translate the operator's actions into command invocations in the middle-tier. The middle-tier, through its centralised and shared processing power, is in charge of accessing databases and accelerator devices. The middle-tier also ensures the coherency of operator actions and shelters resources. It enforces separation between presentation and application logic and provides shared services to many clients.

To achieve this new programming model, a platform is needed to support the middle-tier. The platform provides the infrastructure with all the necessary common basic services, i.e., all parts of a control system that are not specific to accelerator controls. By using such a platform, the developers can concentrate on writing code for the accelerator control components, such as parameter management, setting generation, cycle handling, and trim management; they do not have to write system level services. The platform of choice today is the J2EE, which is an industrial standard defined by a set of specifications and APIs, implemented by many vendors. J2EE is based on the Java programming language and on a component model known as Enterprise JavaBeans (EJB). Components are the key technology used to write a modular object-oriented distributed

The J2EE Architecture
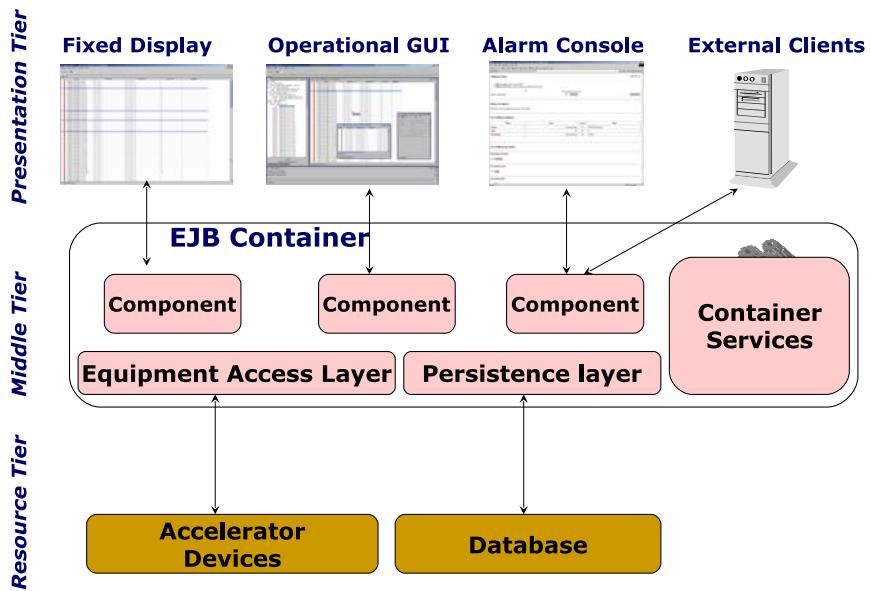
Figure 9.5: The J2EE Architecture.

application. EJB components are "Lego® pieces" that implement a set of interfaces, allowing them to run inside a so-called "EJB container".

As shown in figure 9.5, developers write accelerator-specific code in the form of EJB components, and the EJB container provides the necessary infrastructure to run them, such as remote accessibility, components management, concurrency support, fault tolerance, high availability, scalability, resource pooling, transaction management, and security.

To summarise, the 3-tier approach and the J2EE framework are the basis on which the controls for the LHC are built. This allows effort to be focused on the LHC controls challenges and not on the infrastructure. It exploits existing technology and provides the modular and distributed architecture needed.

9.7.6 The UNICOS framework for industrial controls

Reflecting a trend of the last decade, a single industrial supplier has been chosen for the procurement of the hardware and software for the control of the cryogenic equipment and experimental magnets installed in the LHC accelerator complex. This control system is referred to using the acronym UNICOS, standing for UNified Industrial COntrol System. UNICOS builds on a classic industrial controls architecture, using the PVSS (object-oriented process visualization and control system) SCADA in the Supervision layer, Schneider Quantum PLCs for process control at the Control layer and Schneider Premium PLCs to connect process channels in the Field layer (an alternative is Quantum remote I/O). Communication is based on Ethernet and FIPIO (Factory Instrumentation Protocol Input Output). The software design is an evolution of an object-oriented philosophy used with former control systems [55]. In this approach, each process device (sen-

sor, actuator, or set of devices constituting a process entity) is modelled as an object. This object integrates the process behaviour and the GUI.

9.7.7 The UNICOS object model

In the UNICOS concept, the object implementation is split into two parts:
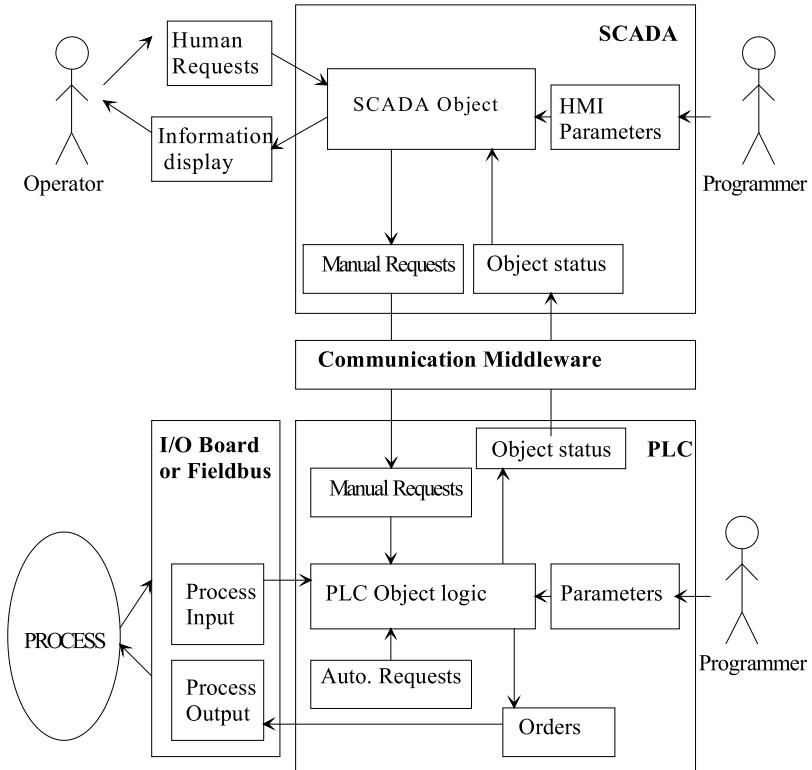
- The GUI functionality - programmed in the SCADA.

- The process behaviour - programmed in the PLC.

The GUI part includes the interaction with the operator by means of graphical components and dedicated panels called "faceplates"; these GUIs inform the operator of the object status, and allow him to send orders. The PLC part contains the process behaviour of the object. The object is linked to the plant through I/O channels that may be linked to the PLC via either a fieldbus or a direct I/O connection. The SCADA and PLC object parts are connected together by a communication layer based on the TCP-Modbus protocol. As shown in figure 9.6, each object has several interfaces and receives the following information:

- Requests from the operator via the SCADA object. These requests are transmitted to the PLC by manual requests through the communication middleware.

- Configuration parameters (GUI or PLC) set during the programming phase and accessible for modification by a program specialist.

- Information from the process (process inputs), consisting of analogue or binary values from sensors and status of other objects.

- Orders from the control logic programmed into an object of a higher hierarchical level via the Auto Requests.

  Three main types of object are defined in the UNICOS architecture:

- Input-output objects which provide the interface to the plant. They link the devices and actuators to the control system. Some basic treatments may be embedded in these objects. Input/output channels are exclusively accessed through such objects.

- Field objects that represent hardware elements, such as valves, heaters, motors, and other devices. Each type of field object has its own associated process logic. This logic integrates specific functions (e.g., alarm generation, transition between set points, interlocking).

- Process control objects that control equipment units grouping several field objects and/or other process control objects. The process logic of these objects is split between a standard part (insuring a homogeneous interface to the environment) and a specific part to handle the process to control.

Figure 9.6: The UNICOS Object Model.

9.8 Control room software

9.8.1 Software for LHC beam operation

The LHC control room applications will be based on a set of common control system services and components, in order to avoid duplication of effort and solutions. The operational software development process relies on common development tools, guidelines, and procedures for construction, testing, integration, deployment, and change management.

9.8.2 Software requirements

The LHC aims at injecting, accelerating, and colliding beams with well controlled beam parameters in an efficient, reliable, and reproducible manner. This is a non-trivial task, since the small aperture, the high stored beam energy, and the sensitivity of the machine to beam losses impose very tight accelerator physics constraints. The superconducting magnets will generate field errors that have large static and dynamic components. The destructive power of the LHC beams and the low tolerances to beam losses will place very stringent demands on the LHC control system. A non-exhaustive list of the main software application categories for LHC is given below:

- **On-line monitoring** of the state and tolerances of every LHC component and interlock system.

- **Measurements** to allow for synchronised acquisition as part of scans, feedback, or at a given point in the ramp.

- **Real time control** to implement feedback on key beam parameters (orbit, tune, chromaticity), plus the feed-forward of corrections from the reference magnets.

- **On-line modeling** including calculation of parameter variations, and feed-forward from the machine into the model.

- **Automatic sequencer** to allow complicated sequences for injection and ramp to be performed systematically.

- **Fixed displays** including transfer lines, beam size, bunch currents, mountain range turn-by-turn, tune FFT, beam loss monitors, global orbit plus crossing angles, beam separation, and transverse position along a batch.

- **Settings management system** to deal with the generation and management of complex settings.

- **Fast, accurate control of the main beam parameters** in both the physics coast and during injection and ramping.

- **Trim facility** incorporating persistent versus geometric correction, scaling, accumulation, smoothing out of errors and corrections, and time and history dependency of errors.

- **Communication with experiments** and other major systems (cryogenics, vacuum, technical services).

- **Scripting environment** for ad-hoc rapid application development for machine development.

- **Miscellaneous support applications** such as an Electronic Logbook.

- **Console Manager** to launch and manage controls applications in a unique manner.

9.8.3 The software development process

The software development follows the Unified Software Development Process, a practical software process model followed by many industrial OO projects. Java is the programming language chosen for the implementation of the high-level services and control room applications, as it enables platform-independent development. XML is playing an increasingly important role in the exchange of data.

The software developers are provided with a suite of selected software tools for code optimisation, quality assurance, and testing, to guarantee the quality of the control room software. Software configuration management facilities are provided on top of the archive engine (RCS) to provide version management services, making it possible to trace and identify any component of an operational application, and to deliver consistent operational software releases. In addition, tools for code building and distribution are available to release operational software components in a multi-versioned repository residing on dedicated fileservers (section 9.4).

Operational software, once released, is deployed locally to the operators' consoles using standard Java-distributed deployment technology, which guarantees automatic delivery of software updates without operator intervention. Local deployment ensures the speed and performance required by operations.

9.8.4 Software for LHC Industrial Systems

Several LHC accelerator industrial subsystems will be accessible from the control consoles via a SCADA supervision interface. SCADA systems are used in a wide variety of industrial domains and therefore typically provide a flexible, distributed, and open architecture to allow customisation to a particular application area. In addition to basic SCADA functionality, these systems also provide strong support for GUI tools, a set of standard interfaces to hardware, as well as an API to enable integration with other applications or software systems. PVSS, the industrial SCADA product recommended at CERN, has the following specific features:
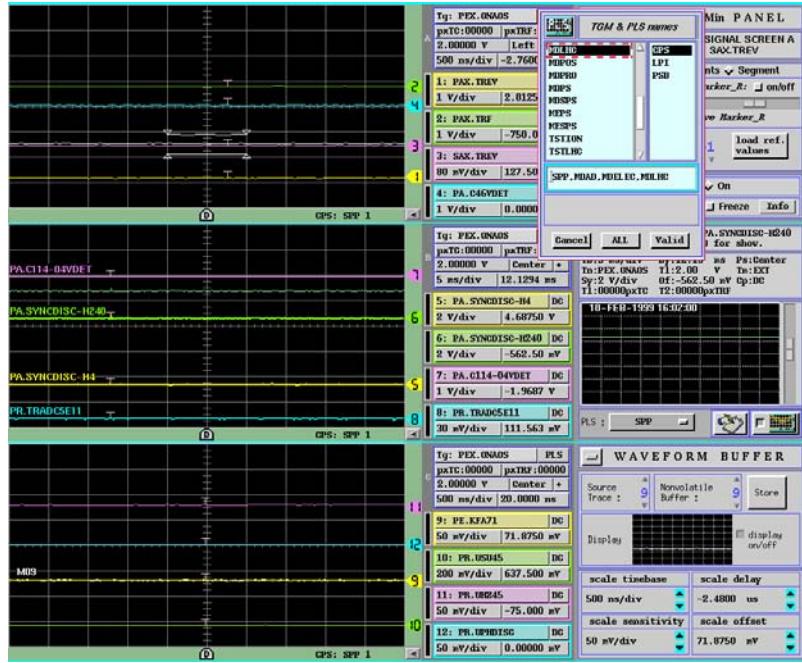
- It can run in a distributed manner.

- It has multi-platform support (Linux and Windows).

- It is device oriented with a flexible structural concept.

- It has advanced scripting capabilities.

- It has a flexible API, allowing access to all features of PVSS from an external application.

The SCADA development process, in particular when based on frameworks such as UNICOS (section 9.7.6), can be based mostly on configuration and graphic editors rather than programming. A unique device configuration database contains all characteristics of the devices, including device addressing, alarm, and data logging parameterisation.

9.9 Services for operations

9.9.1 Analogue signals transmission

While most signals from the LHC will be digitised for internal usage by the respective accelerator systems, some are required for visualisation during tuning and measurement. These include some 200 signals, mainly in the 0 to 10 kHz range from the RF system, and over 300 signals with a typical bandwidth of 50 MHz from the kicker systems for injection and beam extraction. In the injector chain, the nAos system [56] is successfully used to fulfil the need for coherent acquisition and display of analogue signals. The system's main feature is the digitisation of signals in acquisition crates as close as possible to their sources, thereby ensuring optimal fidelity. Whenever possible, in order to save costly oscilloscope modules, signals are multiplexed, allowing some 100 signals to be serviced by one crate containing four two-channel oscilloscope modules. The triggers for all the oscilloscope modules are elaborated from the GMT distribution (section 9.5.1), ensuring a precise time-correlation between signals. The digitised signals are sent through Ethernet to control room

Figure 9.7: Snapshot of nAos GUI.

consoles, where a GUI application (figure 9.7) allows operators to monitor them on four-channel "virtual oscilloscope" screens.

The nAos system is currently being upgraded to more modern, commercial hardware and software platforms. The new version of the system is called Open Analogue Signals Information System (OASIS). It will implement all the above features, including arbitration of resource (i.e., oscilloscopes), allocation to clients, and additional functionality for LHC requirements. This approach will ensure that signals from the injector chain may also be integrated into LHC operation; the older, lower energy machines are more richly instrumented by this system. As with all LHC systems, OASIS must provide information to the Logging (section 9.9.3) and Post Mortem (section 9.9.4) systems. Analogue signals will be monitored by compact PCI-based acquisition systems; the total number of crates will depend on the amount of multiplexing achievable with regard to the number of clients.

9.9.2 Alarms

The detection, collection, management, and distribution of information concerning abnormal situations ranging from severe alarm states to warning states, hereafter referred to as Fault States (FS), uses one global system. The system will accept information concerning any problem associated with the CERN accelerator complex and offer this information, in a structured way, to any interested party. The core part of this system will be the LHC Alarm SERvice (LASER), [57]. As a result of a detailed technology survey, a 3-tier architecture was chosen and is now being implemented according to the J2EE specification (see 9.7.5).

FS detection is performed (figure 9.5) in the resource tier by surveillance software written

by equipment specialists, application programmers, and operators. The LASER system offers a standard interface for these sources to push a FS, by means of either a C or Java API based on the messaging system. FS time stamping at the point of detection, using UTC time, down to the microsecond level if needed, will be crucial in correlating data. The middle-tier will collect the FS by subscribing to all FS sources. A number of services and facilities will be offered at this level including:

- FS persistence.

- Logging of FS transitions using the LHC Logging facility.

- FS dependency and reduction management.

- FS browsing and interaction.

- Administration of the overall system.

- User and configuration management.

- Scaling, using clustering facilities.

- FS distribution according to a FS hierarchy, representing the interest of users.

Finally, the presentation tier will allow clients interested in those services to access them via a Java client interface. The major user of this interface will be the alarm console, which will be used by equipment groups and control centres to select, receive, and display FS, and in order to access all LASER services. Important configuration facilities will allow the alarm console to be personalised.

9.9.3 Logging

The information to be logged is heterogeneous, but usually concerns values of variables that evolve over time, for example cryogenic temperatures, vacuum pressures, magnetic field measurements, bunch intensities, or beam profiles. The total number of logging variables will be on the order of 10^5-10^6, with logging frequencies up to 0.1 Hz. The main purpose of LHC logging is to improve the machine performance and that of the individual subsystems. Therefore the recorded data will be stored and kept accessible over consecutive years, in order to permit comparison of historical data, off-line analysis to search for data correlations, and compilation of operational statistics.

For each of the logged records of the data variables, the date-time value is a key attribute, and therefore correct *"time stamping"* is vital for the exactness of the data. For time stamping, the usage of UTC is endorsed throughout the LHC Logging system (section 9.5.3), with microsecond precision where applicable. In order to enable effective exploitation of the logged data by users such as equipment engineers, control room operators, machine physicists, and CERN managers, the LHC Logging system will employ web-enabled interfaces to graphically visualise the information and to extract it to common desktop tools.

9.9.4 Post mortem

The LHC will be protected by over 10'000 interlock channels, thousands of quench detectors, and around 3'000 beam loss monitors. Many tens of thousands of signals will be available for the operators and engineers to interpret the circumstances of Beam and Power Aborts. The Quench Protection System alone will provide around 80'000 signals for Alarms, Logging, and Post Mortem purposes. Recovery from a perturbation to the nominal magnet cycling will require a minimum of 2 hours (7 TeV back to 7 TeV), which precludes learning by trial and error, as practiced with normal conducting machines.
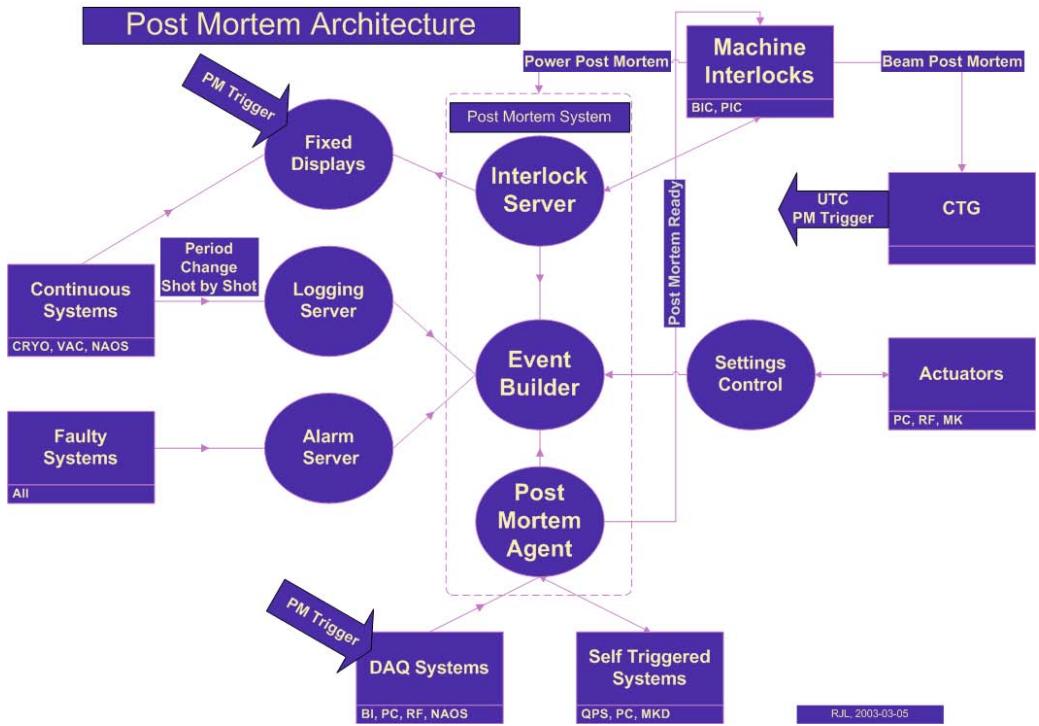
The LHC Post Mortem System (figure 9.8) [51, 58] is required as a suitable diagnostic tool. The purpose of this system is:

- To ensure comprehensive monitoring of machine protection systems.

- To improve the operational efficiency of the LHC by:

    – Providing diagnostics of power and beam aborts - the aim is to quickly identify the origin of failures in order to initiate appropriate action and restore operation,

- Building long-term understanding of accelerator operation,

    – Providing diagnostics for beam losses resulting from equipment malfunction.

- To explain the mechanism if damage occurs.

To achieve these aims, the post mortem data must be *complete* and *coherent* across systems. While it is intended to make full use of diagnostics from Alarms and Logging, these systems will not provide all the facilities required for the understanding of quenches and beam losses in the LHC. In particular, the underlying hardware must capture transient data pertaining to conditions prevailing before, during, and after such events. These transients may be relatively slow when they are provoked by quenches; indeed, in this case, the Logging system will gather some pertinent information, such as cryogenic temperatures. However, in the case of beam losses, the timescales are extended downwards to turns of the machine.

In order to satisfy the aims of being complete and coherent across all LHC systems, the following essential ingredients are required:

- Every piece of LHC equipment and diagnostic system must implement a circular Post Mortem buffer of appropriate depth holding the latest data (for example, 1'000 turns for beam instrumentation).

- This data must be time stamped using a common clock, with a precision related to the corresponding process (see table 9.2).

- The Post Mortem buffers must freeze at the Post Mortem timing event, or by self-triggering in the case of the protection systems.

- Data must be self describing, so that it can be managed by the event builder and analysed by generic tools.

**Figure 9.8**: The LHC Post Mortem Architecture.

The Post Mortem events will be large - several gigabytes - and therefore analysis must be automatic in order to generate digested information for operators. After analysis, the information must be stored in order to build up the longer term history and understanding of the machine. The most relevant data will be stored for the lifetime of the LHC.

Chapter 10

Beam dumping
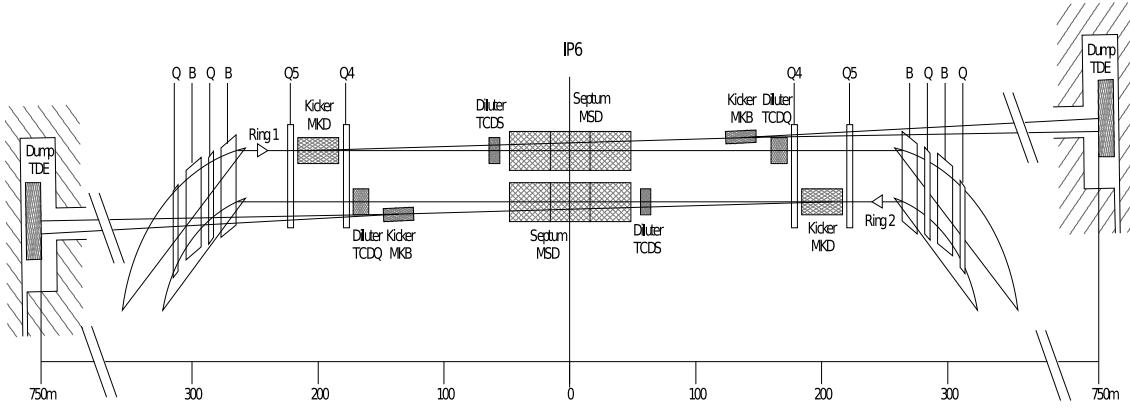
10.1 System and main parameters

The dedicated beam dumping system of the LHC is sited in Point 6. The system is able to fast-extract the beam from each ring in a loss-free way, to an external absorber positioned sufficiently far away to allow for beam dilution, so as not to overheat the absorber material. A loss-free extraction requires a particle-free gap in the circulating beam, during which the field of the extraction kicker magnets can rise to the nominal value. Given the destructive power of the LHC beam, the dumping system must meet extremely high reliability criteria. The system is shown schematically in figure 10.1 and will comprise, for each ring:

- 15 extraction kicker magnets MKD located between the superconducting quadrupoles Q4 and Q5;

- 15 steel septum magnets MSD of three types MSDA, MSDB, and MSDC, located around IP6;

- 10 modules of two types of dilution kicker magnets between the MSD and Q4;

- The beam dump proper, comprising the TDE core assembly and associated steel and concrete shielding, situated in a beam dump cavern ∼750 m from the centre of the septum magnets;

- The TCDS and TCDQ diluter elements, immediately upstream of the MSD and Q4, respectively.

The nominal system parameters are given in table 10.1. The MKD kickers deflect the entire beam horizontally into the high-field gap of the MSD septum. The MSD will provide a vertical deflection to raise the beam above the LHC machine cryostat before the start of the arc sections. The dilution kickers will be used to sweep the beam in an '*e*' shaped form, and after the appropriate drift distance the beam will be absorbed by the TDE assembly. The TCDS and TCDQ will serve to protect machine elements from a beam abort that is not synchronised with the particle-free beam gap.

The beam dumping system must also be able to handle beams that are outside normal parameters, due to equipment failure or abnormal optics settings in the rings. The relevant worst-case

Figure 10.1: Schematic layout of beam dumping system elements around LHC Point 6 (distances in m).

Table 10.1: Overall beam dumping system parameters.

Parameter	Unit	Value
Total horizontal deflection (MKD + Q4)	mrad	0.330
Total vertical deflection (MSD)	mrad	2.400
Dilution horizontal deflection (MKBH)	mrad	± 0.14
Dilution vertical deflection (MKBV)	mrad	± 0.14
Total beam line length (start MKD – end TDE)	m	975
Required particle-free abort gap length	μs	3.0
System Safety Integrity Level (SIL)		3
Beta function at TDE entrance	m	4990 (H), 4670 (V)

Table 10.2: Assumed worst-case LHC beam characteristics for dumping system design.

Beam	Maximum ε_n		Total Orbit [mm]	Beta modulation [%]	Total p+ 10^{14}
	450 GeV [μm]	7 TeV [μm]			
Commissioning	6.0	12.0	± 4	42	0.3
Initial	6.0	12.0	± 4	42	0.8
Nominal	7.5	15.0	± 4	42	3.1
Ultimate	7.5	15.0	± 4	42	5.3

beam characteristics that can be accommodated are given in table 10.2 for the various LHC beams considered.

For the purposes of estimating radiation and heat loads on the TDE, TCDS, and TCDQ, and also for the purposes of the reliability analysis, the assumptions shown in table 10.3 were used for the operational parameters, dump and fault frequencies. In general, these are worst-case assumptions, so as to ensuring that there is an inherent safety factor in the subsequent calculations.

Table 10.3: Assumptions for activation calculations and reliability.

Number of years of LHC operation	20
Number of days of operation per year	200
Number of 7 TeV fills dumped per day (at nominal current)	2
Number of 450 GeV fills dumped per day (at nominal current)	2
Number of dumps at full intensity per beam in LHC operational lifetime	2×10^4
Number of dumps with a missing MKD module per year	1
Number of asynchronous dumps per year	1
Number of total dump system failures per 100 years	1
Total intensity until staged equipment operational (MKB and TDE cooling)	50% of nominal

10.2 Reliability

A fault in the beam dump system could lead to severe damage to the system itself, to the LHC machine, and/or to the LHC experiments, due to uncontrolled beam losses on equipment. It is desired that total beam dump failures will not exceed a rate of 1 failure in 10^6 hours, or roughly one failure in 100 years. This requires the use of high quality components, the introduction of redundancy for critical elements, the provision of redundant signal paths, fault-tolerant subsystems, continuous surveillance, rigorous follow-up, and finally the mandatory use of a check list of validation tests before injecting beam in the LHC. It has to be noted that this is the failure rate for the complete system, comprising the beam dumping sub-system elements, together with the LHC Beam Interlock System, the LHC Beam Energy Meter, and the associated signal transmission. The Beam Energy Meter will be one of the critical elements in the chain of equipment required to dump the beam, since a false estimation of the beam energy could send the full LHC beam into one of the arcs adjacent to the beam dump insertion. Similarly, the extraction kicker magnets, MKD, will also be one of the critical elements in the system.

10.2.1 MKD

First estimates from reliability calculations for the extraction kicker system, MKD, have shown that the reliability requirement can only be obtained with full redundancy of one complete MKD kicker and its generator. Thus the beam can safely be extracted, albeit with the risk of beam loss on the TCDS, with only 14 out of the 15 kicker magnets. In addition, each MKD generator will consist of two parallel discharge circuits, including two switches, with failsafe triggering. The switches will use Fast High Current Thyristor (FHCT) solid-state technology, which is more reliable than conventional gas discharge switches. The energy needed for the kickers will be stored in local capacitors whose voltage will be constantly monitored. If one voltage is found outside the specified value, the beam will be dumped immediately (self-triggering). If a switch closes when not requested, a re-trigger system will immediately close all the other 14 switches with a maximum delay of 700 ns. A redundant UPS system will ensure that a dump action is correctly triggered and executed in the event of a general power failure and all triggering and re-triggering lines will be doubled.

10.2.2 MKB

The dilution kicker, MKB, will not be critical items from a reliability point of view. However, triggering lines will be doubled, since a total dilution failure could lead to damage of the TDE core.

10.2.3 MSD

The reliability of the DC septum magnets, MSD, is also not regarded as critical, since the magnets are based on conventional technology (with current decay constants in the order of seconds). The current in the magnet can be constantly monitored, as could the voltage drop across the magnet if required.

10.2.4 Vacuum system and TDE

The vacuum system of the TD dump line and the pressure vessel of the dump block, TDE, cannot fail in such a way as to threaten the safety of the LHC machine in general. The vacuum systems give adequate warning of degradation, and the beams can still be dumped without risk to the LHC machine proper.

10.2.5 Post-mortem
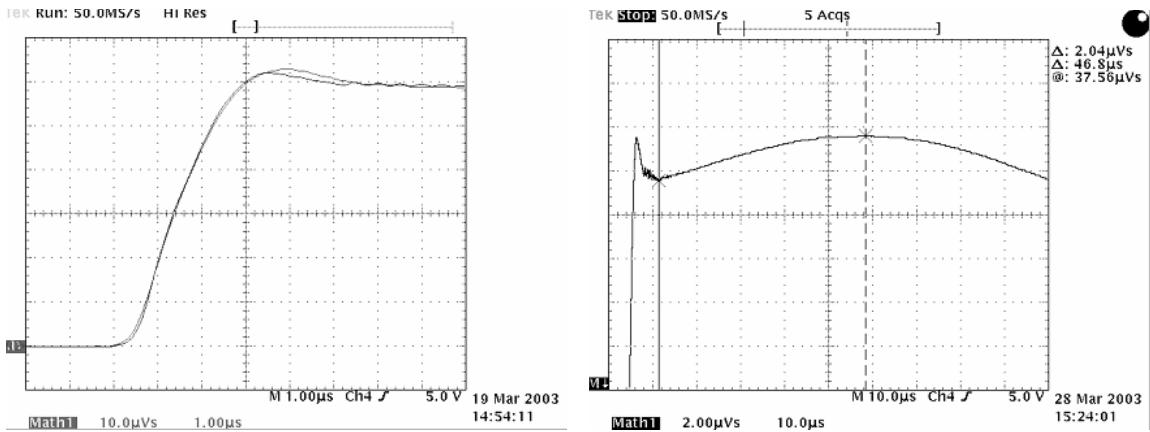
High reliability will be maintained by performing a post-mortem on every beam dump. A dump action without beam shall take place if the last post-mortem was too long ago, for example after a shutdown. It will only be possible to inject beam in the LHC if the post-mortem of the last beam dump and the beam dump status are satisfactory.

10.2.6 Synchronisation

The synchronisation between the RF and the beam dump kickers will be a redundant system, and the loss of the synchronisation of one of the two systems will launch a synchronous beam dump. Transmission is via a direct fibre-optic link.

10.2.7 Energy tracking

In order to get the correct extraction trajectory, the beam energy tracking system will determine the deflection strength of the MKB and MKD kickers and the MSD septa according to the measured beam energy. The tolerances on the kick angles for the MKD and MSD elements are below one percent. The beam energy reference information will be obtained through two redundant Beam Energy Meter systems (BEM), connected to the two main bend power converters located left and right of Point 6. The RF central frequency and integrated orbit corrector fields will affect the beam energy and may need to be taken into account, either via the BEM or via interlocking.

Figure 10.2: Start of MKD magnet current pulse at 450 GeV and 7 TeV with overshoots of 7.5% and 5.2% respectively (left); MKD magnet current pulse over 100 μs at 7 TeV with flat top overshoot of 5.6% (right).

10.2.8   Other protection

Local damage to components in case of certain fault scenarios will be avoided or reduced by the absorbers TCDS and TCDQ. The local orbit feedback will stabilise the beam in the extraction channel, and an interlock on the orbit position will ensure that the beam position remains within specified tolerances to permit a successful abort. Sacrificial absorbers may also be placed in the TD lines.

10.3   Main equipment subsystems

10.3.1   Fast-pulsed extraction magnets MKD

The beam dumping system has two sets of 15 fast-pulsed extraction magnets, MKD. A pulse generator will power each magnet via a low impedance transmission line. At least 14 out of the 15 kicker magnets must operate simultaneously on request. The kicker field rise time is specified as $\leq 3.0\,\mu$s and the kicker field 'flat-top' $\geq 90\,\mu$s. The current pulse is shown in figure 10.2. Any spontaneous triggering of one of the pulse generators must be detected and trigger the other generators within 700 ns at energies above 3 TeV. The kicker field has to track the energy as indicated by the Beam Energy Meter to better than $\pm 0.5\%$.
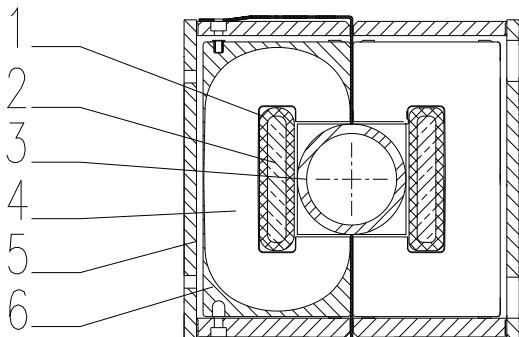
The unipolar voltage is 30 kV. The individual magnet current pulse (figure 10.2) has an amplitude of 18.5 kA with a rise time of 2.85 μs (to which 150 ns total jitter between magnets must be added), and a 'flat top' duration of 90 μs, followed by an approximately exponential decay of 1900 μs. This current corresponds to a magnetic field in the gap of 0.34 T, with up to 0.35 T in the steel. Table 10.4 summarises the main parameters of the MKD kicker system.

The MKD magnets have C-shaped cores made of thin gauge steel in continuous tape form, produced from a cold-rolled grain-oriented silicon-iron alloy of at least 3% Si content. The single-turn HV winding is composed of two insulated OFE copper bars of quasi-rectangular cross-section, with a minimum insulation thickness of 5 mm. The conductors are insulated with hot-pressed

Table 10.4: MKD system parameters.

Number of magnets per system	15	
System deflection angle	0.275	mrad
Kick strength per magnet	0.428	Tm
Vacuum chamber clear aperture (inner diameter)	56	mm
Operating charging voltage range	2 to 30	kV
Magnetic field overshoot at 7 TeV	$\leq$ 7.9	%
Magnetic field overshoot at 450 GeV	$\leq$ 10.0	%
Field flat top duration	$\geq$ 90	μs
Effective magnet length (magnetic)	1.421	m
Yoke length (mechanical)	1.348	m
Magnet vacuum length (mechanical)	1.583	m
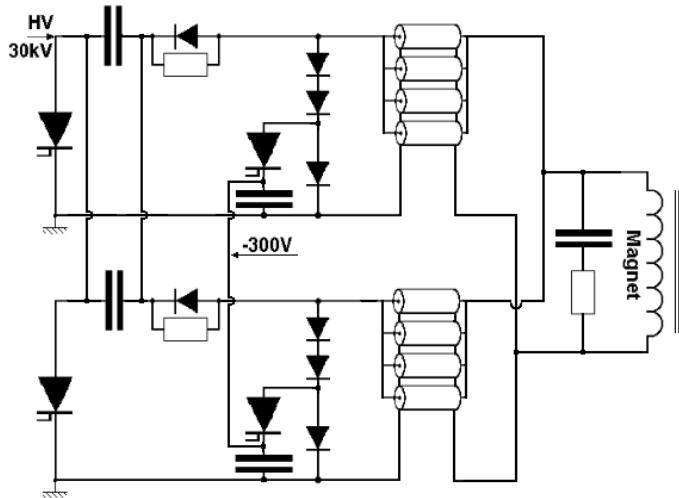
1. **Insulation of high voltage coil**
2. **Conductor of high voltage coil**
3. **Ceramic vacuum chamber**
4. **C-core**
5. **Mechanical frame**
6. **Epoxy moulding**

Figure 10.3: Cross-section of the MKD magnet.
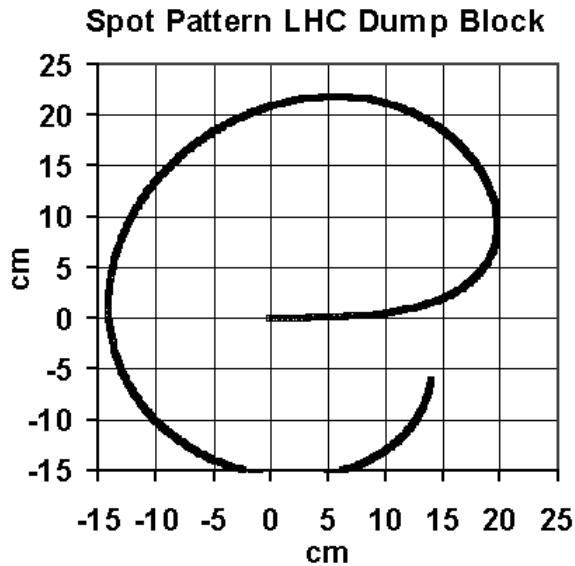
mica tapes with a glass carrier and pre-impregnated with an electrically high-grade epoxy resin. Figure 10.3 shows a cross-sectional view. The service life of the magnets will be $\geq$ 20 years, and during this period the magnets will be exposed to an estimated integrated radiation dose of 10^6 Gy (10^8 rad). The magnet and its excitation coil can be opened horizontally in order to insert the metallised ceramic vacuum chamber. The vacuum system operates in the 10^{-11} mbar range.

10.3.2 Generator

The generator consist of a discharge capacitor in series with a solid-state switch operating at 30 kV . In combination with a parallel diode stack, this generator produces the current pulse shown in figure 10.2. The circuit will be completed with a flat top current droop compensation network, consisting of a low voltage, low stray inductance, high current discharge capacitor. To improve reliability, each generator has a redundant second, parallel branch. The circuitry of the dual branch generator is shown in figure 10.4. Normally, both branches will supply half of the current, but in the event of a switch failure each branch will be capable of supplying the full nominal current.

Figure 10.4: Dual branch generator circuit layout.

Figure 10.5: Beam spot figure on absorber block.

10.3.3 Fast-pulsed dilution magnets MKB

For each extracted beam, a set of four horizontal and six vertical fast-pulsed dilution magnets (MKB) will sweep the beam along an "*e*"-shape path on the upstream face of the absorber graphite core, with a minimum velocity of 10 mm/μs during the dumping process. The MKBH and MKBV magnets will be based on the same technology as the MKDs, using similar C-cores, although no ceramic vacuum chamber will be required for the magnet, which is installed directly in a vacuum tank. Each magnet will be sinusoidally powered by a pulse generator via a low impedance transmission line. Table 10.5 summarises the main parameters of the beam dump dilution kicker system, and figure 10.5 shows the trace of the beam spot on the dump block.

Table 10.5: MKB System parameters.

Horizontal diluter magnet system MKBH		
Number of magnets per system	4	
Max. system deflection angle	0.278	mrad
Kick strength per magnet	1.624	Tm
Magnet beam aperture — horizontal	58	mm
Magnet beam aperture — vertical	32	mm
Operating charging voltage	16.4	kV
Field rise time	18.9	μs
Field oscillating frequency	14.2	kHz
Effective length (magnetic)	1.936	m
Yoke length (mechanical)	1.899	m
Vacuum length (mechanical), 2 magnets	4.582	m
Vertical diluter magnet system MKBV		
Number of magnets per system	6	
Max. system deflection angle	0.277	mrad
Kick strength per magnet	1.077	Tm
Magnet beam aperture — horizontal	66	mm
Magnet beam aperture — vertical	36	mm
Operating charging voltage	22.3	kV
Field rise time	34	μs
Field oscillating frequency	12.7	kHz
Effective length (magnetic)	1.267	m
Yoke length (mechanical)	1.196	m
Vacuum length (mechanical), 2 magnets	4.076	m

10.3.4 Extraction septum magnets MSD
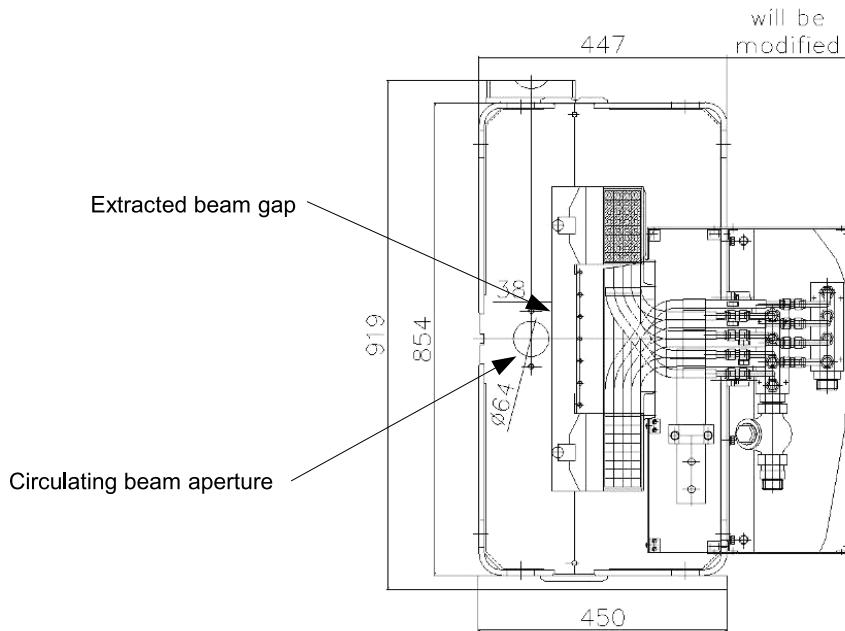
The 30 MSD septum magnets are modified Lambertson-type septa with an all-welded construction. The yoke lamination is 1.0 ± 0.02 mm thick steel, with a 10 μm Fe_3O_4 layer as electrical insulation, a maximum permeability of 4600 ± 80, and a coercivity of 60 ± 12 A/m. There are 3 magnet types, MSDA, MSDB, and MSDC, differing in the number of coil layers and the distance of the circulating beam hole from the pole face. A transverse section of the MSD magnet is shown in figure 10.6 and the main parameters are shown in table 10.6.

10.3.5 Beam dump absorber block TDE

For each ring, the extracted and diluted beam will be directed onto an external beam dump, TDE. The TDE is designed for 2×10^4 beam aborts at 7 TeV with full beam intensity (4.69×10^{14} protons per beam) during an operational lifetime of 20 years. The TDE design has been checked by Monte Carlo energy deposition simulations, heat transfer analyses, and structural assessment at off-normal operating conditions. Carbon was chosen as the most suitable absorbing material for the

Table 10.6: The main parameters of the MSD magnets.

	MSDA	MSDB	MSDC	
Septum core length	4460	4460	4460	mm
Coil core length	4000	4000	4000	mm
Core width	447	447	447	mm
Core height	854	854	854	mm
Gap height	44	44	44	mm
Septum thickness	6	12	18	mm
Number of coil turns (total)	32	40	48	-
Number of coil layers	4	5	6	-
Number of turns per layer	8	8	8	-
Electrical coil resistance at 20 °C	27.1	33.9	40.7	mΩ
Inductance	36	56	79	mH
Dissipated power	22.7	28.3	34.0	kW
Water flow per coil	16.5	20.7	24.8	l/min
Coil water pressure drop	5	5	5	bar
Design current	880	880	880	A
Nominal magnetic field in the gap	0.80	0.99	1.17	T
Magnet weight	10500	10600	10700	kg

Figure 10.6: Connection end view of an MSD magnet (dimensions in mm).

dumps, with the highest melting (sublimation) temperature and the best thermal shock resistance of the investigated materials. The dump core is a segmented carbon cylinder of 700 mm diameter and 7'700 mm length, shrink-fitted in a stainless steel jacket. The jacket incorporates welded tubes for cooling water. Each dump is surrounded by ∼900 tons of radiation shielding blocks constructed from decommissioned ISR dipole-yokes, partially filled with concrete. Each block is 1'298×1'088×2'440 mm and weights 24 tons. Thirty-five blocks in total are required per dump.

10.3.6 Activation

Activation in the surrounding air, rock, and ground water, and dose-rates close to the core and in different parts of the dump, have been estimated. For general access to the dump-caverns with all the dump-shielding in position, total dose-rates from all sources will be at relatively low levels. Only 1 hour after dumping the beam, the dose-rates will be typically below 300 μSv/h. However, most of this will be due to the ^{24}Na in the concrete shielding and walls, so allowing several days for this to decay would be preferable. The dismantling of the dump to exchange the core will require strict control and remote handling.

Chapter 11
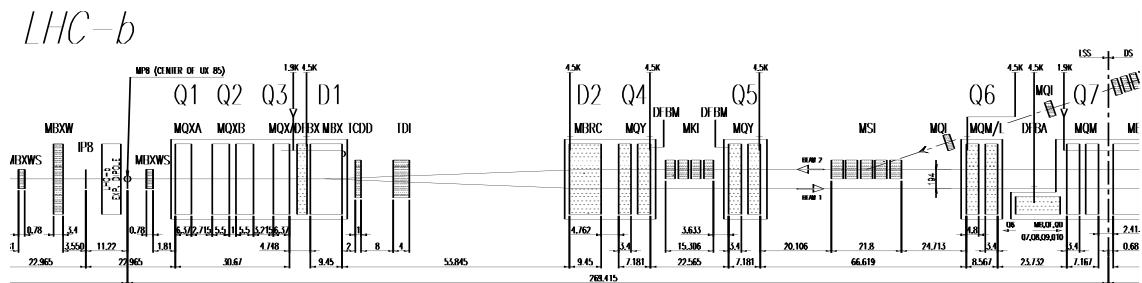
Beam injection

11.1 Overview

Injection into the LHC is performed in the combined experimental and injection insertions in Points 2 and 8. The transfer line TI 2 brings the beam to within ∼150 m left of Point 2 for injection into Ring 1, and TI 8 delivers the beam ∼160 m right of Point 8 for injection into Ring 2 [59].

A schematic layout of the injection region at Point 8 is given in figure 11.1. In both insertions, the beam approaches the LHC from outside and below the machine plane. The beam is directed by a series of dipoles in the injection line, already located in the LHC tunnel, towards a series of five Lambertson-type septum magnets, which deflect the beam horizontally by 12 mrad under the outer ring. A series of four MKI kicker magnets deflects the beam vertically by 0.85 mrad onto the closed orbit. The vertically defocusing quadrupole Q5, between the MSI and the MKI, provides, through its kick enhancement, about one quarter of the required total vertical deflection. To facilitate the setting up of the injection with pilot bunches and to protect the LHC in case of malfunction of the injection kickers, an injection beam stopper, TDI, is placed 15 m upstream of the superconducting recombination dipole D1, supplemented by an additional shielding element, TCDD, 3 m upstream of D1. The protection against injection errors is further complemented by two collimators, TCLI, near the superconducting quadrupole Q6 on the other side of the insertion.

The geometrical layout and arrangement of MSI, MKI and TDI/TCDD is virtually identical for both injection regions. However, despite being based on the same design criteria, the optics varies between Point 2 and Point 8 due to the displaced IP in Point 8. The precision of the injected

Figure 11.1: Schematic layout of the injection region right of IP8 (distances in m).

Table 11.1: Main parameters of the injection septum magnets.
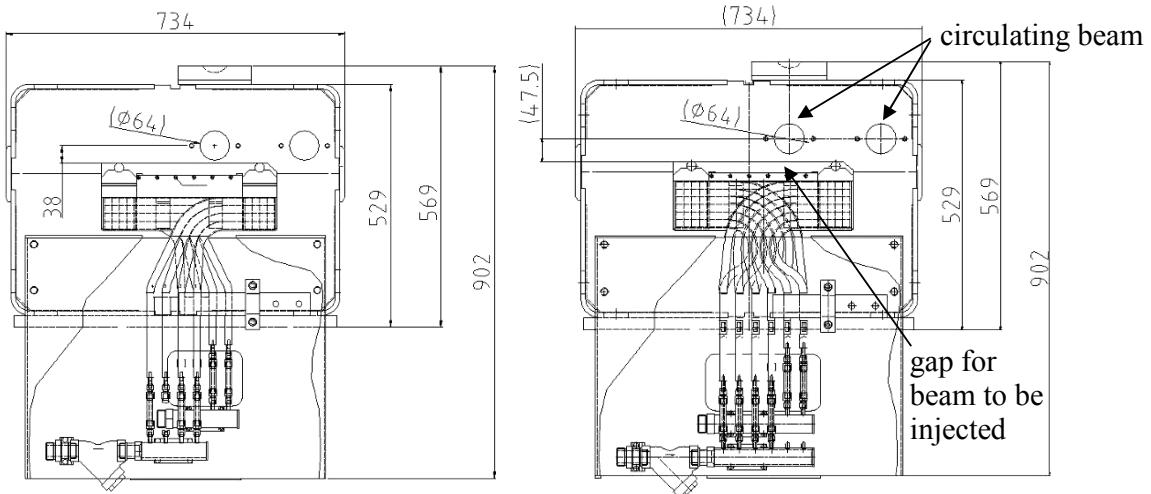
	MSIA	MSIB	
Septum core length	4000	4000	mm
Coil core length	3650	3650	mm
Core width	734	734	mm
Core height	529	529	mm
Gap height	25	25	mm
Septum thickness	6	15.5	mm
Number of coil turns	16	24	-
Number of coil layers	4	6	-
Number of turns per layer	4	4	-
Electrical coil resistance at 20 °C	10.9	16.4	mΩ
Inductance	10.2	23.7	mH
Dissipated power	10.6	15.9	kW
Water flow per coil	7.9	11.8	l/min
Coil pressure drop	5	5	bar
Design current	950	950	A
Nominal magnetic field in the gap	0.76	1.13	T
Magnet weight	9800	9900	kg

beam's position with respect to the LHC closed orbit is specified to be less than $\pm 1.5\sigma$, including SPS closed orbit errors at extraction, ripple and drifts of power supplies, and injection kicker ripple. Further parameters can be found in the descriptions of the individual components.
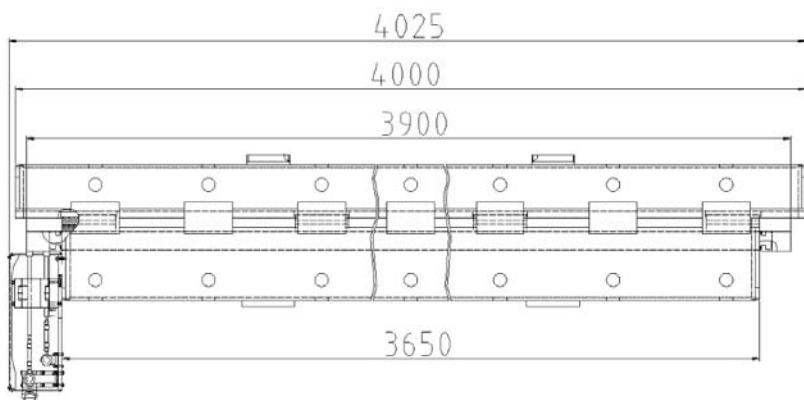
11.2   Injection septa

Five septum magnets (MSI), of two different types (MSIA and MSIB), deflect the incoming beam horizontally by 12 mrad under the outer ring. For injection into Ring 1, the septa are located in RA23 between Q6 and Q5, and similarly for Ring 2 in RA87. The MSIA and MSIB magnets differ in the septum thickness (the distance of the holes for the circulating beams from the pole face) and the coil configuration, and, consequently, the field in the gap. In the beam direction, there are three MSIB magnets followed by two MSIA magnets and, including the inter-magnet gaps, the whole system stretches over 21.8 m. The main parameters of the injection septum magnets are given in table 11.1.

The magnets were designed and built by a collaboration between CERN and the Institute for High Energy Physics (IHEP), Protvino, Russia. See figures 11.2 and 11.3 for views of the magnets. The 1.0 mm thick steel laminations have a 10 μm thick Fe_3O_4 layer as electrical insulation. The magnet yokes are an all-welded construction and are assembled from different half cores, the so-called septum core and the coil core. The septum core contains circular holes for the circulating beams, thus avoiding the need for the careful alignment of the usually wedge-shaped septum blades used in classical Lambertson magnets. The septum core is longer than the coil core to reduce the

Figure 11.2: MSIA (left) and MSIB (right) connection front face view (dimensions in mm).
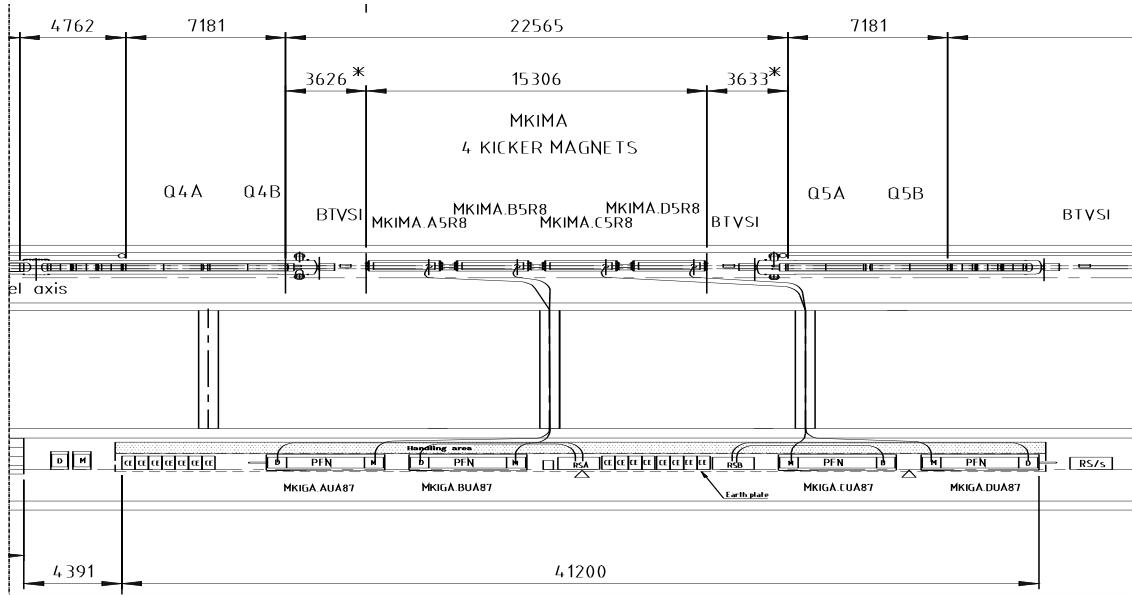

Figure 11.3: MSI side view (dimensions in mm).

stray field extending from the field gap to the circulating beam holes. The coil core holds the single pancake coil. The coils are made from a 15 mm wide OFHC square copper conductor, with a circular cooling hole of ≈ 4.5 mm diameter, insulated with glass fibre tape, and impregnated using a radiation resistant resin. Each coil water outlet carries a thermo-switch, to prevent overheating of the coil by switching off the MSI power converter, through the magnet surveillance system, in the event of a failure in the cooling circuit. The trip temperature on the switch is 65°C.

11.3 Injection kickers

The injection kicker system (MKI) comprises four fast pulsed magnets per injection. The magnets are housed in a separate vacuum tank containing both beam pipes, which has been recovered from the LEP separators. For injection into Ring 1, the magnets are located in RA23, and for Ring 2 injection, in RA87. The pulse generators and part of the power and control electronics are located

Figure 11.4: Injection kicker layout right of Point 8 (plan view) (distances in mm).

in the adjacent underground galleries: UA23 for Point 2 and UA87 for Point 8. The transmission cables pass through two existing holes previously used for wave-guides. Figure 11.4 shows the layout (plan view) around the LHC injection kickers in Point 8.
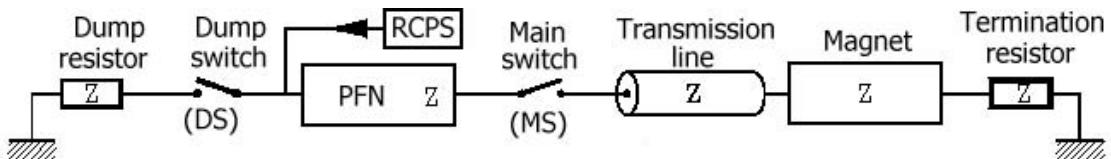
The beam to be injected approaches the kicker system from below at an angle of 0.85 mrad, requiring a total integrated dipole field of 1.2 Tm for deflection onto the central machine orbit. To limit the emittance blow-up at injection, reflections and flat top ripple of the field pulse must stay below $\pm$ 0.5%, which is a very stringent requirement. The pulse repetition time, imposed by the SPS acceleration cycle is 18 s in the case of 3-train extraction. The LHC will be filled with 12 batches of 5.84 μs or 7.86 μs duration, to be deposited successively on the machine circumference, with 11 gaps of 0.94 μs in between them to allow for the injection kicker rise time. One final gap of 3.0 μs allows for the fall time of the injection kickers and allows also for the rise time of the beam dumping kickers. The main parameters are summarised in table 11.2.

Figure 11.5 shows the schematic circuit diagram of the injection kickers. Each magnet is powered by a separate pulse-forming network (PFN). Two PFNs are charged simultaneously from one resonant charging power supply (RCPS). To be able to vary the pulse duration, a main switch (MS) and a dump switch (DS) are needed, one at either end of the PFN. A carefully matched high-bandwidth system is necessary to fulfil the stringent pulse response requirements. The system is therefore composed of a multi-cell PFN and a multi-cell travelling wave kicker magnet, connected by a matched transmission line, and terminated by a matched resistor. To achieve the required kick strength, a low characteristic impedance of 5 Ω was chosen.

The design voltage is 60 kV, as in most SPS kicker installations, allowing the use of several proven components such as transmission lines, connectors, and termination resistors. The voltage on the magnet is half of the PFN voltage. Allowing for overshoot, the design voltage of the magnet is 35 kV.

Table 11.2: Main MKI system parameters.
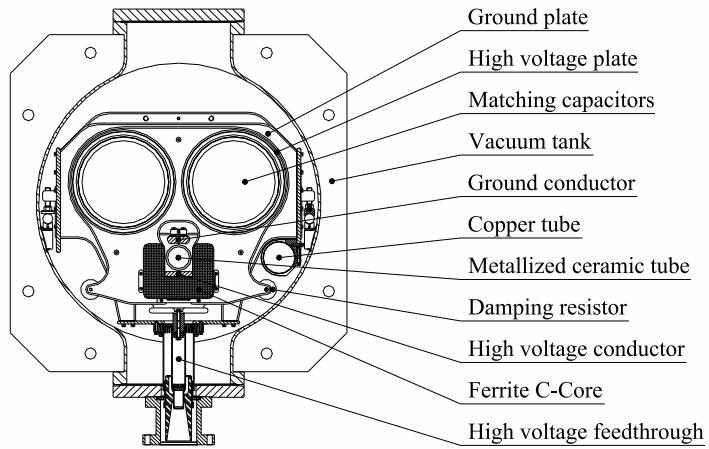
Item	Value	Unit
Number of magnets per system	4	-
System deflection angle (4 magnets)	0.85	mrad
∫ B dl	0.325	Tm
Magnet beam aperture (diameter)	38	mm
Characteristic impedance	5	Ω
Operating charging voltage (PFN)	54	kV
Field flat top ripple	< ± 0.5	%
Field flat top duration	up to 7.86	μs
Field rise time 0.5%–99.5%	0.9	μs
Field fall time 99.5%–0.5%	3.0	μs
Yoke length	2.650	m
Magnet length (mechanical)	3.400	m

Figure 11.5: Schematic circuit diagram.
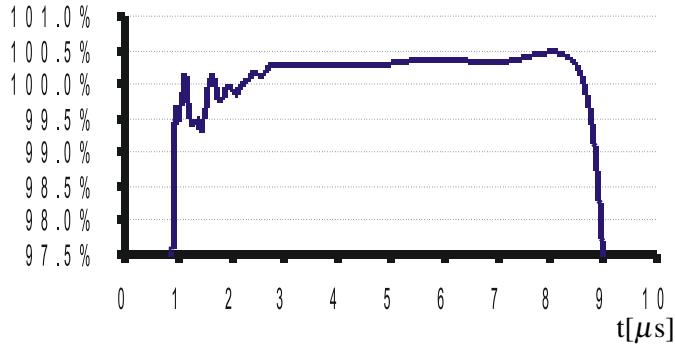
Each kicker magnet consists of a series of 33 cells, which is a compromise between bandwidth and cost. Figure 11.6 shows a cross section of one magnet cell, with matching capacitors mounted between a high voltage and a ground plate. The plates are spaced by three ceramic-metal insulators, which together form an independent cell assembly. To achieve a characteristic impedance of 5 Ω within the space constraint of the 540 mm diameter tanks, two 210 mm diameter ceramic plate capacitors with contoured rims have been used, leading to a nominal self-inductance and capacitance per cell of 101 nH and 4.04 nF, respectively, including the plate end effect.

In order to reduce beam impedance while allowing a fast field rise time, the beam passes through a ceramic pipe with silver stripes on its inner wall. The stripes provide a path for the image current and screen the ferrite yoke against beam induced heating. The stripes are connected to the standard vacuum chambers of the machine directly at one end, and via a decoupling capacitor of 300 pF at the other, using the ceramic pipe itself as dielectric. The pipe is made from a 3 m long extruded ceramic tube with a wall thickness of 4 mm.

The ferrite cores are made from high permeability, high resistivity NiZn, 8C11 grade, and have a C-configuration to allow earthing of the coaxial HV cable input connection and the output connection to the terminating resistor [60]. In addition to their magnetic properties, which are specially adapted to this application, they exhibit very good vacuum performance after appropriate treatment. In order to obtain a fully bakeable design, the conductors are made from stainless steel. The shape of the ground conductor has been optimised to provide a homogeneous field without requiring shims on the ferrites.
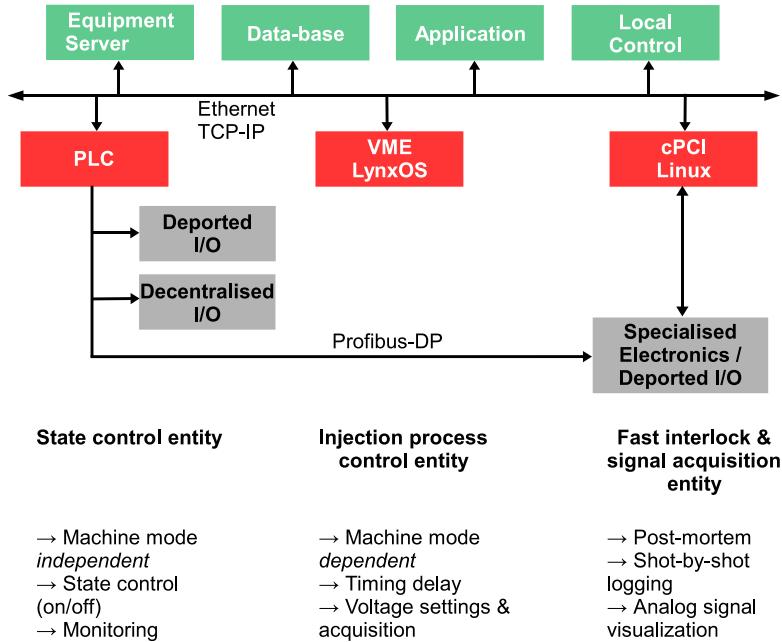
Figure 11.6: MKI magnet cross section.

Figure 11.7: MKI prototype current pulse shape (top part of scale).

PFN type generators are used to produce rectangular pulses with very low ripple. The top part of the current pulse in the prototype magnet is shown in figure 11.7. Main and dump switches have been designed for minimum size and easy maintenance. They use three-gap thyratrons of types CX 2003 and CX 2503, installed in independent tanks, with isolating transformers for heaters, reservoirs, and grid biasing. These switches are mounted directly onto the PFN to save space and cost, as in the SPS injection kicker installation [61].

The pulse is transmitted from the PFNs to the magnets through 10 35 m long parallel RG220 type coaxial cables of 50 Ω impedance. The conductors are drawn from electrolytic copper, and low density polyethylene of high purity is used as dielectric. The cable can be exposed to an integrated radiation dose of at least 10^6 Gy. Cable ends are terminated by moulded high voltage connectors, as already in use in the SPS.

Figure 11.8: MKI control system architecture.
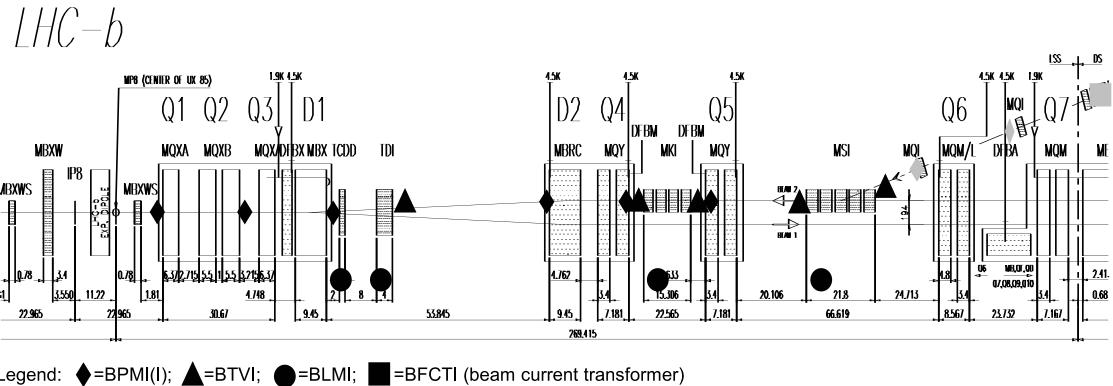
11.4 Control system

The kicker control system, schematically shown in figure 11.8, comprises three independent entities: one for the control of the equipment state (ON, OFF, STANDBY...), one for the control of the injection process (timing system and operational setting management), and one for the control of the fast signal acquisition and interlock logic (protection of the equipment and of the machine), each implemented in an appropriate technology.

The injection process is composed of two consecutive stages which are repeated for each injection. The first a slow stage is divided into two phases: a 1'000 ms long charging phase of the primary capacitor bank, followed by a 2 ms long resonant charging phase for charging the PFNs with a pulse-to-pulse reproducibility of 0.1%. The second, fast stage, of 10 μs duration, is for synchronisation of the timing system with the circulating beam and the 'to-be-injected' beams, triggering of the thyratron switches, discharging of the PFNs, and generation of the magnetic pulse.

11.5 Beam instrumentation

The beam instrumentation around the injection systems is a direct continuation of the transfer line systems in TI 2 and TI 8. The functional specifications for the transfer lines have therefore been used in the design choices for these systems. A schematic overview of the instrumentation in the injection region is given in figure 11.9. The transfer line beam position monitors (BPMI) allow steering of the beam up to the entry of the septum magnets. The BPMs around the injection elements are standard ring BPMs installed on the superconducting quadrupoles. Luminescent screens (BTVI) using the optical transition radiation effect (OTR) are used to determine the transverse

Figure 11.9: Schematic view of injection related instrumentation (case of injection near Point 8) (distances in mm).

beam sizes and centre of gravity upstream and downstream of the major injection elements, and to provide complementary position information during the setting up and steering of the injection. Standard SPS type beam-loss monitors (BLMI) are used to localise the losses linked to the injection process. The installed instruments can cope with the full variety of LHC beams. For proton operation, the intensity varies from a single pilot bunch, namely 5×10^9 protons, to 4 batches of 72 bunches with up to 1.7×10^{11} protons per bunch.

Chapter 12
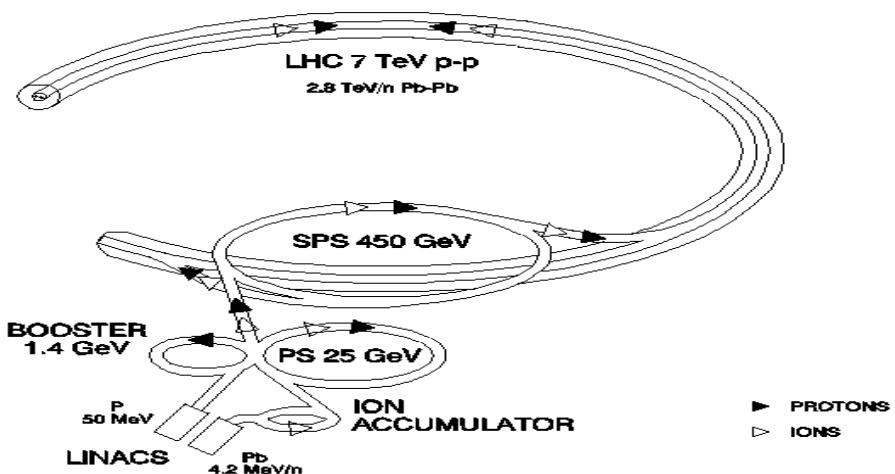
Injection chain

12.1 Introduction

The LHC will be supplied with protons from the injector chain Linac2 — Proton Synchrotron Booster (PSB) — Proton Synchrotron (PS) — Super Proton Synchrotron (SPS), as shown in figure 12.1. These accelerators were upgraded to meet the very stringent needs of the LHC: many high intensity proton bunches (2'808 per LHC ring) with small transverse and well defined longitudinal emittances.

The main challenges for the PS complex are (i) the unprecedented transverse beam brightness (intensity/emittance), almost twice that which the PS produced in the past and (ii) the production of a bunch train with the LHC spacing of 25 ns before extraction from the PS (25 GeV).

Initially, a scheme requiring new Radio Frequency (RF) harmonics of $h = 1, 2$ in the PSB and $h = 8,16, 84$ in the PS, an increase of energy from 1 to 1.4 GeV in the PSB, and two-batch filling of the PS was proposed. After a partial test of this scheme in 1993, a project to convert the PS complex for LHC operation was started in 1995 and completed in 2000 [62]. The major parts of


Figure 12.1: The LHC injector complex.

this project were:

i. new $h = 1$ RF systems in the PSB,

ii. upgrading the PSB main magnet supply from 1 GeV operation to 1.4 GeV,

iii. new magnets, septa, power supplies, and kicker pulsers for the PSB-PS beam transfer,

iv. new 40 and 80 MHz RF systems in the PS,

v. beam profile measurement devices with improved resolution.

About one quarter of the project resources (funds and manpower) was provided by TRIUMF under the Canada-CERN Co-operation Agreement on the LHC. During first beam tests with the complete scheme in 1999, difficulties in producing the LHC bunch train at PS extraction were encountered. The problem was an instability in the coasting beam after adiabatic debunching, just before recapture with the new 40 MHz RF system. As a consequence, the final bunch length at extraction was too large (>5 ns) to fit the SPS 200 MHz RF system. A modified scheme, avoiding debunching in the PS while changing the number of bunches by multiple bunch splitting operations, was proposed. This method is based on using RF harmonics $h = 7, 21, 42$ and 84 in the PS and required the installation of an additional 20 MHz RF system in the PS.

The transverse emittances of the LHC beam have to be maintained at their unusually small size throughout the injector chain. Small amounts of mis-steering and mismatch between the accelerators of the chain, virtually negligible for normal operation, become increasingly important and their effect has to be measurable, calling for high-resolution beam profile monitors. Moreover, various position measurement systems were modified to deal with the new harmonics in the circular machines and to allow bunch-by-bunch observation in TT2.

12.2   LHC and SPS requirements

The equation for luminosity given in chapter 2 summarises the "end-point" beam requirements, but this implies many conditions that have to be satisfied, such as,

- the beam emittance must fit the small aperture of the LHC superconducting magnets;

- the beam intensity is limited by the synchrotron radiation that has to be absorbed by the cryogenic system;

- the beam-beam effect causes a spread in betatron tunes ("footprint") when the beams are colliding, and this has to be kept below a certain limit; and

- the space-charge limits in the injectors have to be respected.

There are also conflicting requirements for the longitudinal emittance. It has to be small at injection to ease beam transport from the SPS through the two ∼2.5 km long lines, but larger at collision to avoid transverse emittance blow-up by intra-beam scattering.

An optimisation procedure, taking into account these boundary conditions, has resulted in the LHC beam parameter set compiled in table 12.1. The "ultimate" performance level corresponds

Table 12.1: LHC nominal and ultimate proton beam parameters.

			Injection	Collision	
	Energy	[GeV]	450	7000	
Luminosity	nominal	[cm^{-2}s^{-1}]		10^{34}	
	ultimate			2.5×10^{34}	
Number of bunches			2808		3564 bunch places
Bunch spacing		[ns]	24.95		
Intensity per bunch	nominal	[p/b]	1.15×10^{11}		
	ultimate		1.70×10^{11}		
Beam current	nominal	[A]	0.58		
	ultimate		0.86		
Transverse emittance (rms, normalized), nominal & ultimate		[μm]	3.5	3.75	Emittances equal in both planes, small blow-up allowed in LHC
Longitudinal emittance, total		[eVs]	1.0	2.5	Controlled blow-up during accel.
Bunch length, total (4σ)		[ns]	1.7	1.0	has to fit into 400 MHz buckets
Energy spread, total (4σ)		[10^{-3}]	1.9	0.45	

to the LHC beam-beam limit, whereas the "nominal" performance combines high luminosity with operational margin. During the first year of physics running, the LHC will be operated at a much lower intensity and luminosity level.

As with the PS complex, the SPS is an "old" machine and is not optimised as an LHC injector. The intensity the SPS is able to accelerate ($\sim 4 \times 10^{13}$ protons per cycle, which is particularly difficult if concentrated on a fraction of its circumference) limits the number of PS pulses per SPS cycle to a maximum of four. The momentum spread acceptance of the PS-SPS line (TT2, TT10) is about $\pm 0.2\%$ in $\Delta p/p$, while the total bunch length has to be below 4 ns to fit into the buckets of the SPS 200 MHz accelerating system, implying a longitudinal emittance of 0.35 eVs per PS bunch. While the longitudinal emittance will be increased from 0.35 to 1 eVs during SPS acceleration, there is little margin for transverse emittance blow-up in this machine. The LHC and SPS requirements define the beam characteristics at PS extraction, summarised in table 12.2 (assuming 100% transmission from PS to LHC). The filling sequence PS-SPS-LHC is sketched in figure 12.2.

12.3 Scheme to produce the LHC proton beam in the PS complex

12.3.1 Space charge issues in PSB and PS
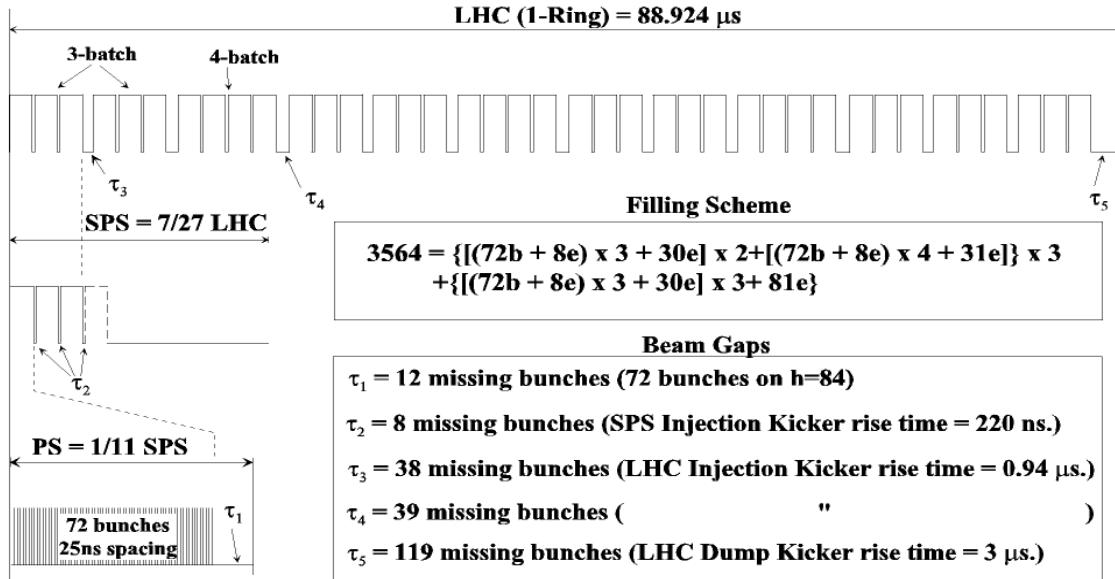
While the intensity required for the LHC is well within the capabilities of the PS complex, the transverse emittance is smaller than usual, yielding a beam brightness about 1.6 times higher than was hitherto achievable. Low-energy synchrotrons suffer from space charge, which can be quantified in terms of the tune shift

$$\Delta Q \propto -\frac{N}{(\beta \gamma^2)_{\mathrm{rel}} \varepsilon_n},$$

where N is the number of protons in the synchrotron. This tune shift would become unmanageable (almost -1) in the PSB at 50 MeV and in the PS at 1 GeV. The measures to overcome this
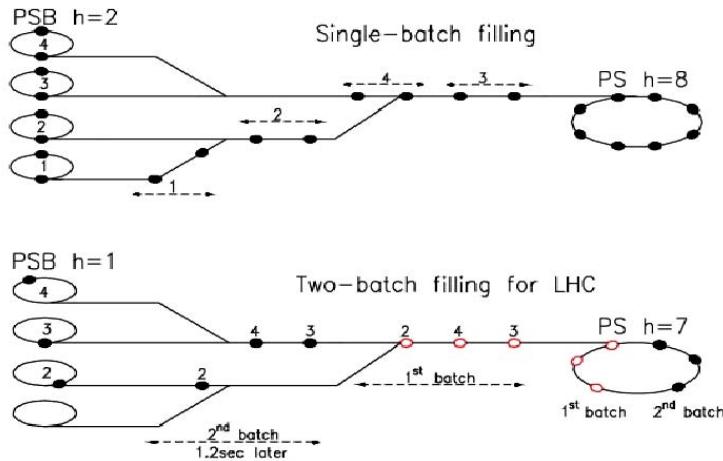
Table 12.2: Beam characteristics at extraction from the PS.

Proton kinetic energy	[GeV]	25	
Number of PS batches to fill SPS		3 or 4	Limited by SPS peak intensity
PS repetition time	[s]	3.6	PS 2-batch filling from PSB
Number of bunches in PS		72	h=84, 12 empty buckets for extraction kicker
Bunch spacing	[ns]	24.97	
Number of protons/bunch N_b - ultimate		1.70×10^{11}	100% transmission assumed
- nominal		1.15×10^{11}	from PS to LHC
Transverse normalised rms emittance	[μm]	3.0	
Bunch area (longitudinal emittance)	[eVs]	0.35	
Bunch length (total)	[ns]	4	Limited by SPS 200 MHz buckets
Relative momentum spread $\Delta p/p$ total (4σ)		0.004	Limited by TT2-TT10 acceptance

Bunch Disposition in the LHC, SPS and PS

Figure 12.2: Proton bunches in the PS, SPS and one LHC ring. Note the partial filling of the SPS (3/11 or 4/11) and the voids due to kicker rise-time. One LHC ring is filled in ~3 min.

fundamental limitation are:

- filling the PS with two consecutive PSB pulses, thus significantly reducing the intensity per pulse and thus ΔQ at 50 MeV;

- raising the PS injection energy from 1 to 1.4 GeV, thus decreasing ΔQ in the PS by a factor 1.5 from $(1/\beta\gamma^2)_{\mathrm{rel}}$.

Figure 12.3: PSB-PS transfer: single-batch filling for SPS physics (top), two-batch filling for LHC (bottom).

The four PSB rings, $1/4$ of the PS circumference each, are normally ejected and transferred sequentially to fill the PS in one go, for example, for the SPS physics beam with two bunches per ring (5 bunches per ring until 1997). However, with only one bunch per ring, up to four bunches can be squeezed into $\sim 1/2$ of the PS, thus leaving space for a second PSB batch 1.2 seconds later. Figure 12.3 shows the standard filling scheme for SPS physics, and the LHC two batch filling scheme, in which three and three (or alternatively four and two) bunches from the PSB are transferred to the PS on consecutive PSB cycles.

To operate with RF harmonic $h = 1$ instead of the former harmonic $h = 5$, the PSB is now equipped with new RF cavities, with a frequency range of 0.6 to 1.7 MHz, and the former $h = 5$ systems have been modified to work on $h = 2$. Also, the PS has to cope with new RF harmonics — an opportunity to equip both machines with Digital Beam Control.

To raise the PSB ejection and PS injection energy from 1 to 1.4 GeV (+26.3% in momentum), the PSB main power supply has been upgraded to provide the higher magnet currents. The elements of the PSB-PS beam transport have to provide higher field levels, which meant replacement of most of the magnets (dipoles, quadrupoles, septa, kickers) and their power supplies.

12.3.2 LHC bunch train generation in the PS

12.3.3 Initial debunching-rebunching scheme

The initially proposed scheme injected two times four PSB bunches (two PSB batches) on harmonic $h = 8$ in the PS. The bunches were then split in two and accelerated on harmonic 16 to 25 GeV. The 25 ns bunch spacing was achieved by debunching and rebunching the beam on h=84, followed by bunch rotation with the new 40 MHz (h=84) and 80 MHz RF systems. Out of the 84 bunches, 81 were transferred to the SPS, and three were expected to be lost due to the PS extraction kicker rise-time.

However, when testing the scheme in 1999, microwave instabilities due to the longitudinal impedance of the PS blew up the momentum spread during the delicate debunching process. At

nominal intensity, there was no way to make the bunches shorter than 5 ns. The decision was then taken to change to a newly proposed scheme using multiple splitting techniques [63], which avoided this instability, provided a gap without particles for the rise-time of the ejection kicker, and introduced flexibility in the bunch train time structure.

12.3.4 Multiple splitting scheme

For the generation of the LHC bunch train with 25 ns spacing in the PS, a multiple splitting scheme is employed. Six PSB bunches (two PSB batches of 3 + 3 or 4 + 2 bunches) are captured on harmonic $h = 7$ in the PS. The bunches are then split into three at 1.4 GeV using appropriate amplitude and phase parameters in three groups of cavities operating on harmonics $h = 7, 14$ and 21. Bunched on harmonic $h = 21$, the beam is accelerated up to 25 GeV where each bunch is split twice in two using the process which has been demonstrated in regular operation. The new 20 MHz and 40 MHz RF systems are required at that stage. Thus, each of the six original bunches has been split into 12, and 72 bunches have been created on harmonic 84. Finally, the 80 MHz systems shorten the bunches to ∼4 ns, so as to fit into the SPS 200 MHz buckets. After injecting only six bunches, the final bunch train contains 72 bunches and 12 consecutive empty buckets, providing a gap of ∼ 320 ns (13 × 25 ns) for the rise-time of the ejection kicker. The change from the debunching-rebunching scheme to the multiple splitting scheme required the installation of a 20 MHz RF system that was not part of the "PS for LHC" conversion project.

The new scheme, though indispensable for longitudinal beam dynamics, has one drawback: There are 72 LHC bunches produced from six PSB bunches, instead of 84 from 8. Thus the intensity per PSB bunch and the beam brightness (due to the fixed emittance) have to be 14% higher than with the debunching-rebunching scheme. The consequence is that the ultimate beam, which is already at the limit of the achievable brightness, can no longer be provided by the PSB. Initially, it was thought that by using up parts of the PS emittance budget and with more experience, one could still achieve the required beam characteristics. This possibility has been ruled out following the observation of beam losses, and alternative RF gymnastics have had to be invoked. A comparison of debunching-rebunching and multiple splitting schemes is given in table 12.3 (the intensities quoted assume 100% transmission from PSB to LHC).

12.4 Overview of hardware changes

The project to convert the PS complex to an LHC pre-injector was launched in 1995. Also in 1995, Canada offered in-kind contributions for the LHC machine (via TRIUMF/Vancouver), which soon developed into an efficient collaboration, with TRIUMF providing ∼1/4 of the resources needed for the PS upgrade project. Major systems and their hardware components are listed in table 12.4, together with Canadian contributions and installation dates. The project was essentially finished by 2001.

Table 12.3: PS complex operation for filling LHC: debunching-rebunching and multiple splitting.

	Debunching-rebunching	Multiple splitting
No. of bunches per PSB ring	1	1
No. of PSB cycles per PS cycle	2	2
No. of bunches from PSB per PS cycle	8	6
Harmonic no. at PS injection	8	7
Bunch splitting at 1.4 GeV	1=>2	1=>3
Harmonic no. from 1.4 GeV to 25 GeV	16	21
No. of bunches from 1.4 GeV to 25 GeV	16	18
Gymnastics at 25 GeV	Debunching-rebunching	Double bunch splitting (1=>4)
Harmonic no. at PS extraction	84	84
No. of bunches to SPS per PS cycle	81 (3 bunches lost due to PS extraction kicker rise time)	72 (empty bucket conserved, provides 320 ns for kicker)
PS intensity at 1.4 GeV for 1.15×10^{11} protons per LHC bunch ("nominal")	9.66×10^{12}	8.28×10^{12}
PSB intensity per ring ("nominal")	1.21×10^{12}	1.38×10^{12}
PS intensity at 1.4 GeV for 1.7×10^{11} protons per LHC bunch ("ultimate")	14.28×10^{12}	12.24×10^{12}
PSB intensity per ring ("ultimate")	1.79×10^{12}	2.04×10^{12}

Table 12.4: Major hardware components of the "PS Conversion for LHC" project.

System	Components	Installation	TRIUMF contribution	Comments
Linac	Inter-tank beam shape monitors (2)	1999, 2000		study very high intensities (180 mA)
50 MeV line	laminated quadrupoles	1997	two magnets	correct optics for protons and ions
PSB RFh=1	RF cavities "C02" (4), tune range 0.6-1.7 MHz	1998	ferrites, HV power supplies	one cavity per ring
PSB RFh=2	RF cavities "C04" (4), tune range 1.2-3.9 MHz	1998		bunch flattening and/or splitting
PSB main magnet supply	double-transformers (5), VAR compensator, quadrupole trim supplies, control circuitry	1998	all transformers, VAR compensator	26% increase of magnet current on PSB main magnets
PSB water cooling	closed-circuit demineralised water	2000		copes with more heating at 1.4 GeV
PSB instrumentation	fast wire scanners (4 rings, H+V, + 2 spares)	2001-2003	10 units, design and fabrication.	standard PS beam profile meas. device
	Q-measurement: electronics, kicker pulser	1999/2000		all four beams are kicked
PSB-PS beam transport	ejection/recombination kicker pulsers (6)	1998, 1999		26% more kick to cope with 1.4 GeV
	ejection, recombination, PS injection septa + power supplies (8)	1997, 1998, 1999		half-sine-wave pulses of 3.5 ms
	15 laminated magnets (vertical bending magnets, quadrupoles, correction dipoles)	1997, 1998	all 15 magnets all (+spare) power supplies	allow pulse-to-pulse modulation between 1.4 GeV (PS) and 1 GeV
PS RFh=84	300 kV fixed-frequency (40 MHz) cavities (1+1 spare installed) "C40"	1996, 1999	model studies, tuners, higher-order-mode dampers, HV supplies	for generating LHC bunch spacing of 25 ns at 25 GeV
PS RFh=168	300 kV fixed-frequency (80 MHz) cavities (2+1 spare installed) "C80"	1998, 1999		for shortening the LHC bunches to 4 ns
PS transverse feedback	new amplifiers, deflector, electronics	2003-2005		damping injection oscillations and instabilities
PS instrumentation	wide-band position monitors (2) in line TT2	1998		bunch-by-bunch position measurement
PS RF h=28, 42	15 kV dual frequency 13.3 or 20 MHz cavity, (1+1 spare installed) "C20"	2003-2004		for various bunch splitting operations in the PS

Chapter 13

LHC as an ion collider

Heavy ion collisions were included in the conceptual design of the LHC from an early stage, and collisions between beams of fully stripped lead ions (^{208}Pb^{82+}) are scheduled for one year after the start-up of the collider with protons. With the nominal magnetic field of 8.33 T in the dipole magnets, these ions will have a beam energy of 2.76 TeV/nucleon, yielding a total centre-of-mass energy of 1.15 PeV and a nominal luminosity of 1.0×10^{27} cm^{-2} s^{-1}. Collisions between ion beams will be provided principally at Interaction Point 2 for the specialised ALICE detector. However, the CMS and ATLAS detectors also plan to study ion collisions with similar luminosities.

While the major hardware systems of the LHC ring appear compatible with heavy ion operation, the beam dynamics and performance limits with ion beams are quite different from those of protons in a number of respects. The LHC also enters new territory where, for example, the copious nuclear electromagnetic interactions in peripheral collisions of the ions can directly limit luminosity and beam lifetime. While these phenomena are present in RHIC, for example, they are not straightforward to observe and do not limit performance. Yet they become critical in the LHC because of the combination of its unprecedented energy and superconducting magnet technology. It is not possible to make firm predictions about factors that may limit the performance of the LHC with ions. In particular, there are substantial uncertainties concerning some vacuum issues and the ion beam parameters during ramping.

13.1 LHC parameters for lead ions

Some aspects of heavy ion beams are similar to those of proton beams. For example, the nominal emittance of the ions has been chosen so that the ion beams have the same geometric size as the nominal proton beams (at beam energies corresponding to the same magnetic field in the dipole magnets). Thus, the most basic considerations of beam size and aperture will be the same as for protons, implying that this is a safe operational value. Despite this, the physics of ion beams is qualitatively and quantitatively different from that of protons, and the values of some parameters are necessarily very different. There are two reference sets of parameters for the lead ion beams:

Table 13.1: LHC beam parameters bearing upon the peak luminosity in the nominal ion scheme.

Beam Parameters		Injection	Collision
Lead ion energy	[GeV]	36'900	574'000
Lead ion energy per nucleon	[GeV]	177.4	2'759
Relativistic "gamma" factor		190.5	2'963.5
Number of ions per bunch		7.0×10^7	7.0×10^7
Number of bunches		592	592
Transverse normalised emittance	[μm]	1.4[a]	1.5
Peak RF voltage (400 MHz system)	[MV]	8	16
Synchrotron frequency	[Hz]	63.7	23.0
RF bucket half-height		1.04×10^{-3}	3.56×10^{-4}
Longitudinal emittance (4σ)	[eV s/charge]	0.7	2.5[b]
RF bucket filling factor		0.472	0.316
RMS bunch length[c]	[cm]	9.97	7.94
Circulating beam current	[mA]	6.12	6.12
Stored energy per beam	[MJ]	0.245	3.81
Twiss function $\beta_x = \beta_y = \beta*$ at IP2	[m]	10.0	0.5
RMS beam size at IP2	[μm]	280.6	15.9
Geometric luminosity reduction factor[d]		-	1
Peak luminosity at IP2	[cm^{-2} s^{-1}]	-	1.0×10^{27}

[a] The emittance at injection energy refers to the emittance delivered to the LHC by the SPS without any increase due to injection errors and optical mismatch.

[b] The baseline operation assumes that the longitudinal emittance is deliberately blown up during, or before, the ramp, in order to reduce the intra-beam scattering growth rates.

[c] Dimensions are given for Gaussian distributions. The real beam will not have a Gaussian distribution, but more realistic distributions do not allow analytic estimates for the IBS growth rates.

[d] The geometric luminosity reduction factor depends on the total crossing angle at the IP.

13.1.1 Nominal ion scheme

A peak luminosity of 1.0×10^{27} cm^{-2} s^{-1} has been the overall performance goal for lead ions for some time [11, 12, 64, 65]. The main parameters of the beams at injection and collision energies are given in table 13.1.

13.1.2 Early ion scheme

The first period of operation of the LHC as a lead-lead collider will be carried out with nominal single bunch parameters but ten times fewer bunches and a larger value of $\beta*$. These relaxed parameters will provide more margin against some of the performance limitations, namely those that depend on the total beam current. The reduced luminosity will nevertheless give access to important physics. The parameters at collision energy for this scheme are given in table 13.2.

Table 13.2: LHC beam parameters bearing upon the peak luminosity in the early ion scheme. Only those parameters that differ from those in the nominal ion scheme (table 13.1) are shown.

Beam Parameters		Injection	Collision
Number of bunches		62	62
Circulating beam current	[mA]	0.641	0.641
Stored energy per beam	[MJ]	0.0248	0.386
Twiss function $\beta_x = \beta_y = \beta^*$ at IP2	[m]	10.0	1.0
RMS beam size at IP2	[μm]	280.6	22.5
Peak luminosity at IP2	[cm^{-2} s^{-1}]	-	5.40×10^{25}

13.2 Orbits and optical configurations for heavy ions

The optics at IP2, for collisions of ion beams in the ALICE detector, will be quite different from that used for protons, in which $\beta^* = 10$ m, and beams are collided with an angle. For ions, collisions will be head-on, with β^* with values down to 0.5 m. Moreover, since this value is somewhat smaller than the limit of $\beta^* = 0.55$ m for the high-luminosity p-p collisions at IP2 and IP5, the peak values of β_x and β_y in the insertion quadrupoles will be higher in the ion collision optics. The lower value of β^* is possible with ions because the separation bumps are smaller (see the following section), leaving more aperture for the increased beam size at the peaks of the beta-functions.

For ion collisions in both IP1 and IP5, the optics can be the same as for protons, or may be adjusted to $\beta^* = 0.5$ m, as in IP2. Elsewhere, the pre-collision optics can be maintained in any IP in which the beams do not collide. Thanks to the modularity and independence of the optics in the various interaction regions, it is in principle straightforward to adapt the optics of the LHC to any set of collision points. However, it should be remembered that switching between the various possible configurations may require some operational time in order to establish the appropriate corrections. In particular, each configuration will contribute differently to the horizontal and vertical dispersion around the ring.

Compared with the nominal proton beams, the relatively low intensities and larger bunch spacing of the lead ion beams lead to weak long-range beam-beam effects which do not, in themselves, require any minimum separation around the interaction points. If these were the only considerations, it might be possible to eliminate the crossing angle entirely. However, this would create additional head-on beam-beam encounters, reducing the beam lifetime. The collisions at additional encounters would also interfere with the trigger for ALICE. Moreover, the ALICE detector has a spectrometer magnet, which is compensated by its own orbit separation bump around IP2. The total separation will be the superposition of this bump and the "external" crossing angle and parallel separation bumps. At the IP, the full crossing angle is given by

$$[\theta_c/\mu\text{rad}] \approx 140 f_{\text{ALICE}} - 340 f_{\text{IP2 bump}},$$

where f_{ALICE} and $f_{\text{IP2 bump}}$ are amplitude factors for the bumps (normalised so that $\theta_c = -200$ μrad for $f_{\text{ALICE}} = f_{\text{IP2 bump}} = 100\%$). It is desirable to use the minimum separation needed because, with the full separation used for protons, the criteria for minimum aperture are violated. Since the ion collision optics in IR2 has higher maximum values of β_x and β_y in the insertion quadrupoles, the

need to observe the minimum physical aperture criteria is another strong reason for reducing the separation bump amplitudes in the collision optics.

13.3   Longitudinal dynamics

Nominal longitudinal parameters for lead ions at injection and collision energies are given in table 13.1. The relatively small injected longitudinal emittance of $\varepsilon_\lambda = 0.7$ eV s/charge is necessary for efficient injection, as long as the 200 MHz capture system (discussed in the Introduction to Chapter 4) is not installed. All parameters given in this chapter assume these conditions. Because of mismatch and nonlinearities, some filamentation to a slightly larger value of emittance after injection is likely. Under these conditions, the bunches occupy about one half of the RF bucket area. However, the relatively short growth times for the longitudinal emittance at nominal intensity imply a further increase in longitudinal emittance if the bunches have to be kept for some time at injection. At some point, ions may start to spill out of the RF bucket. However, since beam-loading will be very small for the foreseen ion beams, a reserve of 50% of the total RF voltage will be available to counter this. Controlled blow up to $\varepsilon_\lambda = 2.5$ eV s/charge is in any case necessary during the ramp to collision energy, to reduce the growth of the transverse emittances from intra-beam scattering.

13.4   Effects of nuclear interactions on the LHC and its beams

When ultra-relativistic lead ions collide at LHC energies, numerous processes of fragmentation and particle production can occur. Some of these have direct consequences as performance limits for the collider. Besides the hadronic nuclear interactions due to direct nuclear overlap,

$$^{208}Pb^{82+} + {}^{208}Pb^{82+} \xrightarrow{\text{nuclear}} X \tag{13.1}$$

for which the cross section is

$$\sigma_H \approx 8 \text{ barn} \tag{13.2}$$
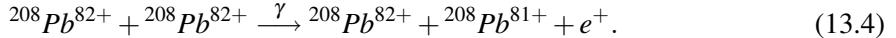
there is an important class of longer-range, or peripheral, collisions, dominated by electromagnetic interactions. When colliding light ions, the cross sections for these processes are small (some are zero in the case of protons) compared with σ_H. For heavy ions (with $Z \geq 30$), and Pb in particular, the cross sections for these electromagnetic interactions are much larger than σ_H. While simple elastic (Rutherford) scattering and free $e^+ e^-$ pair production are of little consequence, other processes change the charge state or mass of one of the colliding ions, creating a secondary beam emerging from the collision point. For a change, ΔQ, in the charge, Q, and ΔA in the number of nucleons, A, the magnetic rigidity of the secondary beam corresponds to an effective fractional momentum deviation given approximately[1] by

$$\delta(\Delta Q, \Delta A) \approx \frac{1 + \Delta A/A}{1 + \Delta Q/Q} - 1 \tag{13.3}$$

---
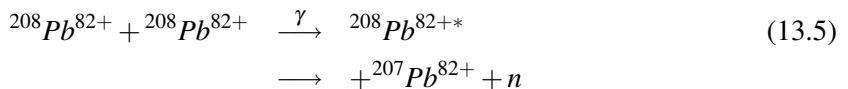
[1]This assumes that the momentum per nucleon of all final state components — for example, emitted neutrons — in the laboratory frame remains close to its value in the initial state. It is easy to see that the approximation is good for the electron capture process. Detailed calculations show that this holds, in an average sense, to a fairly good approximation in the electromagnetic dissociation processes considered.

All contributions to the total cross section for ion collisions will, of course, contribute to the total loss rate and resulting beam lifetime. However, certain processes have consequences beyond this, causing concentrated particle losses, heating and finally magnet quenches. An important example is electron capture from pair production, in which a lead nucleus captures an electron (ECPP),

$$^{208}Pb^{82+} + {}^{208}Pb^{82+} \xrightarrow{\gamma} {}^{208}Pb^{82+} + {}^{208}Pb^{81+} + e^+. \tag{13.4}$$

Another important effect is electromagnetic dissociation, in which a lead ion first makes a transition to an excited state and then decays with the emission of a neutron, leaving a lighter isotope of lead (EMD),

$$
\begin{aligned}
^{208}Pb^{82+} + {}^{208}Pb^{82+} &\xrightarrow{\gamma} \quad {}^{208}Pb^{82+*} \\
&\longrightarrow \quad + {}^{207}Pb^{82+} + n
\end{aligned}
\tag{13.5}
$$

The total cross section for removal of an ion from the beam is,

$$\sigma_T = \sigma_H + \sigma_{\text{ECPP}} + \sigma_{\text{EMD}} \approx 514 \, \text{barn}. \tag{13.6}$$

13.5   Intra-beam scattering

Multiple Coulomb scattering within an ion bunch, known as intra-beam scattering (IBS), is a diffusive process that modifies all three beam emittances. IBS is already significant for protons in the LHC, but it is even stronger for lead ion beams of nominal intensity and determines the acceptable longitudinal emittance, particularly at injection from the SPS. As the emittances increase from the initial nominal values, the growth rates due to IBS will decrease. Figure 13.1 shows how the emittance growth times due to IBS depend on longitudinal emittance.
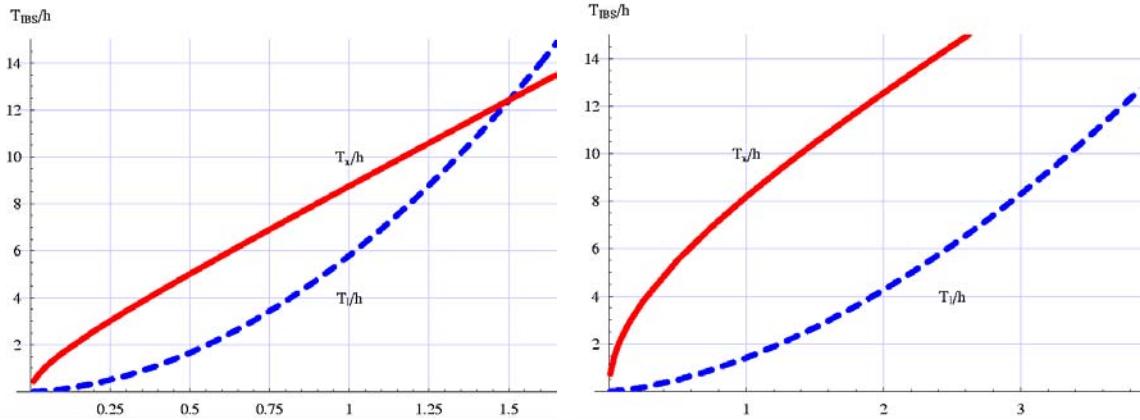
13.6   Synchrotron radiation from lead ions

The LHC is not only the first proton storage ring in which synchrotron radiation plays a noticeable role (mainly as a heat load on the cryogenic system), but also the first heavy ion storage ring in which synchrotron radiation has significant effects on beam dynamics. Surprisingly, perhaps, some of these effects are stronger for lead ions than for protons, because the charges in the nucleus of the ion behave coherently.[2] Quantities such as the energy loss per turn from synchrotron radiation, and the radiation damping time for ions, are obtained from the familiar formulas for electrons by replacing the classical electron radius and the mass by those of the ions. The principal characteristics of the incoherent synchrotron radiation of fully stripped ions of atomic number Z and mass number A can be related to those of protons (assuming the same field in the bending magnets) by,

$$\frac{U_{\text{Ion}}}{U_p} \approx \frac{Z^6}{A^4} \approx 162 \qquad \frac{u_{\text{Ion}}^c}{u_p^c} \approx \frac{Z^3}{A^3} \approx 0.061 \tag{13.7}$$

---

[2]The nuclear radius being much smaller than relevant wavelengths, the nucleus radiates coherently, like a single charge Ze.

Figure 13.1: Emittance growth times from intra-beam scattering as a function of longitudinal emittance for ^{208}Pb^{82+} at injection (left plot) and collision (right plot) energies. The transverse emittances and beam intensities are taken to have their nominal values, and the total circumferential voltages from the 400 MHz RF system, at injection and collision, are VRF = 8 MV and VRF = 16 MV, respectively. Solid and dashed lines correspond to the growth times for horizontal (μm.rad) and longitudinal emittances (eV.s).

$$\frac{N_{\text{Ion}}}{N_p} \approx \frac{Z^3}{A} \approx 2651 \qquad \frac{\tau_{\text{Ion}}}{\tau_p} \approx \frac{A^4}{Z^5} \approx 0.5, \tag{13.8}$$

where U is the energy lost per ion per turn by synchrotron radiation, u^c is the critical energy of the synchrotron radiation photons, N is the number of photons emitted per turn, and τ is the synchrotron radiation damping time. The numerical values are given for the case of the lead ion ^{208}Pb^{82+}. It is notable that radiation damping for heavy ions like lead is about twice as fast as for protons, and that the emittance damping times are comparable with the growth times from intra-beam scattering.

Acknowledgements

LHC machine acronyms

LHC	Large Hadron Collider being built at CERN
LEP	Large Electron Positron collider built at CERN and now decommissioned
IP	Interaction Point at which two opposing beams collide
IR	Interaction Region in which the IP is situated
SSS	Short Straight Section, that occurs in the arcs and contain quadrupole and corrector magnets
LSS	Long Straight Section, that flanks the IPs
MS	Matching Section in the LSS
DS	Dispersion suppressor situated between the MS in the LSS and the arc
MB	Main LHC dipoles
MQ	Main LHC quadrupoles
QF	Focusing Quadrupole
QD	Defocusing Quadrupole
QRL	Cryogenic feed line
HOM	Higher order modes in RF cavities

Bibliography

[1] J.P. Blewett, 200 *GeV intersecting storage accelerators*, *Proceedings of the 8*th *International Conference on High-Energy Accelerators*, CERN, Geneva Switzerland (1971).

[2] E.J. Bleser, *Superconducting magnets for the CBA project*, *Nucl. Instrum. Meth.* **A 235** (1985) 435, see footnote at page 435.

[3] *CBA Brookhaven Colliding Beam Accelerator*, Newsletter No. 2 (Nov. 1982) page 27–31.

[4] *Report of the task force on SSC operations*, SCC-SR-1005 (1985), http://dx.doi.org/10.2172/88535.

[5] J. Billan, et al, *The eight superconducting quadrupoles for the ISR high-luminosity insertion*, *Proceedings of the 11*th *International Conference on High-Energy Accelerators*, Geneva Switzerland (1980), CERN-ISR-BOM-GE-80-22, http://cdsweb.cern.ch/record/879231.

[6] G. Bon Mardion, G. Claudet, P. Seyfert and J. Verdier, *Helium II in low-temperature and superconductive magnet engineering*, *Adv. Cryog. Eng.* **23** (1978) 358.

[7] R. Aymar et al., *Conceptual design of a superconducting tokamak: "Torus II supra"*, *IEEE Trans. Magn.* **15** (1979) 542.

[8] G. Claudet and R. Aymar, *Tore Supra and helium II cooling of large high-field magnets*, *Adv. Cryog. Eng.* **A 35** (1990) 55.

[9] G. Claudet, F. Disdier, P. Lebrun, M. Morpurgo and P. Weymuth, *Preliminary study of superfluid helium cryogenic system for the Large Hadron Collider*, *Proceedings of the ICFA Workshop on Superconducting Magnets and Cryogenics*, BNL 52006, Brookhaven National Laboratory, U.S.A. (1986) page 270.

[10] J. Casas Cubillos, A. Cyvoct, P. Lebrun, M. Marquet, L. Tavian and R. van Weelderen, *Design concept and first experimental validation of the superfluid helium system for the Large Hadron Collider (LHC) project at CERN*, *Cryogenics* **32** (1992) 118.

[11] THE LHC STUDY GROUP collaboration, *LHC — the Large Hadron Collider accelerator project*, CERN-AC-93-03 (known as the "White Book"), http://cdsweb.cern.ch/record/87244.

[12] THE LHC STUDY GROUP collaboration, *LHC — the Large Hadron Collider conceptual design*, CERN-AC-95-05 (known as the "Yellow Book"), http://cdsweb.cern.ch/record/291782.

[13] O.S. Brüning et al. (eds.), *The LHC design report v.1 : the LHC Main Ring*, CERN-2004-003-V-1, http://cdsweb.cern.ch/record/782076; *The LHC design report v.2 : the LHC Infrastructure and General Services*, CERN-2004-003-V-2, http://cdsweb.cern.ch/record/815187; M. Benedikt et al. (eds.), *The LHC design report v.3 : the LHC Injector Chain*, CERN-2004-003-V-3, http://cdsweb.cern.ch/record/823808.

[14] ATLAS Collaboration, *ATLAS: technical proposal for a general-purpose pp experiment at the Large Hadron Collider at CERN*, CERN-LHCC-94-43, http://cdsweb.cern.ch/record/290968.

[15] CMS collaboration, *CMS technical proposal*, CERN-LHCC-94-38, http://cdsweb.cern.ch/record/290969.

[16] LHb collaboration, *LHCb technical proposal*, CERN-LHCC-98-004, http://cdsweb.cern.ch/record/622031.

[17] TOTEM collaboration, W. Kienzle et al, *TOTEM, Total cross section, elastic scattering and diffractive dissociation at the LHC: Technical Proposal*, CERN-LHCC-99-007, http://cdsweb.cern.ch/record/385483.

[18] ALICE collaboration, *ALICE: Technical proposal for a Large Ion collider Experiment at the CERN LHC*, CERN-LHCC-95-71, http://cdsweb.cern.ch/record/293391.

[19] THE LHC STUDY GROUP, *Design study of the large hadron collider (LHC): a multiparticle collider in the LEP tunnel*, CERN-91-03, http://cdsweb.cern.ch/record/220493.

[20] O. Brünning, *Progress report on the LHC optics*, *Presentation to the 10th LHC machine advisory committee*, http://mgt-lhc-machine-advisory-committee.web.cern.ch/mgt-lhc-machine-advisory-committee/lhcmac10/ClosedSession/Bruning.pdf.

[21] E. Willen et al., *Superconducting dipole magnets for the LHC insertion regions*, *Proceedings of the EPAC* 2000, Vienna Austria (2000), http://cdsweb.cern.ch/record/508368.

[22] S. Plate, E. Willen and R. Ostejic, *LHC Interface Specification, LBRS cryo-assemblies — D3 dipoles*, LHC-MBRS-ES-0002, http://cdsweb.cern.ch/record/1069431.

[23] E. Shaposhnikova, *Longitudinal beam parameters during acceleration in the LHC*, LHC-PROJECT-NOTE-242, http://cdsweb.cern.ch/record/691957.

[24] D. Boussard, W. Höfle and T. Linnecar, *The LHC transverse damper (ADT) performance specification*, SL-Note-99-055-HRF http://cdsweb.cern.ch/record/702559.

[25] D. Boussard and T. Linnecar, *The LHC superconducting RF system*, LHC-Project-Report-316, http://cdsweb.cern.ch/record/410377.

[26] J. Tückmantel, *The SPS/LHC longitudinal interface*, *Proceedings of the* 9th *Chamonix workshop*, Chamonix France (1999), CERN-SL-99-007, http://ab-div.web.cern.ch/ab-div/Conferences/Chamonix/chamx99/PAPERS/JT2_1.PDF.

[27] E. Gorbatchev et al., *Transverse damping system for the future CERN LHC*, *Proceedings of the PAC* 2001, Chicago Illinois U.S.A. (2001), http://cdsweb.cern.ch/record/555897.

[28] P. Corredoura, *Architecture and performance of the PEP-II low-level RF system*, *Proceedings of the* 18th *Particle Accelerator Conference*, New York City, U.S.A. (1999).

[29] D. Angal-Kalinin and L. Vos, *Coupled bunch instabilities in the LHC*, *Proceedings of* 8th *European Particle Accelerator Conference*, Paris France (2002), LHC-Project-Report-585, http://cdsweb.cern.ch/record/569462.

[30] D. Brandt and L. Vos, *Resistive wall instability for the LHC: intermediate review*, LHC-PROJECT-NOTE-257, http://cdsweb.cern.ch/record/692031.

[31] K. Eggert, K. Honkavaara and A. Morsh, *Luminosity considerations for the LHC*, CERN-LHC-note-263, http://cdsweb.cern.ch/record/260711.

[32] O. Gröbner, *The LHC vacuum system*, *Proceedings of the PAC* 1997, Vancouver B.C. Canada (1997), LHC-Project-Report-181, http://cdsweb.cern.ch/record/356437.

[33] C. Benvenuti et al., *Vacuum properties of TiZrV non-evaporable getter films for the LHC vacuum system*, *Vacuum* **60** (2001) 57.

[34] M. Zerlauth, A. Yepes Jimeno and G. Morpungo, *The electrical circuits in the LHC reference database*, LHC-LD-ES-0003, http://cdsweb.cern.ch/record/1069436.

[35] K. Dahlerup-Petersen, B. Kazmine, V. Popov, V. Sytchev, L. Vassiliev and V. Zubko, *Energy extraction resistors for the main dipole and quadrupole circuits of the LHC*, *Proceedings of the* 7th *European Particle Accelerator Conference*, Vienna Austria (2000), LHC-Project-Report-421, http://cdsweb.cern.ch/record/466523.

[36] A. Vergara-Fernández, *Reliability of the quench protection system for the LHC superconducting elements*, PhD Thesis, March 2003, LHC-PROJECT-NOTE-350, http://cdsweb.cern.ch/record/745594.

[37] P. Lebrun, *Superconductivity and cryogenics for the large hadron collider*, LHC-Project-Report-441, http://cdsweb.cern.ch/record/473537.

[38] A. Ballarino, A. Ijspeert and U. Wagner, *Potential of high temperature superconductor current leads for cryogenics*, *Proceedings of the* 16th *International Cryogenic Engineering Conference*, Kitakyushu Japan (1996), Elsevier Science, Oxford U.K. (1997) pgg 1139–1142.

[39] J.-P. Koutchouk, *Measurement of the beam position in the LHC main rings*, LHC-BPM-ES-0004, http://cdsweb.cern.ch/record/1068133.

[40] D. Cocq, *The wide band normaliser – a new circuit to measure transverse bunch position in accelerators and colliders*, *Nucl. Instrum. Meth.* **A 416** (1998) 1.

[41] B. Jeanneret and H. Burkhardt, *On the measurement of the beam losses in the LHC rings*, LHC-BLM-ES-0001, http://cdsweb.cern.ch/record/1069442.

[42] R. Jung et al., *The LHC* 450 *GeV to* 7 *TeV synchrotron radiation profile monitor*, *AIP Conf. Proc.* **648** (2002) 220, CERN-SL-2002-015-BI, http://cdsweb.cern.ch/record/556822.

[43] R. Assmann et al., *On the measurement of the relative luminosity at the LHC*, LHC-B-ES-0007, http://cdsweb.cern.ch/record/1069444.

[44] Y. Papaphilippou and F. Zimmermann, *Weak-strong beam-beam simulations for LHC*, *Workshop on Beam-Beam Effects in Large Hadron Colliders*, Geneva Switzerland (1999), http://cdsweb.cern.ch/record/533692.

[45] J.P. Koutchouk, *Correction of the long-range beam-beam effect in LHC using Electro-Magnetic lenses*, *Proceedings of the IEEE PAC* 2001, Chicago U.S.A. (2001), CERN-SL-2001-048-BI, http://cdsweb.cern.ch/record/513685.

[46] *LynuxWorks*, http://www.lynuxworks.com.

[47] *Redhat*, http://www.redhat.com.

[48] *Timing, Trigger and Control (TTC) systems for the LHC*, http://ttc.web.cern.ch/TTC/intro.html.

[49] *Timing working group*, http://lhc-proj-timwg.web.cern.ch/lhc-proj-timwg/.

[50] *Coordinated Universal Time (UTC)*, http://www.its.bldrdoc.gov/fs-1037/dir-009/_1277.htm.

[51] E. Ciapala, F. Rodriguez Mateos, R. Schmidt and J. Wenninger, *The LHC post-mortem system*, LHC-PROJECT-NOTE-303, http://cdsweb.cern.ch/record/691828.

[52] *NTP: the Network Time Protocol*, http://www.ntp.org.

[53] R. Billen and J. Schinzel, *Building, running and dismantling world's largest scientific instrument with the same database tools*, SL-Note-2001-011-MR, http://cdsweb.cern.ch/record/702646.

[54] M. Zerlauth, A. Jimeno, G. Morpurgo and R. Schmidt, *The electrical circuit description for the LHC*, *Proceedings of the EPAC* 2002, Paris France (2002), http://cdsweb.cern.ch/record/584717.

[55] P. Gayet et al., *Application of object-based industrial controls for cryogenics*, *Proceedings of the EPAC* 2002, Paris France (2002), CERN-LHC-2002-007-IAS, http://cdsweb.cern.ch/record/567337.

[56] http://srv1ps.cern.ch/psop/nAos/index.htm.

[57] F. Calderini et al., *LHC alarm system user requirements document*, SL-Note-2002-004-CO,
http://cdsweb.cern.ch/record/702685.

[58] R.J. Lauckner, *What data is needed to understand failures during LHC operation?*,
Proceedings of the 11th *Workshop of the LHC*, Chamonix France (2001),
http://cdsweb.cern.ch/record/567214.

[59] A. Hilaire, V. Mertens and E. Weisse, *Beam transfer to and injection into LHC*, *Proceedings
of the EPAC* 1998, Stockholm Sweden (1998), LHC-Project-Report-208,
http://cdsweb.cern.ch/record/364728.

[60] L. Ducimetière et al., *The LHC injection kicker magnet*, *Proceedings of the PAC* 2003,
Portland U.S.A. (2003), LHC-Project-Report-655, http://cdsweb.cern.ch/record/625014.

[61] E. Frick et al., *Fast pulsed magnet systems for proton and antiproton injection into the
CERN* 400 *GeV proton synchrotron*, *Proceedings of the* 15th *Power Modulator Symposium*,
Baltimore U.S.A. (1982).

[62] M. Benedikt (ed.), *The PS complex as proton pre injector for the LHC — design and
implementation report*, CERN-2000-003, http://cdsweb.cern.ch/record/449242.

[63] F. Blas et al., *Conversion of the PS complex as LHC proton pre-injector*, *Proceedings of the
PAC* 1997, Vancouver Canada (1997), CERN-PS-97-048-DI,
http://cdsweb.cern.ch/record/328735.

[64] THE LHC STUDY GROUP collaboration, *Design study of the Large Hadron Collider (LHC):
a multiparticle collider in the LEP tunnel*, CERN-AC-91-03,
http://cdsweb.cern.ch/record/220493.

[65] D. Brandt, *Review of the LHC ion programme*, LHC-Project-Report-450,
http://cdsweb.cern.ch/record/482035.